Resonance Enhanced Multiphoton Ionisation Spectroscopy of Small Halogenated Molecules

John T. Hennessy

Doctor of Philosophy

The University of Edinburgh

May 1999

"Labour is blossoming or dancing where
The body is not bruised to pleasure soul,
Nor beauty born out of its own despair,
Nor blear-eyed wisdom out of midnight oil"

Among School Children,
W. B. Yeats.

To my father and mother,

without the support of whom any of this would never have been possible.

Acknowledgements

I would like to thank Prof. Robert Donovan for the initial offer of a Ph.D. position and for his constant advice and direction during my years in Edinburgh. Also, I am grateful to Dr. Trevor Ridley for his assistance with the experimental work which was carried out. His considerable expertise regarding experimental matters has proved especially useful. In addition to this, insightful discussions with Trevor, both formal and informal, have proved most useful in analysing the obtained data. Also, the considerable input of Dr. Kenneth Lawley regarding matters of a theoretical nature must not go unrecognised. Robert Maier is thanked too for any technical assistance that he provided. I also thank the technical, administrative and secretarial staff in the Department of Chemistry. Of the secretarial staff, special thanks goes to Margaret Stewart and Annette Roper. The financial assistance provided by the University of Edinburgh to me in the form of a University demonstratorship is acknowledged as well.

I am grateful to the members of the Physical Chemistry section for making my time in Edinburgh both an enjoyable and interesting experience. While working as part of the Donovan group, I have had the pleasure of working with the other members, both past and present. These include such people as Pat O'Keeffe, Shiliang Wang, Neil Macleod, Marc de Vries, Sandy Flexen, Martin Snel, Mike Reilly, Zhiyuan Min, Andy Cormack, David Beattie and Mohammed Al-Kahali.

I also thank all of the people with whom I have shared flats since coming to Edinburgh in October 1995. I especially thank my current flatmates, Andy, Sofie and Cameron, for the quiet and pleasant environment in which has made the writing of this thesis so much easier.

Finally, I must express my special gratitude to my father, mother and brother. I am indebted to them for allowing me to take the opportunity to come to Edinburgh

and gain from what has been a very useful and interesting experience. I would also thank them for their additional support while I was writing this thesis.

Abstract

The results of studies of the higher electronic states of small halogenated molecules using resonance enhanced multiphoton ionisation (REMPI) spectroscopy are presented. A substantial part of this work concerned the Rydberg states of some methyl halides (methyl bromide, methyl iodide and methyl chloride). The assignment of these states was considerably aided by polarisation studies. Also, the propensity rules apparent in the VUV and two-photon spectra of the diatomic halogens and interhalogens were found to be useful. Thus, features comprising the two-photon spectra of the methyl halides were assigned to Ω=0 and Ω=2 components of *nd* and *np* states. In the three-photon spectra, transitions to the above states were observed along with transitions to *ns*, *np*, *nd* and *nf* states, all with Ω=1. In fact, three-photon spectra are seen to be dominated by *nf*;1 series while *nd* series dominate the two-photon spectra. This study involves a considerable reappraisal of the identity of the states underlying Rydberg transitions in these methyl halides, apart from the first *ns* cluster. In a similar vein, Rydberg transitions in trifluoromethyl iodide were also investigated but their vibrational envelopes were found to depart from those seen for the methyl halides. This can be attributed to two causes: first, the increased amount of valence character of the orbital from which an electron is being promoted to a Rydberg orbital, as suggested by the appearance of the photoelectron spectrum, and second, the possibility of Rydberg~ion-pair interactions. This increased amount of valence character in the orbital from which an electron is promoted in a Rydberg transition also complicates the analysis of the two-photon spectrum of dichloromethane, especially in the energy region just below the first ionisation energy. Even so, the observed band systems are assignable to *nd* states of A_1 symmetry. Given that propensity rules in the spectra of the halogens are used to aid the spectral assignment of the above polyatomic molecules, an examination of the VUV spectroscopy of molecular chlorine in the 72000-77000 cm^{-1} region, using (1+1') REMPI, is included as an example of the operation of these propensity rules. Also apparent in this energy region is extensive Rydberg~ion-pair interaction. All expected components of the 4p cluster are seen with only the [3/2]4p;0_u^+ Rydberg state

interacting with the nearby F′ 0_u^+ ion-pair state. This complements other studies involving bound-free-bound excitation of other ungerade ion-pair states lying in the vicinity of the F′ 0_u^+ state.

Table of Contents

List of Figures

List of Tables

Chapter 1

Introduction and Basic Principles

1.1 Introduction

Spectroscopy is concerned with the study of the energy levels in atoms and molecules involved in the absorption, emission or scattering of radiation. Of particular interest are the reasons why some energy states are involved in some processes and others are not. These energy levels are generally discrete which results in sharp variation in the absorption, emission or scattering intensity with change in wavelength. It is this property that allows the determination of the energies above the ground state level of the observed states. This kind of data can be especially useful in molecular reaction dynamics. Spectroscopy can also provide valuable information on the physics and chemistry of atoms and molecules in their excited states. Applications of this type of information are found in areas such as photochemistry, atmospheric chemistry, plasma chemistry and combustion studies.

Of particular interest in this thesis are those excited states which lie 50000 cm^{-1} or more above the ground state. Until relatively recently, the only means of examining states in this energy region for any atom or molecule was through the use of vacuum ultraviolet (VUV) absorption spectroscopy with its inherent experimental difficulties. However, with the development of the tunable lasers, these states can now be accessed by the simultaneous absorption of two or more photons with wavelengths in the more convenient visible and near ultraviolet (UV) regions of the electromagnetic spectrum.

1.2 The Excited States

In this work, it is the identity of the electronically excited states involved in the absorption of radiation by molecules that is of most interest. In this vein, the

properties of electronically excited states are introduced here. Given the differences between the classes of molecules examined in this work, only a general discussion will be given here with further details specific to the class of molecule in question being given in the relevant chapter. Molecular electronically excited states can be classified into two main types: valence states and Rydberg states. Different valence electronic states arise from different arrangements of electrons within the outer valence shell of a molecule. While many valence states dissociate to produce neutral fragments given sufficient energy, some dissociate to give pairs of ions. These are known as ion-pair states and possess unusual properties which will be discussed later. Rydberg states result from the promotion of an electron from the outermost molecular orbital into an orbital which lies to higher energy of the valence orbitals and has a higher quantum number. The electronic ground states of molecules can be either conventional valence or ion-pair in character. For the molecules discussed in this thesis, the majority of which have closed shell ground states, the electronic ground states are of conventional valence character. Because of the energy region being investigated for the molecules of interest, Rydberg transitions are more common than those to valence excited states.

1.2.1 Rydberg States

Before considering molecular Rydberg states, it is useful to describe their atomic counterparts with which they share many of their characteristics. For the purposes of this discussion, atomic Rydberg states will be discussed using a hydrogenic picture because this is also applicable to molecules. For the hydrogen atom[1], Rydberg transitions occur when an electron is promoted from the ground state (1s) orbital to one of higher principal quantum number n. In these, the Rydberg orbital is always larger than the orbital from which the Rydberg electron originates. As a consequence, an atom in a Rydberg state can essentially be regarded as an electron, called the Rydberg electron, associated with a positively charged ion, the ionic core. Also, Rydberg states form series, examples of which are shown in Figure 1-1, converging upon ionisation limits according to the following equation:

$$T_n = \text{I.E.} - \frac{R}{(n-\delta)^2} \qquad \textbf{1-1}$$

where T_n is the transition energy for the Rydberg state with respect to the electronic ground state, I.E. is the ionisation energy upon which this series converges, R is the Rydberg constant at infinite mass (109737 cm^{-1}), and δ is the quantum defect. Although δ is independent of energy, and *n*, it varies significantly with *l*, the orbital angular momentum. This is a direct consequence of the reduced penetration of the ionic core by the wavefunction of the Rydberg electron, with increasing angular momentum. In other words, there is a lower probability of finding the Rydberg electron near the ionic core in Rydberg states with higher *l*. This behaviour can be explained if the shapes of the atomic and Rydberg orbitals are considered. In atomic orbitals of higher *l*, more nodes occur at their centres or at the ionic core in the case of Rydberg orbitals. Since the value of δ is a direct indicator of the amount of core

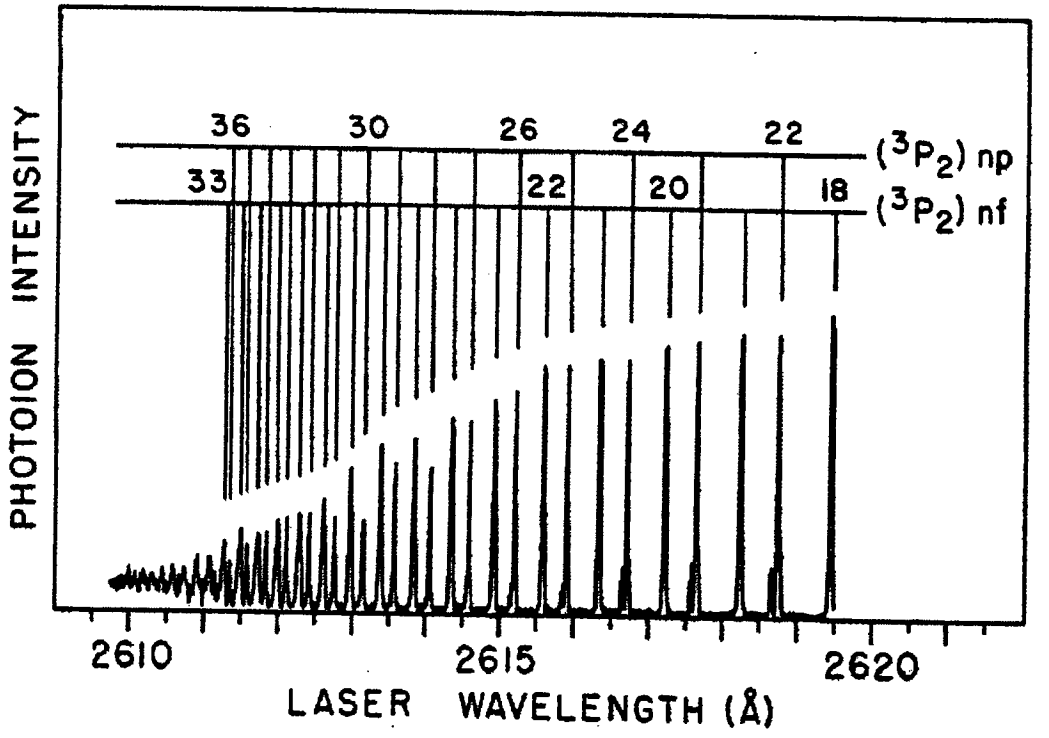

Figure 1-1: Higher members of *np* and *nf* Rydberg series converging upon the $^3P_2$ ionisation limit in atomic iodine. This spectrum, taken from the work of Pratt[2], was obtained using two-photon spectroscopy, the basis of which is discussed in a later section.

penetration, it is hardly surprising that it decreases in the sequence $ns > np > nd > nf$. Also, because δ dictates the energies where members of a Rydberg series lie, it can prove of some value in assigning spectra. Not only does the degree of penetration of the ionic core by a Rydberg electron decrease with increasing l but it also decreases with increasing n. This itself is a direct result of the increase in the radius of a Rydberg orbital with n^2. The decreasing penetration has a number of consequences for successive members of a Rydberg series. Firstly, the consequential decrease in the time spent by a Rydberg electron near the ionic core reduces the window within which relaxation processes can occur. The Rydberg state lifetime generally shows a direct dependence upon n^3. Correspondingly, the transition strengths of members of a Rydberg series show an inverse proportionality to n^3.

While a similar hydrogenic picture to that described above can be adopted for molecular Rydberg states, some differences are apparent. Firstly, not all molecular Rydberg transitions occur with a change in n and the first members of *nd* and *nf* series in molecules containing only main group atoms are examples of this. The assertion that transitions to the corresponding orbitals can be classified as Rydberg in nature is justified because they are the lowest energy *nd* and *nf* orbitals which essentially make no contribution to molecular bonding. The Rydberg nature of transitions to these states would be further confirmed by their quenching in condensed phases. Another difference between atoms and molecules is that there is greater scope for Rydberg state relaxation in the latter. In atoms, Rydberg state relaxation is limited to emission and autoionisation. Autoionisation involves the ejection of the Rydberg electron due to coupling of the Rydberg state with a nearby ionisation continuum. In molecules, Rydberg state decay can also occur as a result of predissociation. Predissociative interactions involve potential energy curve or surface crossings between Rydberg states and nearby valence states prior to the dissociation limit of the Rydberg state. These valence states may be bound or unbound in the vicinity of the Rydberg state. Interactions involving both of these cases are illustrated in Figure 1-2 for a hypothetical homonuclear diatomic molecule. While interactions with unbound states lead to lifetime shortening, those involving bound states can lead

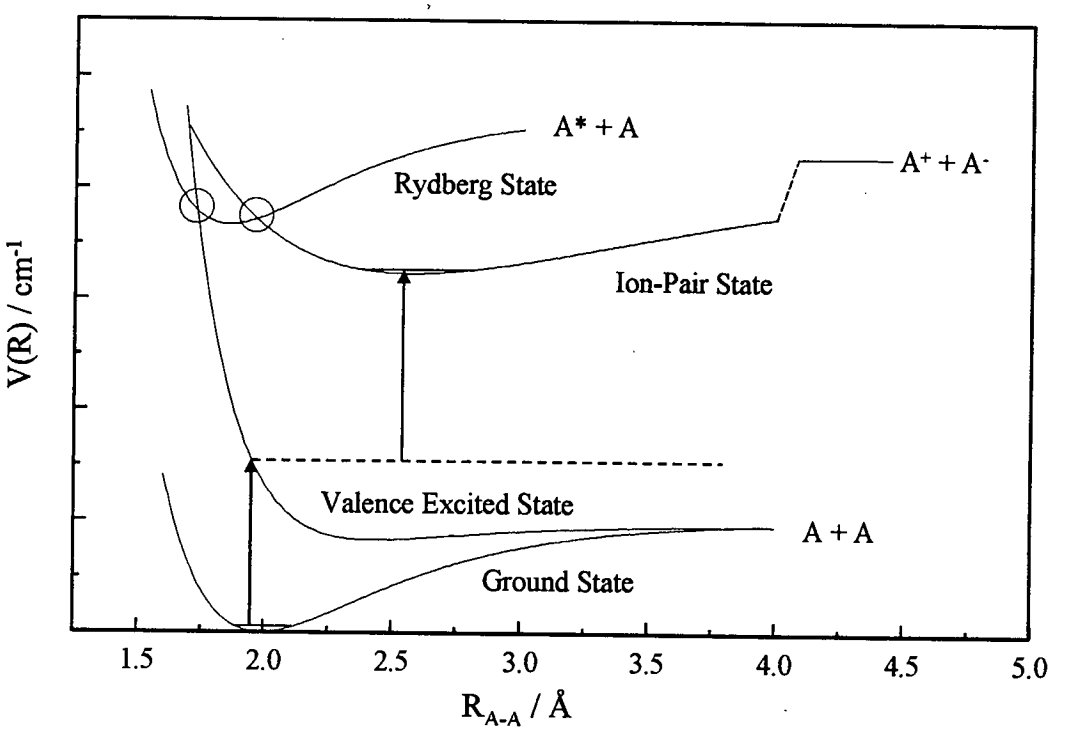

Figure 1-2: Potential energy diagram for a hypothetical homonuclear diatomic molecule A_2. The superimposed arrows and dotted line indicate a bound-free-bound excitation scheme, which is discussed later.

to a greater spectral complexity which makes spectral analysis more difficult. The increased spectral complexity can result from Rydberg~valence interactions allowing the population of excited states not otherwise accessible from the electronic ground state.

While molecules have a more intricate electronic structure than atoms, the major difference between the spectroscopy of atoms and that of molecules is the presence of rotational and vibrational structure in the latter. The rovibronic assignment of Rydberg transitions is made easier if spectroscopic data regarding the relevant ionic state is available. However, the usefulness of such data can prove somewhat limited if the Rydberg states are perturbed. This can occur through Rydberg~valence interactions as mentioned previously or through valence contamination of the Rydberg orbital[3]. The latter can occur if Rydberg orbitals mix with unoccupied valence orbitals to give Rydberg~valence conjugates. Another consequence of the presence of the rotational and vibrational energy levels in

molecules is that interactions between Rydberg states and nearby ionisation continua are enhanced with respect to atoms where only electronic autoionisation can occur.

One thing held in common by both atoms and molecules is the influence that quantum defect values have on the energies where Rydberg states lie. For the purposes of the work described in this thesis, quantum defect values are used and obtained in an empirical manner. In the past, energetic data from atomic spectroscopy has been used to aid the assignment of molecular Rydberg transitions. However, the additional complexity of molecular electronic structure means that there are many other ways in which Rydberg states can be perturbed. This means that care is required when using atomic data as an aid to the understanding of molecular spectra. An example where atomic data has proved misleading in the assignment of molecular spectra was recently seen in the diatomic halogens[4]. Thus, more information is required before secure assignments can be presented and some means for obtaining this are described in Chapter 3.

The factors controlling quantum defect values have attracted a great deal of interest theoretically[5,6]. In the past, quantum defect theory has focused largely upon higher n Rydberg states where the extent of relaxation as a result of strong interactions with the ionic core is reduced. More recently, added impetus for the study of these states and their properties came from the need to explain the mechanism behind a recently developed type of photoelectron spectroscopy, known as ZEro Kinetic Energy (ZEKE) photoelectron spectroscopy. This will be discussed later. The approach used in quantum defect theory is similar to that used in electron-ion scattering calculations. The interaction between the Rydberg electron and the ionic core at long range is considered to be coulombic but short range interactions are considered in terms of a collision complex. In this way, autoionisation is thought of as resulting from the transfer of energy from the ionic core to the Rydberg electron while predissociation results from energy transfer in the opposite direction. Also in line with the scattering formalism, the bound states comprising an individual Rydberg series and its associated ionisation continuum are considered as closed and open parts

of a single channel, respectively. Multichannel Quantum Defect Theory (MQDT) considers the interactions between different channels and hence, states belonging to different Rydberg series. Only recently has the effect of nearby unbound valence states upon a Rydberg series been considered in any detail[7]. It is this transfer of electronic energy from the Rydberg electron to the ionic core that needs to be investigated more extensively. In this way, Rydberg~valence interactions and any energetic displacements of the Rydberg states could be examined. It is only then that MQDT might prove useful for lower n Rydberg states ($n < 30$) , such as those investigated in this thesis.

1.2.2 Conventional Valence and Ion-Pair States

It might seem surprising that the spectra discussed in this thesis are dominated by transitions to Rydberg states. Transitions to valence states are also expected but most of the valence excited states lie below 50000 cm^{-1} in the molecules of interest in this work. The only valence states of interest, above this energy, are ion-pair states.

Because of electronic configurations where at least one electron occupies an anti-bonding orbital and the effect of the long-range Coulombic attraction between the ions, ion-pair states[8] display an unusual combination of properties. These states have longer equilibrium bondlengths, R_e, smaller equilibrium vibrational frequencies, ω_e, and larger equilibrium dissociation energies, D_e, than the electronic ground state. While the smaller ω_e and larger D_e make for a greater number of possible vibronic transitions, very few of these can be seen in spectra recorded using vertical excitation schemes. This is a direct consequence of the Franck-Condon principle which states that electronic transitions occur without any change in the position or momentum of the nuclei. Thus, because of the large geometry changes involved, transitions to low vibrational levels of ion-pair states, from the electronic ground state, are disfavoured. Even so, higher members of the vibrational manifold in the ion-pair potential can occur within the Franck-Condon window of the ground state and as a result, may be observed. This is the case for molecules such as ICl and IBr[8] but not for the molecules

of interest in this work. There still remains the possibility of Rydberg~ion-pair interactions which can complicate spectral analysis.

1.3 Multiphoton Spectroscopy

Because of its greater ease of use than VUV spectroscopy, multiphoton spectroscopy has found great applicability in the study of higher energy atomic and molecular states. It is also much used in studies of molecular reaction dynamics. The general features of this kind of spectroscopy are introduced here because it has proved so useful in the studies described in this thesis. Multiphoton spectroscopy, when used with ion detection, is known as Resonance Enhanced Multiphoton Ionisation (REMPI) and two typical schemes are depicted in Figure 1-3. In the schemes illustrated, three or four photons are used to ionise the atom or molecule and the ion signal is enhanced whenever coincidences occur near *real* energy levels at some intermediate point in the REMPI pathway, |1> and |2> in Figure 1-3. The non-resonant steps involve *virtual* intermediate states. Of particular interest in this thesis are those energy states which enhance the ion signal at the two- or three-photon level. A discussion of the experimental aspects of REMPI is deferred to the next chapter.

Not only can the simultaneous absorption of two or more photons provide an easier means of observing transitions which otherwise occur in the VUV region of the electromagnetic spectrum but transitions which cannot be seen by any other means are also seen. These new states can be seen as the selection rules for electronic transitions differ with the number of photons absorbed. This can lead to a relaxation of the selection rules which apply to one-photon transitions. For example, in atoms[1], the selection rule $\Delta l = \pm 1$ is strictly observed at the one-photon level. This selection rule arises as a result of conservation of angular momentum and symmetry restrictions. Again conserving angular momentum and following symmetry selection rules, $\Delta l = 0$, ± 2 and $\Delta l = \pm 1$, ± 3 selection rules apply for two- and three-photon atomic transitions, respectively.

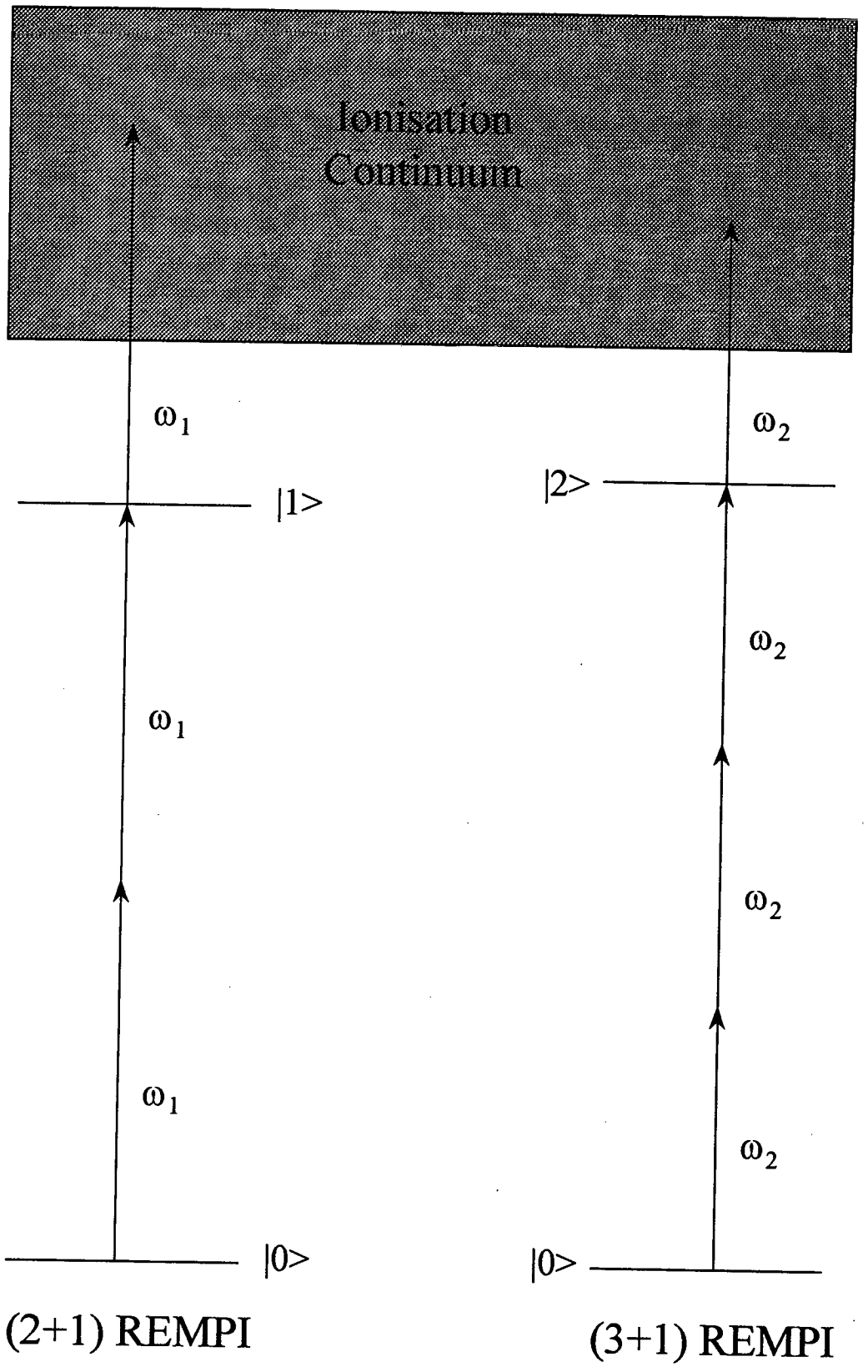

Figure 1-3: Some schemes for Resonance Enhanced Multiphoton Ionisation (REMPI).

The sequential absorption of more than one photon, through *real* intermediate states, is another means for examining electronically excited states which cannot be examined using vertical excitation schemes. The usefulness of sequential multiphoton excitation is well recognised in molecular spectroscopy. One example of the use of sequential multiphoton excitation is Optical-Optical Double Resonance (OODR) spectroscopy. Here, the first photon is resonant with a vibrational level of some bound excited state which has good Franck-Condon overlap with the ground state. A second photon is then absorbed which can populate vibrational levels in an electronically excited state not accessible through vertical excitation from the ground electronic state. A variant of the OODR technique involves either a repulsive intermediate state or the continuum of a bound state. It is then called bound-free-bound excitation and an example of this is illustrated in Figure 1-2. Here, the Franck-Condon window of the electronic ground state is much extended through bond-stretching following the absorption of the first photon. Both of these techniques have been used to study the ion-pair states of the diatomic halogens.

Another use for OODR excitation schemes is that they can be used to observe transitions that are otherwise weak or forbidden by the spin selection rule, $\Delta S = 0$, where S is the total spin angular momentum. However, this is only feasible for molecules containing relatively heavy atoms, such as the diatomic halogens Cl_2, Br_2 or I_2. Because of coupling of the spin angular momenta of the outermost pair of electrons, electronic states can have singlet or triplet spin multiplicity in an atom or molecule with a closed shell ground state. Singlet spin multiplicity arises when $S = 0$ as a result of both spin angular momentum vectors being antiparallel to one another. If these spin angular momentum vectors are not antiparallel, then $S = 1$ and triplet spin multiplicity results. Since, most molecules have closed shell ground states of singlet spin multiplicity, only transitions to other singlet states are observed, for the most part, using direct excitation. Nevertheless, the spin selection rule can be relaxed if the electron spin and orbital angular momentum are sufficiently strongly coupled. This is known as spin-orbit coupling and is particularly prevalent in heavier atoms and any molecules containing them. Not only does this result in mixing of singlet and triplet

states of the same M_s but it also increases the strength of triplet ← singlet or singlet ← triplet transitions. An example of this is the B ← X transitions in the heavier diatomic halogens mentioned already. Thus Λ, the projection of orbital angular momentum upon the internuclear axis, is no longer defined and Ω, the projection of total angular momentum upon the internuclear axis, becomes the more applicable (Ω results from coupling of Λ and Σ). Thus, an OODR excitation scheme involving the B 0_u^+ state, which is triplet in character, can lead to the observation of transitions to other triplet states not accessible by any other means. For example, some triplet ion-pair states of Cl_2 have been studied recently through employing the continuum of the B state as a real intermediate[9].

1.4 Photoelectron Spectroscopy

While atomic and molecular ionisation energies are worthy of attention in their own right, they are of special interest with regard to the spectroscopy of Rydberg states. This is because Rydberg series converge upon the energy levels of the ion. Therefore, knowledge of where these energy levels lie with respect to the corresponding neutral atomic or molecular electronic ground state can greatly aid the electronic assignment of Rydberg spectra by using the Rydberg formula, given in Equation 1-1. Conversely, values for ionisation energies can be obtained by extrapolation of Rydberg series. The assignment of Rydberg transitions is always easier and more secure if accurate ionisation energy values are available from other sources. For some of the molecules discussed in this thesis, newly reported ionisation energy values are used. Some of these were obtained using ZEKE photoelectron spectroscopy which can achieve sub-wavenumber resolution[13].

Until quite recently, the resolution of photoelectron spectroscopy has proved somewhat limited. In the longest established methods of photoelectron spectroscopy (PES), molecules are ionised using monochromatic radiation, typically at wavelengths of 584 Å (He I) or 304 Å (He II), which is produced using a helium discharge lamp. Because the photon energy is always greater than the measured ionisation energies,

excess energy is removed from the molecule by the ejected electron in the form of kinetic energy. This process is depicted in the ionisation scheme shown in Figure 1-4(a). Ionisation energies are then obtained using Equation 1-2:

$$h\nu - K.E._1 = I.E. \qquad \textbf{1-2}$$

where $h\nu$ is the photon energy, $K.E._1$ is the electron kinetic energy and I.E. is the ionisation energy. It is the necessity of determining the kinetic energies of the photoelectrons that has limited the resolution of conventional PES. Other techniques for PES requiring kinetic energy analysis such as synchrotron PES or REMPI-PES have the same disadvantage. While vibrational resolution is routinely achievable for most small molecules using these methods, rotational resolution remains elusive for all but the lightest molecules.

However, photoelectron spectroscopy can be carried out without the need for electron kinetic energy determination. This is possible because, at threshold, some photoelectrons have near-zero kinetic energy. It is possible to discriminate in favour of these near-zero kinetic energy or threshold photoelectrons using a number of techniques, most of which involve either time-of-flight or penetrating field spectrometers. This is essentially the basis of threshold photoelectron spectroscopy[11] (TPES), the ionisation scheme for which is depicted in Figure 1-4(b), where only the electrons with near-zero kinetic energies, sometimes as low as 3 meV, are detected. The resolution of the spectra obtained then depends only on the bandwidth of the radiation used.

A new PES technique improving on the resolution of TPES by using lasers, delayed electric fields and time-of-flight spectrometers, was reported by Müller-Dethlefs et al.[12] in 1984. This technique, called ZEro Kinetic Energy (ZEKE) PES[13], has proved of great value to the understanding of the photoelectron spectra of neutral molecules. The basis of this is that all neutral molecules possess Rydberg states. Rydberg state lifetimes generally increase with n^3 and so Rydberg states with

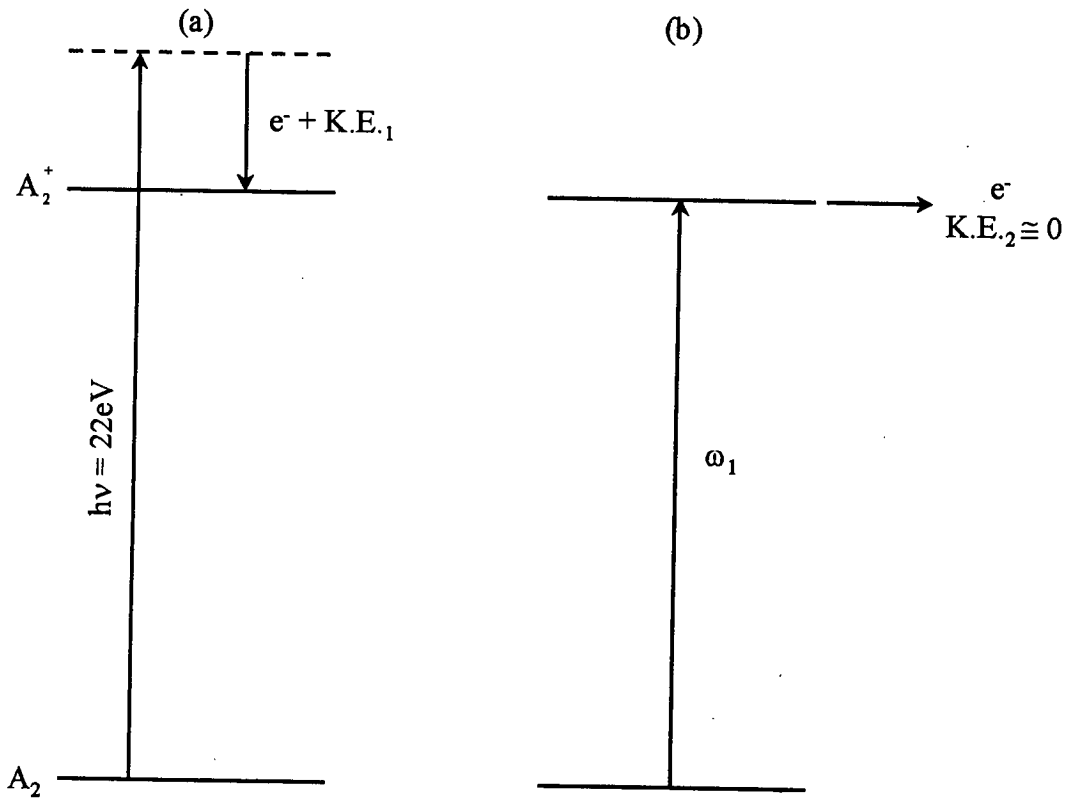

Figure 1-4: The ionisation schemes used in two different forms of photoelectron spectroscopy are illustrated for a hypothetical molecule A_2. The energy scheme for He I PES is shown in (a) while (b) depicts the scheme for TPES.

higher n are quite long-lived. However, the lifetimes of Rydberg states with $n > 100$ extend into the microsecond time domain[6] and, moreover, they seem to depend upon n^5. The reasons for this are still subject of some discussion but mixing of different l and m_l states by stray electric fields seems to have been accepted as the main explanation. This has the effect of essentially keeping the Rydberg electron away from the ionic core, hindering any decay processes as a result. These high n Rydberg states or ZEKE states lie less than 10 cm^{-1} below the adiabatic ionisation limit upon which the series is converging. Therefore, if an electric field, typically less than 6 Vcm^{-1}, is introduced, the ionisation energy of the atom or molecule is depressed and electrons ejected from the ZEKE states, enhancing the ZEKE signal. Also, if a time delay is introduced before this electric field is turned on, all of the fast electrons will have departed before the ZEKE electrons are produced and only the latter will be

detected. The resulting increase in ZEKE signal makes higher resolutions easier to achieve. The technique referred to as ZEKE-PFI where PFI stands for pulsed field ionisation. Resolutions of ZEKE-PFI spectra are dependent upon that of the radiation source and not the resolution of the detector. Hence, with the use of a coherent laser source, sub-wavenumber resolution can be achieved and rotational structure resolved. This kind of resolution makes the determination of ionisation energies of atoms or molecules, and hence the limits of any Rydberg series not only much easier but also much more accurate than before.

While ZEKE-PFI PES is very useful in the provision of accurate energies, the intensity information available from the spectra obtained is not always reliable. This is not only due to power variations in the radiation source with changes in wavelength, which can easily be corrected, but also arises from autoionisation processes. It is mainly because of autoionisation that band intensities in ZEKE-PFI spectra are not solely dependent upon either Franck-Condon or Hönl-London factors, which govern the linestrengths of vibrational and rotational transitions, respectively. Comparison with He I PES, which does involve direct ionisation, establishes whether or not the intensity information from ZEKE-PFI spectra is reliable. Once proved reliable, intensity information from ZEKE-PFI spectra can be used to aid the rovibronic assignment of Rydberg transitions.

ZEKE-PFI photoelectron spectroscopy has the advantage over that more detailed spectroscopic studies of ion states can be undertaken. In this way, electronic state splittings in the ion can be observed. Since these increase the number of Rydberg states present, they have a disproportionate effect upon the electronic structure of the neutral molecule. These ion state splittings can occur as a result of spin-orbit coupling or static Jahn-Teller interaction[10], for example. While spin-orbit coupling can occur in both atoms and molecules, Jahn-Teller interaction is restricted to polyatomic molecules. In degenerate states, the molecular geometry is distorted in order to break the coincidence of energy levels. Static Jahn-Teller interaction, the more important in relation to the spectroscopy of Rydberg states, causes the splitting of electronic states,

while dynamic Jahn-Teller interaction splits vibrational energy levels. Static Jahn-Teller interaction would be best exhibited in the electronic ground states of the methyl halide ions were it not for effective quenching by spin-orbit coupling. Regarding molecules, ZEKE-PFI photoelectron spectroscopy is particularly valuable when the greater spectral complexity caused by the presence of rotational and vibrational energy levels is considered. Since a Rydberg state arises from the long-range association of an electron with an ion core, ion-like characteristics are expected. Thus, Rydberg states are expected to display vibrational and rotational envelopes very similar to those of the ionic states upon which they are based. It is clear therefore that an understanding of molecular photoelectron spectroscopy can greatly assist the rovibronic analysis of molecular Rydberg transitions.

1.5 Arrangement of the Thesis

The greater part of this thesis is concerned with a discussion of the systematic assignments of higher energy transitions in the heavier methyl halides CH_3X (X = Cl, Br and I). The relative simplicity of their spectra lends itself to a detailed discussion of the underlying propensity rules and the electronic configurations of the observed states. Following discussion of the methyl halides, other molecules are discussed which have more complex spectra. In CF_3I and CH_2Cl_2, this additional complexity arises from the greater degree of vibrational activity present. Because Rydberg transitions are expected to dominate, photoelectron data is useful in aiding assignments. However, interactions between different electronic states can complicate matters further. A classic case of this is seen in the VUV spectrum of Cl_2, part of which is discussed in Chapter 7.

1.6 References

1. T. P. Softley, *Atomic Spectra*, Oxford Science Publications, Oxford, **1994**.
2. S. T. Pratt, *Phys. Rev. A*, **1985** 32 928.
3. M. B. Robin, *Higher Excited States of Polyatomic Molecules Vol. 1*, Academic Press, New York, **1974**.

4. R. J. Donovan, A. C. Flexen, K. P. Lawley and T. Ridley, *Chem. Phys.*, **1998** 226 217.

5. C. H. Greene and C. Jungen, *Adv. Atom. Mol. Phys.*, **1985** 21 51.

6. F. Merkt, *Ann. Rev. Phys. Chem.*, **1997** 48 675.

7. C. Jungen and S. C. Ross, *Phys. Rev. A*, **1997** 55 R2503-R2506.

8. K. P. Lawley and R. J. Donovan, *J. Chem. Soc. Faraday Trans.*, **1993** 89 1885.

9. M. S. N. Al-Kahali, R. J. Donovan, K. P. Lawley and A. J. Yarwood, *J. Phys. Chem.*, **1995** 99 3978.

10. G. Herzberg, *Molecular Spectra and Molecular Structure III: Electronic Spectra and Electronic Structure of Polyatomic Molecules*, Van Nostrand Reinhold, New York, **1966**.

11. G. C. King and K.-H. Schartner, in *VUV and Soft X-Ray Photoionisation* (Edited by U. Becker and D. A. Shirley), Plenum Press, New York, **1996** p.355-400.

12. K. Müller-Dethlefs, M. Sander and E.W. Schlag. *Chem. Phys. Lett.*, **1984** 112, 291.

13. K. Müller-Dethlefs and E. W. Schlag, *Angew. Chem. Int. Ed.*, **1998** 37 1347.

Chapter 2

Experimental Details

2.1 Introduction

In this chapter, the experimental equipment used to obtain the results reported in this thesis will be described. The experimental setup used essentially consists of a tunable laser system, a supersonic molecular beam, a time-of-flight mass spectrometer and appropriate data acquisition equipment. Where necessary, additional details relating to any specific experiments carried out will be discussed in the relevant chapters. Schematic diagrams depicting overviews of the experimental arrangements for one- and two-colour experiments are given in Figure 2-1 and Figure 2-2, respectively.

2.2 Resonance-Enhanced Multiphoton Ionisation (REMPI)

Multiphoton ionisation[1,2] occurs when an atom or molecule simultaneously absorbs two or more photons before it is ionised. When a real resonance is accessed at any of the intermediate levels in the ionisation pathway, an enhancement in ion signal is observed. One advantage of REMPI is that it allows the observation of high energy atomic and molecular states using tunable lasers, which operate in the ultraviolet (UV) and visible regions of the electromagnetic spectrum. Otherwise, these transitions could only be observed using vacuum ultraviolet (VUV) excitation with its inherent technical difficulties.

The absorption cross-sections for simultaneous absorption of two or more photons tabulated in Table 2-1, are much smaller than that of a one-photon transition[3]. Although the possibility of multiphoton transitions was noted first in

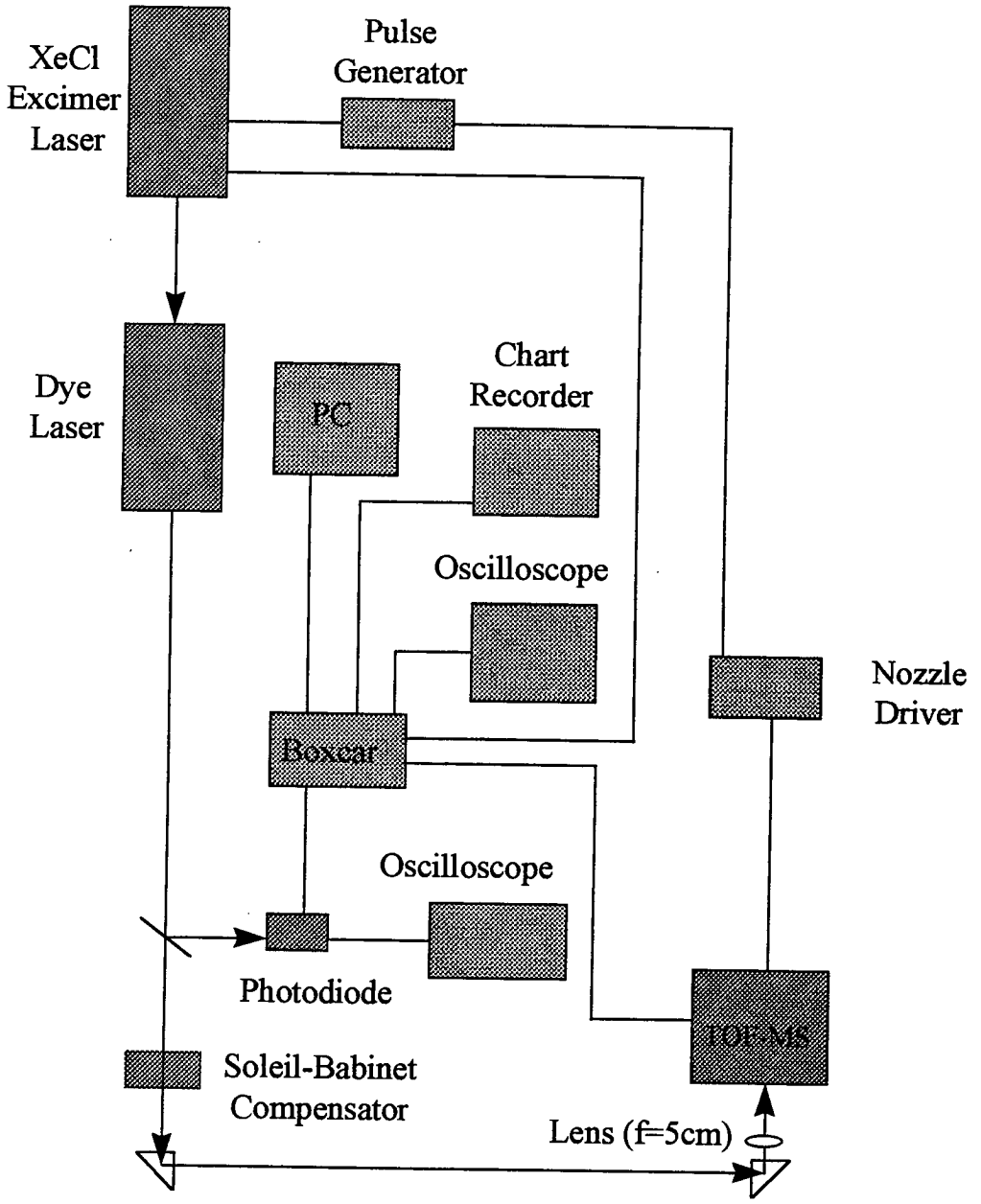

Figure 2-1: Schematic diagram of the typical setup for a one-colour polarisation-resolved REMPI experiment with associated dye laser power monitoring equipment.

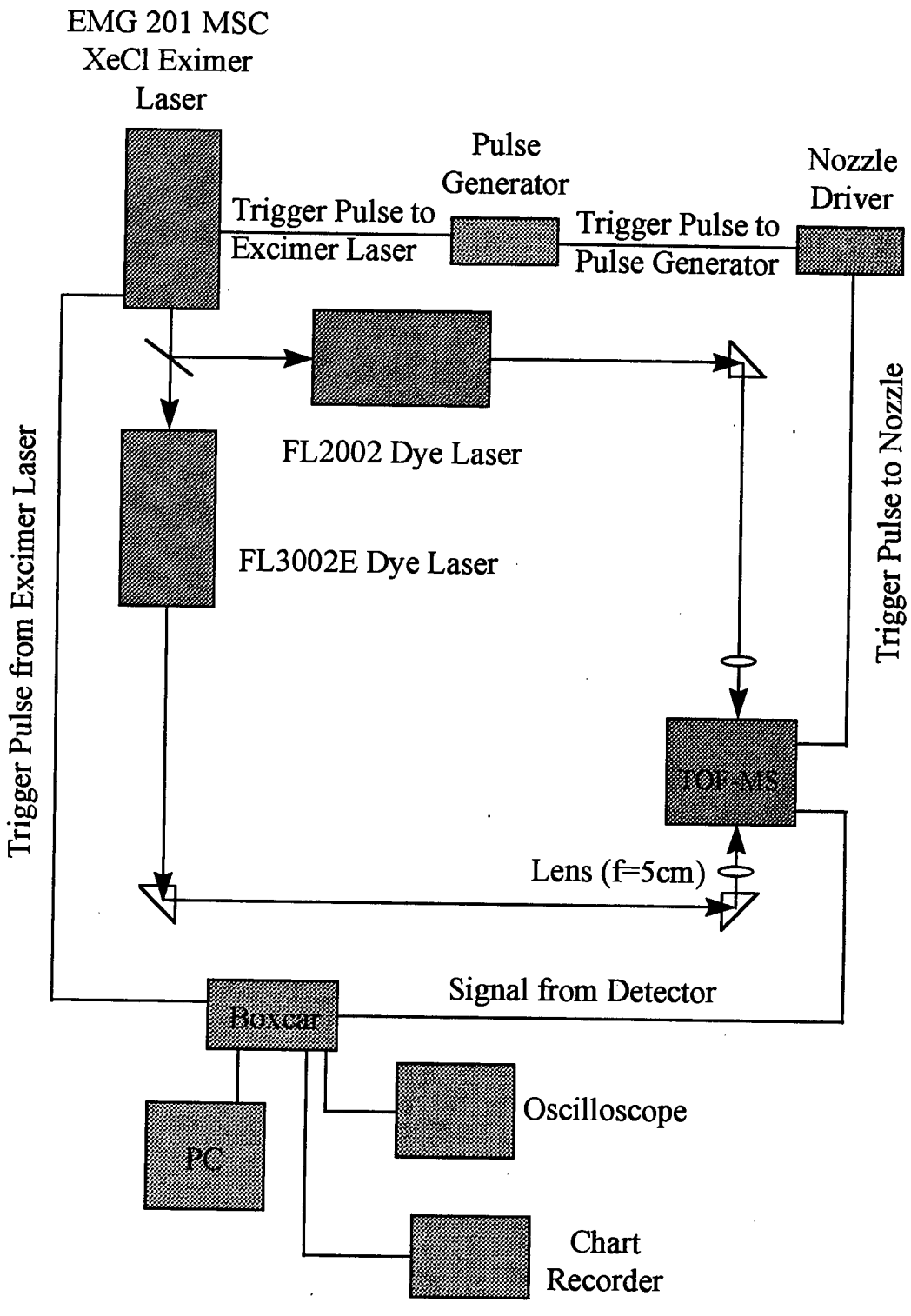

Figure 2-2: Schematic diagram of a typical setup for a two-colour REMPI experiment.

Excitation	Cross-Section
One-Photon	$\sim 10^{-18}$ $cm^2 molecule^{-1}$
Two-Photon	$\sim 10^{-50}$ $cm^4 s.molecule^{-1}$
Three-Photon	$\sim 10^{-82}$ $cm^6 s^2 molecule^{-1}$

Table 2-1: Typical cross-sections for the absorption of one or more photons[3].

1929[4], their low absorption cross-sections precluded their study until the advent of lasers, with their high intensity. For example, the laser intensity required to achieve a rate sufficient for a two-photon process as high as that of a one-photon one is of the order of 10^{28} photons.$cm^{-2}s^{-1}$. This is equivalent to a 300 μJ pulse with a laser power of 100 $MWcm^{-2}$ in the 200-300nm wavelength region[5]. The lasers used in this work are discussed in the next section.

2.3 The Laser System Employed

The laser radiation, used to probe the multiphoton transitions in the molecules which form the greater portion of the subject matter of this thesis, was generated using dye lasers pumped by an excimer laser. A Lambda Physik EMG 201 MSC excimer laser[6] was used to generate radiation with a wavelength of 308 nm, a pulselength of 25 ns and a maximum energy of 400mJ/pulse, typically at a repetition rate of 5 Hz. For one-colour experiments, this was used to pump a Lambda Physik FL3002E dye laser[7] which in turn produced tunable radiation in the UV and visible regions. In the case of two-colour experiments, the excimer laser beam was split, using a 50/50 or 75/25 beam splitter as required, so as to simultaneously pump a Lambda Physik FL2002 dye laser[7], in addition to the FL3002E. These dye lasers produce radiation in the UV and visible regions with a maximum laser energy of 20 mJ, a pulselength of 10ns and a bandwidth of 0.2 cm^{-1}. A brief description of the modes of operation of these laser types is given next.

2.3.1 Excimer Laser

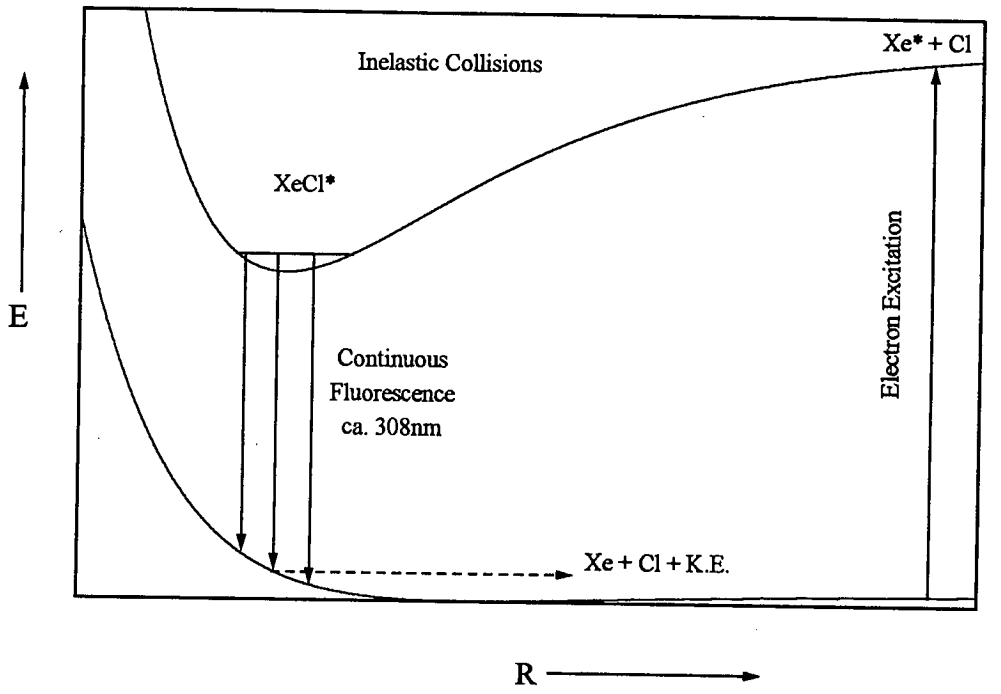

Figure 2-3: Schematic potential energy diagram depicting the lasing action in a XeCl excimer laser.

Excimer lasers[8-10] are a family of gas-discharge lasers where the lasing action results from the emission from an excited state of a bound molecular complex. These complexes are more strongly bound in the excited state than in the ground state and are generally known as exciplexes. More specifically, excimers are exciplexes where all partners in the complex are the same and those where they are different are termed heteroexcimers. In this class of laser, the emitting species are heteroexcimer and thus should be called exciplex lasers. However, the term excimer laser has endured and will be adopted here.

An overview of the laser mechanism in given in Figure 2-3 above. The initial step in an excimer laser is preionisation. This can be achieved in a number of ways but in the EMG 201 MSC, an electric discharge is applied transversely across the laser cavity containing a mixture of xenon, hydrogen chloride, helium and neon (the latter

two being buffer gases). Thus, a plasma is formed whereby free electrons can collide with ground state xenon atoms either exciting or ionising them. Following this, excimers can be generated in two manners as shown in schemes (2.1) and (2.2) below. Once excited, the chemical behaviour of xenon atoms is essentially like that of alkali metals ensuring that the rate of formation of XeCl* (B state) is very fast. Process (2.2) will also occur at high rate in the presence of M, an atom from one of the buffer gases.

$$\begin{aligned} &Xe + e^- \rightarrow Xe^* + e^- \\ &Xe^* + HCl \rightarrow XeCl^* + H \end{aligned} \qquad (2.1)$$

$$\begin{aligned} &Xe + e^- \rightarrow Xe^+ + 2e^- \\ &Xe^+ + Cl^- + M \rightarrow XeCl^* + M \end{aligned} \qquad (2.2)$$

Figure 2-3 depicts a very shallow bound ground state for XeCl. The dissociation energy of this complex is sufficiently weak for it to spontaneously fragment at room temperature, that is at energy kT. This ensures prompt removal of XeCl subsequent to B $\rightarrow$ X emission. In contrast, XeCl* has a lifetime long enough to ensure a population inversion and hence, lasing action. Once excimers are generated in sufficient numbers, a population inversion can occur, giving rise to the lasing action.

2.3.2 Dye Laser Operation

The lasing action in a dye laser[8-10] is based upon the ability of certain organic dye molecules to fluoresce with high efficiency. Quantum yields of near unity are most desirable. One advantage of using a XeCl excimer laser to pump dye lasers is that its lasing wavelength of 308nm can be used to excite a large variety of lasing dyes[7]. This gives a better coverage of the UV and visible regions than if, say, a Neodymium-YAG (Yttrium Aluminium Garnet) laser were used as the pump laser.

Figure 2-4 gives an overview of a typical lasing cycle of a dye laser. In this case, we are dealing essentially with a four-level lasing system. The first step involves excitation from the ground state, S_0, to a singlet excited state. This could either be an $S_1 \leftarrow S_0$, as shown in Figure 2-4, or an $S_2 \leftarrow S_0$ transition. For efficient lasing action, the dye molecule must have a high extinction coefficient. Because of differences in molecular geometry between the electronic ground and excited states, it is higher vibrational levels of the excited state that are populated in the excitation step.

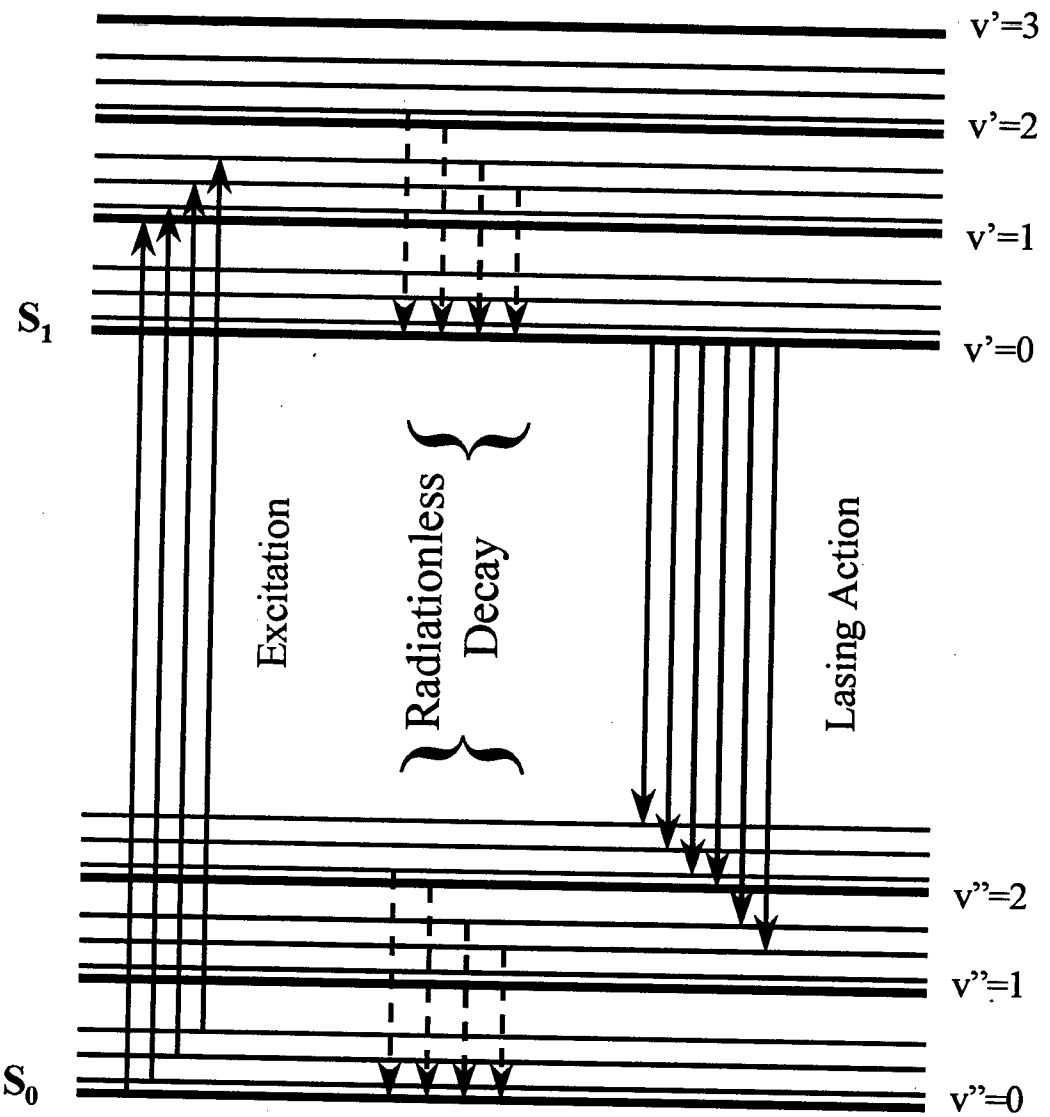

Figure 2-4: Schematic diagram of part of a typical singlet manifold in a laser dye indicating how lasing action arises.

Following excitation, non-radiative decay populates the lowest vibronic level in the S_1 manifold. The molecule then fluoresces to populate high vibrational levels of the ground state, again due to Franck-Condon factors. Because the fluorescence lifetime is typically of the order of 1 ns and non-radiative relaxation takes only 10 ps, a population inversion can occur[11]. The possibility of a population inversion is further enhanced if the ground state vibrational levels populated by fluorescence are sufficiently energetic so as to inhibit their population at room temperature according to the Boltzmann distribution. Yet another condition for efficient lasing action is that the laser radiation should not be absorbed by the dye solution.

In the Lambda Physik FL3002E and FL2002, 20% of the excimer laser beam is directed into a dye cell within the laser cavity, called the oscillator/preamplifier cuvette. The output beam from the oscillator/preamplifier cuvette is directed into another cuvette, called the amplifier cuvette, which resides outside the laser cavity. In addition, 80% of the pump beam is directed into the same dye cell perpendicular to the oscillator beam. In this cuvette, additional amplification over and above that taking place inside the laser cavity occurs. Dye solutions are circulated to reduce degradation of the dye and so extend their operating lifetimes.

Because of the complexity of the dye molecules used, there is a very high density of vibronic levels. Also, because the dyes are used in solution, collisional broadening of the fluorescent transitions involved in the laser cycle can occur. This results in continuous laser action over a given wavelength range, affording tunability. The lasing ranges for the dyes used in the work described in this thesis are given in Table 2-2. The laser can be tuned using a diffraction grating which forms one end of the laser cavity. The grating also reduces the bandwidth in the frequency domain to a level which is extremely useful for spectroscopy. In the dye lasers used here, the FL3002E and FL2002, the bandwidth of the laser radiation produced was $0.2cm^{-1}$. The wavelength of the laser radiation was tuned by altering the angle of the grating using a precision milled screw. Diffraction gratings also change order depending on

the wavelength region which extends tunability to the whole UV and visible regions. The wavelength of the laser radiation can be controlled either manually or using stepper motors under computer control. In the case of the FL3002E, the laser was tuned solely by means of a microcomputer mounted on the side of the laser. In contrast, the FL2002 was tuned using an external microcomputer.

Dye	Wavelength Range nm
PTP	332-350
DMQ	346-377
QUI	368-402
PBBO	386-420
Stilbene 3	405-428
Coumarin 120	423-462
Coumarin 2	432-475
Coumarin 47	440-484
Coumarin 102	460-510
Coumarin 307	479-553
Coumarin 153	522-600
Rhodamin 6G	569-608
Rhodamin B	588-644
Rhodamin 101	614-672
DCM	632-690

Table 2-2: Wavelength ranges for fundamentals of the laser dyes used in the work described in this thesis.

2.3.3 Second Harmonic Generation

Because of the energy losses which occur, the wavelength of fluorescence is always red-shifted, or Stokes-shifted, from the excitation wavelength. As a result of the excitation wavelength being 308 nm, wavelengths shorter than 332 nm could not be covered with the dye fundamentals alone. However, shorter wavelengths can be

achieved as a result of the non-linear optical properties of non-isotropic crystals[11,12]. The dielectric polarisation of such a crystal or any other non-linear medium can be written in terms of its nonlinear susceptibility χ and the electric field component E of the incident light:

$$P = \varepsilon_0(\chi^{(1)}E + \chi^{(2)}E^2 + \chi^{(3)}E^3 + ...) \qquad \textbf{2-1}$$

where $\chi^{(k)}$ is the k^{th} order susceptibility tensor of rank k. The $\chi^{(2)}E^2$ term in Equation 2.1 is referred as the hyperpolarisability term. In noncentrosymmetric crystals, the second order or hyperpolarisability term is significant. Since E depends upon $\cos(\omega.t)$ in the case of light, E^2 depends upon $\cos^2(\omega.t)$ and hence $\cos(2\omega.t)$ implying frequency doubling or second harmonic generation (SHG). SHG is maximised when dispersion is minimised. This is determined by the refractive index of the material which itself is wavelength dependent. Therefore, the optimum angle of incidence of the fundamental beam also changes with change in wavelength. As a result, the crystal position has to be tuned as the laser wavelength is being tuned and this was achieved using a computer controlled autotracker. The materials used for SHG in obtaining the results for this thesis were β-Barium Borate (BBO) and Potassium Dihydrogen Phosphate (KDP). The wavelength ranges for these materials are given in Table 2-3.

Crystal	**Wavelength Range nm**	
	Second Harmonic	**Fundamental**
BBO Type II (FL37-2)	205-222	410-442
BBO Type I (FL37-1)	220-315	440-630
KDP (FL30)	265-335	530-670

Table 2-3: Frequency doubling crystals used in the work described in this thesis, and their wavelength ranges[7].

Because of the relative inefficiency of frequency doubling crystals, some of the dye laser fundamental always passes through. For example, the laser power of the second harmonic produced in the laser system used to carry out the work discussed in this thesis was about 10 % that of the fundamental. Thus, the second harmonic has to be separated from the fundamental using dispersion by a series of four Pellin Broca prisms positioned at each corner of a rectangular mounting unit. To prevent beam walk while the laser was being tuned, a compensator prism (Lambda Physik FL301) was placed between the Pellin Broca unit (Lambda Physik FL35) and the frequency doubling crystal. This ensures that the second harmonic always exits the Pellin Broca unit in the same direction during a laser scan.

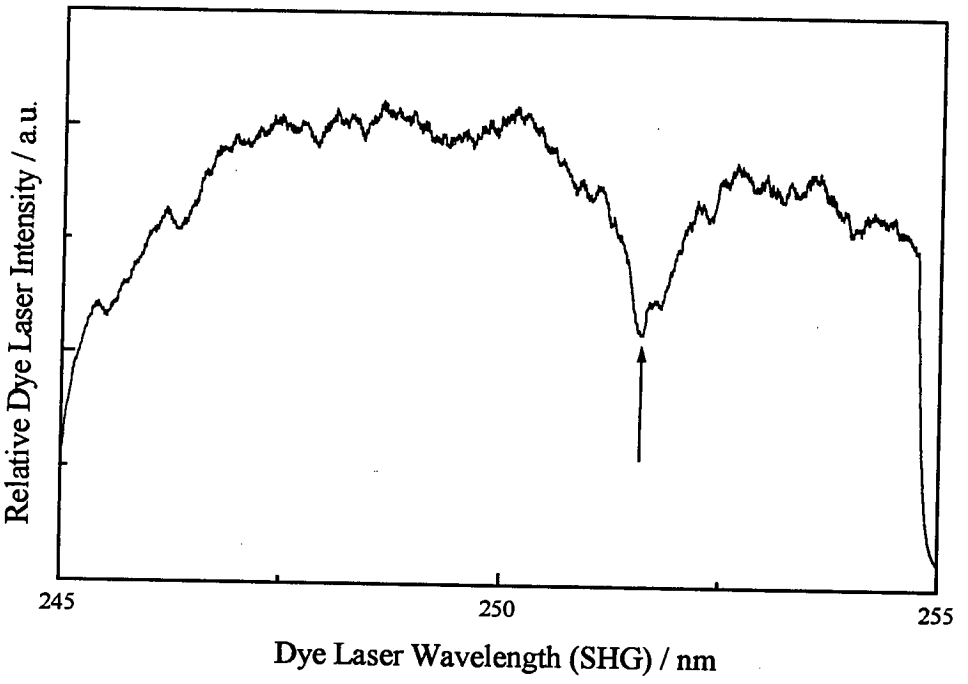

Figure 2-5: Power spectrum of the second harmonic of Coumarin 307 showing the dip in dye laser power (highlighted by the arrow) resulting from interference resulting from a back reflection from the frequency doubling crystal.

One difficulty which can be experienced when frequency doubling at shorter wavelengths is that back reflections from either the doubling or compensator prisms can enter the oscillator cuvette and destructively interfere with the lasing action. This

was circumvented most of the time by altering the position of either crystal. An example of the result of this interference is shown in Figure 2-3. Apart from this, tuning in the 210-335 nm range, where frequency doubling is necessary, is relatively continuous.

2.4 The Molecular Beam

A molecular beam[11] is generated by pulsing a sample gas seeded in carrier gas through a nozzle from a high pressure chamber to one of very low gas pressure. As the gas pressure is increased in the higher pressure chamber, the average distance travelled by atoms or molecules between collisions, that is, the mean free path λ, is reduced. When the mean free path is much less than the nozzle diameter, the beam is supersonic. The increase in the number of collisions increases conversion of the internal energy of an atom or molecule to kinetic energy. From the Born-Oppenheimer approximation, the internal energy of molecules can be partitioned as follows:

$$E = E_{tr.} + E_{rot.} + E_{vib.} + E_{el.},$$

2-2

that is, it can be split up into translational, $E_{tr.}$, rotational, $E_{rot.}$, vibrational, $E_{vib.}$ And electronic, $E_{el.}$, components. The conditions in a supersonic molecular beam are more effective at changing translational energy than rotational energy than vibrational energy. As the molecules in the beam are almost always in their ground electronic state, electronic energy disposal need not be considered. This removal of internal energy reduces the number of molecules occupying the higher rotational and vibrational levels. Because of rotational and vibrational cooling, the number of transitions seen in a spectrum is decreased. This results in the dramatic simplification of molecular spectra which makes their analysis more tractable.

The beam is termed supersonic because the atoms and molecules in it can have high Mach numbers of the order of 100. The Mach number M is defined as:

$$M = \frac{u}{a}$$

2-3

where u is the mass flow velocity and a is the local speed of sound, given by:

$$a = \sqrt{\frac{\gamma k T_{tr}}{m}}$$

2-4

where m is the mass of the gas particles, k is the Boltzmann constant, T_{tr} is the translational temperature and γ is the ratio of the specific heat capacities of the carrier gas at constant pressure and constant volume (C_p/C_v). The high Mach numbers result not from the mass flow velocity but from the low value of T_{tr}, and hence a.

In this work, a General Valve Series 9 pulse valve, with an orifice of diameter 250 μm driven by a solenoid with a Teflon tip, was used as the nozzle. The nozzle opening time and repetition rate was controlled by a General Valve Iota One pulse driver, referred to as the nozzle driver for the remainder of this discussion. A gas mixture of total pressure 0.5-1 atm, typically composed of 20% sample and 80% carrier gas, which was always helium, was passed through the nozzle into a high vacuum cell to produce the molecular beam. The jet cell was pumped down to about 2×10^{-6} torr using a 6 inch diffusion pump, with liquid nitrogen trap, backed by a Maruyama Type 150 rotary pump. The pressure was monitored using Pirani and Penning gauges (Edwards). A rotational temperature of the order of 10 K in the beam was obtainable.

2.5 The Time-of-Flight Mass Spectrometer

Initially, REMPI experiments were carried out at room temperature using an ionisation cell filled with a given pressure of the gas of interest and using two electrodes to collect total ion signal. This is disadvantageous when transitions are observed via fragment ion channels that do not belong to the parent molecule or the

molecule of interest. One example of this is methyl iodide, where atomic iodine transitions are seen superimposed upon the molecular spectrum[13]. In time-of-flight mass spectrometry, the ion current is not measured instantaneously but as a function of the time elapsed since the laser pulse. The resulting production of a mass-spectrum allows the selection of a particular ion signal whereby the variation in its intensity can be monitored with respect to wavelength, largely without any interference from other ion signals. In fact, a number of ion signals can be monitored simultaneously and the additional information can be used to decide the carrier of any transitions observed, that is, whether it is the parent molecule or a fragment species.

2.5.1 Production of Ions in the Jet Cell

In the experiments described in this thesis, one or two laser beams were focused on the molecular beam using lenses of focal length 5 cm. The spatial overlap of the laser and molecular beams was optimised using an XYZ translator to control the lens positions. A Farnell PG102 pulse generator was used to optimise the temporal overlap of the laser and molecular beams. This was triggered by the nozzle driver and then sent a 15 V trigger pulse to the excimer control unit. Upon multiphoton ionisation of the species in the molecular beam, ground state molecular ions are produced with any excess electronic energy being imparted to the electron in the form of kinetic energy. The nascent ions are then accelerated down an electric field gradient generated between a conical repeller electrode at a potential of about +2100V and a conical ground electrode (0V), orthogonal to the propagation directions of the laser and molecular beams. The ions are then collimated or focused into the field free drift region of a time-of-flight tube using an Einzel lens, 6 mm in diameter with a 2 mm orifice, set to a potential of about 800V. The arrangement of the electrodes in the jet or ionisation cell is shown in Figure 2-6. The applied voltages were produced using two Brandenberg Model 472R high voltage power supplies, one for the repeller electrode and one for the Einzel lens.

2.5.2 Time-of-Flight Mass Spectrometry

The main principal behind time-of-flight mass spectrometry[14] is that different ions travel in the field-free drift region at different velocities. Because all the ions experience the same acceleration in the repeller field, they reach the same kinetic energy $\frac{1}{2}mv^2$ and ions with greater mass have a smaller velocity and hence have longer flight times. The time-of-flight of a given ion can be represented as follows:

$$t = l\sqrt{\frac{m}{2Ue}} \qquad \textbf{2-5}$$

where t is the flight time, l is the length of the flight tube, m is the mass, U is the accelerating potential and e is the charge of an electron. In this work, the length of the flight tube was 50cm. Because l, e and U can taken as constant for a given system, Equation 2-5 can be simplified to give:

$$t = A\sqrt{m} \qquad \textbf{2-6}$$

Because there is a delay between the sending of a trigger pulse to the oscilloscope from the excimer laser and the laser firing, Equation 2-6 becomes:

$$t_m - t_d = A\sqrt{m} \qquad \textbf{2-7}$$

where t_m is measured flight time and t_d is the delay. Thus, ions will have different flight times which allows their respective ion currents to be monitored independently in the majority of cases. The exception to this is when an extremely strong ion signal

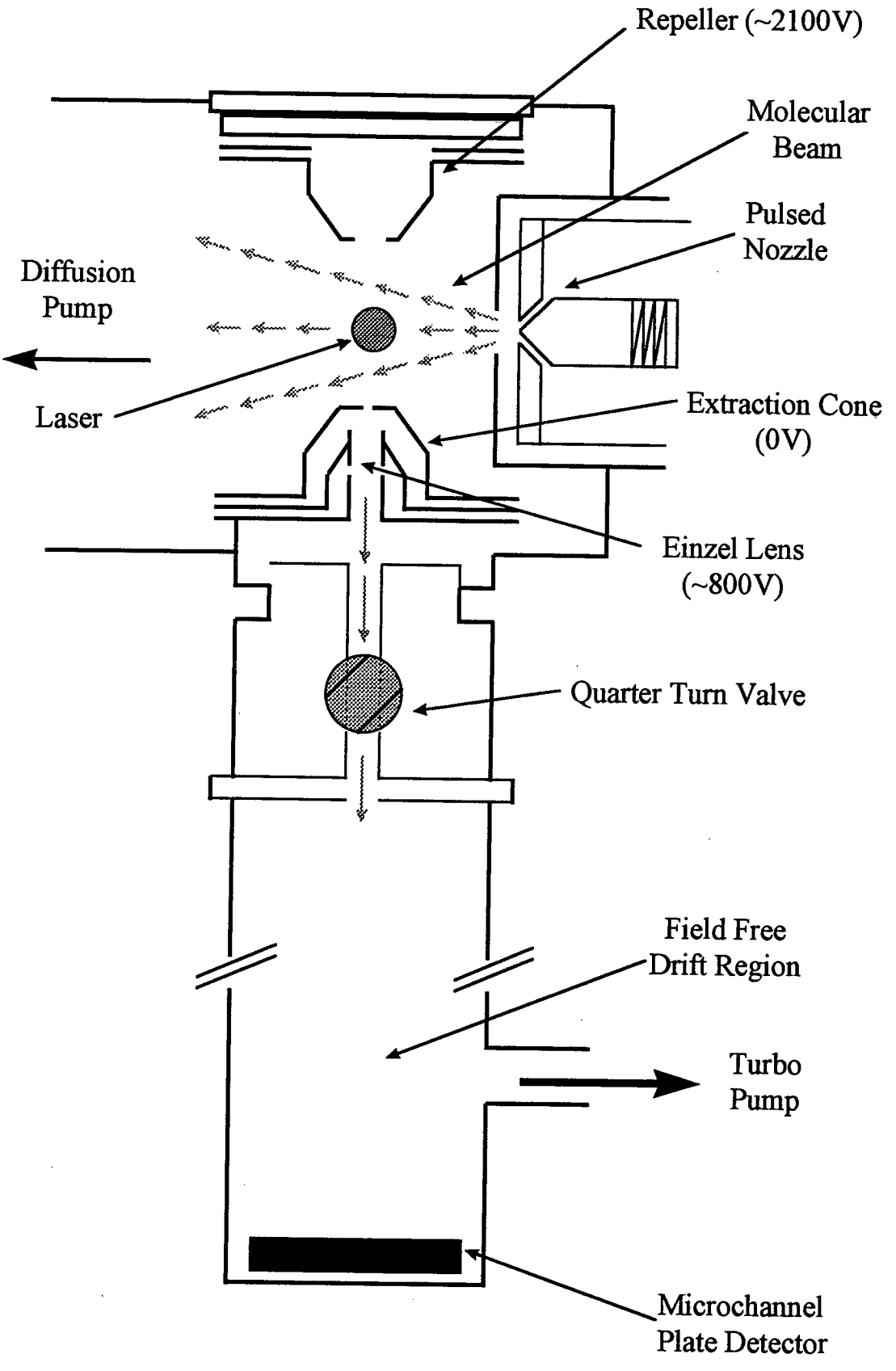

Figure 2-6: A schematic diagram detailing the linear time-of-flight mass spectrometer used.

saturates the microchannel plate detector and interferes with other ion signals which have somewhat similar flight times. An example of this can occur in methyl iodide where a strong atomic iodine signal overlaps with that of the molecular ion resulting in dips in the molecular ion spectrum. This occurs as a result of the Einzel lens focusing ions upon the detector. A schematic diagram of the time-of-flight mass spectrometer is shown in Figure 2-6.

2.6 Signal Collection and Processing

The ions signal was collected and amplified using a microchannel channel plate detector and then passed to a Stanford Research Systems (SRS) SR250 gated integrator and boxcar averager. The output of the boxcar was monitored using an oscilloscope (LeCroy 9400A initially and then a LeCroy 9344A) and chart recorder (Kipp and Zonen BD8) and stored on an IBM PC XT desktop computer.

2.6.1 Detection of Ion Signal

The ions were detected by a microchannel plate detector positioned at the bottom of the flight tube. A microchannel plate detector is essentially a type of electron multiplier[15] and amplifies the ion signal as well as detecting it. It is made up of two plates, the first being at ground potential, with an anode at a large negative potential. For the earlier part of this research, a potential of up to -4.1 kV was applied across the anode using a Brandenberg Type S.0530/10 high voltage power supply. For the latter part, a potential of up to -5 kV was applied using a Wallis high voltage power supply. When the ions collide with the first plate, a cascade of electrons is produced which liberates more electrons. Amplification occurs because each collision displaces more than one electron. With such high voltages being applied, it is important to keep background pressure low. Initially, a four inch diffusion pump was used to reduce this pressure to less than 2×10^{-6} torr but later, a turbo pump (Turbotronik NT150/360) was used for this purpose. A rotary pump, Maruyama Type 150, was used to back both.

2.6.2 The SRS SR250 Gated Integrator and Boxcar Averager

At their simplest, boxcar integrators consist of a switch or gate and an averaging device such as a low pass filter[15]. The SRS SR250[16] consists of a gate generator, fast gated integrator and an averaging facility. An adjustable delay is possible by means of the gate generator which can be triggered either internally or externally. Here, it was triggered using a trigger pulse from the excimer laser control unit and every second laser shot was sampled. This delay was used to probe the wavelength dependence of a given peak on the mass spectrum, thus exploiting the main advantage of using time-of-flight mass spectrometry for REMPI spectroscopy. The width of the gate, the length of time over which sampling occurs, can also be adjusted. This was generally kept to 30μs but was expanded to 100μs when flight times were seen to change rapidly over the course of a scan. This was liable to occur as a result of changes in the time lag between the trigger pulse being sent from the excimer laser and the laser actually firing. One disadvantage of larger gate widths is that the signal-to-noise ratio suffers. The fast gated integrator converts a pulsed signal into a continuous one for the duration of the gate. An exponential averager is then used to amplify signal and improve the signal to noise ratio. In the experiments described in this thesis, averaging was carried out usually over ten samples and also over thirty samples where better signal to noise ratios were required, such as the recording of rotational band contours or spectra containing very weak features. It was the averaged output that was monitored with the chart recorder and oscilloscope, and stored on the computer.

2.6.3 Computer Handling and Storage of Data

The averaged output from the SRS SR250 boxcar system was passed via an SRS SR245 computer interface to a computer. Once on the computer, the output data were stored and manipulated using the SRS SR265 software package. For a laser scan, the software was set up for up to three channels with 5000-5500 binaries storable for each channel. Upon terminating the scan, the start and finish wavelengths were input before storing any spectra produced.

2.7 Additional Details

2.7.1 Power Normalisation

The variation of dye laser power over the lasing range of a given dye can affect the observed relative intensities of any features seen. Thus, it is important to normalise the spectral intensities in order to correct for this variation. The dye laser power over the course of a scan was monitored by splitting off 10% of the dye laser beam and directing it onto a photodiode. The output from the photodiode was monitored using an oscilloscope (Tektronix 2445A) as well as being sent to a boxcar. The boxcar output was monitored using a chart recorder and stored on a computer in the usual manner. Because the transition probability for an n-photon transition, W_n, is related to the laser intensity, I, as follows:

$$W_n \propto I^n, \qquad \text{2-8}$$

two- and three-photon spectra are normalised to the square and the cube, respectively, of the laser power. It should be noted, however, that this will only apply where no real intermediate resonances are involved. Because a photodiode measurement of laser power is relative, a joulemeter (Gentec ED-200) was used whenever absolute measurements were required, for example, when optimising the dye laser power.

2.7.2 The Soleil-Babinet Compensator

As the greater part of the work discussed in this thesis relates to polarisation studies of multiphoton transitions, a discussion of how linearly and circularly polarised light is generated is in order. A Soleil-Babinet compensator[12,17] (Newport RSA-1) was used to polarise light for the purpose of the work carried out and discussed in this thesis. This device is one of a broader class of such devices, called retarders. The compensator is based upon having two quartz crystalline plates, each cut so that their

optic axes are parallel to their surfaces, stacked upon each other. Any retardation in one crystal is cancelled out by the other when they are of equal thickness and their optic axes are perpendicular. However, in the compensator, one of the quartz plates is replaced by two quartz wedges which are stacked so as to act essentially as a quartz plate of variable width. By changing the effective width, retardation can be introduced and controlled by means of a micrometer screw. Hence, the desired polarisation state of light can by produced.

Light is made up of an electric field with two helicity states, $\sigma = +1$ and $\sigma = -1$. These states correspond to clockwise (right circular polarisation) and anticlockwise (left circular polarisation) motions of the electric field component about the direction of travel, respectively. Plane or linearly polarised light results from a superposition of these two states. But the circular birefringence of quartz allows one helicity state or polarisation to be selected over another. Hence, at the correct setting, one handedness of circularly polarised light can be selected and produced using a Soleil-Babinet compensator. However, because the compensator was placed before the final prism, directing the laser beam into the chamber, one of the spin states became scrambled by the prism. This means that care is required when setting up the compensator so as to use the unscrambled handedness of polarisation.

Not only is quartz circularly birefringent but it is also linearly birefringent. It is this property which allows the production of vertical and horizontal linearly polarised light. The light produced by the dye lasers in this work is vertically polarised for the dye fundamental and horizontally polarised in the case of the second harmonic. The Soleil-Babinet was set up to rotate the plane of polarisation by 90° in producing linearly polarised light. This was to ensure that the linear polarisation produced was essentially pure.

2.7.3 Calibration

Because of the turning action of the precision milled screw used to vary the position of the diffraction grating and so select the output wavelength of the dye laser,

a sinusoidally varying discrepancy occurs between the wavelength displayed on the microcomputer and the actual wavelength of the light emitted. For the vast majority of the band positions reported in this thesis, this has been corrected by means of calibrating the observed spectra. Two methods were used to achieve this. The first arises as a consequence of using time-of-flight mass spectrometry in that it is possible to record a spectrum of atomic transitions while simultaneously recording a molecular spectrum in another ion channel. From a comparison with known values, an internal calibration is provided whenever possible. Where atomic lines were absent, optogalvanic transitions in neon[18] were used instead. Here, a portion (10%) of the dye laser beam was directed into a hollow cathode lamp (Pye Unicam with a Cathodean C601 power supply) filled with neon and the directed to a boxcar and a slow scan over the region of interest recorded. Again, a direct comparison with known values in conjunction with a table of vacuum corrections[19] allows calibration of the dye laser and the band positions of any features present.

2.8 References

1. M. N. R. Ashfold, *Mol. Phys.*, **1986** 58 1.
2. M. N. R. Ashfold and S. D. Howe, *Ann. Rev. Phys. Chem.*, **1994** 45 57.
3. P. M. Johnson and C. E. Otis, *Ann. Rev. Phys. Chem.*, **1987** 87 745.
4. M. Göppert-Mayer, *Ann. Physik*, **1931** 9 273.
5. G. G. M^{c}Fadyen, *Ph. D. Thesis*, University of Edinburgh, **1991**.
6. *Lambda Physik EMG 201-204 MSC Instruction Manual*, **1985,** Göttingen.
7. *Lambda Physik FL 3001/2 Instruction Manual*, **1986,** Göttingen.
8. J. Hecht, *The Laser Guidebook* (2nd Ed.), **1992**, TAB Books, Pasadena.
9. O. Svelto, *Principles of Lasers* (3rd Ed.), **1989**, Plenum Press, New York.
10. W. Demtröder, *Laser Spectroscopy* (2nd Ed.), **1996,** Springer Verlag, Berlin.
11. J. M. Hollas, *Modern Spectroscopy* (2nd Ed.), **1992**, John Wiley and Sons, Chichester.
12. R. Guenther, *Modern Optics*, **1990**, John Wiley and Sons., New York.
13. A. Gedanken, M. B. Robin and Y. Yafet, *J. Chem. Phys.*, **1982** 76 4798.

14. E. De Hoffmann, J. Charette and V. Stroobant, *Mass Spectrometry: Principals and Applications*, **1996**, John Wiley & Sons., Chichester.

15. R. P. Wayne, *Chemical Instrumentation*, **1994**, Oxford Science Publications, Oxford.

16. *Operation and Service Manual: Model SR250 Gated Integrator and Boxcar Averager*, Stanford Research Systems, Palo Alto.

17. *Melles Griot Optics Guide 5*, **1990**.

18. S. H. Ashworth and J. M. Brown, *An Atlas of Optogalvanic transitions in Neon*, CLRC Rutherford Appleton Laboratory, **1991**.

19. B. Edlén, *Vacuum Corrections to Three Decimal Places*, Lund, **1951**.

Chapter 3

Multiphoton Spectroscopy of the Rydberg States of Methyl Bromide and Methyl Bromide-d_3

3.1 Introduction

The REMPI spectra of the methyl halides CH_3X (X = Cl, Br, I) are discussed both in this chapter and the one immediately following it. This chapter introduces the electronic structure of the methyl halides using methyl bromide as an example. The assignments of the observed multiphoton transitions of methyl bromide (CH_3Br and CD_3Br) are described. In the next chapter, the observed propensity rules for Rydberg transitions in methyl bromide will be used to aid the reassignment of the spectra of methyl iodide and methyl chloride.

Like the diatomic halogens[1,2], methyl halide multiphoton spectra almost exclusively consist of Rydberg transitions. Thus, a consideration of the propensity rules seen in the VUV (Vacuum UltraViolet) absorption and REMPI spectra of molecular bromine[1,2] may well be useful when assigning the spectra of methyl bromide. This is especially apparent when one considers that essentially the same description can be used for Rydberg states in both molecules. Initially, the two-photon spectra of the diatomic halogens[3] were assigned using the trends seen in atomic halogen spectroscopy. Upon recent re-examination of these spectra using two-photon polarisation studies[1,2], they were subsequently re-assigned. Following this, the assignments of the VUV spectra of these molecules were reviewed[2]. Thus, given the success of the systematic re-assignment of the Rydberg spectra of the

halogens, a systematic assignment, and in some cases, reassignment, of the (2+1) and (3+1) REMPI spectra of the methyl halides was undertaken.

It might seem surprising to use the Rydberg states of methyl bromide for elucidating the propensity rules for Rydberg transitions in methyl halides, given that they have not attracted the same amount of interest as those of methyl iodide or methyl chloride. Before now, the Rydberg states of methyl bromide have only been studied using VUV photoabsorption[5-8] but never REMPI. This is in contrast to the Rydberg states of methyl iodide[9] and methyl chloride[10], which have been the subject of REMPI studies. However, a more complete set of data were more easily obtainable using REMPI in the case of methyl bromide. Moreover, it can be seen from the two-photon spectra of molecular bromine[1] and molecular iodine[11] that there is much stronger interaction between molecular states in the case of the latter than in the former. As little evidence for Rydberg-valence interaction was seen in the (2+1) REMPI spectrum of molecular bromine, trends in the assignment of its one- and two-photon spectra have been used to aid the assignment of the spectra of other halogen molecules such as iodine and iodine monochloride[2]. The methyl halides will be treated similarly for the same reason.

3.1.1 Photoelectron Spectroscopy of Methyl Bromide

Because Rydberg states are expected to reflect the vibronic structure of the ion core state upon which they are based, a discussion of the photoelectron spectrum is useful. Because of this, the photoelectron spectroscopy of the methyl halides, taking methyl bromide as an example, is discussed here prior to a discussion of the VUV spectroscopy of methyl bromide. While only methyl iodide[12,13] has been studied using ZEKE-PFI photoelectron spectroscopy, its VUV ZEKE spectrum[13] is essentially identical to its He(I) spectrum[14] except for the increased resolution of the ZEKE technique. In light of this and since most of this chapter is concerned with the Rydberg states of methyl bromide, the He(I) photoelectron spectrum of CH_3Br (CD_3Br) will be used as an example for the other methyl halides.

The ground state electronic configuration of methyl bromide, in common with the other methyl halides, is $(core)(1a_1)^2(2a_1)^2(1e)^4(3a_1)^2(2e)^4$. In the He(I) photoelectron spectrum[14] of methyl bromide, discrete features are apparent in the 10.5-12 eV region with much broader bands due to continuum excited states of CH_3Br^+ (CD_3Br^+) occurring to higher energy. The discrete structure results from the removal of an electron from the 2e orbital which is essentially of non-bonding character and based mainly upon the bromine atom. The resulting $\tilde{X}\ ^2E$ ionic state is split into $^2E_{3/2}$ and $^2E_{1/2}$ components by competing Jahn-Teller and spin-orbit interactions. Because the electron is being removed from an orbital of non-bonding character little change in molecular geometry occurs upon ionisation to give the $^2E_{3/2}$ and $^2E_{1/2}$ states. Therefore, most of the intensity of the vibronic envelopes of these states is concentrated upon the origin bands with some weaker vibrational structure built upon them. Since the vast majority of the Rydberg states occurring below the first ionisation energies of the methyl halides are based upon these two ionic states, the simple vibronic envelopes implied by the photoelectron spectrum greatly simplifies the analysis of their Rydberg spectra. In fact, with increasing energy, vibrational structure is no longer apparent with only the origin bands of Rydberg states being seen. This is due both to the decreasing transition strength in successive members of a Rydberg series and increasing spectral congestion upon going to higher energy. This disappearance of vibrational structure upon going to higher energy should make the methyl halides ideal examples for the examination of the Rydberg states of a polyatomic molecule.

3.1.2 UV and VUV Spectroscopy of Methyl Bromide

Since this chapter is mainly concerned with Rydberg transitions in methyl bromide, a discussion of previous work relating to methyl iodide and methyl chloride will be deferred to the next chapter. Given that studies of the ultraviolet absorption spectrum (UV and VUV) of methyl bromide[5-8] have mainly dealt with CH_3Br apart from one study of CD_3Br[7] dealing with its 5s cluster, this discussion will concentrate on the former.

The UV spectrum of methyl bromide, in common with the other methyl halides, consists of a single broad feature[15] due to transitions to the $^3Q_1$, $^3Q_0$ and $^1Q_1$ states. The parallel transition to the $^3Q_0$ component dominates. In methyl bromide, this continuum absorption begins at 235 nm and extends to 178 nm.

The remainder of the VUV spectrum of methyl bromide consists of sharp features which extend from 180 nm up to the second ionisation limit. These features have been assigned to *ns*, *np* and *nd* Rydberg states by previous authors[5-8]. The assignments were made largely on energetic grounds. Since the electron excited in a Rydberg transition originates in an orbital that is essentially non-bonding in character and localised upon the bromine atom, it was thought that quasi-atomic selection rules might explain the observed spectrum. Also as a result of this perceived atomic character, comparisons with the spectra of atomic krypton were used to aid the assignment of the observed features[5,6,8]. However, the interpretation of Hochmann et al.[5] implied that *ns* and *np* series dominated the spectrum with *nd* transitions being very weak. Hochmann et al.[5] arrived at their conclusions using both rare gas correlation and comparison of the spectra of methyl iodide, methyl bromide and methyl chloride. Causley and Russell[6] independently assigned their spectrum of methyl bromide to *ns*, *np* and *nd* Rydberg states as well. In addition to these assignments, they also reported vibrational analyses of the 5s and 5p clusters. The vibrational analysis of the 5s system was subsequently extended by Felps et al.[7] and included CD_3Br as well as CH_3Br.

Baig et al.[8] have re-analysed the absorption spectrum at wavelengths shorter than 125 nm with much higher resolution. Their spectrum was obtained using synchrotron radiation where the previous studies had used discharge tube sources. The increase in VUV intensity allowed the spectra to be recorded at a spectral resolution in excess of 0.005 Å. This meant that in their study, any uncertainty in the band measurements did not result from the resolution of the VUV source but from the intrinsic width (FWHM) of the molecular Rydberg bands themselves. They assigned all of the features that they observed to members of two *nd* series but it is not

immediately clear how this assignment follows on from earlier interpretations of the spectrum. However, upon closer inspection, it can be seen that some bands assigned to members of the *nd* series of Baig et al.[8] coincide, within the combined uncertainties of the band measurements, with some of those previously assigned as members of *ns* series by Causley and Russell[6]. This opens up two possibilities: either the bands reported by Baig et al.[8] are the continuation of the previously assigned *ns* series, or, the higher members of the *ns* series of Causley and Russell[6] are in fact due to *nd* states. This disagreement in the interpretation of the VUV spectrum of methyl bromide is resolved by the present work.

3.1.3 Description Used for the Rydberg States of the Methyl Halides

The Rydberg states of the methyl halides are discussed here using a description which has already proved successful for Rydberg states of the diatomic halogens. In the halogens, Ω, which corresponds to the component of total angular momentum about the internuclear axis **r**, has been shown to remain a good quantum number. Ω arises from (Ω_c, ω_{Ryd}) coupling of the Rydberg electron to the ionic core. Here, Ω_c, the projection of total angular momentum along **r**, arises in the ionic core as a result of spin-orbit coupling. Also, spin-orbit coupling in the Rydberg orbital couples λ, the projection of Rydberg orbital angular momentum, l, along **r**, and m_s, the component of Rydberg electron spin about **r**, to produce ω_{Ryd}. The Rydberg states are then described using $\Omega = \Omega_c \pm \omega_{Ryd}$, the component of total angular momentum about **r**.

In addition to Ω, consideration of the microconfigurations of Rydberg states has also aided the understanding of the halogen spectra. Microconfigurations are discussed using a (Ω_c, λ, m_s) description. This is largely equivalent to the (Ω_c, ω_{Ryd}) description given above, the only difference being that ω_{Ryd} would still remain a good quantum number if the uncoupling of l from the molecular axis were to occur in the Rydberg orbital. Microconfigurations are of the form $[....]_c \lambda^{m_s}$ where $[...]_c$ is the electronic configuration of the ionic core. λ indicates one projection of Rydberg

orbital angular momentum along **r** while $\underline{\lambda}$ denotes the opposite projection. m_s is indicated by + (α or spin up) or - (β or spin down). The configurations of individual valence electrons of the ionic core are indicated in a similar fashion to that of the Rydberg electron. From a microconfiguration with $M_S = 0$, one singlet and one triplet state can result. However, these are mixed by spin-orbit coupling in the Rydberg orbital. For the purposes of this discussion, states of mixed singlet and triplet character shall be referred to as singlet states.

The Rydberg states of the methyl halides can be described in a similar manner except that **r** now corresponds to the symmetric top axis of the molecule which lies along about the C-X bond. Indeed, a similar description has been used for the Rydberg states of methyl iodide[9] previously but they were defined using Λ, the projection of total orbital angular momentum along **r**, rather than Ω. Given that one would expect spin-orbit coupling to be important in both the diatomic halogens and the methyl halides, Λ should be uncoupled from the internuclear axis in the latter and hence can no longer remain a good quantum number. Thus, Ω would appear to be the more appropriate quantum number for the description of methyl halide Rydberg states. Thus, the labelling scheme adopted when discussing the Rydberg states studied in this work will be as follows: $[\Omega_c]nl;\Omega$ where n is the principal quantum number of the Rydberg orbital.

For the methyl halides, an alternative description based upon molecular symmetry could also be used but an (Ω_c, ω_{Ryd}) or (Ω_c, λ, m_s) description would appear to be the more applicable. This is because the spin-orbit interaction in the ionic core appears to be sufficiently strong to effectively quench the Jahn-Teller interaction. If the latter were to prevail in the ion, then a description employing molecular symmetry would be more appropriate. Ω does appear to remain a good quantum number based upon polarisation studies, the basis of which is discussed next.

3.1.4 Two-Photon Polarisation Dependence

In previous studies of methyl halide Rydberg states, assignments have been made largely on energetic grounds. However, recent two-photon polarisation studies of the two-photon spectra of the halogens[1,2] has proved that quantum defect criteria cannot be used on their own as a basis for assigning spectra. This marked polarisation dependence seen for the intensities of two-photon transitions can be used equally well to aid assignments in the spectra of the methyl halides.

The two-photon polarisation rules used in the halogen studies[1,2] were derived by Bray and Hochstrasser[16] for diatomic molecules. Since the Rydberg states in methyl halides also can be described using Ω, these rules should also be useful here as well. In order to discuss these, it is necessary to define the two-photon polarisation ratio, ρ_2:

$$\rho_2 = \frac{\sigma_{cc}}{\sigma_{ll}} \qquad 3.1$$

where σ_{cc} is the cross-section of a two-photon transition excited with circularly polarised light and σ_{ll} is cross-section of the same transition excited with linearly polarised light, assuming constant laser power and saturation of the detection step. From the results of Bray and Hochstrasser[16], all rotational transitions of the second rank, that is, all those comprising all rotational branches of all electronic transitions except those comprising the Q-branch of a transition with $\Delta\Omega=0$, were found to have $\rho_2 = 1.5$. In contrast, rotational transitions of the zeroth rank, that is, all rotational lines in the Q-branch of a transition with $\Delta\Omega = 0$, have $\rho_2 < 1$. There are two cases: parallel bands have $\rho_2 = 0.25$ and perpendicular bands have $\rho_2 = 0.07$. Parallel bands are defined here as being observed when each step in the two-photon excitation involves a transition having its transition moment parallel to the symmetric top axis. Similarly, perpendicular bands are seen when the two-photon excitation involves two

simultaneous transitions with transition moments perpendicular to the symmetric top axis. In many two-photon transitions with $\Delta\Omega=0$, the zeroth rank component dominates the rotational contour. Of the second rank component, P and R branches are absent with the O and S branches being very weak. Thus, for the purposes of this investigation, which are largely diagnostic, this means that any band with $\rho_2 < 1$ must arise from a transition with $\Delta\Omega=0$. However, transitions with $\Delta\Omega=1$ and $\Delta\Omega=2$ cannot be distinguished using two-photon polarisation data alone. While rotational band contour analysis can be used to achieve this distinction in molecules such as bromine[1], this proved unsuccessful in methyl bromide because of the broader bandwidths. Nevertheless, three-photon polarisation studies can be used to distinguish $\Delta\Omega=1$ and $\Delta\Omega=2$ transitions and the basis of these is discussed below.

3.1.5 Three-Photon Polarisation Dependence

Three-photon polarisation studies were used to distinguish between $\Delta\Omega=1$ and $\Delta\Omega=2$ transitions in the methyl halides. The trends described here are taken from a REMPI study of OCS[17] where rotational band contour analysis also cannot be applied. The trends summarised by Berger et al.[17] are based upon the results of rotational linestrengths calculations reported by Dixon et al.[18] and Nieman[19] for three-photon resonances in polyatomic molecules. As in the two-photon case, the three-photon polarisation ration, ρ_3 is defined as:

$$\rho_3 = \frac{\sigma_{ccc}}{\sigma_{III}} \qquad 3.2$$

where σ_{ccc} is the cross-section of a three-photon transition excited with circularly polarised light and σ_{III} is the cross-section of the same transition excited with linearly polarised light, assuming constant laser power and saturation of the detection step. For rotational transitions of the third rank, that is, every rotational transition comprising every rotational branch for every electronic transition except for those comprising the P, Q and R branches of $\Delta\Omega=0$ and $\Delta\Omega=1$ transitions, ρ_3 is 2.5.

Rotational transitions of the first rank include those comprising the P, Q and R branches of $\Delta\Omega=0$ and $\Delta\Omega=1$ transitions and these have $\rho_3 < 1$. Because the ratio of first and third rank components of the rotational structure of $\Delta\Omega=0$ and $\Delta\Omega=1$ transitions can vary, some caution is required when interpreting three-photon polarisation experiments. For example, if the first rank component dominates, then $\rho_3 < 1$ but if the third rank component is dominant ρ_3 may well be 2.5. The ideal confirmation for electronic assignments would come from an analysis of the rotational structure but a combined two- and three-photon polarisation study, as discussed here, is almost equally valid. Thus, if two features appear in the three-photon spectrum, one with $\rho_2 = 1.5$ and $\rho_3 < 2.5$ and the other with $\rho_2 = 1.5$ with $\rho_3 = 2.5$, then they can be assigned with some certainty to $\Delta\Omega=1$ and $\Delta\Omega=2$ transitions, respectively. To be even more certain of three-photon polarisation behaviour, comparison with two-photon polarisation studies must be undertaken. Thus, three-photon polarisation studies can introduce a distinction between $\Delta\Omega=1$ and $\Delta\Omega=2$ transitions which would allow them to be distinguished.

3.2 Additional Experimental Details

The (2+2), (2+1) and (3+1) REMPI spectroscopy of methyl bromide and methyl bromide-d_3 was studied using UV and visible light in the 230-460 nm region. The molecular beam was produced by pulsing methyl bromide seeded in helium through a nozzle. The total backing pressures used were typically 500-750 torr with the proportion of methyl bromide used typically being 20% of the total pressure. Where a comparison of the relative intensities of the observed features in a particular spectrum is required, spectra are normalised to the square or cube of the dye laser power as required. But when polarisation behaviour is discussed, comparisons are made between spectra that are not necessarily power normalised. However, this comparison still remains valid because the spectra were recorded sequentially to ensure that little change in dye laser power occurred between both scans concerned. Most tabulated band positions have been calibrated using transitions in atomic bromine[4] but optogalvanic transitions in neon[20] were used where the former method did not prove applicable. Uncertainties in the reported band positions mainly result

from the widths of the bands themselves. Since bandwidths vary over the whole spectral region discussed, a single value cannot be given for the uncertainty in any band measurement as a result of the width of the band. Nevertheless, an uncertainty of ± 10 cm^{-1} is typical. Some additional uncertainty is introduced through the calibration procedure but this is less than ± 3 cm^{-1}.

3.3 (2+2) and (2+1) REMPI Spectroscopy of Methyl Bromide

Figure 3-1 depicts the overall two-photon spectrum of CH_3Br in the 65000-85000 cm^{-1} region while Figure 3-2 depicts the equivalent spectral region for CD_3Br. The strongest ion signals were observed in the CH_3^+ (CD_3^+) ion channels in the two-photon spectra. That the observed resonances arose from the parent species was confirmed by their presence in the $^{79}Br^+$ and $^{81}Br^+$ channels. However, the molecular ion signal was either very weak or absent in the spectral regions of interest here. The absence or low intensity of the molecular ion signal is most likely to be due to fragmentation of the molecular ion upon absorption of a further photon following ionisation. This is a general feature, not only of the two-photon spectra but also of the three-photon spectra, discussed later. Thus, all the depicted REMPI spectra in this chapter have been recorded in the CH_3^+ or CD_3^+ ion channels, depending upon which isotopomer is being studied.

The first noticeable difference in the general appearance of the spectra of CH_3Br and CD_3Br depicted in Figures 3-1 and 3-2 is the height of the lowest energy peak vis-à-vis the other features on the spectrum. This is due, at least in part, to the different bandwidths seen in the spectra of both isotopomers. In a recent Femtosecond Transition State (FTS) spectroscopic[21] study of some Rydberg states of methyl iodide, it was shown that the Rydberg states of the deuteride are less predissociated than those of the hydride. The decay in the molecular ion signal produced in a REMPI scheme via different Rydberg bands was monitored with time. Janssen et al.[21] argued that this predissociation occurred via a tunnelling mechanism. In order to explain the

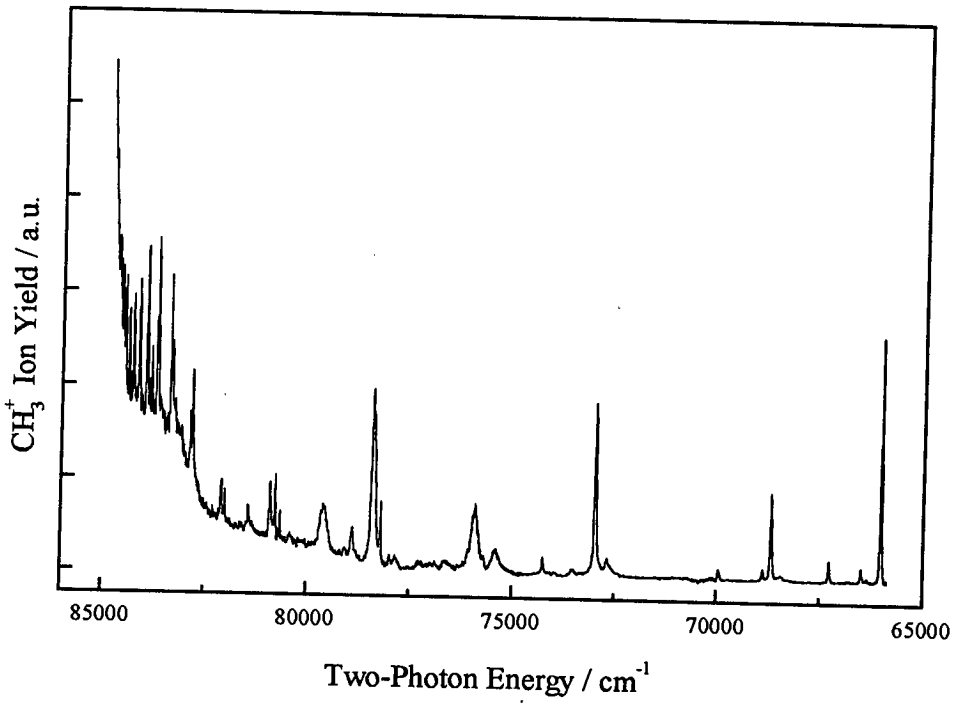

Figure 3-1: Power-normalised (2+1) REMPI spectrum of CH_3Br in the 65000-85000 cm^{-1} region.

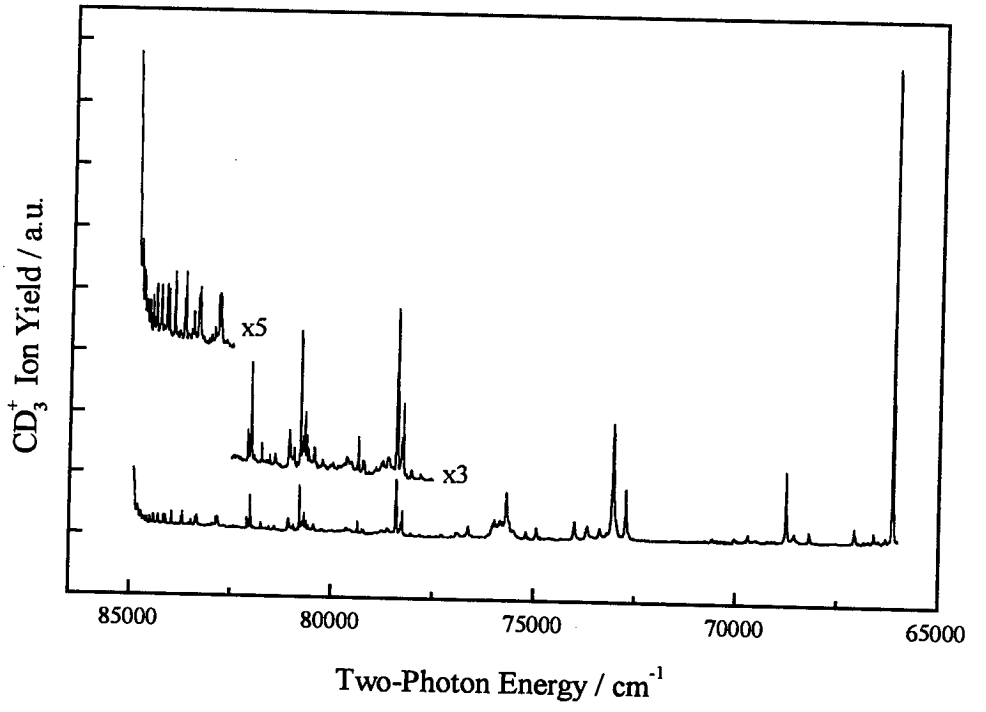

Figure 3-2: Power-normalised (2+1) REMPI spectrum of CD_3Br in the 65000-85000 cm^{-1} region. The intensity scale used here is different to that in Figure 3-1.

isotope dependence, it was suggested using theoretical calculations that the predissociation involved some C-H(D) bond stretching along with extension of the C-I bond which was being broken. It is a general feature of the spectra of CD_3Br that peaks are sharper than those of the hydride. This applies not only to two-photon spectra but also to one- and three-photon spectra. Thus, when comparing transition strengths between the different isotopomers, peak areas are more useful than peak heights. This, along with fluctuations in dye laser power, also applies when comparing intensities of different transitions over the course of a one-, two- or three-photon spectrum of a particular isotopomer. Features arising from transitions to different states display differing bandwidths due to varying degrees of predissociation.

3.3.1 Ionisation Energies

For an initial consideration of the assignment of Rydberg transitions, accurate ionisation energies are needed to calculate quantum defects. However, no ZEKE-PFI spectrum of methyl bromide has been reported. Thus, the previous best estimate for ionisation energies comes from the work of Baig et al.[8] These values, 85017 ± 1 cm^{-1} for the $^2E_{3/2}$ state and 87565 ± 1 cm^{-1} for the $^2E_{1/2}$ state, were extrapolated from the *nd* series assigned in their study of the VUV spectrum of CH_3Br. The best value for the other isotopomer comes from photoelectron spectroscopy which is of insufficient accuracy for the purposes of this study.

In light of the previous work, new values for the $^2E_{3/2}$ and $^2E_{1/2}$ ionisation energies were sought for CD_3Br and CH_3Br. From the data presented in this work, there are two means of obtaining a new value for the ionisation energy corresponding to the $^2E_{3/2}$ ionic state. Firstly, measuring half-way up the rising edge of the two-photon photoionisation curve and correcting for the effect of an external d.c. electric field gives a value of 85029 cm^{-1} for CH_3Br and 85107 cm^{-1} for CD_3Br. The d.c. field correction takes the form $6\sqrt{E}$ where E is the d.c. electric field in volts/cm. Alternatively, a plot of threshold measurements versus $\sqrt{E}$ should produce a straight line approximately of slope 6 with the ionisation energy at zero field as the intercept. The latter method has been used for the deuteride while the value for the

hydride has been obtained using the former. In addition, values can also be obtained in an extrapolation from *nd* series seen up to $n = 19$ in the two-photon spectrum. The values obtained by extrapolation, 85030 ± 10 cm^{-1} and 85100 ± 5 cm^{-1} for the hydride and deuteride respectively, are in reasonable agreement with the values obtained from the photoionisation cross-sections.

However, a large disparity exists between the value given above for the $^2E_{3/2}$ ionisation energy of CH_3Br and the value reported by Baig et al.[8] Moreover, the extrapolation of a reliable ionisation energy from a Rydberg series only works if there is little or no variation of n^* with n. As in the diatomic halogens[1,2], there is some variation of n^* with n in methyl bromide. In this light, the ionisation energy obtained by extrapolation from the longer *nd* Rydberg series reported by Baig et al.[8] would seem the more secure. Also, members of the [3/2]*nd* series of Baig et al.[8] with $n = 20$-23 display quantum defect values which depart from those displayed by the other members of the series. The two-photon *nd* series assigned in this work cannot be continued above the energy region where Baig et al.[8] observed *nd* states that are somewhat perturbed. If these perturbations were to occur in two-photon *nd* series, they would have a disproportionate effect upon the extrapolated ionisation limits. These arguments favour the ionisation energy reported by Baig et al.[8] but they do not explain the disagreement with the values from the photoionisation cross-sections. This can be explained if one considers the difficulty in judging where the rise in a photoionisation curve occurs. This is seen in a plot of ionisation energy versus $\sqrt{E}$ for CD_3Br where the slope of the straight line fit is seen to be nearer 5 than 6, the latter being the expected value. Therefore, on the basis of the above arguments, the value for the ionisation energy given by Baig et al.[8] will be adopted here for CH_3Br.

Although the $^2E_{3/2}$ ionisation energy of 85109 cm^{-1} obtained from the two-photon data is possibly the best estimate to date for CD_3Br, the previous comments regarding the $^2E_{3/2}$ ionisation energy of the hydride cannot be ignored. Also, upon comparison of the values for the $^2E_{3/2}$ ionisation energies obtained from two-photon photoionisation thresholds, an isotopic shift of 78 cm^{-1} is seen in CD_3Br

relative to CH_3Br. Using this shift with the $^2E_{3/2}$ ionisation energy of Baig et al.[8] for CH_3Br, an alternative value of 85095 cm^{-1} is obtained for the $^2E_{3/2}$ ionisation energy of CD_3Br. This value for the $^2E_{3/2}$ ionisation energy of CD_3Br adopted for the remainder of this discussion is 85095 cm^{-1}.

Because the series converging upon the $^2E_{1/2}$ limit assigned in this work are of insufficient length to contradict the value for this ionisation energy reported by Baig et al.[8], their value of 87565 cm^{-1} will be used here for CH_3Br. In light of the isotopic shift noted already, the $^2E_{1/2}$ ionisation limit used for CD_3Br is 87643 cm^{-1}. Thus, in this discussion of the assignments of the two- and three-photon spectra, the previous values for the ionisation energies are adopted for CH_3Br and corrected, using the isotope shift, for use in the case of CD_3Br.

3.3.2 General Features of the Assignment

In the light of polarisation studies, the two-photon spectra of methyl bromide are seen to be dominated by transitions with $\Delta\Omega=0$. Given that the ground state of methyl bromide, in common with those of the other methyl halides and the diatomic halogens, has a closed shell configuration, it can be said that the two-photon spectrum is dominated by transitions to states with $\Omega=0$. In the VUV spectrum of atomic bromine[4], two sets of Rydberg transitions can be picked out based the range of their quantum defect values, tabulated in Table 3-1: those with half-integer quantum defect values such as *np* and *nd* states and those with near-integer quantum defect values, that is, *ns*, *nd* and *nf* states. Similarly, those features in the two-photon spectrum of methyl bromide with quantum defect values of about 2.5 are assigned to members of short *np* series. From polarisation studies, the more intense bands with half-integer quantum defect values are due to *np* states with $\Omega=0$. However, the

Rydberg Series	Quantum Defect
ns	3.00-3.15
np	2.35-2.71
nd	1.15-1.6
nf	<0.05

Table 3-1: Typical quantum defects for Rydberg transitions in atomic bromine[4].

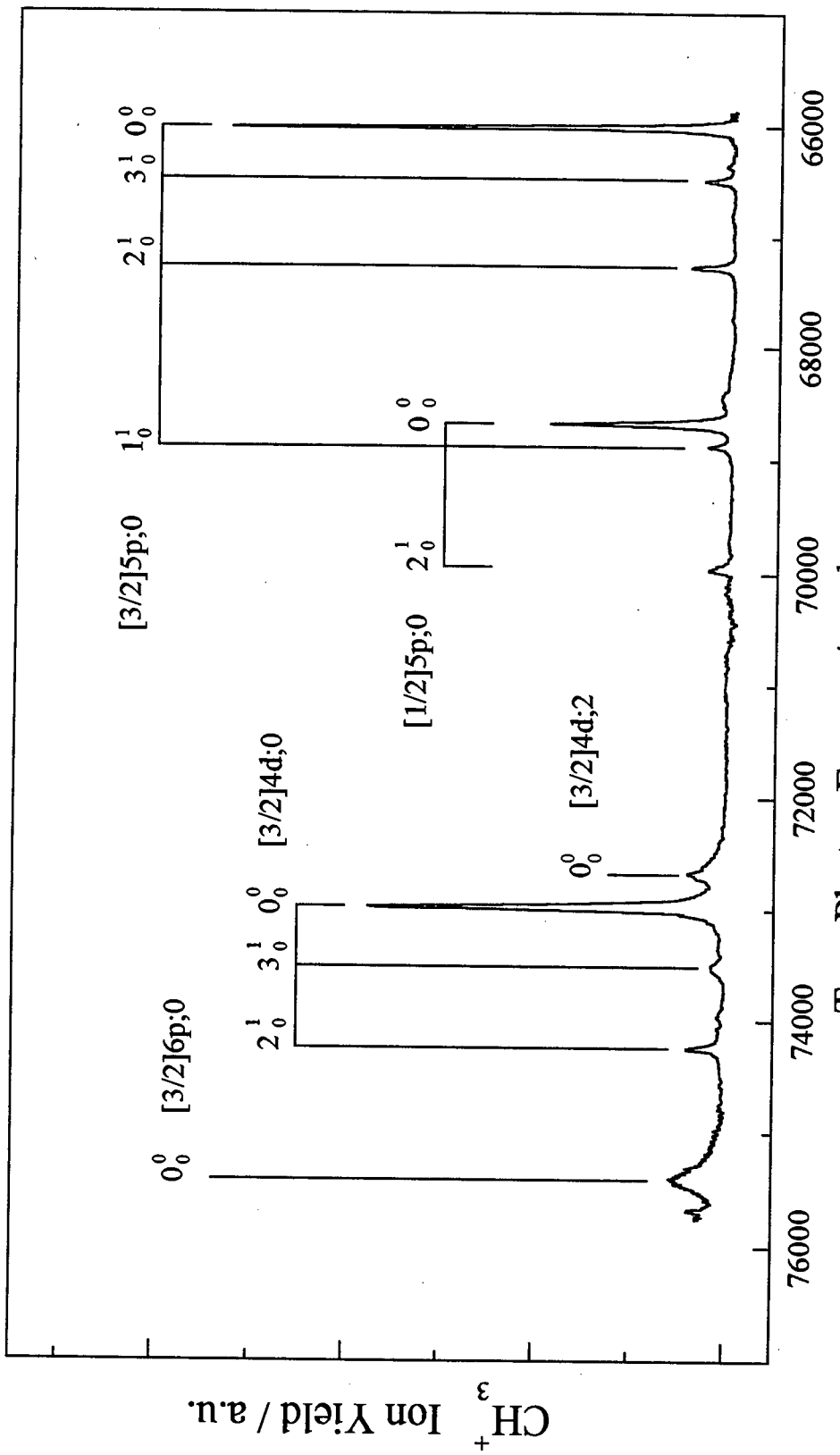

Figure 3-3: Two-photon spectrum of lower Rydberg states of CH_3Br

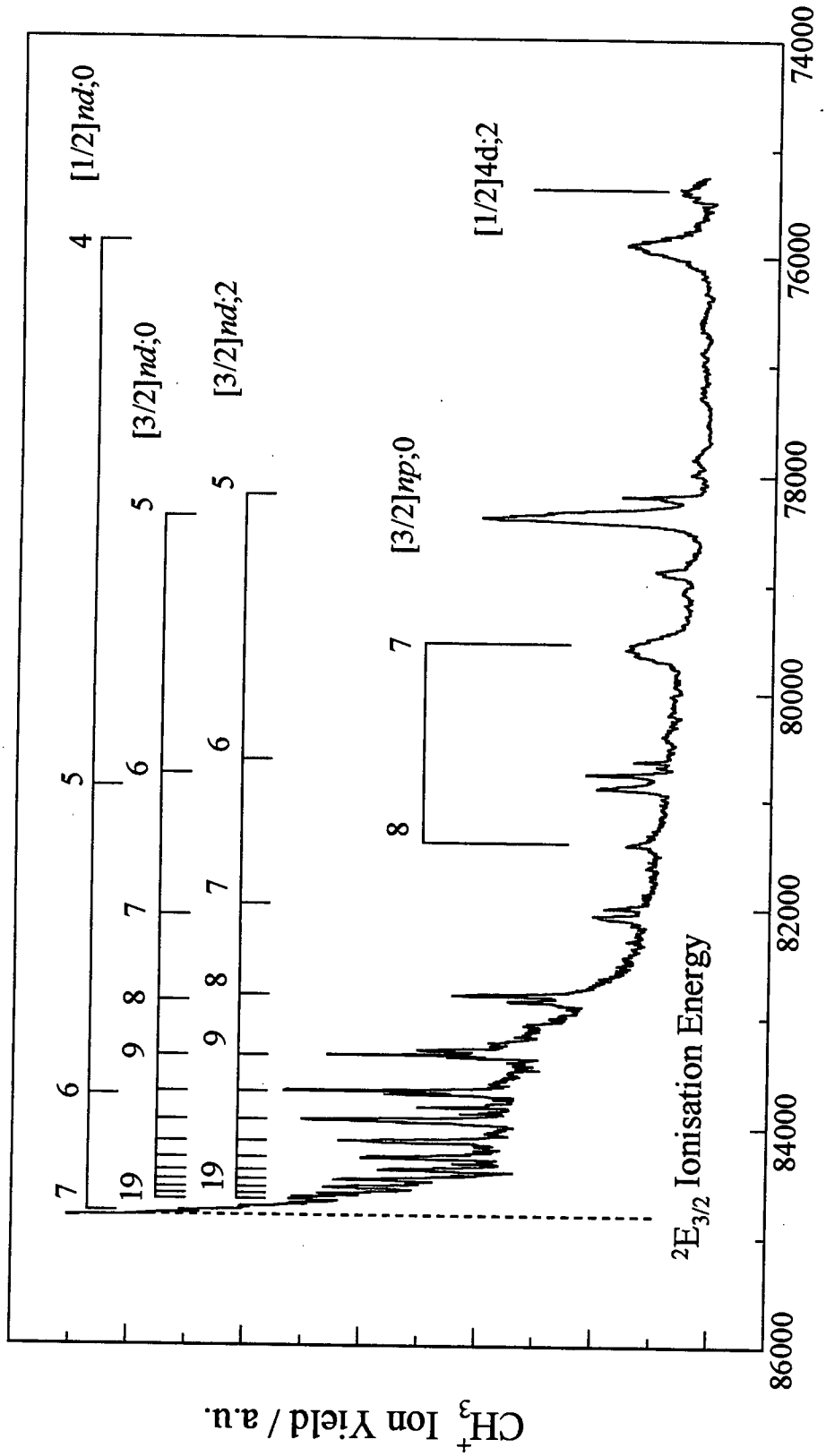

Figure 3-4: Two-photon spectrum of CH_3Br in the 75000-85000cm^{-1} region

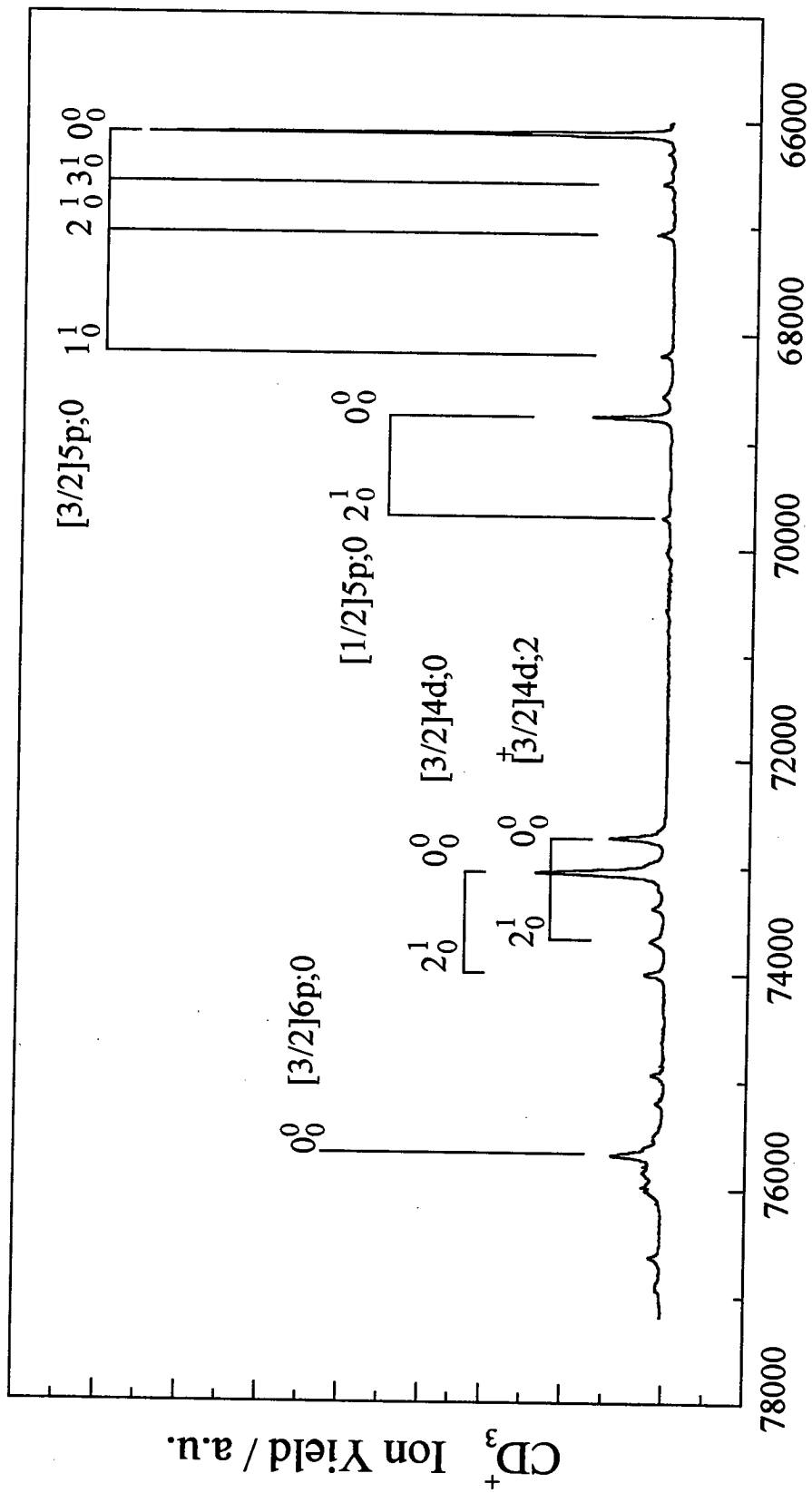

Figure 3-5: Two-photon spectrum of lower Rydberg states of CD_3Br

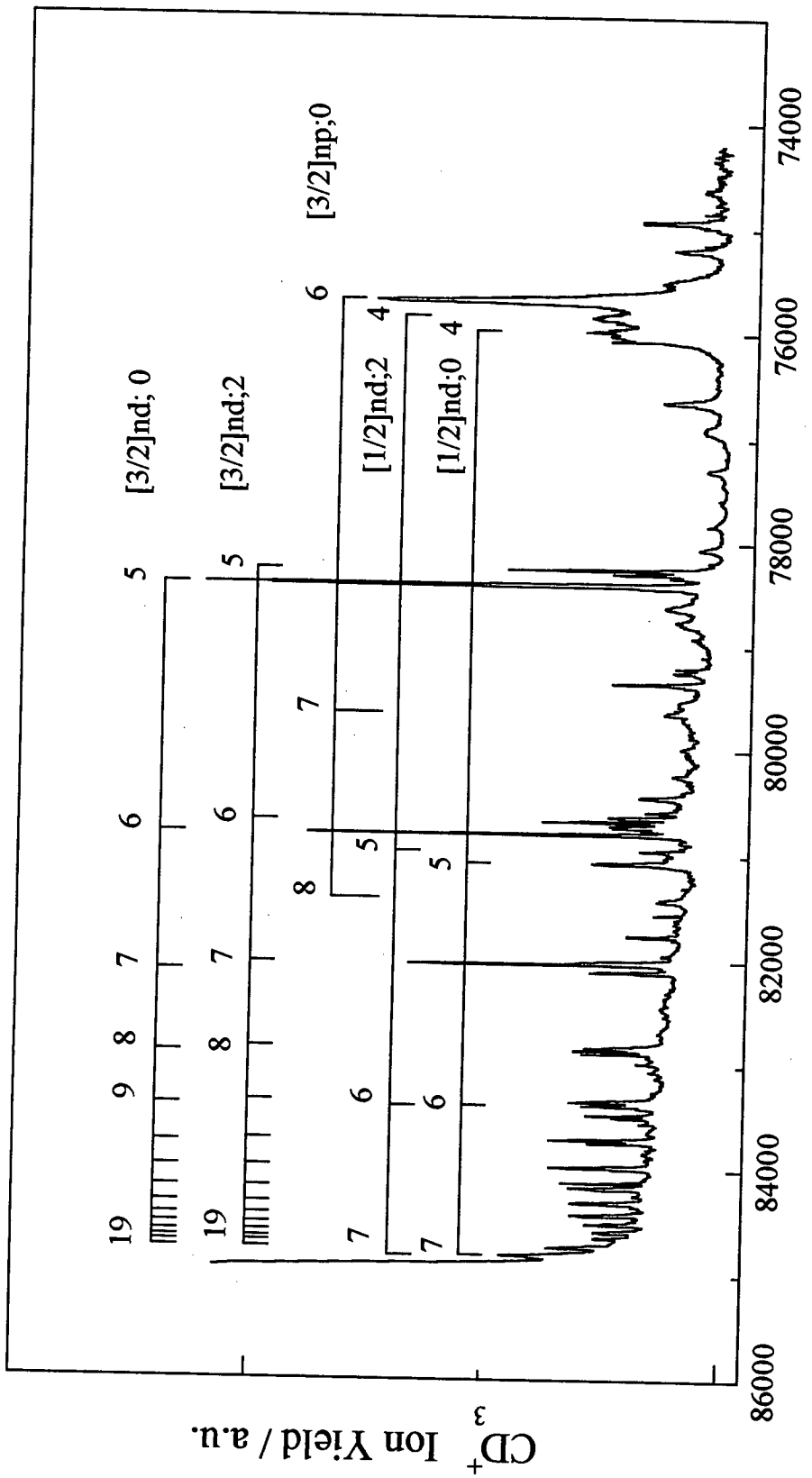

Figure 3-6: Two-photon spectrum of CD_3Br in the 75000-85000cm^{-1} region

Assignment	CH_3Br		CD_3Br		ρ_2
$[\Omega_c]nl;\ \Omega$	Band Position cm^{-1}	$(n-\delta)$	Band Position cm^{-1}	$(n-\delta)$	
[3/2]5s;1	56065	1.95	56284	1.95	+
[1/2]5s;0	58465	1.94	58645	1.95	-
[1/2]5s;1	59109	1.96	59252	1.97	+
[3/2]5p;0	66007	2.40	66112	2.40	-
[1/2]5p;2	68444	2.40	68536	2.40	+
[1/2]5p;0	68674	2.40	68737	2.41	-
[3/2]4d;2	72655	2.98	72737	2.98	+
[3/2]4d;0	72977	3.02	73050	3.02	-
[3/2]6p;0	75418	3.38	75667	3.41	-
[1/2]4d;2	75682	3.04	†		+
[1/2]4d;0	75889	3.07	75997	3.07	-
[3/2]5d;2	78193	4.01	78264	4.01	+
[3/2]5d;0	78401	4.07	78415	4.05	-
[3/2]7p;0	79610	4.51	79665	4.50	-
[3/2]6d;2	80623	5.00	80711	5.00	+
[3/2]6d;0	80741	5.07	80831	5.07	-
[1/2]5d;2	†		80983	4.06	+
[1/2]5d;0	80857	4.04	81100	4.10	-
[3/2]8p;0	81327	5.45	81463	5.50	-
[3/2]7d;2	81980	6.01	82049	6.00	+
[3/2]7d;0	82057	6.09	82123	6.08	-
[3/2]8d;2	82795	7.03	82861	7.01	+
[3/2]8d;0	82846	7.11	82913	7.09	-
[3/2]9d;2	83310	8.02	83383	8.01	+
[3/2]9d;0	83351	8.12	83415	8.08	-
[1/2]6d;2	83298	5.07	†		+
[1/2]6d;0	83356	5.11	83419	5.10	-
[3/2]10d;2	83669	9.02	83741	9.00	+
[3/2]10d;0	83704	9.14	83771	9.10	-
[3/2]11d	83934	10.07	84000	10.01	*
[3/2]12d	84122	11.07	84191	11.02	*
[3/2]13d	84270	12.12	84358	12.20	*
[3/2]14d	84378	13.10	84453	13.07	*
[3/2]15d	84471	14.17	84541	14.07	*
[3/2]16d	84538	15.13	84614	15.10	*
[3/2]17d	84599	16.20	84674	16.14	*
[3/2]18d	‡		84712	16.93	*
[3/2]19d	‡		84764	18.20	*
[1/2]7d	84761	6.26	84838	6.25	*

Table 3-2: Electronic assignment of the two-photon spectrum of methyl bromide, CH_3Br and CD_3Br. The polarisation ratio, ρ_2, is denoted + where it equals 1.5, - where it is less than 1 and * where features arising from $\Omega=2$ and $\Omega=0$ states are blended. The † denotes where a feature has blended with another lying nearby and ‡ denotes a feature present in one isotopomer but absent from another. For the hydride, the $^2E_{3/2}$ and $^2E_{1/2}$ series limits used to calculate the above $(n-\delta)$ values are 85017 cm^{-1} and 87565 cm^{-1}, respectively. The $(n-\delta)$ values tabulated for the deuteride were calculated using 85095 cm^{-1} and 87643 cm^{-1} as the values of the $^2E_{3/2}$ and $^2E_{1/2}$ series limits.

majority of features arising from transitions to Ω=0 states have near-integer quantum defect values. Following the trends apparent in the case of molecular bromine[1], the features with near integer quantum defect values are assigned to *nd*;0 states. Features with a non-zero Ω-value occurring immediately to the red of those assigned to *nd*;0 states are assigned to *nd*;2 states in line with the assignments of the two-photon spectrum of molecular bromine[1]. Further support for the *nd*;2 assignments comes from three-photon polarisation studies which are discussed later. In both molecular bromine[1] and methyl bromide, the quantum defect values for *nd* states are just outside the range in atomic bromine[4], tabulated in Table 3-1. This implies that Rydberg transitions cannot be assigned on the basis of their quantum defects alone but need further information such as that from polarisation studies. The electronic assignments of the two-photon spectrum of methyl bromide are detailed in Table 3-2 and depicted in Figures 3-3, 3-4, 3-5 and 3-6.

3.3.3 The 5s Cluster

Although the 5s cluster has been studied exhaustively in a previous VUV study[3] and this study concentrates on the higher Rydberg states, the polarisation behaviour of the origin bands of the 5s states will be discussed here as an example for the higher energy states. (Ω_c, ω_{Ryd}) coupling in the 5s cluster produces the [3/2]5s;2, [3/2]5s;1, [1/2]5s;0 and [1/2]5s;1 components. Of these, the Ω=1 states possess singlet character while the others are triplet states. Figure 3-7 shows the polarisation behaviour of the origin band of the [1/2]5s;1 state of CD_3Br. The 0_0^0 [1/2]5s;1 band has $\rho_2 \cong 1.5$, consistent with an Ω=1 assignment and the 0_0^0 [3/2]5s;1 band displays similar polarisation behaviour.

While the 5s;1 states follow the Bray and Hochstrasser rules[16], the band previously assigned by Felps et al.[7] to the origin of the [1/2]5s;0 state apparently does not. Thus, an alternative assignment of this band to the 1_0^1 [3/2]5s;1 transition seems more likely in the light of its polarisation behaviour. Also, there is a band at

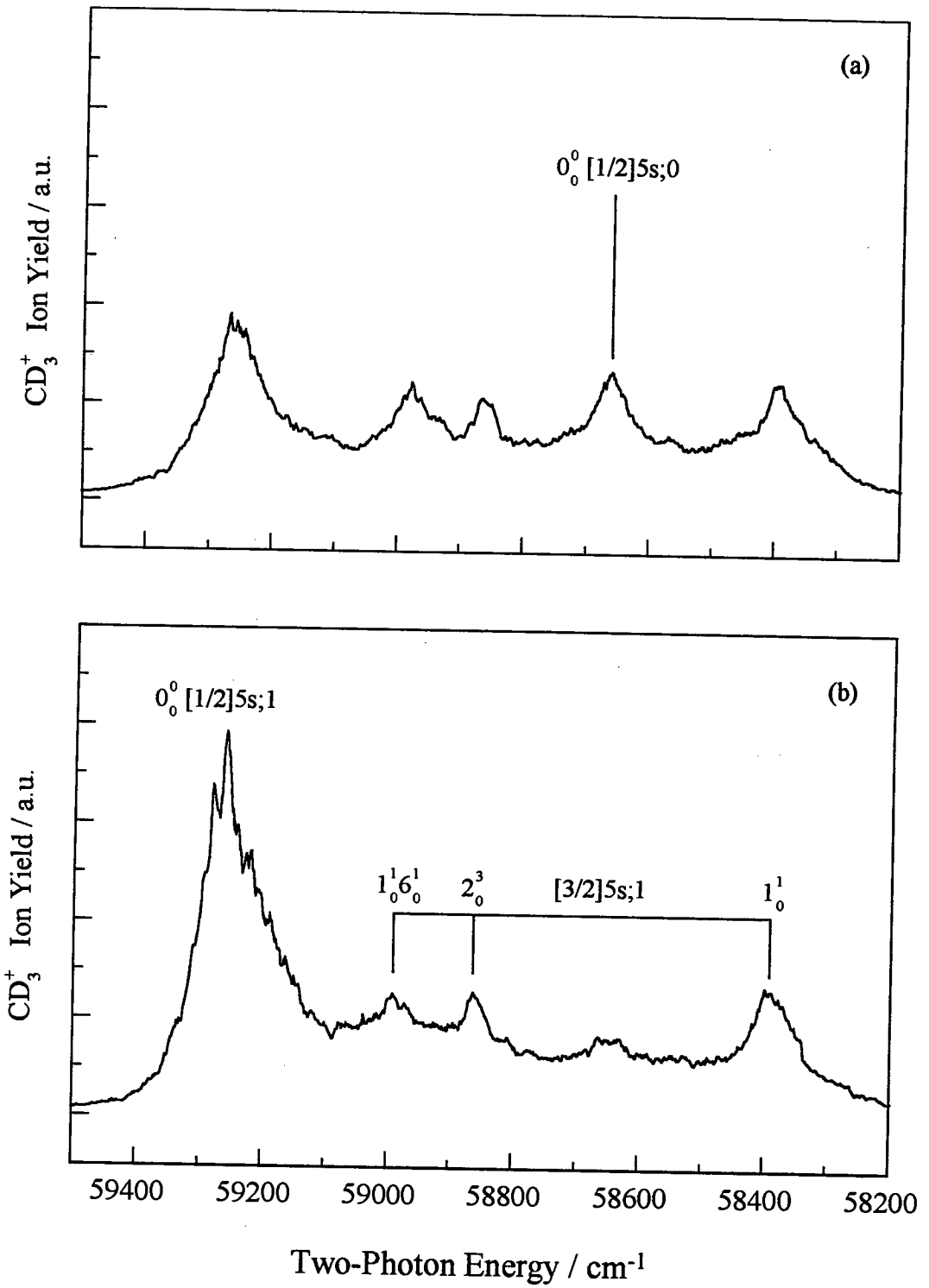

Figure 3-7: Polarisation behaviour of the [1/2]5s origin bands. Panel (a) depicts the spectrum recorded using linearly polarised light while panel (b) depicts the same spectral region but recorded using circularly polarised light. Neither spectrum has been normalised to the square of the laser power but since they were recorded sequentially, little variation in laser power is expected. This comment applies equally to the other figures depicting polarisation behaviour in this chapter.

58645 cm^{-1}, which was formerly attributed to $2_0^2 6_0^1$ [3/2]5s;2 and 5_0^3 [3/2]5s;2 transitions[7], which has $\rho_2 < 1$. Because of its polarisation dependence, this band is now assigned to the origin of the [1/2]5s;0 state. This leaves a band that was previously assigned[7] to the 6_0^1 [1/2]5s;0 transition and this is reassigned here to the $1_0^1 6_0^1$ [3/2]5s;1 transition.

The origin bands of all but the Ω=2 component of the 5s cluster were observed using two-photon excitation. A similar situation occurs in methyl iodide[22] where the Ω=2 component of the 6s state is absent. Given the propensity rules seen in higher energy transitions, the triplet character of the state could explain this except for the presence of the [1/2]5s;0 component (another triplet state). An alternative reason that has been suggested previously for the absence of the Ω=2 state in the lowest Rydberg cluster of methyl iodide[9] is that it is selectively predissociated by a continuum state. Barring enhancement of the Ω=0 component through interaction with another state, selective predissociation would appear to be the most likely explanation for the absence of the [3/2]5s;2 state.

3.3.4 *np* States

Short *np*;0 series are depicted in Figures 3-3 to 3-6 and the polarisation behaviour typical of these features is depicted in Figure 3-8. The curtailment of the *np*;0 series is somewhat surprising considering that some features comprising the 5p band system are among the strongest in the two-photon spectrum. In fact, the origin band of the [3/2]5p;0 state is the most intense in the spectrum of CD_3Br. However, upon further examination, it can be seen that successive members of the [3/2]*np*;0 series not only become weaker but also more diffuse. This suggests that predissociation is at least one of the underlying causes of this curtailment. There are a number of possible channels for predissociation. One channel involves interaction with the valence states giving rise to the continuum absorption band in the UV[15]. and two further channels open up above 75000 cm^{-1}. The first of these involves the

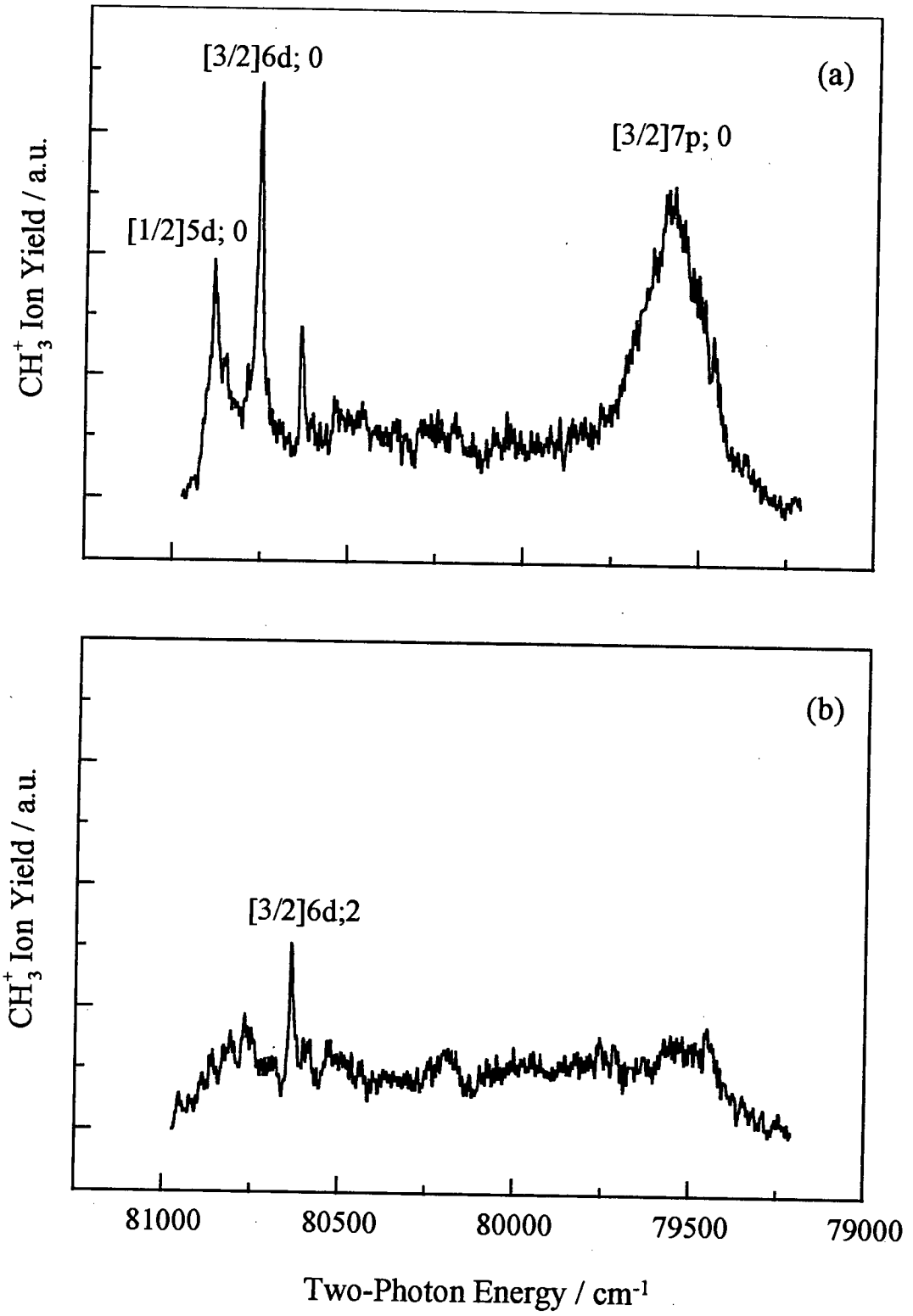

Figure 3-8: Polarisation behaviour of features in the 79000-81500 cm^{-1} region of the two-photon spectrum of CH_3Br. Panel (a) depicts the spectrum recorded with linearly polarised light and panel (b) shows the spectrum recorded using circularly polarised light.

continuum of the lowest-lying ion-pair state while the other involves the lowest Rydberg state based upon the $\tilde{A}\ ^2A_1$ ionic core.

In homonuclear diatomic molecules such as molecular bromine, ion-pair states dissociate to produce Br^+ and Br^-. In polyatomic molecules such as methyl bromide, different ion-pair states dissociate to produce different pairs of ions. For example, in CH_3Br, some ion-pair states dissociate to give CH_3^+ and Br^- and others dissociate to produce Br^+ and CH_3^-. The lowest thermodynamic threshold for ion-pair production in methyl bromide is 76470 cm^{-1} and this corresponds to the CH_3^+ ($\tilde{X}\ ^1A_1'$) and Br^- ($^1S_0$) dissociation limit. The value for the above threshold, was calculated using the dissociation energy of ground state methyl bromide[23], D_0 = 24302 cm^{-1}, the ionisation potential of methyl radical[24], I.E.(CH_3) = 79349 cm^{-1}, and the electron affinity of atomic bromine[25], E.A.(Br) = 27181 cm^{-1}. Conserving symmetry (or Ω) and spin, only one ion-pair state can dissociate to produce CH_3^+ ($\tilde{X}\ ^1A_1'$) and Br^- ($^1S_0$) and, correspondingly, this has Ω=0. Following the nomenclature employed in the diatomic halogens, this is denoted as the D (0) state.

Because the first ion-pair continuum in methyl bromide is associated with a state having Ω=0, bound Ω=0 states lying in its vicinity are predissociated since homogeneous interactions are favoured. However, this means that the observed *nd*;0 series should be curtailed as well. and it is clear from Figures 3-4 and 3-6 that this is not the case. Moreover, there is one further difference between *np* and *nd* states. This is the greater probability of penetration of the ionic core by an electron in an *np* Rydberg orbital compared with an electron in an *nd* orbital. This greater penetration increases the time spent by the Rydberg electron near the ionic core, increasing the probability of predissociation. Thus, the curtailment of the *np*;0 series suggests that predissociation of Rydberg states in methyl bromide is *l*-dependent. This contrasts with the ion-pair excitation spectra of the I_2 and ICl[2] where there is no *l*-dependence in the dissociation of Rydberg states via the ion-pair continuum.

While *l*-dependent predissociation might explain the curtailment of *np*;0 series in methyl bromide, there is one inconsistency. For a series to be curtailed in the manner of the *np*;0 series in the two-photon spectrum, the amount of penetration of the ionic core should remain at least constant over the course of the series. This contrasts with the expectation that penetration should decrease with successive *n*, decreasing the likelihood of predissociation. However, other factors need to be considered such as the positions of the potential energy surface crossings between the [3/2]*np*;0 Rydberg and D (0) ion-pair states on the [3/2]*np*;0 potential surfaces. These will be considered in light of the potential energy diagram depicted in Figure 3-9.

Although the electronic states in methyl bromide should be described using potential energy surfaces, the potential curves depicted in Figure 3-9 were generated assuming that methyl bromide behaves in a quasi-linear fashion. Since Ω is a good quantum number and the D (0) ion-pair state dissociates to give CH_3^+ and Br^-, this is not unreasonable. The potential curves of the ground, Rydberg, ionic and ion-pair states are represented by Morse potentials. The repulsive curves were generated using the model developed by Bersohn and Shapiro[26] for the equivalent states in methyl iodide. Strictly speaking, the use of a Morse potential to describe an ion-pair state is not correct because of the Coulombic attraction between the partners in an ion pair. However, the effect of the Coulombic attraction is more important at larger separations. Because the shape of the curve at short bondlengths is of most interest here, a Morse potential is adequate in this case.

The data required to generate a Morse potential are the equilibrium bondlength, R_e, the equilibrium vibrational frequency, ω_e, the equilibrium dissociation energy, D_e, the reduced mass, μ, and the equilibrium term value, T_e. For calculation of the reduced mass, the mass of the CD_3 group was taken as m_1 and that of the bromine atom was taken as m_2. For R_e, the D_3C-Br distance was used. However, some of the data required was unavailable and, as a result, some assumptions had to be made. Firstly, the equilibrium bondlengths of the Rydberg and ionic states were assumed to

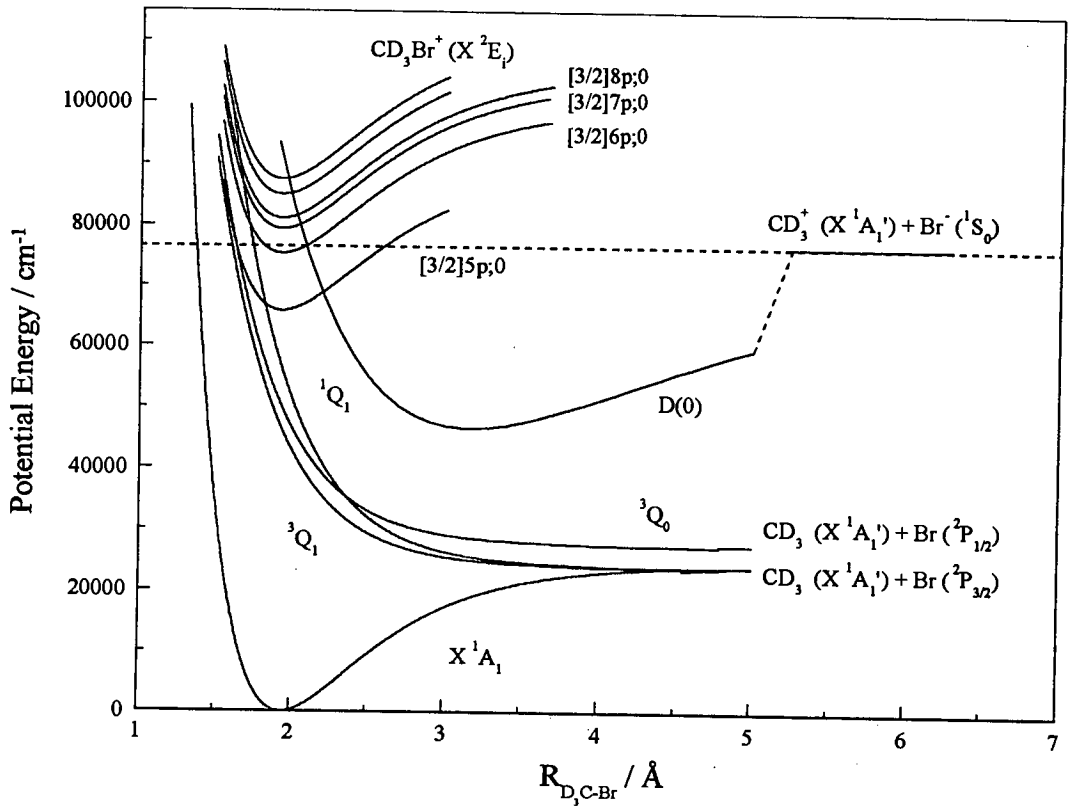

Figure 3-9: Potential energy diagram of CD_3Br depicting selected electronic states of the neutral molecule and its ion. The generation of the depicted potential energy curves is discussed in the text.

be similar to those of the ground state. This assumption is validated by the amount of vibrational activity in the two- and three-photon spectra of methyl bromide. Also, there is practically no data available regarding the ion-pair states of the methyl halides. Thus, trends in the diatomic halogens were used to deduce sensible values for the quantities required for the calculation of the ion-pair potential curve. In light of the similarities in Rydberg state D_3C-Br bondlengths to those of the halogens, a typical bondlength of an ion-pair state in molecular bromine[27], 3.2 Å, was adopted. A typical value for the dissociation energy for ion-pair states in molecular bromine[27] is 30000 cm^{-1} and this was adopted also. This value for the dissociation energy of ion-pair states in Br_2 was obtained by subtracting the term values[27] of several ion-pair states dissociating to produce Br^+ ($^3P_2$) and Br^- ($^1S_0$) from the transition energy corresponding to this ion-pair threshold[2], 84059 cm^{-1}, and comparing the resulting values. The equilibrium term value of the first-tier ion-pair state in CD_3Br,

T_e = 46470 cm^{-1}, was calculated by subtracting D_e from the value for the thermodynamic threshold for ion-pair formation, 76470 cm^{-1}. In the halogens, ω_e for an ion-pair state is generally half that of the ground electronic state[27]. This trend was used to calculate an ω_e value for an ion-pair state in CD_3Br.

The first point clear from Figure 3-9 is that the [3/2]5p;0 lies below the first ion-pair threshold. Thus, the strength of two-photon transitions to this state might be explained by its not being predissociated by the ion-pair continuum. Another point of note is that the positions of the curve crossings with the D (0) state occur lower on the potential curves in successive members of the [3/2]*np*;0 series. Thus, while the window available for predissociation is reduced by the greater amount of time spent away from the ionic core by the Rydberg electron, the effect of the ion-pair continuum might be increased by the changing positions of the curve crossings.

The other predissociation channel above 75000 cm^{-1} involves the 5s state based upon the $\tilde{A}\ ^2A_1$ ionic core. In the photoelectron spectrum[14], the $\tilde{A}\ ^2A_1$ ionic state is seen to be repulsive. Thus, it would not be unreasonable for any Rydberg state based upon this ionic core to be repulsive also. Moreover, A[3/2]*ns* and A[1/2]*ns* states have been observed in the VUV spectra of the halogens as a result of coupling with nearby X[3/2]*np* and X[1/2]*np* states. Thus, the $\tilde{A}\,[^2A_1]$5s state would be expected to interact with *np* states in methyl bromide as well. Previous comments regarding the means by which the *np*;0 series might be shortened through interaction with the D (0) ion-pair continuum apply here also.

Therefore, the curtailment of the observed [3/2]*np*;0 series can be explained by *l*-dependent predissociation. Also, the positions of the crossings with the predissociative states on the potential energy surfaces of the [3/2]*np*;0 states may have a part to play. This because less time is spent by the Rydberg electron near the ionic core in successive members of a Rydberg series and this should reduce the probability of predissociation occurring.

The [1/2]*np*;0 series seems even shorter than the [3/2]*np*;0 series with only the first member being seen, but blending with features arising from members of *nd* series cannot be discounted. Even so, it is not expected to be longer than the [3/2]*np*;0 series and, as evidenced by the relative intensities of the origin bands of the

Assignment		**CH_3Br**		**CD_3Br**
Electronic	Vibrational	One-Photon $\bar{\nu}$/cm^{-1}	Two-Photon $\bar{\nu}$/cm^{-1}	Two-Photon $\bar{\nu}$/cm^{-1}
[3/2]5p;0	3_1^0	65616	–	–
[3/2]5p;0	3_1^1	65877	–	–
[3/2]5p;0	0_0^0	66003	66007	66112
[3/2]5p;0	3_1^2	66341		-
[3/2]5p;0	3_0^1	66482	66507	66583
[3/2]5p;0	6_0^1	66650	-	-
[3/2]5p;0	3_0^2	66990	-	-
[3/2]5p;0	5_0^1	67093	-	-
[3/2]5p;0	2_0^1	67246	67256	67052
[3/2]5p;0	6_0^2	67437	-	-
[3/2]5p;0	$2_0^1 3_0^1$	67720	-	-
[3/2]5p;0	5_0^2	68256	-	-
[3/2]5p;0	2_0^2	68504	-	-
[3/2]5p;0	1_0^1	68848	68860	68167
[1/2]5p;0	3_1^1	68504	-	-
[1/2]5p;0	0_0^0	68659	68674	68737
[1/2]5p;0	3_0^1	69105	-	-
[1/2]5p;0	3_0^2	69581	-	-
[1/2]5p;0	2_0^1	69932	-	69682
[3/2]4d;2	0_0^0	-	72655	72737
[3/2]4d;2	2_0^1	-	-	73703
[3/2]4d;0	0_0^0	-	72977	73050
[3/2]4d;0	3_0^1	-	73529	-
[3/2]4d;0	2_0^1	-	74258	72999

Table 3-3: Vibrational structure of the 5p and 4d states of methyl bromide. The one-photon data is taken from the work of Causley and Russell[6].

[3/2]5p;0 and [1/2]5p;0 states, should be much weaker. The difference in relative intensities of the [3/2]5p;0 and [1/2]5p;0 states is, in itself, somewhat surprising, although consistent with the VUV spectrum[6]. This consistency with the one-photon absorption spectrum rules out differences in ionisation efficiencies as the underlying cause.

Some vibrational structure built upon the origins of both the [3/2]5p;0 and [1/2]5p;0 states is seen. This is summarised in Table 3-3. In the [3/2]5p;0 state, this is limited to one quantum of excitation in each of the symmetric vibrational modes ν_1 (C-H stretch), ν_2 (CH_3 out-of -plane bend) and ν_3 (C-Br Stretch) with the 2^1_0 band being the most intense after the origin. It is even more limited in the higher spin-orbit state with only the 2^1_0 band being seen but this is not surprising considering the intensity of the origin band relative to that of the [3/2]5p;0 state. This dearth of vibronic activity is not surprising considering the appearance of the photoelectron spectrum[14]. The vibronic assignments are in agreement with those of Causley and Russell[6].

3.3.5 *nd* States

Because the bands comprising the 5s system are seen with reasonable intensity one might expect the series to continue, especially if there are features with similar quantum defects occurring to higher energy. This has been the way Rydberg transitions in the two-photon spectra of methyl iodide[9] and methyl chloride[10] were assigned. The consequence of this would be that the two-photon spectrum of methyl bromide should be dominated by features which have ρ_2=1.5. Given that the type of polarisation behaviour seen in Figure 3-8 is typical of the majority of features with near integer quantum defects in the two-photon spectrum, the *ns* assignment can be discounted even if it appears perfectly reasonable on energetic grounds.

The polarisation behaviour of the [3/2]6d cluster, depicted in Figure 3-8, is not only typical of other such features in the two-photon spectrum of methyl bromide

but is also typical for similar features in the two-photon spectrum of molecular bromine[1]. In the [3/2]6d cluster, the higher energy feature has $\rho_2 \cong 0$ and the lower energy one has $\rho_2 > 1$. While there can be no doubt that the former belongs to a state with $\Omega=0$, the latter can arise from a transition to a state with $\Omega=1$ or $\Omega=2$. It is because this type of behaviour is also seen in the two-photon spectrum of molecular bromine[1] that the features of interest here are similarly assigned to [3/2]6d;0 and [3/2]6d;2 states. Since similar behaviour is seen for the [1/2]5d cluster, even if the $\Omega=2$ component is weaker, it is assigned accordingly. In the case of molecular bromine[1], $\Omega=1$ and $\Omega=2$ states were distinguished using rotational band contour simulation. From this, it was seen that features due to $\Omega=1$ states were much weaker than those due to $\Omega=2$ states. It was suggested that this might arise from destructive interference between both excitation pathways terminating in an $\Omega=1$ state. That this is also the case in methyl bromide as well is supported by three-photon polarisation studies, discussed later. Thus, the dominant series in the (2+1) REMPI spectrum of methyl bromide can be assigned based upon the trends seen in the spectra of molecular bromine.

The polarisation behaviour described for the bands in Figure 3-8 is typical of all members of *nd* series seen in the two-photon spectrum of methyl bromide. However, the splitting between $\Omega=0$ and $\Omega=2$ components is inversely proportional to n^3. Thus, as is evident from Figure 3-10, the features due to both components eventually blend. That the polarisation behaviour already discussed applies here as well is shown by the perceptible narrowing of bands in the spectrum recorded using linearly polarised light.

Even though the dominant bands in the two-photon spectrum of methyl bromide are assigned to *nd* states, features arising from transitions to *nf* states are also expected. Also, there are extra features in the two-photon spectrum which may arise from transitions to *nf* states. These extra features are seen about the [3/2]5d;2 and [3/2]6d;2 bands in Figure 3-6 and blending of such features would explain the

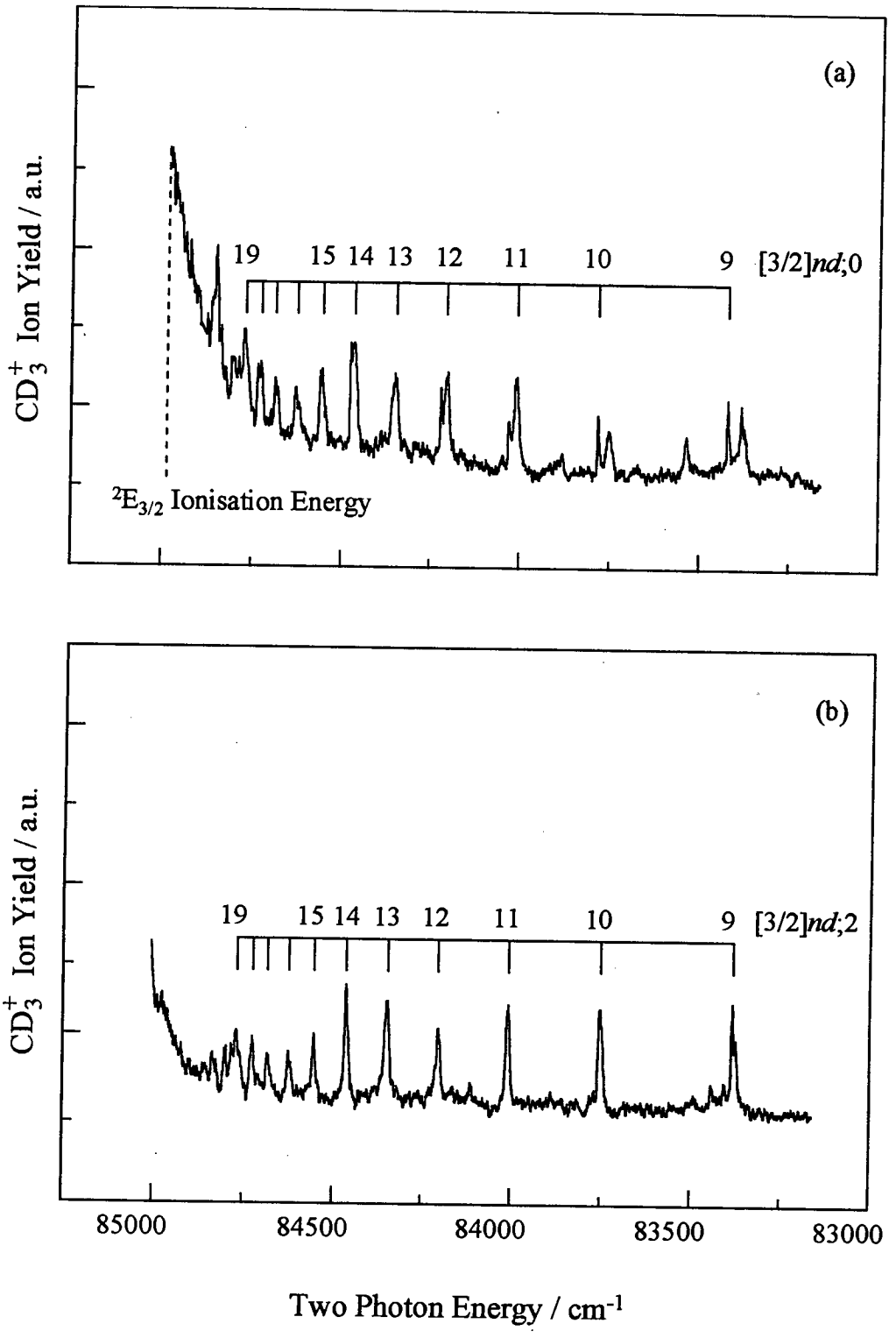

Figure 3-10: Polarisation behaviour of features in the 83000-85250 cm^{-1} region in the two-photon spectrum of CD_3Br. Panel (a) depicts the spectrum recorded using linearly polarised light and panel (b) depicts the spectrum recorded using circularly polarised light.

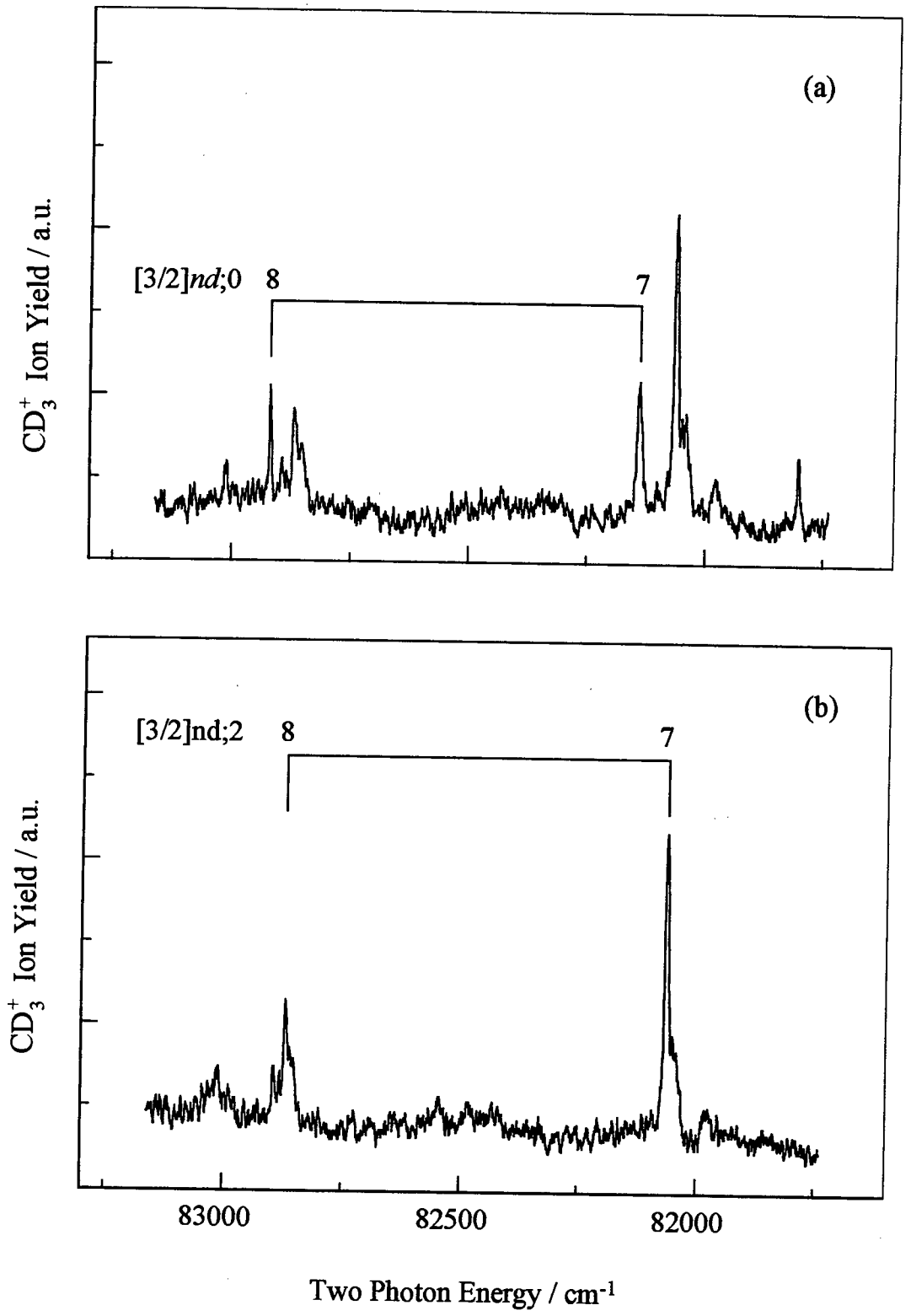

Figure 3-11: Two-photon spectrum of CD_3Br in the 81700-83300 cm^{-1} region. The intensity of the [3/2]7d;2 band is discussed in the text. Panel (a) depicts the spectrum recorded using linearly polarised light and panel (b) depicts the spectrum recorded using circularly polarised light.

increased intensity of the [3/2]7d;2 band in Figure 3-11. A discussion of this possibility and the possibility of *nf* transitions dominating the two-photon spectrum of methyl bromide is deferred to later because of the dominance of *nf* transitions in its three-photon spectrum, discussed below.

3.4 (3+1) REMPI Spectroscopy of Methyl Bromide

The (3+1) REMPI spectroscopy of methyl bromide has been studied in the 65000-85000 cm^{-1} energy region. While transitions seen in the two-photon spectrum are apparent in the three-photon spectrum, it is dominated by features which are either very weak in or absent from the two-photon spectrum. Polarisation studies indicate that these features are due to transitions with $\Delta\Omega=1$. These extra features are assigned to *ns*;1, *np*;1, *nd*;1 and *nf*;1 states. Features arising from transitions with $\Delta\Omega=3$ are expected but are not seen which is somewhat surprising. This means that any features not seen in the two-photon spectrum but which occur in the three-photon spectrum should hence be apparent in the VUV spectrum. However, the *nf*;1 series dominating the three-photon spectrum does not conform with this expectation, implying that *l* remains a good quantum number in methyl bromide where Rydberg transitions are concerned.

While two-photon polarisation studies aid interpretation of the results of three-photon polarisation studies, the opposite can also be true. The example of particular interest here is the confirmation of the *nd*;2 assignments in the two-photon spectrum of methyl bromide using three-photon polarisation studies. This shows that the inability to undertake rotational band contour simulations need not hamper the assignment of a multiphoton spectrum. The electronic assignments of the three-photon spectra of CH_3Br and CD_3Br are tabulated in Table 3-4.

Assignment	CH_3Br		CD_3Br	
	Energy / cm^{-1}	$(n-\delta)$	Energy / cm^{-1}	$(n-\delta)$
[3/2]5p;2	-	-	65871	2.39
[3/2]5p;0	66015	2.40	66131	2.40
[3/2]5p;1	67503	2.50	67609	2.51
[1/2]5p;2	-	-	68565	2.40
[1/2]5p;0	68672	2.41	68764	2.41
[1/2]5p;1	69803	2.49	69959	2.49
[3/2]4d;1	70194	2.72	70318	2.73
[3/2]4d;2	72676	2.98	72713	2.98
[3/2]4d;0	72968	3.02	73048	3.02
[1/2]4d;1	73601	2.80	73648	2.80
[3/2]6s;1	73601	3.10	73648	3.10
[3/2]6p;0	75416	3.38	75667	3.41
[1/2]4d;0	75872	3.01	76050	3.08
[1/2]6s;1	76174	3.10	76374	3.12
[3/2]6p;1	76742	3.64	76623	3.60
[3/2]5d;1	77293	3.77	77295	3.75
[3/2]4f;1′	77794	3.90	77923	3.91
[3/2]4f;1	77985	3.95	78045	3.95
[3/2]5d;2	78210	4.02	78265	4.01
[3/2]5d;0	78363	4.06	78427	4.06
[3/2]7s;1	78638	4.15	78661	4.13
[1/2]5d;1	80046	3.82	80196	3.84
[3/2]6d;1	80230	4.79	80278	4.77
[1/2]4f;1′	80451	3.90	-	-
[1/2]4f;1	80541	3.95	80614	3.95
[3/2]5f;1	80541	4.95	80614	4.95
[3/2]8s;1	80881	5.15	80950	5.15
[1/2]7s;1	81077	4.11	-	-
[3/2]6f;1	81916	5.95	81973	5.93
[3/2]9s;1	81996	6.03	82054	6.01
[3/2]7f;1	82735	6.93	82817	6.94
[1/2]5f;1	83103	4.96	83179	4.96
[3/2]8f;1	83293	7.98	83339	7.91
[3/2]9f;1	83653	8.97	83720	8.93
[3/2]10f;1	83704	9.14	83778	9.13
[3/2]13f;1	84371	13.03	-	-
[3/2]14f;1	84476	14.24	-	-
[3/2]15f;1	84537	15.12	-	-

Table 3-4: Electronic assignments of the three-photon spectrum of methyl bromide. $(n-\delta)$ values have been calculated using the ionisation energies already used to calculate the $(n-\delta)$ values of the observed two-photon transitions.

3.4.1 5p Cluster

The three-photon spectra of the 5p cluster of CH_3Br and CD_3Br are shown in Figure 3-12. The first thing to be noted is the richer spectrum of the deuteride when compared with that of the hydride. The amount of structure seen in the 5p region in the deuteride even surpasses that seen in the two-photon spectrum in the same energy region. This is in marked contrast to the hydride where the appearance of the 5p system is practically unchanging in the one-, two-, and three-photon spectra. The majority of the extra features in the three-photon spectrum of CD_3Br can be assigned to vibrational structure built upon the 5p;0 origin bands. Symmetric vibrational modes again dominate but ν_6, the CH_3 rock, an asymmetric mode, is also seen.

The power output of the dye laser in the 420-460 nm region might explain the presence of vibrational bands built upon the 5p;0 origins in the three-photon spectrum of CD_3Br that are absent from its two-photon spectrum. However, there are other features which cannot be explained in this way. One of these is the band at 67609 cm^{-1} and this has a counterpart lying at 67503 cm^{-1} in the three-photon spectrum of the hydride. The clear proximity of both features, with a not unreasonable zero point energy shift, confirms the assignment of a new electronic origin. Because three-photon polarisation studies of the hydride show that all features making up the 5p system have $\rho_3 < 1$, the feature at 67503 cm^{-1} in the hydride and 67609 cm^{-1} in the deuteride are assigned to a [3/2]5p;1 state in both isotopomers.

Similarly, the feature at 69803 cm^{-1} in the hydride and 69959 cm^{-1} in the deuteride are assigned to a [3/2]5p;1 state in each species. Features with $\rho_3 < 1$ which are absent from the two-photon spectrum are more likely to arise from transitions to Ω=1 states than those to Ω=0 states. This conclusion is further justified by polarisation studies of higher energy regions of the three-photon spectrum.

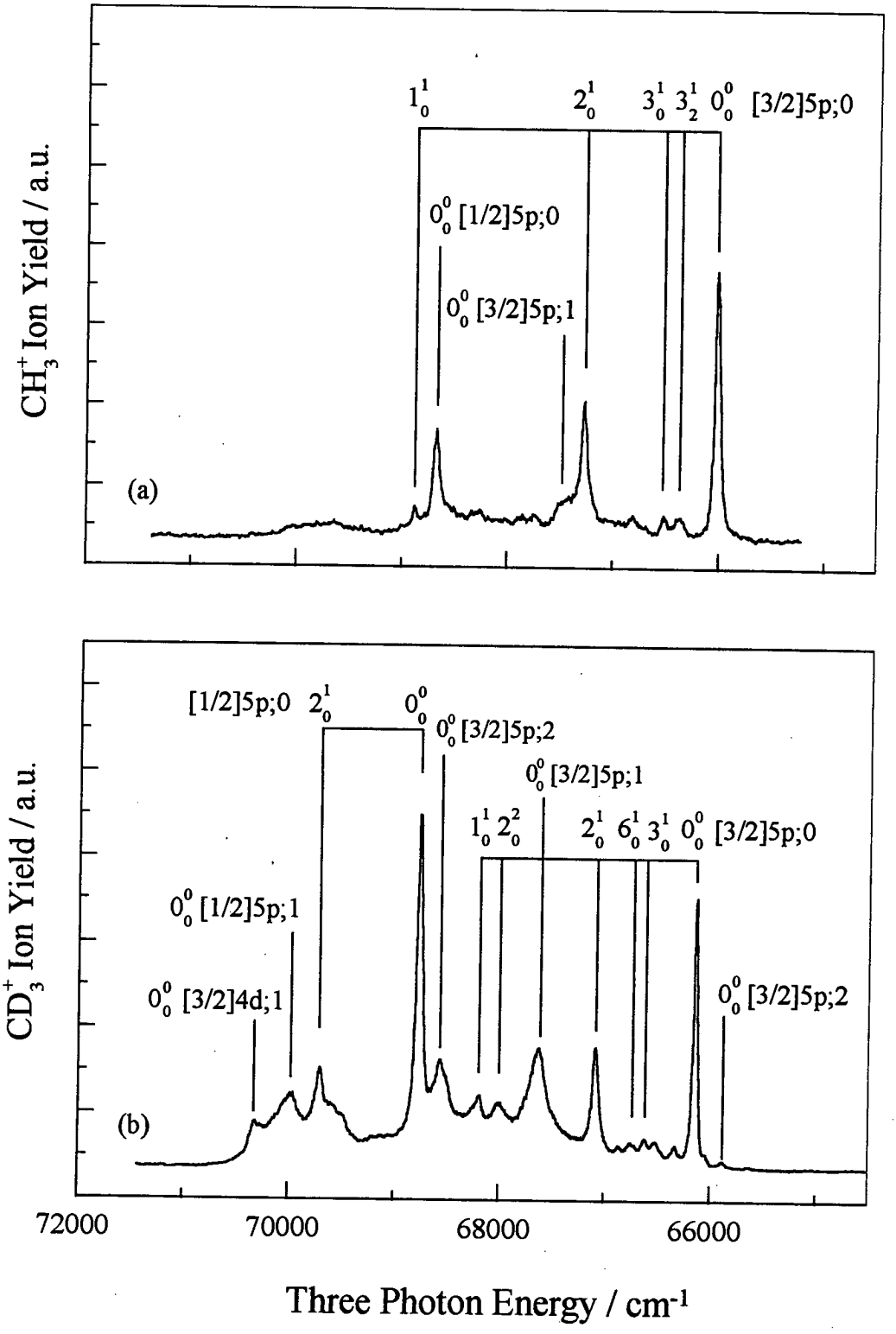

Figure 3-12: (3+1) REMPI of the 5p cluster of (a) CH_3Br and (b) CD_3Br. The spectra depicted here have not been normalised to the cube of the laser power so caution must be exercised when comparing relative intensities of the features depicted above.

Assignment	CH_3Br		CD_3Br
	One-Photon cm^{-1}	Three-Photon cm^{-1}	Three-Photon cm^{-1}
3_1^0 [3/2]5p;0	65616	–	–
3_1^1 [3/2]5p;0	65877	–	–
0_0^0 [3/2]5p;0	66003	66015	66131
$2_0^1 3_1^0$ [3/2]5p;0	-	-	66321
3_1^2 [3/2]5p;0	66341	66357	-
3_0^1 [3/2]5p;0	66482	66505	66606
6_0^1 [3/2]5p;0	66650	66711	66701
3_0^2 [3/2]5p;0	66990	–	-
5_0^1 [3/2]5p;0	67093	–	-
2_0^1 [3/2]5p;0	67246	67262	67073
6_0^2 [3/2]5p;0	67437		-
$2_0^1 3_0^1$ [3/2]5p;0	67720	-	–
5_0^2 [3/2]5p;0	68256	-	-
2_0^2 [3/2]5p;0	68504	–	67995
1_0^1 [3/2]5p;0	68848	68879	68179
3_1^1 [1/2]5p;0	68504	-	-
0_0^0 [1/2]5p;0	68659	68672	68764
3_0^1 [1/2]5p;0	69105	-	-
3_0^2 [1/2]5p;0	69581	-	-
2_0^1 [1/2]5p;0	69932	-	69702

Table 3-5: Vibronic structure of the 5p system in the three-photon spectrum. The one-photon data comes from the work of Causley and Russell[6].

The extra features so apparent in the spectrum of the deuteride are not so obvious in the hydride spectrum. One explanation for this is that a greater degree of predissociation is taking place in the hydride. This predissociation results in band broadening which may well occur to such an extent that some features are barely visible above the baseline. This would explain the remarkable similarity of the two- and three-photon spectra of the 5p region in CH_3Br while they are so different in CD_3Br.

Given that a comprehensive study of the VUV spectrum of CD_3Br has yet to be reported, there is little evidence to suggest that assignments to Ω=0 and Ω=1 states are in any way unreasonable. There are other features in the spectrum of the deuteride which are either weak or absent from the spectrum of the hydride and these are assigned to Ω=2 states. Thus, Ω=2, Ω=0 and Ω =1 components based upon each ionic core, and in that energy ordering, are apparent in the three-photon spectrum of the deuteride. The apparent absence of some features from the hydride is best explained by a greater degree of predissociation. Vibronic assignments in the 5p system are detailed in Table 3-5.

3.4.2 70000-77000cm^{-1} Energy Region

In the 70000-77000 cm^{-1} region of the two-photon spectrum, transitions to 4d;2, 4d;0 and 6p;0 states are present. However, in the same energy region of the three-photon spectrum, additional features are seen along with these. Because of their polarisation behaviour, confirmed later, and their absence from the two-photon spectrum, these are assigned to Ω=1 states. There is an extremely broad feature about 71000 cm^{-1} and this is assigned to a [3/2]4d;1 state. As shown in Figure 3-13(b) and 3-13(d), an additional strong feature is seen to higher energy of the [3/2]4d;0 and [3/2]4d;2 states already seen in the two-photon spectra. This band can equally well be assigned to [1/2]4d;1 or [3/2]6s;1 transitions. However, given the sharpness of the feature in question, a [3/2]6s;1 assignment seems more likely. This is because the appearance of a feature due to a [1/2]4d;1 state should be similar to that of a feature due to its counterpart with the $^2E_{3/2}$ ionic core. Since the feature in the three-photon spectrum of methyl bromide assigned to a [3/2]4d;1 state is broad, any feature due to a [1/2]4d;1 state is expected to be broad also. The [3/2]6s;1 assignment is further confirmed by the ability to extend the *ns*;1 series. The quantum defects of the features assigned to members of the [3/2]*ns*;1 series also follow the trends in the Rydberg spectra of the iodine monochloride[2]. The quantum defects of the first *ns* cluster depart from those exhibited by higher members of the same series in both molecules. In iodine monochloride[2], the [3/2]6s;1 state has δ=4.02 while the [3/2]7s;1 state has

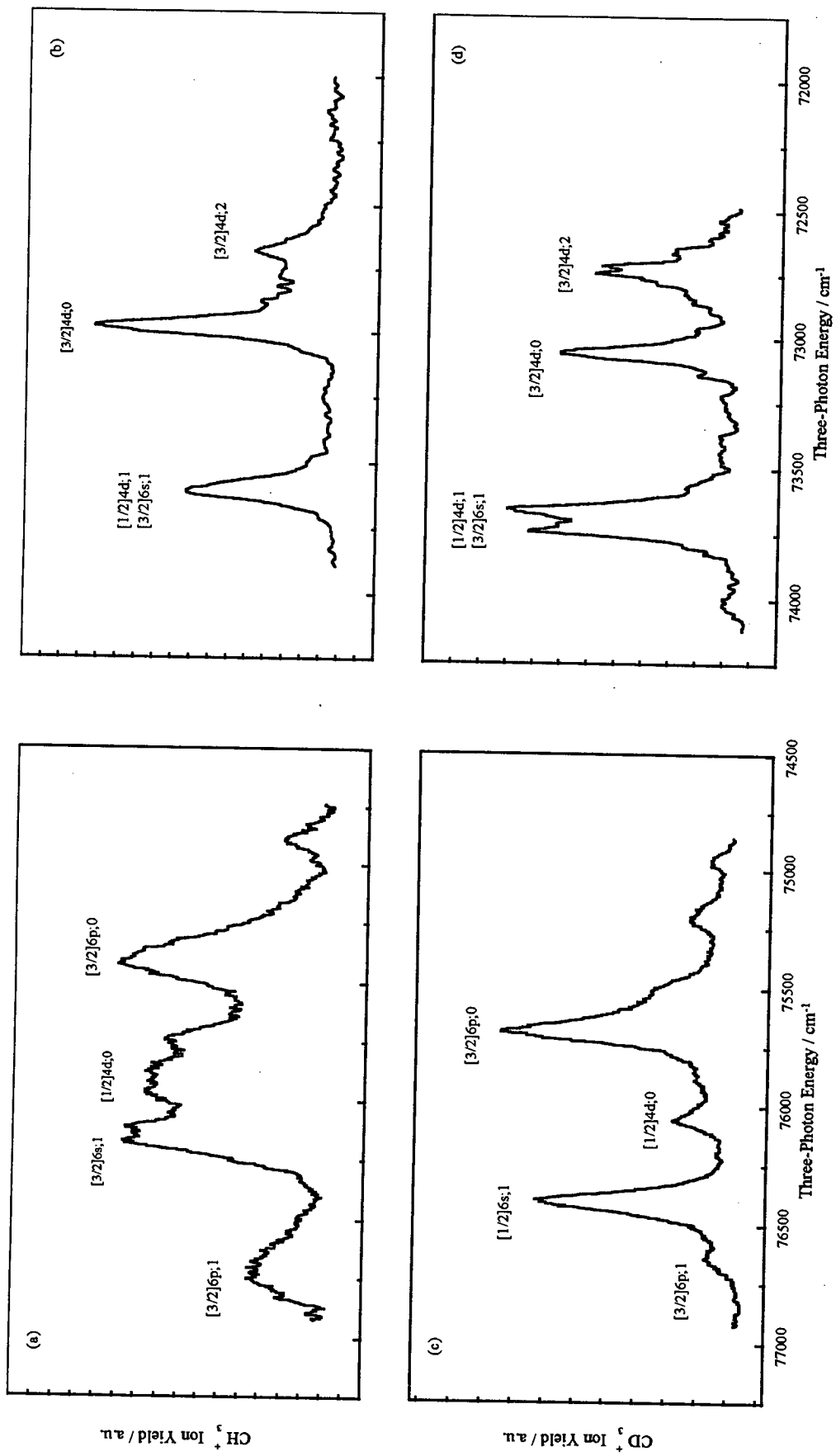

Figure 3-13: Power-normalised three-photon spectra of CH_3Br, (a) and (b), and CD_3Br, (c) and (d), in the 72000-77000 cm^{-1} region

δ=3.89. Similarly, in methyl bromide, the [3/2]5s;1 state has δ=3.05 and the [3/2]6s;1 state has δ=2.90. This departure in the lowest *ns* cluster can be attributed to Rydberg-valence interactions.

Figure 3-13 depicts the three-photon spectra of CH_3Br, (a), and CD_3Br, (c), in the 75000-77000 cm^{-1} region. Some of the observed features are assigned to the higher spin-orbit counterparts of the states seen in the 72000-74000 cm^{-1} region discussed above. The assignment of the feature at 76174 cm^{-1} in the hydride and at 76374 cm^{-1} in the deuteride to the [1/2]6s;1 state provides even more confirmation for the assignment of the feature at 73601 cm^{-1} in the hydride and at 73648 cm^{-1} in the deuteride to the [3/2]6s;1 state. In addition to this, other features are assigned to [3/2]6p;0 and [3/2]6p;1 states.

3.4.3 77000-85000cm^{-1} Energy Region

This region of the three-photon spectrum is dominated by features which are absent from both one- and two-photon spectra. These features have near-integer quantum defect values and comprise series converging upon the first and second ionisation limits. The absence of a corresponding feature in the 72000-77000 cm^{-1} region suggests an *nf* assignment. Polarisation studies, the results of which are discussed below and shown in Figure 3-14, indicate that these states have Ω=1. The extent of these series, up to n = 16 in the hydride, is shown in Figure 3-15 for both hydride and deuteride. Apparent from these spectra is the appearance of a two-photon resonance at 56065 cm^{-1} in the hydride and 56284 cm^{-1} in the deuteride. These two-photon energies correspond to three-photon energies of 84098 cm^{-1} and 84426 cm^{-1}, respectively. The corresponding feature in both isotopomers is assigned to the origin of the [3/2]5s;1 state. This band, observed by (2+2) REMPI, obscures part of the three-photon spectrum and hence, part of the observed *nf*;1 series in both species.

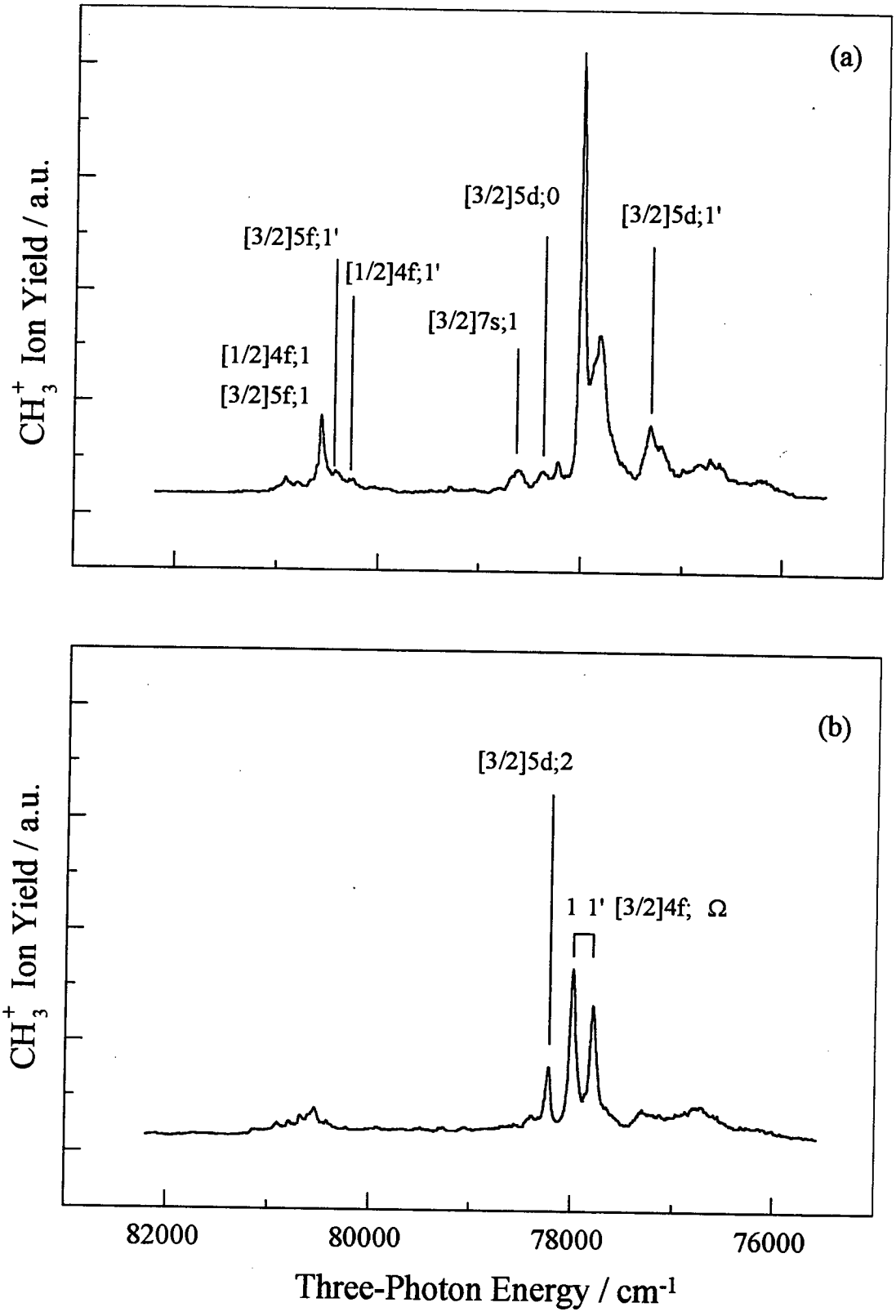

Figure 3-14: Polarisation behaviour of features in the 76000-82000 cm^{-1} region of CH_3Br. The spectrum recorded using linearly polarised light is shown in panel (a) while panel (b) depicts the spectrum recorded with circularly polarised light.

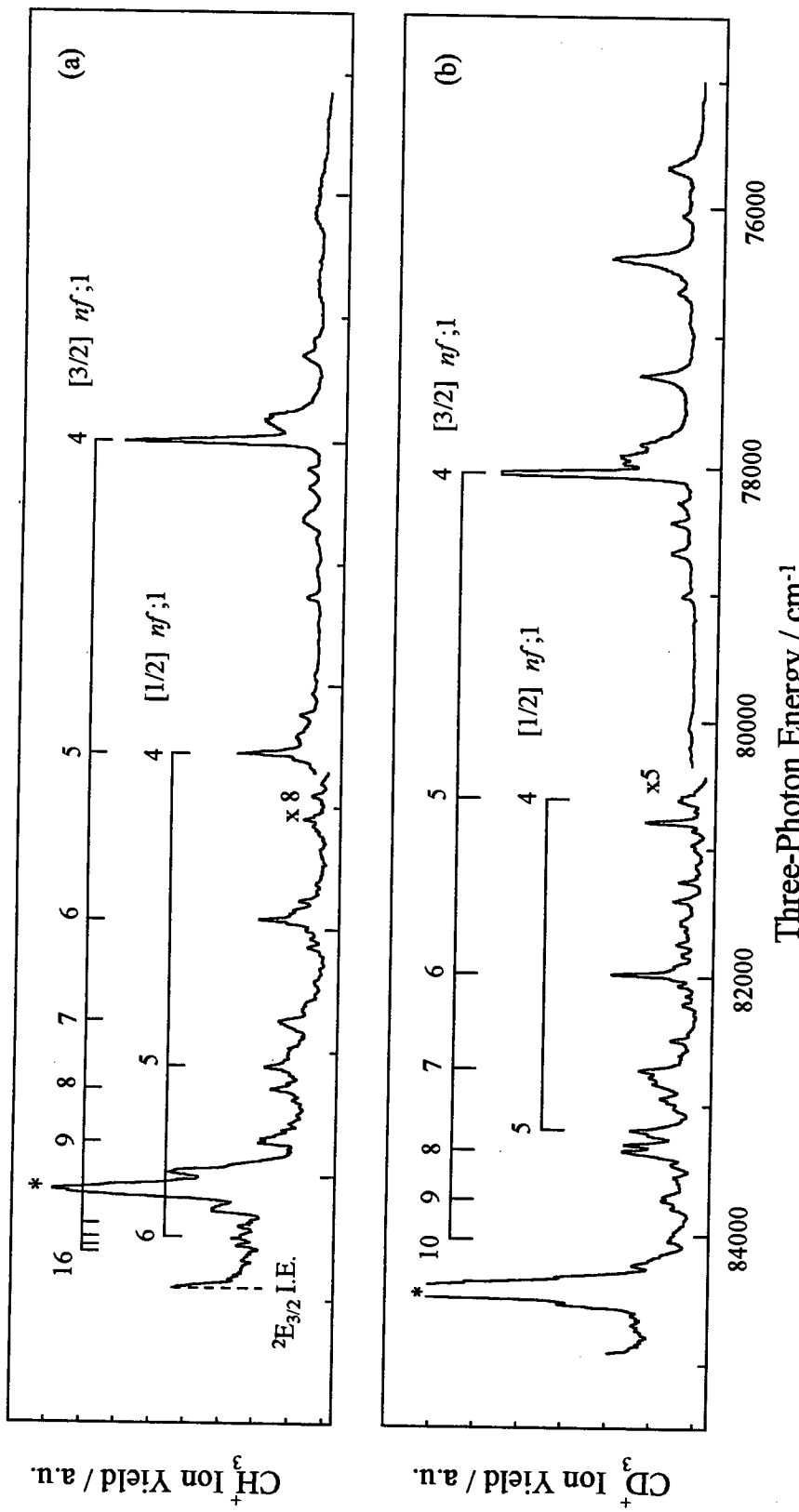

Figure 3-15: Three-photon spectra of (a) CH_3Br and (b) CD_3Br in the 75000-85000 cm^{-1} region depicting dominant *nf*;1 series. Discontinuities in the baseline are due to different laser scans being depicted without normalising them to the cube of the dye laser power. The * denotes the origin band of the [3/2]5s;1 state observed via (2+2) REMPI. This feature obscures some of the features occurring in this region as a result of three-photon transitions.

It is apparent from Figure 3-14 that the majority of the bands in the 76000-82000 cm^{-1} region of the three-photon spectrum of CH_3Br have a three-photon polarisation ratio less than unity. An exception is the band assigned to a [3/2]5d;2 state which has $\rho_3 \cong 2.5$. It is this type of polarisation behaviour that supports the assignment of *nd*;2 states in the two-photon spectrum of methyl bromide. It also confirms further that Ω is a good quantum number in methyl bromide. The situation depicted in Figure 3-14 where the majority of the observed bands display three-photon polarisation ratios less than unity is typical of the whole three-photon spectrum of methyl bromide. This type of polarisation behaviour is displayed by all of the features that are seen with appreciable intensity in the three-photon spectrum but are either absent or very weak in the two-photon spectrum. This clearly rules out the possibility of assignments to Ω=3 states because these would have to display polarisation behaviour similar to that of the [3/2]5d;2 band which clearly is not the case. Thus, Ω=1 assignments seem more reasonable, especially when the propensity rules in the two-photon spectra are considered. Features of this type not only include members of the *nf*;1 series discussed above but also several features assigned to *nd*;1 and *ns*;1 states. A possible exception to this trend is the feature assigned to the [3/2]4f;1′ state. The change in appearance of this band with change in the polarisation of the incident radiation might indicate the presence of overlapping features due to [3/2]4f;0 and [3/2]4f;2(3) states. Still, the low intensity of the equivalent feature in the two-photon spectrum would suggest that the [3/2]4f;1′ assignment is more likely correct.

The surprising thing about the *nf*;1 series seen to dominate the three-photon spectrum of methyl bromide is that the corresponding features are apparently absent from its VUV spectrum[8]. The band positions of the features assigned to [1/2]4f in this study and [1/2]5d in the VUV work[8] do not coincide within the combined uncertainties of both experimental techniques as they should if they were members of the same series. These bands are picked for comparison because the [1/2]5d band is the lowest energy assignment in the work of Baig et al.[8] and the higher energy band measurements will converge towards each other as the ionisation limits of their

respective series are approached, limiting the usefulness of these in any comparison. One possibility is that transitions to *nf*;1 states might be favoured by real intermediate states at either the first and/or second photon level. Because the polarisation behaviour exhibited by the [3/2]5d;2 band follows that expected for a coherent three-photon transition with $\Delta\Omega=2$, the possibility of three-photon transitions via real intermediate states can be discounted. One other possibility is that l is a good quantum number in methyl bromide. Thus, another propensity rule would arise in the one-photon spectrum which is that $\Delta l = 0, \pm 1$. This would mean that transitions to *nf* states would be forbidden in the VUV spectrum, explaining their absence. This would imply a departure from trends in the diatomic halogens where *nf* states are seen in the VUV spectrum implying that l is no longer good. However, Rydberg transitions in the halogens involve the promotion of an electron from a molecular orbital having some anti-bonding character whereas in methyl bromide, the electron being promoted in a Rydberg transition originates from an orbital of lone-pair character essentially localised on the bromine atom. This distinction may well account for l remaining a good quantum number in methyl bromide but not in the halogens. The appearance of *nf*;1 series in the three-photon spectrum of methyl bromide but not its VUV spectrum suggests that, along with Ω, l remains good in the methyl halides.

3.5 Discussion

3.5.1 Further Comments Regarding the Nature of the Rydberg States of Methyl Bromide

The assignments of the two- and three-photon spectra of methyl bromide have several consequences not only for the assignment of the spectra of the other methyl halides but also for other polyatomic molecules. Rydberg transitions of the methyl halides have previously been assigned in a comparison with atomic transitions and several authors have thought that they were quasi-atomic in nature[5,6,8]. This is at least partly due to the atomic-like spectral appearance and the fact that an electron involved in a Rydberg transition in the methyl halides originates from what is essentially a non-bonding orbital localised upon the halogen atom in the molecule. In methyl bromide,

this is essentially a 4p orbital based on the bromine atom. This situation would imply that Rydberg transitions in methyl bromide would follow atomic-like selection rules and the VUV spectrum should consist solely of *ns* and *nd* transitions. Similarly, the two-photon spectrum would comprise only of transitions to *np* and *nf* states. The first piece of evidence suggesting that quasi-atomic symmetry restrictions are relaxed is the appearance of intense bands which can only be assigned to 5p states in the one-photon spectrum[6]. The dominance of *nd* states in the two-photon spectrum and *nf* states in the three-photon spectrum further expresses this point. Although, the propensity rules governing Rydberg transitions in methyl bromide closely follow those of the diatomic halogens, the possibility of l remaining a good quantum number cannot be ruled out entirely, especially considering that the *nf* transitions dominating the three-photon spectrum are absent from the VUV spectrum.

The evidence for *nd* series in the two-photon spectrum comes from polarisation studies which show similarities between methyl bromide and the halogens[1,2]. This similarity helps the assignment of the spectrum of methyl bromide. Polarisation studies also show that Ω is good and the (Ω_c, ω_{Ryd}) description used for the Rydberg states of methyl bromide is correct. This is especially true of the three-photon studies where differences between an (Ω_c, ω_{Ryd}) description and one using C_{3v} point group symmetry would be apparent. With Ω being a good quantum number, the absence of Ω=1 states from the two-photon spectrum is easier to explain. As in the halogens and other diatomic molecules, two possible excitation pathways exist when a transition to an Ω=1 state occurs. The first involves a parallel transition followed by a perpendicular one while the second involves a perpendicular transition first and then a parallel one. It may be possible that these two pathways destructively interfere with each other, diminishing the intensity of a $\Delta\Omega$=1 transition. Hence, the propensity for Ω=0 and Ω=2 states in the two-photon spectrum. In the three-photon spectrum, transitions to states with Ω=1 give rise to some of the strongest features, confirming that transitions to states with Ω=1 are weakened in some manner for two-photon excitation. Surprisingly, transitions with $\Delta\Omega$=3 are absent but a possible explanation for this is Ω-dependent predissociation.

3.5.2 Use of Rydberg State Microconfigurations in the Spectral Assignment

In the diatomic halogens[1,2], apart from those based upon Ω, other propensity rules are apparent. The lower propensity for transitions with $\Delta\Omega=1$ in the two-photon spectra of the diatomic halogens has already been discussed. Also, transitions to states with some singlet character were seen almost exclusively, especially as *n* increases. The latter propensity rule is confirmed upon examination of Rydberg state microconfigurations. These two propensity rules greatly simplify an analysis of the VUV and two-photon spectra of the halogens. A consequence of the operation of these propensity rules is the absence of *ns* transitions with $n>5$ from the two-photon spectrum of molecular bromine[1]. When one considers the microconfigurations for *ns* states, given in Table 3-6, it is seen that *ns* states with non-unity Ω-values have pure triplet character. This, in combination with a reduced propensity for $\Delta\Omega=1$ transitions is most likely to explain the absence of *ns* states with $n>5$ from the two-photon spectrum of Br_2. Given that *ns* states with $n>5$ are also absent from the two-photon spectrum of methyl bromide, the propensities seen in the spectra of the diatomic halogens[1,2] should aid the assignment of its two- and three-photon spectra of methyl bromide. This approach is based on the assumption that CH_3Br (CD_3Br) behaves as a quasi-linear system.

While spin and Ω propensity rules can explain the absence of *ns* states from

Ω_c	Ω	$^{2S+1}\Lambda$	Microconfiguration $[....]_c(\lambda m_s)_{Ryd}$
3/2	1	$^{1,3}\Pi$	$[1^+1^-\underline{1}^+]_c0^-$
,,	2	$^3\Pi$	$[1^+1^-\underline{1}^+]_c0^+$
½	1	$^{1,3}\Pi$	$[1^+1^-\underline{1}^-]_c0^+$
,,	$0^\pm$	$^3\Pi$	$\frac{1}{\sqrt{2}}([1^+1^-\underline{1}^-]_c0^- \pm [\underline{1}^+\underline{1}^-1^+]_c0^+)$

Table 3-6: A complete listing of Rydberg state microconfigurations for *ns* states in an (Ω_c, *l*, m_s) coupling scheme.

the two-photon spectrum, they also reduce the number of components of *np*, *nd* and *nf* transitions that are seen. In light of these propensities and the respective Rydberg state microconfigurations given in Table 3-7, only two *np* components based upon each ionic core are expected in the two-photon spectrum. The *np*;2 states are extremely weak with only the [1/2]5p;2 state being seen. The features comprising series of *np*;0 states are much more intense. Like the *np* states, two components of *nd* states based upon each core are expected upon examination of Rydberg state microconfigurations, given in Table 3-8. Unlike the *np* states, however, both Ω=2 and Ω=0 components of *nd* states are seen in the two-photon spectrum. Using a consideration of microconfigurations, the two-photon spectrum of methyl bromide can be understood relatively easily.

Extra features are seen in the three-photon spectrum of methyl bromide which

Ω_c	Ω	$^{2S+1}\Lambda$	Microconfiguration $[....]_c(\lambda m_s)_{Ryd}$
3/2	2	$^{1,3}\Delta$	$[1^+1^-\underline{1}^+]_c1^-$
,,	1	$^{1,3}\Pi$	$[1^+1^-\underline{1}^+]_c0^-$
,,	$0^\pm$	$^{1,3}\Sigma^\pm$	$\frac{1}{\sqrt{2}}([1^+1^-\underline{1}^+]_c1^- \pm [\underline{1}^+\underline{1}^-1^-]_c1^+)$
,,	3	$^3\Delta$	$[1^+1^-\underline{1}^+]_c1^+$
,,	2	$^3\Pi$	$[1^+1^-\underline{1}^+]_c0^+$
,,	1	$^3\Sigma^-$	$[\underline{1}^+\underline{1}^-1^-]_c1^-$
½	2	$^{1,3}\Delta$	$[1^+1^-\underline{1}^-]_c1^+$
,,	1	$^{1,3}\Pi$	$[1^+1^-\underline{1}^-]_c0^+$
,,	$0^\pm$	$^{1,3}\Sigma^\pm$	$\frac{1}{\sqrt{2}}([1^+1^-\underline{1}^-]_c1^+ \pm [\underline{1}^+\underline{1}^-1^+]_c1^-)$
,,	1	$^3\Delta$	$[1^+1^-\underline{1}^-]_c1^-$
,,	1	$^3\Sigma^-$	$[\underline{1}^+\underline{1}^-1^+]_c1^+$
,,	$0^\pm$	$^3\Pi$	$\frac{1}{\sqrt{2}}([1^+1^-\underline{1}^-]_c0^- \pm [\underline{1}^+\underline{1}^-1^+]_c0^+)$

Table 3-7: A complete listing of Rydberg state microconfigurations for *np* states in an (Ω_c, *l*, m_s) coupling scheme.

Ω_c	Ω	$^{2S+1}\Lambda$	Microconfiguration $[....]_c(\lambda m_s)_{Ryd}$
3/2	3	$^{1,3}\Phi$	$[1^+1^-\underline{1}^+]_c2^-$
,,	2	$^{1,3}\Delta$	$[1^+1^-\underline{1}^+]_c1^-$
,,	1	$^{1,3}\Pi$	$[1^+1^-\underline{1}^+]_c0^-$
,,	1	$^{1,3}\Pi$	$[\underline{1}^+\underline{1}^-1^+]_c2^-$
,,	$0^\pm$	$^{1,3}\Sigma^\pm$	$\frac{1}{\sqrt{2}}([1^+1^-\underline{1}^+]_c\underline{1}^- \pm [\underline{1}^+\underline{1}^-1^-]_c1^+)$
,,	3	$^3\Delta$	$[1^+1^-\underline{1}^+]_c1^+$
,,	2	$^3\Pi$	$[1^+1^-\underline{1}^+]_c0^+$
,,	1	$^3\Sigma^-$	$[\underline{1}^+\underline{1}^-1^-]_c1^-$
,,	$0^\pm$	$^3\Pi$	$\frac{1}{\sqrt{2}}([1^+1^-\underline{1}^+]_c\underline{2}^+ \pm [\underline{1}^+\underline{1}^-1^-]_c2^-)$
½	3	$^{1,3}\Phi$	$[1^+1^-\underline{1}^-]_c2^+$
,,	2	$^{1,3}\Delta$	$[1^+1^-\underline{1}^-]_c1^+$
,,	1	$^{1,3}\Pi$	$[1^+1^-\underline{1}^-]_c0^+$
,,	$0^\pm$	$^{1,3}\Sigma^\pm$	$\frac{1}{\sqrt{2}}([1^+1^-\underline{1}^-]_c\underline{1}^+ \pm [\underline{1}^+\underline{1}^-1^+]_c1^-)$
,,	2	$^3\Phi$	$[1^+1^-\underline{1}^-]_c2^-$
,,	2	$^3\Pi$	$[\underline{1}^+\underline{1}^-1^+]_c2^+$
,,	1	$^3\Delta$	$[1^+1^-\underline{1}^-]_c1^-$
,,	1	$^3\Sigma^-$	$[\underline{1}^+\underline{1}^-1^+]_c1^+$
,,	$0^\pm$	$^3\Pi$	$\frac{1}{\sqrt{2}}([1^+1^-\underline{1}^-]_c0^- \pm [\underline{1}^+\underline{1}^-1^+]_c0^+)$

Table 3-8: A complete listing of Rydberg state microconfigurations for *nd* states up to Ω=3 in an (Ω_c, *l*, m_s) coupling scheme.

are either very weak or absent from the two-photon spectrum. Polarisation studies indicate that these have Ω=1 which confirms that Rydberg transitions in methyl bromide follow the propensity rules already seen for those of the diatomic halogens[1,2]. Upon examination of state microconfigurations, it can be seen that there are sufficient possible transitions to states having some singlet character with Ω=1 to

Ω_c	Ω	$^{2S+1}\Lambda$	Microconfiguration $[....]_c(\lambda m_s)_{Ryd}$
3/2	3	$^{1,3}\Phi$	$[1^+1^-\underline{1}^+]_c2^-$
,,	2	$^{1,3}\Delta$	$[1^+1^-\underline{1}^+]_c1^-$
,,	2	$^{1,3}\Delta$	$[\underline{1}^+\underline{1}^-1^-]_c3^+$
,,	1	$^{1,3}\Pi$	$[1^+1^-\underline{1}^+]_c0^-$
,,	1	$^{1,3}\Pi$	$[\underline{1}^+\underline{1}^-1^+]_c2^-$
,,	$0^\pm$	$^{1,3}\Sigma^\pm$	$\frac{1}{\sqrt{2}}([1^+1^-\underline{1}^+]_c\underline{1}^- \pm [\underline{1}^+\underline{1}^-1^-]_c1^+)$
,,	3	$^3\Delta$	$[1^+1^-\underline{1}^+]_c1^+$
,,	2	$^3\Pi$	$[1^+1^-\underline{1}^+]_c0^+$
,,	1	$^3\Sigma^-$	$[\underline{1}^+\underline{1}^-1^-]_c1^-$
,,	1	$^3\Delta$	$[\underline{1}^+\underline{1}^-1^-]_c3^-$
,,	$0^\pm$	$^3\Pi$	$\frac{1}{\sqrt{2}}([1^+1^-\underline{1}^+]_c\underline{2}^+ \pm [\underline{1}^+\underline{1}^-1^-]_c2^-)$
½	3	$^{1,3}\Phi$	$[1^+1^-\underline{1}^-]_c2^+$
,,	2	$^{1,3}\Delta$	$[1^+1^-\underline{1}^-]_c1^+$
,,	2	$^{1,3}\Delta$	$[\underline{1}^+\underline{1}^-1^+]_c3^-$
,,	1	$^{1,3}\Pi$	$[1^+1^-\underline{1}^-]_c0^+$
,,	$0^\pm$	$^{1,3}\Sigma^\pm$	$\frac{1}{\sqrt{2}}([1^+1^-\underline{1}^-]_c\underline{1}^+ \pm [\underline{1}^+\underline{1}^-1^+]_c1^-)$
,,	3	$^3\Gamma$	$[1^+1^-\underline{1}^-]_c3^-$
,,	3	$^3\Delta$	$[\underline{1}^+\underline{1}^-1^+]_c3^+$
,,	2	$^3\Phi$	$[1^+1^-\underline{1}^-]_c2^-$
,,	2	$^3\Pi$	$[\underline{1}^+\underline{1}^-1^+]_c2^+$
,,	1	$^3\Delta$	$[1^+1^-\underline{1}^-]_c1^-$
,,	1	$^3\Sigma^-$	$[\underline{1}^+\underline{1}^-1^+]_c1^+$
,,	$0^\pm$	$^3\Pi$	$\frac{1}{\sqrt{2}}([1^+1^-\underline{1}^-]_c0^- \pm [\underline{1}^+\underline{1}^-1^+]_c0^+)$

Table 3-9: A complete listing of Rydberg state microconfigurations for *nf* states up to Ω=3 in an (Ω_c, *l*, m_s) coupling scheme.

account for the extra features. It is surprising, however, that all these additional features correspond to states with Ω=1 and that none are due to Ω=3 states. While

the [3/2]5p;3 state is of pure triplet character, there are *nd*;3 and *nf*;3 states with singlet character. Since, these transitions are allowed by the selection and propensity rules, selective predissociation is one possible explanation for their absence which cannot be discounted.

3.5.3 The Possibility of *nf* Series in the Two-Photon Spectrum

Unlike homonuclear diatomic molecules where symmetry selection rules are more restrictive, transitions to *nf* states are allowed in the two-photon spectrum of methyl bromide. Given that the an *nf* state in methyl bromide has a lower principal quantum number than the equivalent *nd* state occurring in the same energy region, the transition strength for the former should be greater than that of the latter. Hence, *nf* states should dominate the two-photon spectrum of methyl bromide like they do in its three-photon spectrum. This would mean that features assigned to members of *nd* series with $n > 5$ may in fact be due to *nf* series. There are some features are apparent to lower energy of the [3/2]5d cluster in the two-photon spectra of both CH_3Br and CD_3Br which might be assigned to [3/2]4f;1 and [3/2]4f;1′ states. The features assignable to [3/2]4f states are much weaker than those assigned to [3/2]5d states. While this might confirm that the two-photon spectrum of methyl bromide is dominated by *nd* states, it must be remembered that transitions with $\Delta\Omega=1$ are very weak in the two-photon spectrum of molecular bromine[1]. However, comparison of the [3/2]5d;0 and [3/2]4d;0 origin band intensities should establish whether *nf* or *nd* series are dominant. The 4d cluster has no *(n-1)f* counterpart while the features assigned to the [3/2]5d cluster might be due to states comprising the [3/2]4f cluster. Whereas in the three-photon spectrum, the [3/2]4f;1 band is far more intense than the [3/2]4d;1 one, this type of behaviour is not apparent in the two-photon spectrum. Thus, on intensity grounds, there is little to challenge the *nd* assignment.

However, a consideration of microconfigurations reveals that, for *nf* states, two $\Omega=2$ states and one $\Omega=0$ state based upon each ionic core are expected in the two-photon spectrum, upon examination of Table 3-9. While there is little evidence for additional series of $\Omega=2$ states in the two-photon spectrum of CH_3Br, there are

additional features, displaying polarisation behaviour typical of Ω=1 or Ω=2 states, seen in the spectrum of CD_3Br where features due to [3/2]5d;2 and [3/2]6d;2 states are expected. Also, the intensity of the feature assigned to the [3/2]7d;2 state in Figure 3-11 is much greater than expected. The majority of the extra features could be explained by their assignment to [3/2]*nd*;2 and [3/2]*nf*;2 states. This would also explain the anomalous intensity of the feature assigned to a [3/2]7d;2 state. All this suggests that features due to *nf* states are apparent in the two-photon spectrum of methyl bromide. Nevertheless, there is little evidence on intensity grounds to suggest that transitions to *nf* states dominate the two-photon spectrum of methyl bromide.

3.5.4 Comparison of the Assignments of the One-, Two- and Three-Photon Spectra

The one-, two- and three-photon spectra of methyl bromide are each dominated by different series. As noted earlier, there is some disparity between the assignments of Causley and Russell[6] and those of Baig et al.[8] Given the additional information available from multiphoton spectroscopy and the work on the diatomic halogens, it may be possible to reconcile both sets of assignments. Using a comparison between the data of Causley and Russell[6] and the two-photon data from this work, features coinciding on both spectra can be assigned to lower energy *nd*;0 and *np*;0 states and these are detailed in Table 3-10. The presence of *ns*;1 states in the three-photon spectrum confirms the altered assignments even though the features arising from transitions to *ns*;1 states are apparently absent from the VUV spectrum. The majority of the remaining features in Causley and Russell's VUV[6] spectrum fit in with being lower members of Baig et al.'s *nd* series[8]. These can be said to be members of an *nd*;1′ series and will be labelled as such for the remainder of this discussion. These *np*;0, *nd*;0 and *nd*;1′ assignments reconcile the assignments of the VUV spectra of CH_3Br.

While multiphoton spectroscopy has helped to reconcile the two differing interpretations of VUV spectrum, all the features seen in this spectrum should also

appear in the three-photon spectrum and vice versa. However, series with Ω=1 are apparent in the three-photon spectrum that are not seen in the VUV spectrum and vice versa. The prime example of this is the dominant *nf*;1 series but the absence of these features can be explained if *l* remains a good quantum number. The absence of features arising from transitions to *nd*;1 and *ns*;1 states in the VUV spectrum can be explained if one-photon transitions to these states are too weak to be seen against the

Electronic Assignments of Causley and Russell[6]	Band Positions cm^{-1}	Altered Assignments in Light of This Work
[3/2]5s	56111	[3/2]5s;1
[1/2]5s	59158	[1/2]5s;1
[3/2]5p	66003	[3/2]5p;0
[1/2]5p	68659	[1/2]5p;0
[3/2]4d	70083	[3/2]4d;1
[3/2]6s	72152	[3/2]4d;1′
[1/2]4d	72957	[3/2]4d;0
[1/2]6s	74687	[1/2]4d;1′
[3/2]6p	75822	[1/2]4d;0
[3/2]7s	77871	[3/2]5d;1′
[3/2]4f	78157	[3/2]5d;2
[1/2]6p	78372	[3/2]5d;0
[3/2]7p	79544	[3/2]7p;0
[1/2]7s	80427	[1/2]5d;1′
[3/2]8s	80511	[3/2]6d;1′
[1/2]4f	80758	[3/2]6d;0
[3/2]8p	81257	[3/2]8p;0
[3/2]9s	81869	[3/2]7d;1′
[1/2]7p	82050	[3/2]7d;0

Table 3-10: Features in the VUV spectrum of Causley and Russell[6] reassignment in light of the two- and three-photon data presented in this work.

others mentioned previously, depending upon the brightness of the VUV source. The absence of *nd*;1′ series from the two-photon spectrum can be easily explained but its absence from the three-photon is less clear. However, transitions to *nd*;1 states are also weak and this may be due to predissociation as suggested by the appearance of the band assigned to the [3/2]4d;1 state. Even with dominant *nf*;1 series, at least the first members of the *nd*;1′ series should be seen but are not. Given *nd*;1′ states must be sufficiently long-lived and have at least some singlet character to dominate the VUV spectrum, the only other possible explanation is destructive interference between different three-photon excitation pathways. Since the three-photon spectrum is dominated by Ω=1 states, this seems somewhat unusual.

3.6 Conclusion

Multiphoton Rydberg transitions in methyl bromide have been assigned. The two-photon spectrum is seen to be dominated by *nd* states with shorter *np* series also being seen. Only the first *ns* cluster is seen. The similarities between the two-photon spectra of methyl bromide and molecular bromine[1] aid the assignment of the former. The three-photon spectrum comprises of transitions to states already accessed in the two-photon spectrum along with additional features displaying three-photon polarisation behaviour typical of transitions to Ω=1 states. The three-photon spectrum is seen to be dominated by *nf*;1 series. Other features with similar polarisation behaviour are assigned to *ns*;1, *np*;1 and *nd*;1 states. All of the assignments are aided both by polarisation data and a comparison with the equivalent spectra of the diatomic halogens[1,2]. In light of this study, a more consistent understanding of the VUV spectrum would involve assignments to 5s, *np*;0, *nd*;0 and *nd*;1′ states. The results of this study call for a complete re-appraisal of the multiphoton spectra of methyl iodide and methyl chloride which are dealt with in the next chapter.

3.7 References

1. R. J. Donovan, A. C. Flexen, K. P. Lawley and T. Ridley, *Chem. Phys.*, **1998** 226 217.
2. R. J. Donovan, A. C. Flexen, K. P. Lawley, R. R. J. Maier, A. Mank and T. Ridley, *to be submitted.*
3. T. Ridley, K. P. Lawley, R. J. Donovan and A. J. Yencha, *Chem. Phys.*, **1990** 148 315.
4. J. L. Tech, *J. Res. Nat. Bur. Stand.*, **1963** 67A 505.
5. P. Hochmann, P. H. Templet, H-T. Wang and S. P. McGlynn, *J. Chem. Phys.*, **1975** 62 2588
6. G. C. Causley and B. R. Russell, *J. Chem. Phys.*, **1975** 62 848.
7. W. S. Felps, P. Hochmann, P. Brint and S. P. McGlynn, *J. Mol. Spectrosc.*, **1976**, 59, 355.
8. M. A. Baig, J. Hormes and J. P. Connerade, *J. Phys. B: At. Mol. Phys.*, **1982** 15 L5.
9. M. R. Dobber, W. J. Buma and C. A. de Lange, *J. Chem. Phys.*, **1993** 99 836.
10. M. G. Szarka, D. S. Green, D. T. Cramb and S. C. Wallace, *J. Phys. Chem. A*, **1997** 101 1818.
11. K. P. Lawley, T. Ridley, Z. Min, P. J. Wilson, M. S. N. Al-Kahali and R. J. Donovan, *Chem. Phys.*, **1995** 197 37.
12. A. Strobel, I. Fischer, A. Loschmidt, K. Müller-Dethlefs and V. E. Bondybey, *J. Phys. Chem.*, **1994** 98 2024.
13. Y-F. Zhu and E. R. Grant, *J. Phys. Chem.*, **1993** 97 9582.
14. J. L. Ragle, I. A. Stenhouse, D. C. Frost and C. A. McDowell, *J. Chem. Phys.*, **1970** 50 178.
15. A. Gedanken and M. D. Rowe, *Chem. Phys. Lett.*, **1975** 34 39.
16. R. G. Bray and R. M. Hochstrasser, *Mol. Phys.*, **1976** 31 1199.
17. J. P. Berger, J. Baker and S. Couris, *J. Chem. Phys.*, **1996** 105 6147.
18. R. N. Dixon, J. M. Bayley and M. N. R. Ashfold, *Chem. Phys.*, **1984** 84 21.

19. G. C. Nieman, *J. Chem. Phys.*, **1981** 75 584.

20. S. H. Ashworth and J. M. Brown, *An Atlas of Optogalvanic Transitions in Neon*, CLRC Rutherford Appleton Laboratory, 1991.

21. M. H. M. Janssen, M. Dantus, H. Guo and A. H. Zewail, *Chem. Phys. Lett.*, **1993** 214 281.

22. S. Couris, P. Agapaki and P. Brint, *Laser Chem.*, **1993** 13 151

23. E. N. Ofako and E. Whittle, *Int. J. Chem. Kin.*, **1975** 7 287.

24. J. A. Blush, P. Chen, R. T. Wiedmann and M. G. White, *J. Chem. Phys.*, **1993** 98 3557.

25. H. Hotop and J. C. Lineberger, *J. Phys. Chem. Ref. Data*, **1985** 14 731.

26. R. Bersohn and M. Shapiro, *J. Chem. Phys.*, **1981**.

27. T. Ishiwata, T. Hara, K. Obi and I. Tanaka, *J. Chem. Phys.*, **1987** 87 2513.

Chapter 4

Re-analysis and Extension of the Multiphoton Spectra of Methyl Iodide and Methyl Chloride

4.1 Introduction

In the previous chapter, the multiphoton Rydberg spectra of methyl bromide were analysed in light of the previous re-assignment of the spectra of the halogens and interhalogens[1,2]. Because of the similarities in the electronic structures of methyl bromide, methyl iodide and methyl chloride, their Rydberg states can be described in a like manner, that is, using the description introduced in the preceding chapter. Moreover, the similarity of electronic structures has previously proved useful in understanding the spectra of the halogens and interhalogens[1,2]. Also, the same propensity rules were seen to apply in all the halogens and interhalogens studied. As described in the previous chapter, these propensity rules are also applicable to Rydberg transitions in methyl bromide. In this chapter, the trends described already for methyl bromide will be used to gain an understanding of the Rydberg spectroscopy of methyl iodide and methyl chloride. However, the two- and three-photon spectra of methyl iodide[3] and parts of those of methyl chloride[4] have been studied previously but the assignment of the observed features is incompatible with the assignment of the spectra of methyl bromide. Thus, these assignments will be reconsidered in light of the newly presented polarisation data for both molecules which form the subject of this chapter and revised as necessary. The selection rules governing the polarisation behaviour of multiphoton transitions has been discussed already in the previous chapter.

Since methyl iodide is a model system for the study of the spectroscopy and reaction dynamics of a polyatomic molecule, it is especially important to extend the system of assignments used for the REMPI spectra of methyl bromide to those of methyl iodide. Also, unlike either methyl bromide or methyl chloride, the first two ionisation energies of methyl iodide have been determined using ZEKE-PFI PES[5] to be 76934±1 cm^{-1} and 81983 cm^{-1} for the $^2E_{3/2}$ and $^2E_{1/2}$ ion states, respectively. Thus, this provides a further opportunity for confirming that any conclusions based upon polarisation studies are energetically consistent.

In the case of methyl chloride[3], the REMPI study was not complete in that it did not extend to the first ionisation limit. Thus, in this study, the two- and three-photon spectra are extended to higher energy, up to the first ionisation limit in the case of the two-photon spectrum. Another possibility arising in this study is the measurement of a reliable value for the first ionisation energy. The only previous values available were measured using techniques such as conventional photoelectron spectroscopy, electron impact studies and extrapolation from Rydberg series. The values obtained from these techniques have quite large uncertainties. However, given that information from studies of the multiphoton spectroscopy of methyl bromide and methyl iodide can be used to aid the assignment of the equivalent spectra of methyl chloride, the measurement of accurate values for the ionisation limits is not as crucial as if the molecule was studied in isolation. Even so, an improved value for the first ionisation energy is suggested as it is of some use in assigning the spectra.

The two- and three-photon REMPI spectra of methyl iodide and methyl chloride are reviewed and extended. It will be seen that there are great similarities between the multiphoton spectra of the different methyl halides discussed in this and the preceding chapters and that where differences occur, they do not affect the overall understanding of the spectra. Although this study is largely concerned with the electronic assignment of the observed multiphoton spectra, some vibrational assignments are made where necessary. Previous assignments of the VUV absorption

spectra will also be discussed in light of the current work and some re-assignments may be suggested for the observed features.

4.1.1 Previous Work Relating to Methyl Iodide

Of the methyl halides discussed in this chapter and the one immediately preceding it, it is the higher excited states of CH_3I that have been the subject of the most attention since they were first examined by Price[6] over a half-century ago using VUV excitation. It would also appear to give rise to a richer VUV spectrum than either methyl bromide or methyl chloride and also contains the sharpest features.

Consistent with the other methyl halides, its UV spectrum is dominated by a broad absorption band[7] between 230 nm and 300 nm which is due to transitions to three repulsive valence states. Dissociation of these excited states has been subject of numerous studies. One of the more recent of these[8] concluded that the transition to the $^3Q_0$ state is much stronger than those to the $^3Q_1$ and $^1Q_1$ states than was considered previously[7].

To higher energy of the continuum UV band lie features which are due to members of the 6s cluster. These and higher energy Rydberg states in the VUV absorption spectrum of CH_3I were re-investigated by McGlynn and co-workers[9-12]. The earliest[9] of these studies, which concerned the spectrum recorded at medium resolution, resulted in the assignment of *ns* and *np* series converging on both spin-orbit ionisation limits along with the assignment of features to [3/2]5d and [1/2]5d states. These assignments were arrived at by a comparison of the quantum defects of methyl iodide, methyl bromide and methyl chloride aided by a correlation with quantum defects of the relevant rare gases. In a subsequent paper[10], an analysis of the medium resolution spectrum[9] reported earlier using Single Channel Quantum Defect Theory (SQDT) in conjunction with a comparison of the spectra of hydrogen iodide and xenon was used to extend the previous assignments to higher energy. It was found that *ns* and *np* series were only observed up to n=11. *nd* series were also assigned and found to continue up to the first and second ionisation limits. One point

to bear in mind when considering these assignments is that SQDT does not include electronic, vibronic or rovibronic interactions which may perturb the observed spectrum and invalidate the assumption that the Rydberg states of CH_3I are of a quasi-atomic nature which is inferred as a result of the comparison with atomic xenon. The first hint that the Rydberg states of methyl iodide are not truly atomic-like is the presence of *np* series in the VUV spectrum. Further theoretical consideration of the VUV spectrum involving Multichannel Quantum Defect Theory (MQDT) is necessary to take into account not only the molecular character of these Rydberg states. Rydberg states can be displaced though interactions with other Rydberg states and valence electronically excited states. This type of behaviour cannot be modelled using SQDT which excludes excited state interactions. However, the resolution of this VUV spectrum was insufficient for MQDT analysis.

The earlier medium resolution work[9,10] was followed by a re-examination[11] of the VUV spectrum recorded with much higher spectral resolution using a synchrotron radiation source. As in the medium resolution spectrum, members of *ns* and *np* series with $n \leq 11$ were observed. Again, the spectrum was seen to be dominated by *nd* series converging on both ionisation limits which were extended in the higher resolution spectrum. By extrapolation from the *nd* series, the $^2E_{3/2}$ and $^2E_{1/2}$ ionisation limits were determined to be 76930±1 cm^{-1} and 81979±1 cm^{-1}, respectively. This was followed by an MQDT analysis of the higher resolution spectrum[12] which identified a further [3/2]*nd* series. In this study, electronic interactions were included but it was found that a consistent analysis could be obtained without the inclusion of vibrational or rotational interactions. No consideration of the effects of predissociation or autoionisation was invoked in the analysis.

The vibrational structure of the 6s cluster in the VUV has been examined in great detail[13]. It has also been the subject of one- and two-colour REMPI studies[14-16]. The one-colour experiments were carried out with room temperature[14] and jet-cooled[15] samples. Three out of a possible four components are observed, that is, the [3/2]6s;1, [1/2]6s;0 and [1/2]6s;1 states are observed with the [3/2]6s;2 state

being too weak to be observed. Any vibrational structure, that was seen, was much weaker than the origin bands. Dobber et al.[3] re-examined the 6s cluster using REMPI-PES but also did not observe the origin band of the [3/2]6s;2 state.

In addition to the above, Dobber et al.[3] also extended the two-photon spectrum, with the aid of REMPI-PES to confirm their assignments and corrected some of the assignments made in the earlier room temperature work of Gedanken et al.[17] Dobber et al.[3] assigned their two-, three- and four-photon spectra to *ns* series and some components of the 6p cluster. These assignments were based mainly on energetic considerations with no polarisation studies being undertaken. However, the advantage of REMPI-PES is that it allows both the identification of the ionic core upon which a Rydberg state is based and the vibronic assignment of the feature in question. The assignments of the REMPI spectra of methyl iodide are reviewed here as this molecule is of such fundamental interest.

4.1.2 Previous Work Pertaining to Methyl Chloride

Like methyl bromide, the Rydberg states of methyl chloride have not been subject of as much attention as those of methyl iodide. Its UV spectrum[7] consists of a continuum absorption band centred about 193 nm with much sharper features due to Rydberg transitions extending from 165 nm to shorter wavelengths. The features due to Rydberg transitions seen in the one-photon spectrum are broader than those seen in the equivalent spectra of methyl bromide and methyl iodide. The most comprehensive of the earlier studies of the VUV spectrum of methyl chloride[6] resulted in its assignment to *ns* and *np* series with assignments to the first members of *nd* series. This study also concerned methyl iodide and methyl bromide and the assignments were arrived at in the manner described above in the discussion of previous work relating to methyl iodide. In a later study, Truch et al.[18] assigned the spectrum to *ns* and *np* series with the latter dominating but no *nd* assignments were made. Again, these assignments were made solely on energetic grounds but were in contrast to studies of the VUV spectra of methyl bromide[19] and methyl iodide[11] where the dominant transitions were assigned to *nd* states. The 4s cluster has been studied in

detail in the VUV by Felps et al.[13] but assignments were somewhat hampered by the small spin-orbit splitting and the larger bandwidths observed. There have been numerous other investigations of the VUV spectrum of methyl chloride but only those concerning assignments of the majority of features in the spectrum are considered here.

Like methyl iodide, methyl chloride has also been subject of REMPI studies[4]. Although the polarisation dependence of the observed features was reportedly studied, little reference was made to the results of these polarisation studies and the assignments were mainly justified on energetic grounds. Any features observed were attributed to *ns*, *np* and *nd* states in an assignment similar to that of Hochmann et al.[6] for the VUV spectrum. The most extensive REMPI study does not extend all the way up to the first ionisation limit but stops at about 83000 cm^{-1}. In this chapter, the previous assignments of the two- and three-photon spectra of methyl chloride are reviewed and the spectra extended to higher energy.

4.2 Additional Experimental Details

The (2+2), (2+1) and (3+1) REMPI spectra of methyl iodide and methyl chloride were recorded using radiation in the 280-510 nm region and in the 217-430 nm region, respectively. The molecular beam was produced by pulsing methyl iodide and methyl chloride seeded in helium through a nozzle. The total backing pressures used were typically 500-700 torr with the proportion of the total pressure due to the sample typically being 40% in the case of methyl iodide and 20% in the case of methyl chloride.

Because, at lower energy, the observed band systems in the spectra of methyl iodide and methyl chloride are more widely spaced than in methyl bromide, it is not as easy to determine the relative intensities of features due to different electronic states. Thus, one is referred to methyl bromide, discussed in the previous chapter, for an example of intensity distribution in a methyl halide Rydberg spectrum. This means that spectra are normalised to the square or the cube of the laser power only where

relative intensities of different features are sought and it is easy to do so reliably. Where polarisation behaviour is discussed, comparisons often are made between two spectra that are not power normalised. However, these comparisons still remain valid because both spectra concerned were recorded sequentially, thus ensuring that little or no change in dye laser power occurs between both scans. All tabulated band positions have been calibrated using transitions in atomic iodine[20] and atomic chlorine[21].

4.3 Two-Photon Spectroscopy of Methyl Iodide

Assignment	[3/2]			[1/2]		
	$\bar{\nu}$ / cm^{-1}	(n-δ)	ρ_2	$\bar{\nu}$ / cm^{-1}	(n-δ)	ρ_2
6s;0	~	~	~	54055	1.98	-
6s;1	~	~	~	54654	2.00	+
6p;2	58333	2.43	+	63492	2.44	+
6p;0	58926	2.47	-	64815	2.52	-
5d;0′	60687	2.60	-	~	~	~
5d;1	63030	2.81	~	~	~	~
5d; 2	64184	2.93	+	69042	2.91	+
5d; 0	64672	2.99	-	69540	2.97	-
6d; 2	70071	4.00	+	~	~	~
6d; 0	70210	4.04	-	~	~	~

Table 4-1: Electronic assignment of the two-photon spectrum of methyl iodide, CH_3I. The polarisation ratio, ρ_2, is denoted + where it equals 1.5 and - where it is less than 1. ~ indicates either the absence of a feature or that it was not studied. The $^2E_{3/2}$ and $^2E_{1/2}$ series limits[5] used for calculation of the above (n-δ) values are 76934 cm^{-1} and 81983 cm^{-1} respectively.

Long Rydberg series like those seen in the two-photon spectrum of methyl bromide cannot seen in the case of methyl iodide. This is because of the inability of two-photon transitions to compete efficiently with dissociation via one of the repulsive valence states at the first-photon level. In methyl iodide, coherent two-photon transitions must compete with one-photon dissociation over most of the two-photon spectrum. Therefore, for two-photon transitions to be observed, they must compete effectively with one-photon dissociation. However, transition strength decreases for successive members of a Rydberg series with n^3. The reduction in transition strengths with successive n means that, after a certain point, two-photon Rydberg transitions would no longer compete effectively with dissociation at the

first-photon level. This might well explain the consistent absence of Rydberg states with n>6 from the two-photon spectrum of methyl iodide.

In this section, the two-photon polarisation data of CH_3I are reported. The assignments of Dobber at al.[3] for the two-photon spectrum of CH_3I are reviewed and, in some cases, revised in light of this new data. Justification for some of these re-assignments comes, not only from a comparison with the multiphoton spectroscopy of methyl bromide, but also from polarisation studies of the three-photon spectrum discussed later. The electronic assignments of the two-photon spectrum following revision in light of polarisation studies are given in Table 4-1.

However, given the presence of repulsive valence states at the first photon level, it is surprising that no one-colour bound-free-bound transitions are observed. This is qualified by the polarisation behaviour of any features observed between 280 nm and 300 nm. A bound-free-bound transition would involve the sequential absorption of two photons. Given that one-photon transition strengths are not affected by changing the polarisation of the incoming light from linear to circular, this implies unity polarisation ratios. Not all the features occurring in this wavelength range exhibited this type of polarisation behaviour indicating that excitation to Rydberg states in this region occurs as a result of the simultaneous absorption of two photons.

4.3.1 Polarisation Behaviour of the [1/2]6s States.

Although the 6s cluster has been subject of exhaustive studies heretofore[13-16], even including a two-photon polarisation study[14], the polarisation behaviour of the origin bands of the [1/2]6s;0 and [1/2]6s;1 states is presented here because it can be used as a benchmark for interpreting that exhibited by higher Rydberg states of methyl iodide since the state assignments are certain with both components of the [1/2]6s cluster being seen. It should also help to validate the application of an (Ω_c, ω_{Ryd}) description to the Rydberg states of CH_3I. The spectra of the [1/2]6s;0 and

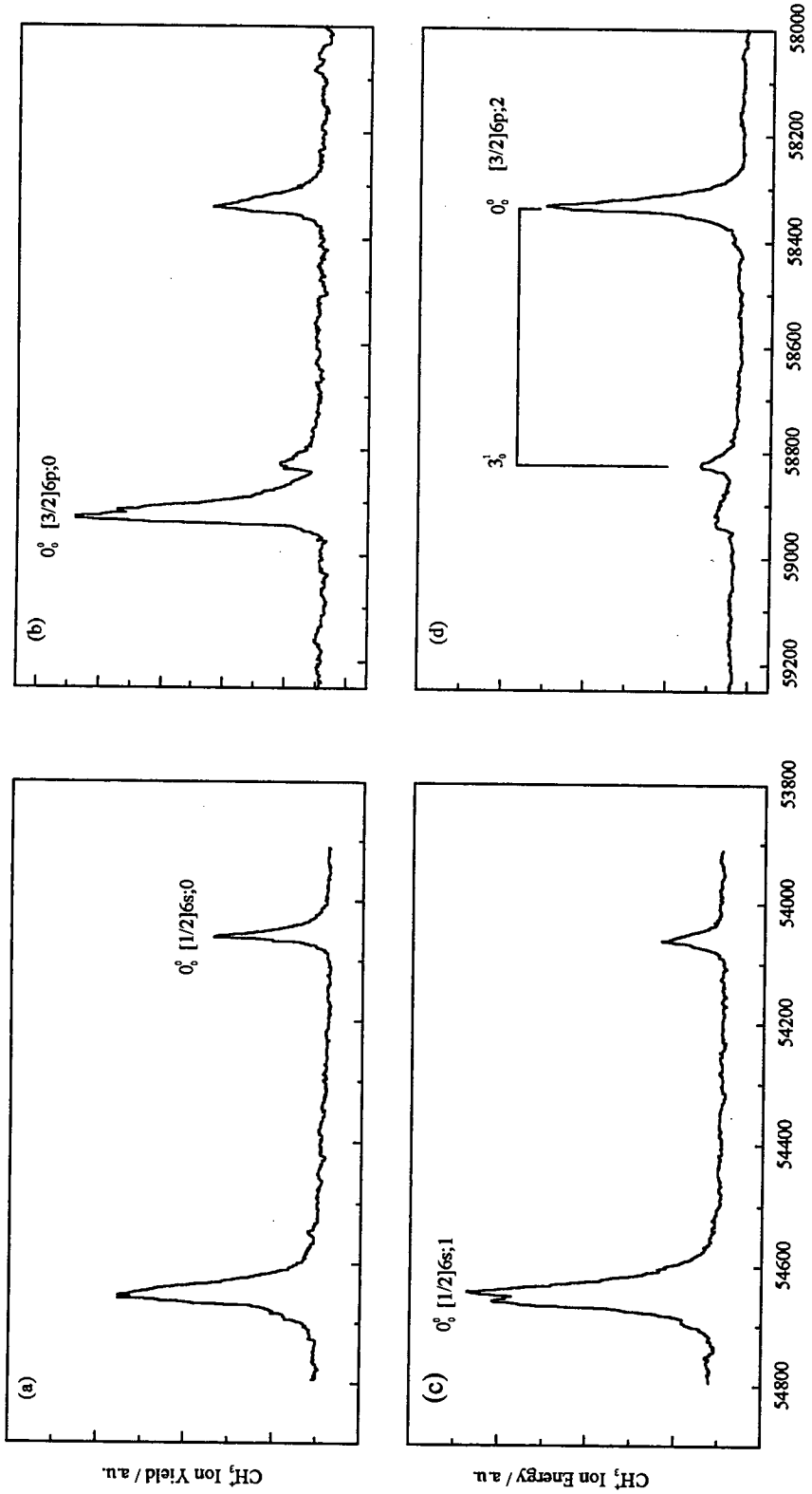

Figure 4-1: Two-photon polarisation behaviour of features arising from transitions to states comprising the [1/2]6s and [3/2]6p clusters in CH_3I. (a) and (c) depict the spectra recorded in the 53800-54900 cm^{-1} region with linearly and circularly polarised light, respectively. (b) and (d) depict spectra in the 58000-59250 cm^{-1} region also recorded using linearly and circularly polarised light, respectively. The overall intensity scales of figures depicting the same energy region, but with different polarisations of light, are the same.

[1/2]6s;1 origin bands recorded using linearly and circularly polarised light are depicted in Figure 4-1(a) and (c), respectively. As expected, based on what is seen for methyl bromide, the former feature has $\rho_2<1$ and the latter $\rho_2>1$. Therefore, the polarisation behaviour of the [1/2]6s cluster confirms the validity of using the same criteria in interpreting the polarisation behaviour of features in the multiphoton spectra of methyl iodide as used in the case of methyl bromide.

4.3.2 The 6p and [3/2]5d Clusters

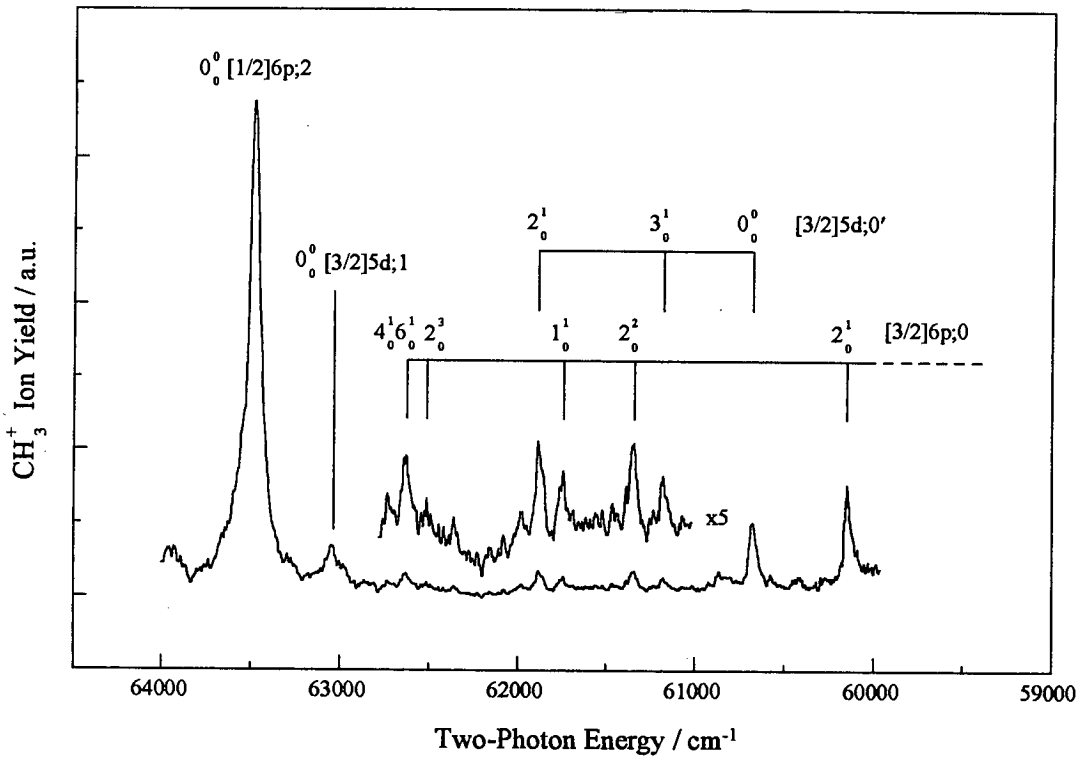

Figure 4-2: Two-photon spectrum of CH_3I in the 59000-64500 cm^{-1} region.

The polarisation behaviour of components of the [3/2]6p cluster is detailed in Figure 4-1(b) and (d). It is obvious that the origin band of the [3/2]6p;0 state is much less intense in the spectrum recorded with circularly polarised light. Hence, the assignment of an Ω-value of 0 is justified. However, there are two features depicted which do not decrease in intensity when excited with two circularly polarised photons. These belong to states with a non-zero Ω-value. Polarisation studies of the three-photon spectrum indicate that these are due to a [3/2]6p state with Ω=2.

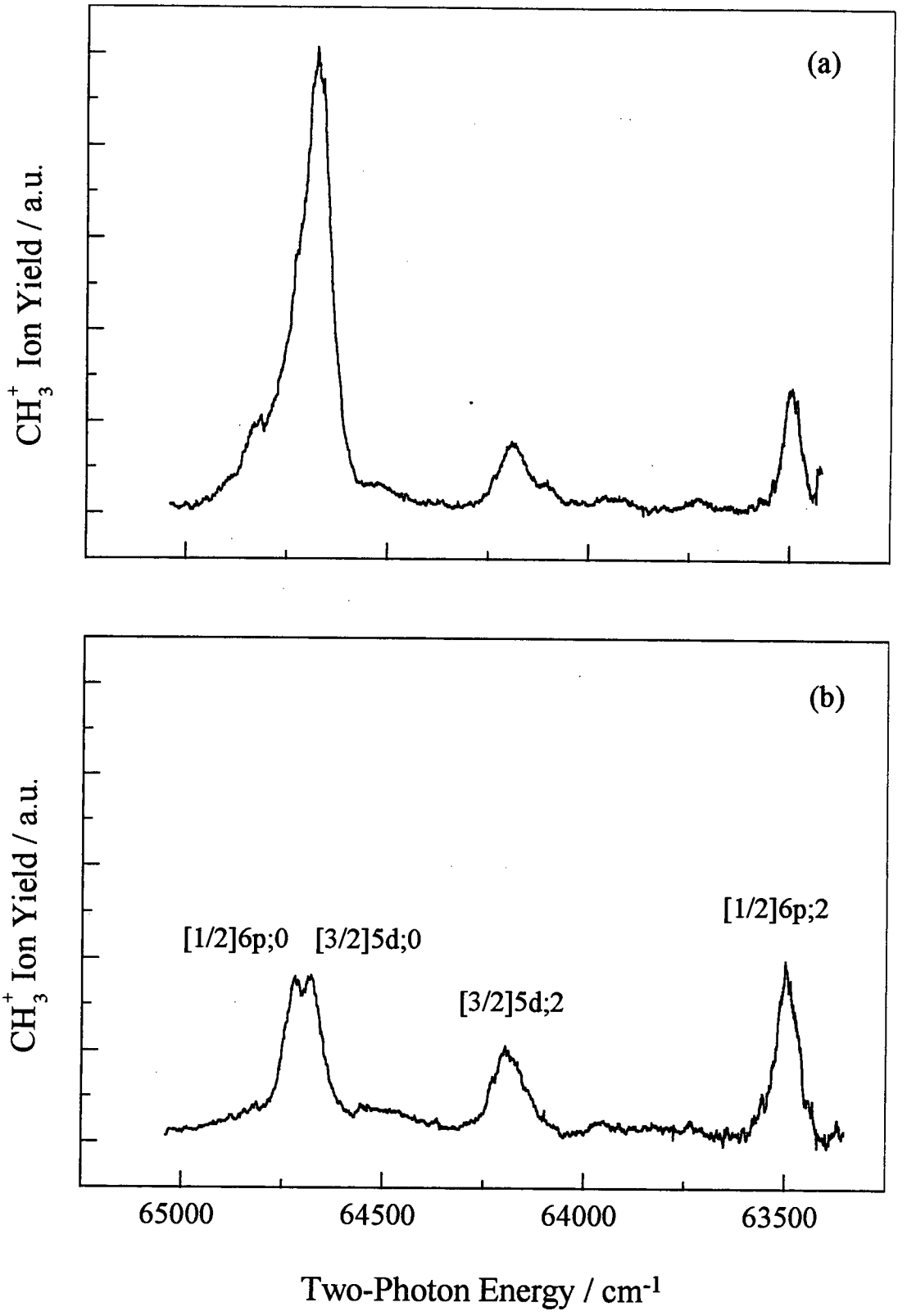

Figure 4-3: Two-photon spectra recorded with (a) linearly and (b) circularly polarised light depicting the polarisation dependence of the [1/2]6p;2, [3/2]5d;2, [3/2]5d;0 and [1/2]6p;0 states.

In addition to the two [3/2]6p states discussed already, Dobber et al.[3] assigned a group of weak features, depicted in Figure 4-2, to a further 6p state with an origin at 60687 cm^{-1}. From REMPI-PES studies it was concluded that this state was based upon the $^2E_{3/2}$ ionic core. From Table 4-1, the quantum defect corresponding to the origin band is seen to be much larger than the other *np* states placing it at the energetic boundary between [3/2]6p and [3/2]5d states, based on considerations of transitions in atomic iodine[20]. Also, this feature has a two-photon polarisation ratio less than unity, introducing the possibility that it might form part of the vibrational structure built upon the strong [3/2]6p;0 origin already discussed. However, the spacing between new origin and the [3/2]6p;0 origin does not fit any reasonable vibrational frequency or combination of frequencies built upon the latter. The additional origin might be due to another [3/2]6p;0 state. However, only two Ω=0 components are expected for the [3/2]6p cluster, one of mixed singlet-triplet character and the other of pure triplet character. Based upon these propensity rules, one might expect the higher energy [3/2]6p;0 state to give rise to more intense features. This is not the case here with the lower energy origin being the more intense. Although the energy orderings of Rydberg states may be disrupted by Rydberg~ion-pair interactions, a much more likely explanation is that the extra features are due to a [3/2]5d;0 state of pure triplet character. This is the assignment adopted here and the state labelled [3/2]5d;0′.

Figure 4-3 shows the two-photon polarisation behaviour of features in the 63500-65000 cm^{-1} region. Previously, the assignment of this region has proved somewhat contentious. Dobber et al.[3] corrected the previous assignment of Gedanken et al.[17] by re-assigning a band at 64672 cm^{-1}, previously assigned to the 6_0^1 vibronic transition built upon a [3/2]6p origin, to a [3/2]7s;1 origin. There are still some outstanding issues regarding these features that need to be addressed here. Aside from the re-assignment of 7s states to 5d states, the basis of which will be discussed later, only one of the expected two components of the [1/2]6p cluster has been assigned[3]. Three features are present in the 63500-65000 cm^{-1} region with appreciable intensity: one with polarisation behaviour typical of a state with Ω=0 and two assignable to

states with Ω=2, an assignment confirmed by three-photon polarisation studies. Two states with Ω=0, [1/2]6p;0 and [3/2]5d;0, are expected and these can be accounted for if features arising from transitions to both these states were overlapped. Dobber et al.[3] investigated the REMPI-PES of the feature at 64672 cm^{-1}, assigned here to [1/2]6p;0 and [3/2]5d;0 states, and the resulting photoelectron spectrum showed structure due to both the $^2E_{3/2}$ and $^2E_{1/2}$ ionic states. This confirms the assignment adopted here. The REMPI-PES of the features at 63492 cm^{-1} and 64148 cm^{-1} was also investigated and showed the former to arise from a state based upon the $^2E_{1/2}$ ionic core and that the latter is due to a state based upon the $^2E_{3/2}$ ionic core. Therefore, the feature at 63492 cm^{-1} is assigned to the singlet [3/2]6p;2 state and the one at 64148 cm^{-1} is assigned to the singlet [3/2]5d;2 state. Thus, in summary, the features formerly attributed to [3/2]7s;2 and [3/2]7s;1 states are now reassigned to

Assignment	Band Measurement cm^{-1}	Vibrational Spacing cm^{-1}
[3/2]6p;2 0_0^0	58333	0
[3/2]6p;2 3_0^1	58823	490
[3/2]6p;0 0_0^0	58926	0
[3/2]6p;0 3_0^1	59368	442
[3/2]6p;2 2_0^1	59580	1247
[3/2]6p;0 2_0^1	60161	1235
[3/2]5d;0' 0_0^0	60687	0
[3/2]6p;2 1_0^1	61186	2853
[3/2]6p;0 2_0^2	61349	2423
[3/2]6p;0 1_0^1	61748	2822
[3/2]5d;0' 2_0^1	61890	1203
[3/2]6p;0 2_0^3	62517	3591
[3/2]6p;0 $4_0^1 6_0^1$	62632	3706
[1/2]6p;2 0_0^0	63492	0
[1/2]6p;2 3_0^1	63958	466
[1/2]6p;2 3_0^2	64442	950
[1/2]6p;2 2_0^1	64719	1227

Table 4-2: Vibrational assignments of the 6p and 5d clusters cluster of CH_3I.

[3/2]5d;0, [1/2]6p;0 and [3/2]5d;2 states in light of polarisation studies. The reassignment of features attributed to *ns* states with n>6 will be discussed in more detail later.

A very weak band is observed 462cm^{-1} to the red of the [1/2]6p;2 origin as shown in Figure 4-2. This spacing is inconsistent with any ground state vibrational spacing and the band is too intense to be a vibrational transition built upon any of the observed [3/2]6p origins. On energetic grounds, it is most likely to be the origin of an additional [3/2]5d state, probably with Ω=1.

Figures 4-1 and 4-2 depict some vibrational structure built upon [3/2]6p and [3/2]5d origins although it is obvious from the figures that the electronic origin bands are much stronger than the vibrational structure built upon them. As in methyl bromide, the symmetric vibrations are most active. Also, the vibrational modes are defined in the same manner for all the methyl halides. Vibronic assignments of the 6p and [3/2]5d clusters are given in Table 4-2.

4.3.3 Further Comments Regarding *nd* Assignments.

As discussed in the previous section, the features attributed to [3/2]7s states by Dobber et al.[3] are now assigned to [3/2]5d states. The reasons supporting this re-assignment and that of higher energy features also previously assigned to *ns* states are discussed here. The polarisation behaviour depicted in Figure 4-3 and 4-4 is at odds with the original assignment to *ns* states. For example, it can be seen from Figure 4-3 that the feature previously assigned as the origin band of the [3/2]7s;1 has ρ<1. This polarisation behaviour indicates that this feature arises from a state with Ω=0. In an (Ω_c, ω_{Ryd}) coupling, a [3/2]7s;0 state cannot arise but an alternative possibility is that the feature is the origin band of a [3/2]5d;0 state which can arise in the (Ω_c, ω_{Ryd}) coupling limit.

In Figure 4-4, the polarisation behaviour of the transitions assigned to [1/2]7s

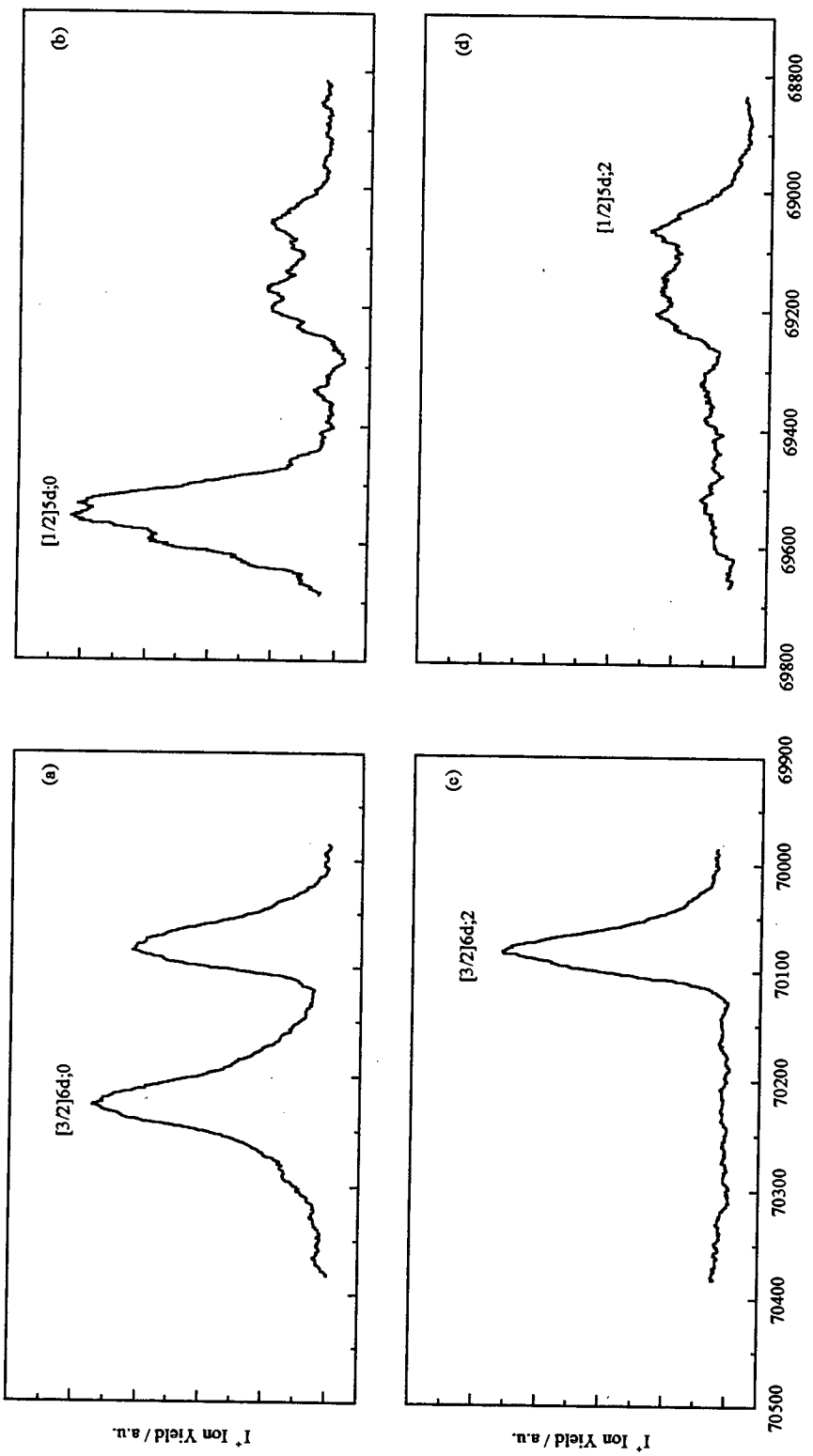

Figure 4-4: Two-photon spectra recorded with linearly and circularly polarised light depicting the polarisation behaviour of the [1/2]5d and [3/2]6d clusters. Panel (a) shows the spectrum of the [3/2]6d cluster recorded using linearly polarised light while panel (c) depicts the equivalent spectrum recorded using circularly polarised light. Panels (b) and (d) show the equivalent spectra for the [1/2]5d cluster. These spectra have been recorded in the I^+ ion channel because of interference by a CH_3 4p resonance in the CH_3^+ channel[24].

and [3/2]8s states by Dobber et al.[3] are shown. As before, REMPI-PES[3] was used to determine the ionic core of the Rydberg states giving rise to the respective features. Again, features assigned to states with Ω=1 are seen to possess polarisation ratios of less than unity. Clearly this requires the reassignment of these features to [1/2]5d;0 and [3/2]6d;0 states. This leaves us with the features previously assigned to the origin bands of the [3/2]7s;2, [1/2]7s;0 and [3/2]8s;2 states. It is obvious from Figure 4-4 that the band previously assigned to the [1/2]7s;0 state has $\rho_2 < 1$ which is again at odds with its original assignment. Thus, following the trend seen in methyl bromide, the features here which were previously assigned to [3/2]7s;2, [1/2]7s;0 and [3/2]8s;2 states are now reassigned to [3/2]5d;2, [1/2]5d;2 and [3/2]6d;2 states. These assignments are further strengthened by three-photon polarisation studies of the [3/2]5d cluster.

4.4 Three-Photon Spectroscopy of Methyl Iodide

In the (3+1) REMPI of methyl iodide, the majority of the features already seen in the two-photon spectrum are also observed. However, there are additional features apparent which are assigned to Ω=1 states following examination of their polarisation behaviour. This is similar to the situation regarding the three-photon spectrum of methyl bromide where transitions due to states with Ω=0, Ω=1 and Ω=2 are present and transitions with $\Delta\Omega$=3 are absent. However, the spectrum of CH_3I is curtailed due to the inability of three-photon transitions to efficiently compete with very strong two-photon 6s transitions which occur above 49500 cm^{-1}, that is, above 74250 cm^{-1} at the three-photon level. Thus, only the lower Rydberg states could be studied along with their polarisation behaviour. Also, in agreement with the two-photon spectrum, there would seem to be a greater degree of interaction between Rydberg states and valence or ion-pair states in methyl iodide than in methyl bromide. The spectral region investigated here using three-photon excitation is shown in Figure 4-5 and the electronic assignments detailed in Table 4-3.

However, several features unreported by Dobber et al.[3] have been seen in this study. The 6p cluster, not investigated using three-photon excitation by Dobber et

al.[3], is examined here using three-photon polarisation studies. Some features apparent in the CH_3^+ and I^+ ion channels concurrently have not been reported previously. These include 5d;1 and *ns*;1 resonances. Their simultaneous appearance in the aforementioned ion channels suggests that they arise in the parent molecule and not any fragments formed as a result of photodissociation. This fragmentation of the molecular ion is typical also of both methyl bromide and methyl chloride, the latter to be discussed later.

Band Measurement cm^{-1}	**Assignment**	**n-δ**		ρ_3
		$^2E_{3/2}$	$^2E_{1/2}$	
58022	[3/2]6p;1′	2.41	~	-
58308	[3/2]6p;2	2.43	~	+
58903	[3/2]6p;0	2.47	~	-
59527	[3/2]6p;1	2.51	~	-
59679	[3/2]6p;1	2.52	~	-
61530	[3/2]5d;1	2.67	~	-
61692	[3/2]5d;1	2.68	~	-
62041	[3/2]5d;1	2.71	~	-
63203	[1/2]6p;1′	~	2.42	-
63491	[1/2]6p;2	~	2.44	+
64173	[3/2]5d;2	2.93	~	+
64473	[1/2]6p;1	~	2.50	-
64680	[3/2]5d;0	2.99	~	-
64829	[1/2]6p;0	~	2.53	-
65699	[3/2]7s;1	3.13	~	-
66608	[1/2]5d;1	~	2.67	-
66943	[1/2]5d;1	~	2.70	-
69751	[3/2]4f;1	3.91	~	-
70225	[3/2]6d;0	4.04	~	-
70699	[3/2]8s;1	4.19	~	-
71017	[1/2]7s;1	~	3.16	-

Table 4-3: Assignments of the three-photon spectrum of CH_3I. Again (n-δ) values were calculated using the values for the ionisation limits obtained from ZEKE-PFI PES[5]. ρ_3, the three-photon polarisation behaviour is indicated by - if it is appreciably less than 2.5 and + if it is near 2.5.

Not all features are seen only in the CH_3^+ and I^+ ion channels but some also give rise to molecular ion signal as well. This is true of features comprising the [3/2]6p and [3/2]5d clusters and is quite unlike the situation in methyl bromide and

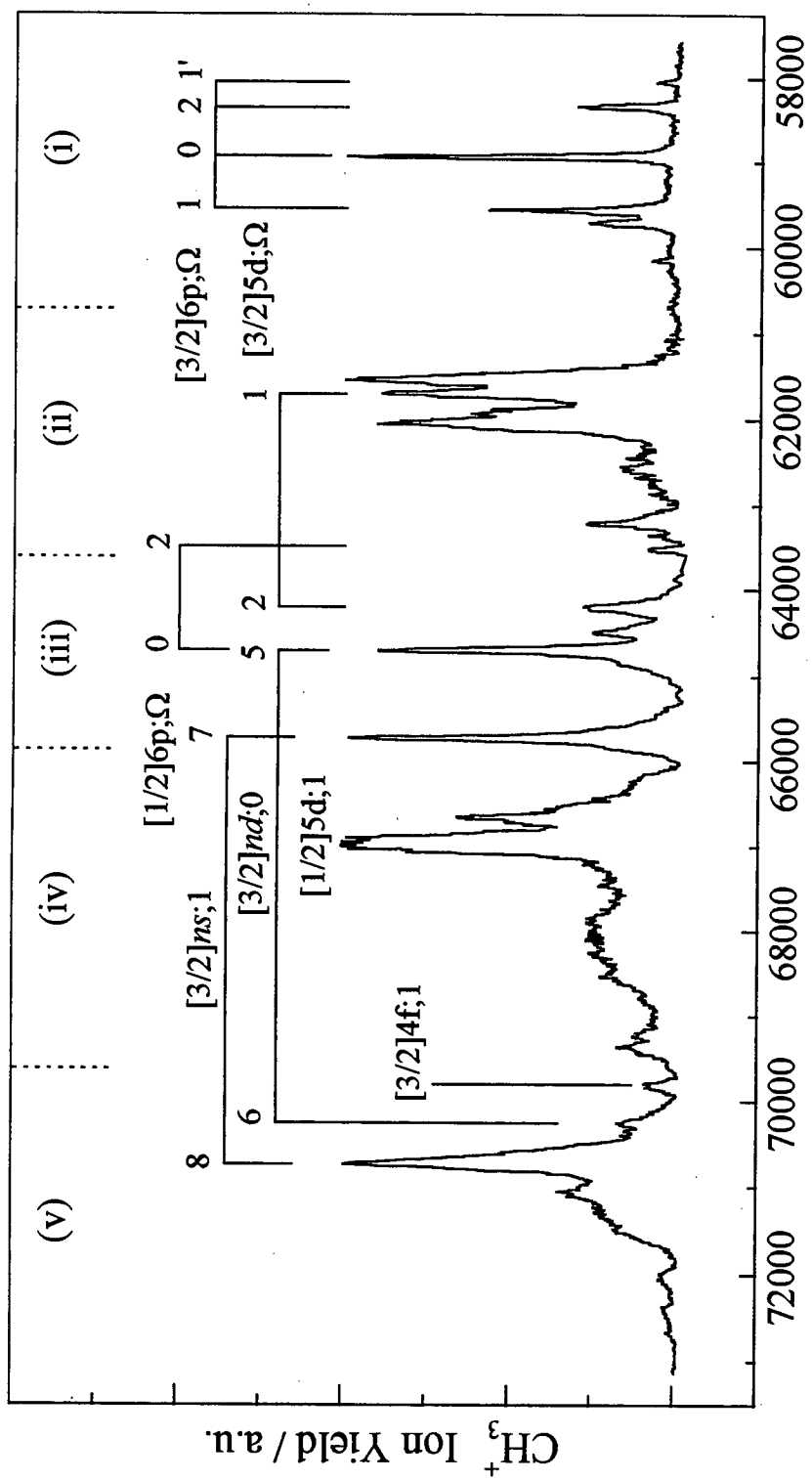

Figure 4-5: Composite plot detailing the three-photon spectroscopy of CH_3I. The component spectra have not been power normalised so caution is required when comparing the relative intensities of the observed features. The most intense feature in each spectrum is kept to the same intensity in this plot. The relevant laser dye regions have been demarcated at the top of the plot as follows: (i) Coumarin 307, (ii) Coumarin 102, (iii) Coumarin 47, (iv) Coumarin 120 and (v) Stilbene 3.

methyl chloride. In fact, features comprising the former cluster give stronger signals in the molecular ion channel than in the fragment channels. Since the ejected electron removes all excess energy in a REMPI process, the molecular ion is produced in its electronic ground state. Therefore, a further photon must be absorbed before fragmentation can occur. Sufficient energy is available for a one-photon dissociation of the molecular ion[23], even for the lowest energy resonances investigated in the three-photon spectrum of CH_3I. However, this energy corresponds to the dissociation limit of the electronic ground state of CH_3I^+ and transitions to vibrational levels of the electronic ground state of CH_3I^+ near this dissociation limit are absent from its photoelectron spectrum. Therefore, any fragmentation of the molecular ion must occur via its repulsive $\tilde{A}\ ^2A_1$ state. The $\tilde{A}$ band, due to the $\tilde{A}\ ^2A_1$ state, in the photoelectron spectrum[24] is centred about 100819 cm^{-1} and has a FWHM (Full Width at Half Maximum) of about 6049 cm^{-1}. The involvement of $\tilde{A}\ ^2A_1 \leftarrow \tilde{X}\ ^2E_{3/2}$ and $\tilde{A}\ ^2A_1 \leftarrow \tilde{X}\ ^2E_{1/2}$ transitions in the fragmentation of the molecular ion would best explain the differences in the mass spectra produced using different three-photon resonances. These comments are pertinent to the two-photon spectrum of methyl iodide also.

4.4.1 The [3/2]6p cluster

The three-photon polarisation behaviour of the [3/2]6p cluster is depicted in Figure 4-6. As in methyl bromide, all components of the cluster having at least some singlet character are seen. The assignment of features to a [3/2]6p;2 state in the two-photon spectrum is confirmed indisputably by their polarisation behaviour. However, two closely-spaced features are seen at 59527 cm^{-1} and 57679 cm^{-1} where a single feature due to the singlet [3/2]6p;1 state is expected. Both of these display the same polarisation behaviour. Either feature cannot be attributed a vibrational assignment built upon the [3/2]6p;0 origin even though their three-photon polarisation behaviour would be compatible with such an assignment. Also, the features of interest are absent from the two-photon spectrum but present in the VUV

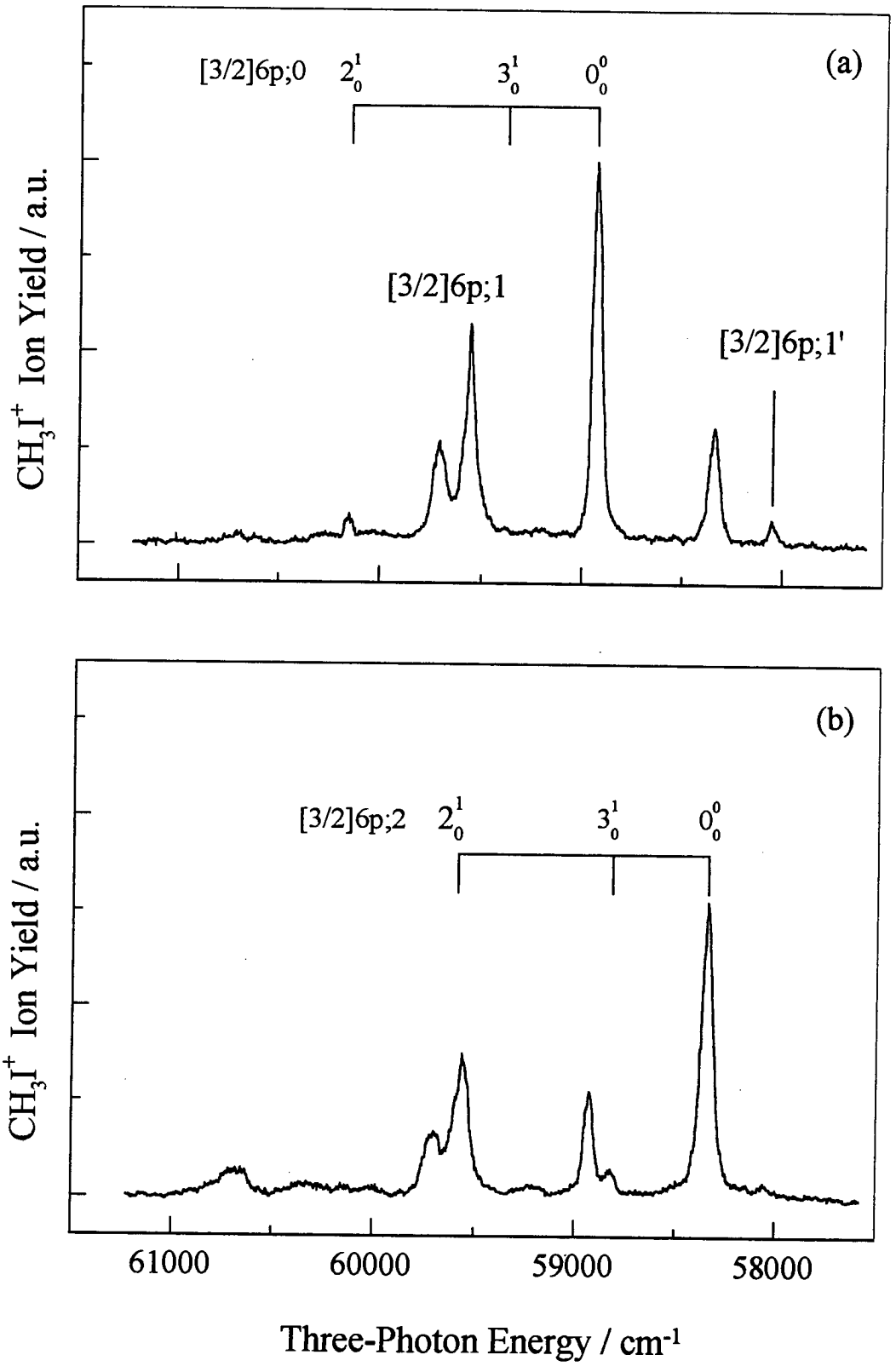

Figure 4-6: Three-photon polarisation behaviour of the [3/2]6p cluster of CH_3I. The spectrum recorded with linearly polarised light is depicted in panel (a) while panel (b) shows the spectrum of the same energy region recorded with circularly polarised light.

Ion-Pair	I.E. cm^{-1}	E.A. cm^{-1}	$D_0(H_3C\text{-}I)$ cm^{-1}	Threshold Energy cm^{-1}
$CH_3^+ (\tilde{X}\ ^1A_1') + I^- (^1S_0)$	79349 [25]	25003 [27]	19652 [29]	73998
$I^+ (^3P_2) + CH_3^- (\tilde{X}\ ^1A_1')$	84295 [20]	645 [28]	19652 [29]	103302
$CH_3^+ (\tilde{A}\ ^3E') + I^- (^1S_0)$	119047 [26]	25003 [27]	19652 [29]	113696

Table 4-4: Table of transition energies corresponding to three thermodynamic thresholds for ion-pair formation in methyl iodide and the values used to calculate them. The references from which values are taken are indicated in square brackets.

spectrum[6]. Thus, they are more likely to be due to either one or two Ω=1 states. The energy separation between both features in question is 152 cm^{-1} which rules out any vibrational assignment built upon a [3/2]6p;1 origin being attributed to the second feature. However, this spacing raises the possibility of vibronic coupling with a nearby valence or ion-pair state. Upon comparison of the term values[30] of several ion-pair states dissociating to produce I^+ ($^3P_2$) and I^- ($^1S_0$) with the transition energy corresponding to this ion-pair threshold[2], 72062 cm^{-1}, a typical value for the dissociation energy of ion-pair states in I_2 is seen to be 30000 cm^{-1}. Taking this value for the dissociation energy of ion-pair states in methyl iodide and subtracting it from the values for the ion-pair thresholds, given in Table 4-4, gives predicted term values for ion-pair states in methyl iodide. Upon examination of these, it can be concluded that the only ion-pair state occurring in the 59000-60000 cm^{-1} region in methyl iodide is the first-tier ion pair state, having a term value of about 43988 cm^{-1}. This has Ω=0 and therefore cannot couple homogeneously with a 6p;1 state. However, since Rydberg~valence interactions can occur also, the features at 59527 cm^{-1} and 59679 cm^{-1} are assigned to the singlet [3/2]6p;1 state. Also seen in the three-photon spectra is a weaker feature to lower energy of the [3/2]6p;2 origin and this is assigned to a triplet [3/2]6p;1 state. Details of the vibronic assignment of the [3/2]6p cluster are given in Table 4-5.

Band Measurement cm^{-1}	Assignment	Vibrational Spacing cm^{-1}
58022	0_0^0 [3/2]6p;1′	0
58308	0_0^0 [3/2]6p;2	0
58788	3_0^1 [3/2]6p;2	480
58903	0_0^0 [3/2]6p;0	0
59527	[3/2]6p;1	0
59679	[3/2]6p;1	152
60122	2_0^1 [3/2]6p;0	1219

Table 4-5: Three-photon vibronic assignments of the [3/2]6p cluster.

4.4.2 The 60500-67000 cm^{-1} Region

In the 60500-67000 cm^{-1} of the three-photon spectrum, [1/2]6p, [3/2]5d and [3/2]7s states are apparent as can be seen in Figure 4-5 and the polarisation behaviour of the stronger features is depicted in Figure 4-7. This polarisation behaviour further confirms the [3/2]5d;2 and other *nd*;2 assignments in the two- and three-photon spectra of methyl iodide. This comment equally applies to features reassigned to the [1/2]6p;2 state. The discussion regarding the assignment of features to the [3/2]7s;1 and other *ns*;1 states is deferred to later.

Of the [1/2]6p cluster, features seen in the two-photon spectrum which arise from transitions to the singlet [1/2]6p;0 and [1/2]6p;2 components are again present in the three-photon spectrum. However, there is less certainty regarding the question of whether features are present which can be assigned to the Ω=1 component. One possibility is that its origin band may have blended with that of the [3/2]7s;1 state. Another possibility is that an additional feature which appears between those of the [3/2]5d;2 and [3/2]5d;0 states is due to the [1/2]6p;1 state. This feature is absent from the two-photon spectrum which, in line with its polarisation dependence, would seem to strengthen the [1/2]6p;1 assignment. However, if this were so, it would mean that the energy ordering of Ω-components in the [1/2]6p cluster differs from that seen in the [3/2]6p cluster. This implies that the energy ordering of the Ω-components is disrupted, possibly because of interactions between the singlet [1/2]6p;0 state and the first-tier Ω=0 ion-pair state.

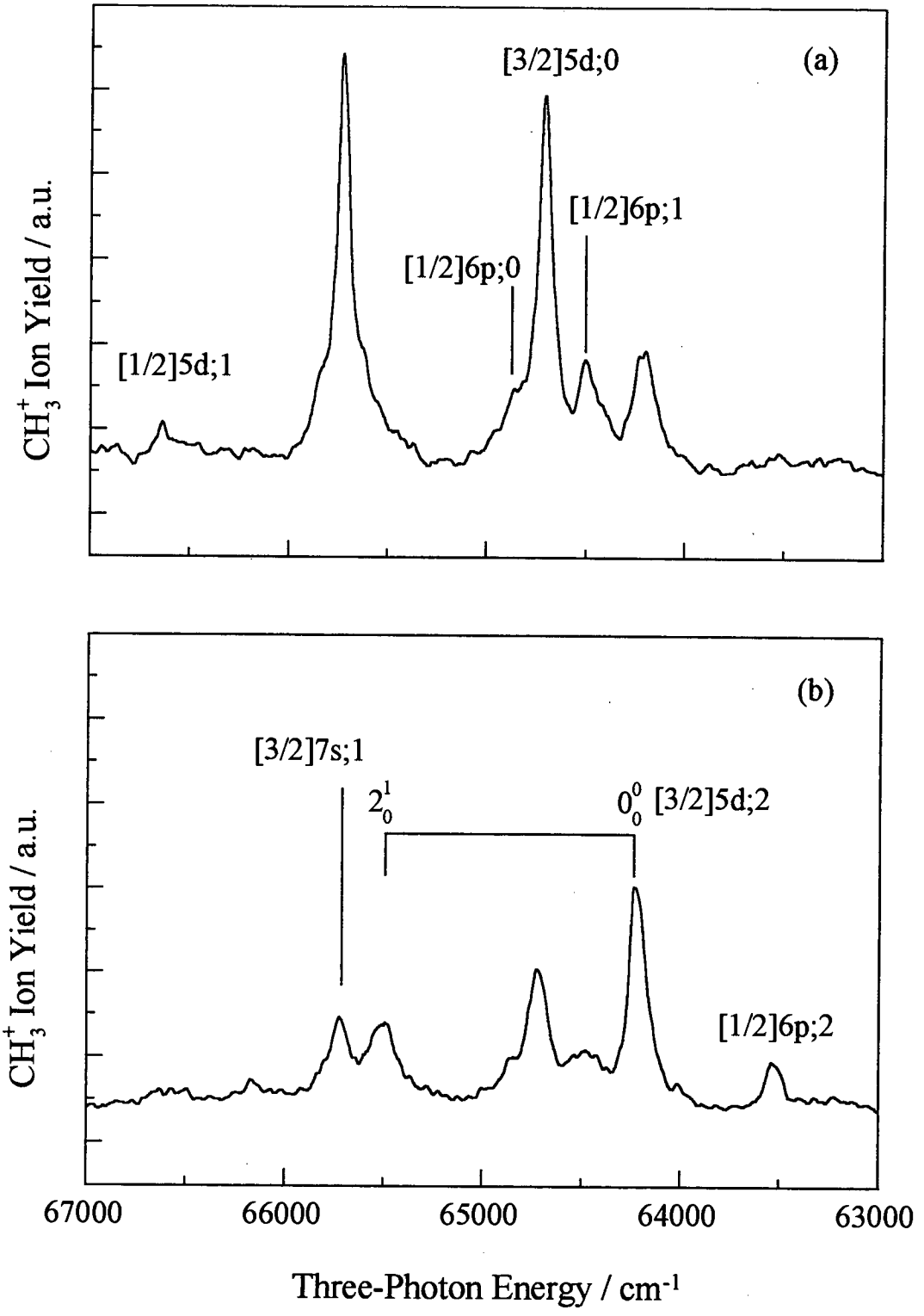

Figure 4-7: Polarisation studies of features in the 63000-67000 cm^{-1} region of the three-photon spectrum of CH_3I. The spectrum recorded using linearly polarised light is shown in panel (a) while panel (b) depicts the spectrum recorded using circularly polarised light.

In the case of the [3/2]5d cluster, the singlet Ω=1, Ω=2 and Ω=0 components are present. For the [3/2]5d;1 state, three features of similar intensity are seen. If these were to be due to individual Ω=1 states, only two features should be seen. The presence of additional features is more likely due to Rydberg~valence interactions because, as discussed earlier for the singlet [3/2]6p;1 state, no Ω=1 ion-pair state is available.

4.4.3 The 67000-72000 cm^{-1} Region

This region of the three-photon spectrum appears to be dominated by transitions to states with Ω=1. The components of the [1/2]5d and [3/2]6d clusters seen in the two-photon spectrum are only seen weakly in the three-photon spectrum. There are no features which might be assigned to higher members of *np* series, in agreement with the two-photon spectrum. Thus, the stronger features in this region are assigned to *ns*;1 and *nd*;1 states. Two features are apparent where singlet [1/2]5d;1 states might be expected and these are assigned accordingly. Other strong features in the three-photon spectrum above 65000 cm^{-1} which are assigned to *ns*;1 states display quantum defects with typical values of about 3.85. A feature at 69751 cm^{-1}, with a quantum defect of 0.09 based on the [$^2E_{3/2}$] ionic core, is assigned to a [3/2]4f;1 state. The presence of a feature which can be attributed a [3/2]4f;1 assignment at least suggests that *nf*;1 series should at least be present, if not dominant, in the three-photon spectra of methyl halides other than methyl bromide.

4.5 Two- and Three-Photon Spectroscopy of Methyl Chloride

The two- and three-photon spectroscopy of CH_3Cl is reinvestigated in light of the polarisation data now available for methyl bromide and methyl iodide. Here, the two-photon spectrum is now extended up to the first ionisation energy while the three-photon spectrum is extended to as high an energy as practically possible. The spectra of the 4s cluster have not been examined in this study because they have been subject of sufficient attention in the past[4,13]. Moreover, sufficient data is available

Assignment	[3/2]			[1/2]		
	$\bar{\nu}$ / cm^{-1}	(n-δ)	ρ_2	$\bar{\nu}$ / cm^{-1}	(n-δ)	ρ_2
4p;2	70970	2.34	†	71644	2.34	†
4p;0	71081	2.34	-	71750	2.34	-
3d;2	78922	3.00	+	79590	3.00	+
3d;0	79181	3.03	-	79795	3.03	-
5p;0	80843	3.27	-	81660	3.30	-
4d;0′	82734	3.63	-			
4d;2	84333	4.03	+	84973	4.03	+
4d;0	84570	4.11	-	85228	4.11	-
5d;1	86123	4.71	+	~	~	~
5d;2	86676	4.99	+	87307	4.98	+
5d;0	86744	5.03	-	87390	5.03	-
6d;0	88089	6.06	-	88681	6.00	-
7d;0	88859	7.04	-	~	~	~
8d;0	89386	8.06	-	~	~	~
9d;0	89739	9.06	-	~	~	~
10d;0	89990	10.05	-	~	~	~
11d;0	90166	10.98	-	~	~	~
12d;0	90405	12.79	-	~	~	~

Table 4-6: Two-photon assignments to Rydberg states based upon the $\tilde{X}\ ^2E_{3/2}$ and $\tilde{X}\ ^2E_{1/2}$ ionic cores. † indicates a feature for which the two-photon polarisation has not been investigated. The two-photon polarisation ratio, ρ_2, is denoted + where it equals 1.5 and - where it is less than 1. Values used for the respective ionisation limits are 91076 cm^{-1} and 91726 cm^{-1}, as determined in this work. Their determination is discussed in the text.

Assignment	[3/2]			[1/2]		
	$\bar{\nu}$ / cm^{-1}	(n-δ)	ρ_3	$\bar{\nu}$ / cm^{-1}	(n-δ)	ρ_3
4p;1′	70362	2.30	-	~	~	~
4p;0	71083	2.34	-	71727	2.34	-
3d;1	ca. 77251	2.82	-	ca. 77901	2.82	-
3d;2	78907	3.00	+	79584	3.00	+
3d;0	79197	3.03	-	79788	3.03	-
5s;1	79655	3.10	-	80487	3.12	-
5p;0	80843	3.27	-	~	~	~
5p;1	81989	3.48	+	82720	3.49	-
4d;0′	82720	3.63	-	~	~	~
4d;1	83091	3.71	+	83751	3.71	~
4f;1″	83608	3.84	+	~	~	~
4f;1′	83934	3.92	-	~	~	~
4f;1	84075	3.96	-	~	~	~

Table 4-7: Three-photon assignments to Rydberg states of CH_3Cl based upon the $\tilde{X}\ ^2E_{3/2}$ and $\tilde{X}\ ^2E_{1/2}$ ionic cores. The values used for the respective ionisation limits are the same as those obtained in the two-photon work. Three-photon polarisation ratios, ρ_3, are indicated by + if ρ_3 is near 2.5 and - if ρ_3 is appreciably less than 2.5. States that were either not observed or not investigated are indicated by ~.

from methyl bromide and methyl iodide to aid the assignment of the spectra of methyl chloride without any recourse to the two-photon polarisation behaviour of the 4s cluster. The spectra are understood as following the same propensity rules as for the aforementioned methyl halides. Assignments of features in the two-photon spectrum to states based upon the $\tilde{X}\ ^2E_{3/2}$ and $\tilde{X}\ ^2E_{1/2}$ ionic cores are given in Table 4-6.

The three-photon study is not as complete as the two-photon one. This is at least partly due to the lower cross-sections exhibited by three-photon transitions. This means that the dye laser power required for three-photon transitions to be seen is higher than that for two-photon transitions. This rules out the possibility of using radiation produced by second harmonic generation to record (3+1) REMPI spectra and only the 70000-84000 cm^{-1} region of the three-photon spectrum will be discussed here. However, sufficient data was obtained to aid the re-interpretation of the work of Szarka et al.[4]. The electronic assignment of the three-photon spectrum is given in Table 4-7.

4.5.1 Ionisation Limits

The power-normalised two-photon spectrum of CH_3Cl in the 84000-91000 cm^{-1} region, composed of several shorter scans, is shown in Figure 4-8. As in the spectra of methyl bromide, the observed features are observed most strongly in the CH_3^+ ion channel. These features are also observed in the Cl^+ and CCl^+ ion channels, confirming that they arose from the parent molecule. Molecular ion signal only appears above the first ionisation energy, suggesting that dissociation in the molecular ion was responsible for the ion signals observed via Rydberg transitions.

The ionisation threshold indicated in Figure 4-8 and observed more clearly in the molecular ion channel (see inset in Figure 4-9) has been used to determine a better value for the $\tilde{X}\ ^2E_{3/2}$ ionisation energy than those reported previously. Thresholds were measured at different repeller voltages in the manner described in the previous

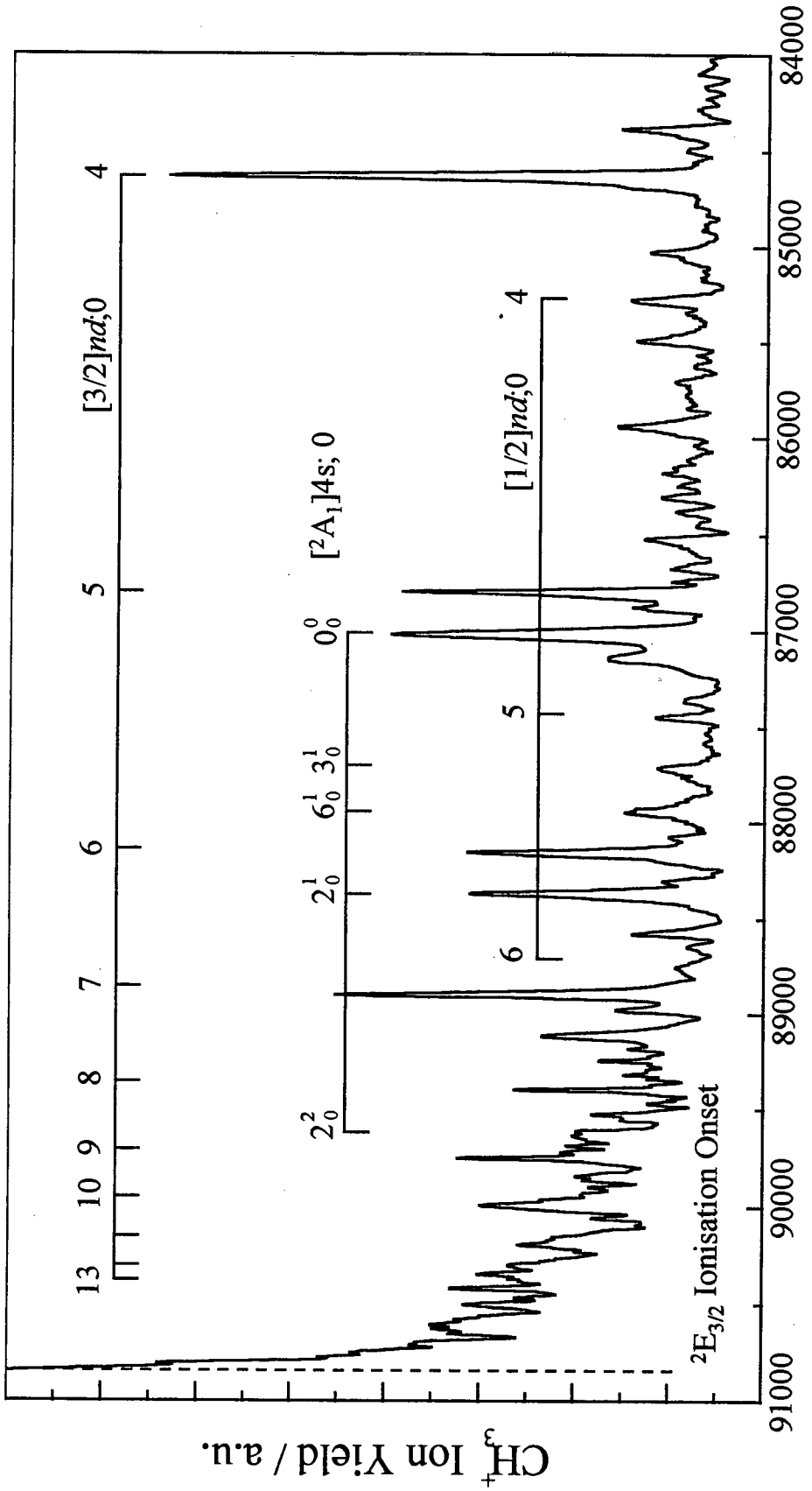

Figure 4-8: Two-photon spectrum of CH_3Cl in the 84000-91000 cm^{-1} region.. The figure is composed of several scans with different laser dyes. which were joined once they were power normalised.

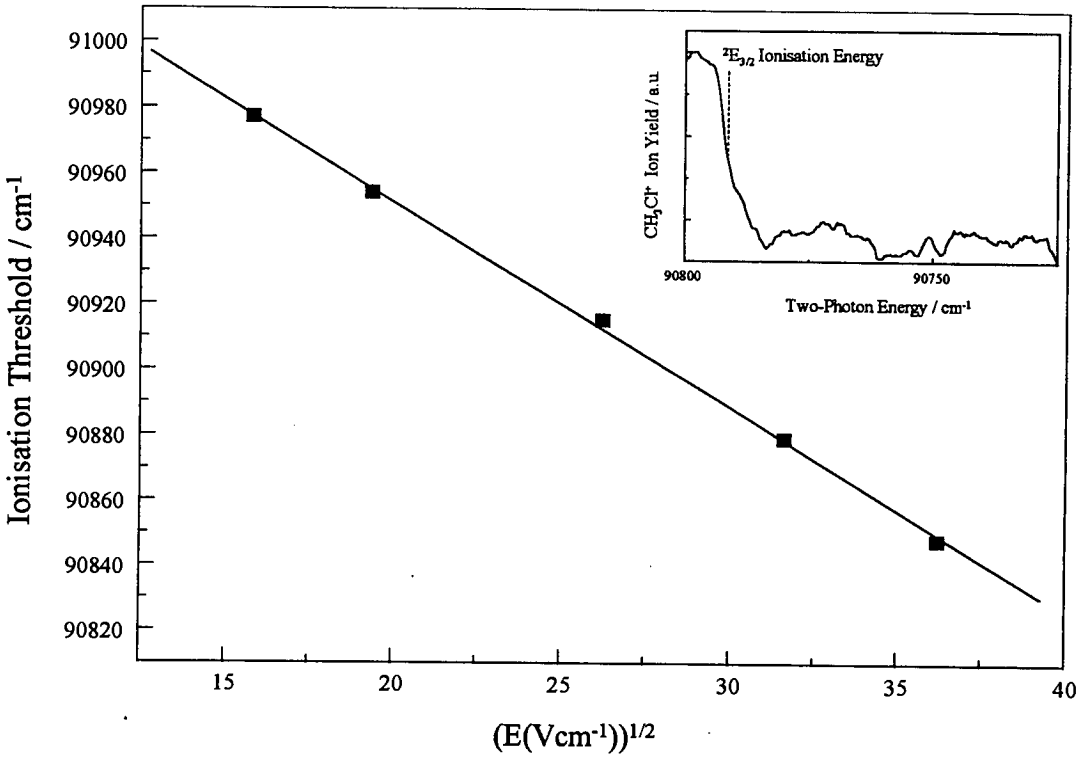

Figure 4-9: A plot of threshold ionisation energy versus repeller electric field for CH_3Cl is shown in the main figure. The slope of the line is -6.3 which is close to the expected value of -6. A two-photon spectrum recorded in the CH_3Cl^+ channel in the 90725-90800 cm^{-1} region showing the full extent of the $^2E_{3/2}$ ionisation curve is inset. The ionisation curve in the inset was displaced by an applied electric field of 1312 Vcm^{-1} which results from the application of 2.1 kV across the repeller electrode.

chapter. These energies were then plotted against the square root of the applied electric fields as in Figure 4-9. From the intercept of this plot a value of 91076 cm^{-1} was obtained for the $\tilde{X}\ ^2E_{3/2}$ ionisation energy. The value obtained here compares well with a previous value of 91060 cm^{-1} obtained from He (I) PES[24]. The value for the spin-orbit splitting is seen to be 650 cm^{-1} in the 4p, 3d and 4d Rydberg states studied. Therefore, when this value is adopted, a value of 91726 cm^{-1} is obtained for the $\tilde{X}\ ^2E_{1/2}$ ionisation energy. Even though increased penetration of the ionic core in lower Rydberg states could distort the spin-orbit splitting observed, the value adopted here is in agreement with the value of 627 cm^{-1} obtained from conventional photoelectron spectroscopy[24].

4.5.2 *np* States

Several features appear, some with appreciable intensity, in the 70000-74000 cm^{-1} region which have previously been assigned to [3/2]4p;0 and [1/2]4p;0 states by Szarka et al.[4] The two-photon polarisation behaviour of the stronger features comprising this cluster is shown in Figure 4-10. It is apparent from Figure 4-10 that the polarisation behaviour displayed by the two features at 71977 cm^{-1} and 72663 cm^{-1} differs from that displayed by other bands depicted. Szarka et al.[4] assigned the features at 71977 cm^{-1} and 72663 cm^{-1} to [3/2]4p;0 3^1_0 and [1/2]4p;0 3^1_0 transitions respectively, which is inconsistent with their polarisation behaviour. Given their polarisation behaviour, these features could be assigned to the origins of 4p;2 and/or 4p;1 states. The latter possibility can be discounted because the propensity rules observed in the two-photon spectra of methyl iodide and methyl bromide are expected here also. The former possibility can also be rejected because this would be at odds with the energy ordering seen for components of the first *np* clusters in both methyl bromide and methyl iodide. Moreover, Szarka et al.[4] noted that there was a perceptible amount of broadening of the 4p;0 origin bands, much more so than in the study presented here, when excited using circularly polarised light in both the two- and three-photon spectra. This is most likely to be due to blending of the origin bands of the singlet 4p;0 and 4p;2 states. Features arising from transitions to 4p;2 states are expected if the propensity rules apparent in the spectra of methyl iodide and methyl bromide also apply to those of methyl chloride. This blending occurs as a result of the reduced energy separation between 4p;0 and 4p;2 states in methyl chloride. The smaller splitting can be attributed to weaker (Ω_c, ω_{Ryd}) coupling in methyl chloride compared to either methyl bromide or methyl iodide. This type of behaviour has already been seen in the homonuclear diatomic halogens[1]. One further possibility regarding the features at 71977 cm^{-1} and 72663 cm^{-1} is that they arise from [3/2]4p;0 6^1_0 and [3/2]4p;0 6^1_0 transitions, respectively. This would be consistent with the observed vibrational spacings, especially upon comparison with the

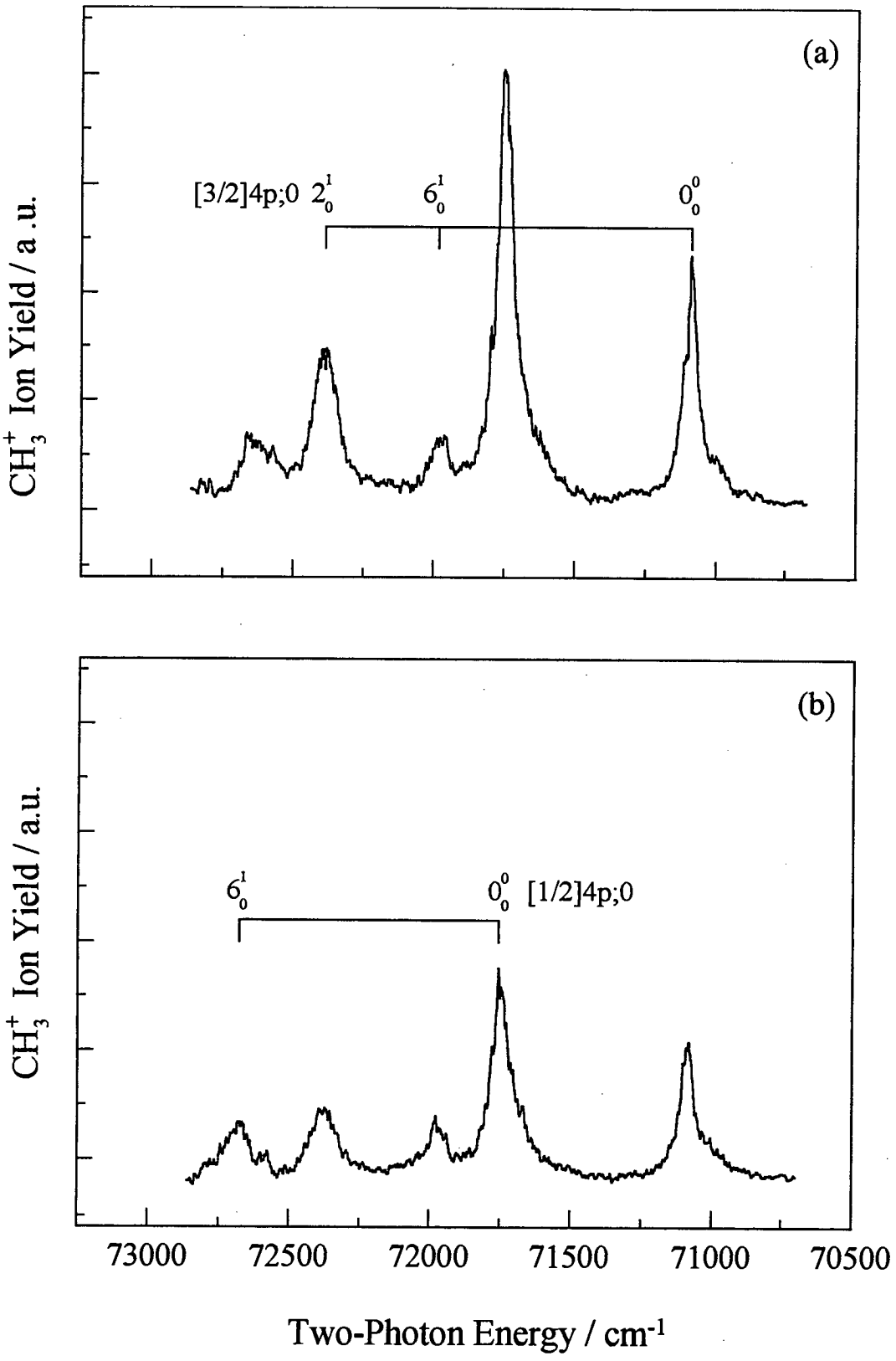

Figure 4-10: Two-photon polarisation behaviour of the 4p cluster of CH_3Cl. The spectrum recorded using linearly polarised light is shown in panel (a) while panel (b) depicts the spectrum recorded using circularly polarised light.

Band Positions cm^{-1}	**Assignment**	**Vibrational Spacing** cm^{-1}
70362	0_0^0 [3/2]4p;1′	0
70970	0_0^0 [3/2]4p;2	0
71081	0_0^0 [3/2]4p;0	0
71623	0_0^0 [3/2]4p;2	0
71750	0_0^0 [1/2]4p;0	0
71977	6_0^1 [3/2]4p;0	896
72394	2_0^1 [3/2]4p;0	1313
72491	$2_0^1 3_0^1$ [3/2]4p;0	1410
72663	6_0^1 [1/2]4p;0	913
73104	2_0^1 [1/2]4p;0	1354
73336	$2_0^1 3_0^1$ [3/2]4p;0	2366
73336	$3_0^1 6_0^1$ [1/2]4p;0	1586
73938	1_0^1 [3/2]4p;0	2857

Table 4-8: Vibronic assignments of the 4p cluster in methyl chloride.

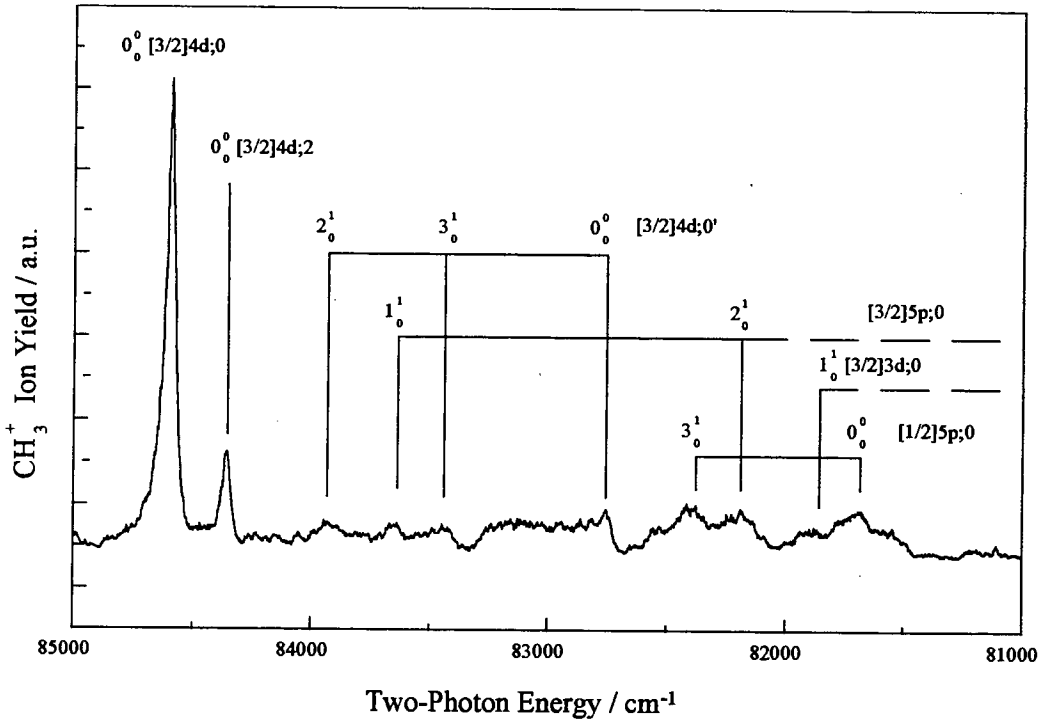

Figure 4-11: Two-photon spectrum of CH_3Cl in the 81000-85000 cm^{-1} region.

vibrational frequencies of the neutral ground state. Vibrational activity in an antisymmetric mode is unexpected but has been seen in the photoelectron spectrum[24]. Also, the symmetry of ν_6, the CH_3 rock, may contribute to the unexpected polarisation behaviour of the features at 71977 cm^{-1} and 72663 cm^{-1}. Therefore, the assignment involving ν_6 is adopted here. An additional feature is seen in the present jet-cooled three-photon spectrum which was previously assigned as a 3_1^0 hot band built upon the [3/2]4p;0 origin. In light of the spectrum of the [3/2]6p region in CH_3I, a more likely assignment for this feature in CH_3Cl is to a [3/2]4p;1 state of triplet character, labelled here as [3/2]4p;1′. The assignment of the 4p cluster is given in Table 4-8.

In the 80000-83000 cm^{-1} region of the two-photon spectrum, weak diffuse structure is apparent. Szarka et al.[4] have assigned some of these features to 5p states. Although most of their assignments are accepted here, the more important point to be drawn from these features is their intensity. As can be seen from Figure 4-11, they are much weaker than those comprising the [3/2]4d band system. This implies that *np* series die out while *nd* series extend to much higher energy has already been considered for methyl bromide. As in the case of methyl bromide, *l*-dependent predissociation is the most likely explanation for the curtailment of *np* series in methyl chloride. Vibronic assignments for the 5p cluster are given in Table 4-9.

Band Positions cm^{-1}	**Assignment**	**Vibrational Spacing** cm^{-1}
80843	0_0^0 [3/2]5p;0	0
81660	0_0^0 [1/2]5p;0	0
82170	2_0^1 [3/2]5p;0	1327
82358	3_0^1 [1/2]5p;0	698
83629	1_0^1 [3/2]5p;0	2786

Table 4-9: Vibronic assignments of the 5p cluster in methyl chloride.

4.5.3 *nd* States

nd series are also seen to dominate the two-photon spectrum of methyl chloride as was seen in those of methyl bromide and methyl iodide. The first members of these series are apparent in the 78500-83000 cm^{-1} region. These were originally assigned to 5s states by Szarka et al.[4] in line with the assignments of the two-photon spectrum of methyl iodide reported by Dobber et al.[3] In light of the two-photon polarisation behaviour presented in Figure 4-12 for the stronger features comprising this system, the features originally assigned to 5s states are now reassigned to 3d states, bringing the assignment of the spectrum of CH_3Cl into line with CH_3Br and CH_3I. The vibronic assignments of the 3d system are given in Table 4-10. The polarisation behaviour exhibited by the 3d cluster is also typical of the majority of the features lying to higher energy, confirming the dominance of *nd* series in the two-photon spectrum of methyl chloride just as in the case of both methyl bromide and methyl iodide. However, ρ_2 is higher for Ω=0 states in methyl chloride than in either of the other two methyl halides, as seen in Figure 4-12. It is not entirely clear how this might arise although the observed polarisation ratios are sufficient justification for the Ω=0 assignments in the diagnostic treatment given here.

The extent of the observed *nd* series with Ω=0 is shown in Figure 4-8. However, the [3/2]*nd*;0 series can only be extended up to n=12 in methyl chloride which is not as extensive as in methyl bromide. The underlying reason for this may well be predissociation. That curtailment did not result from an electric field shift of the ionisation energy was confirmed by recording the higher energy portion of the two-photon spectrum with lower voltages being applied across the repeller electrode without extra features being seen. Also, it can be seen that the features comprising the VUV spectrum of methyl chloride are less sharp than those exhibited in the spectra of either methyl bromide or methyl iodide[3]. This is best exhibited in the appearance of the lowest Rydberg cluster in methyl chloride vis-à-vis those of the other two

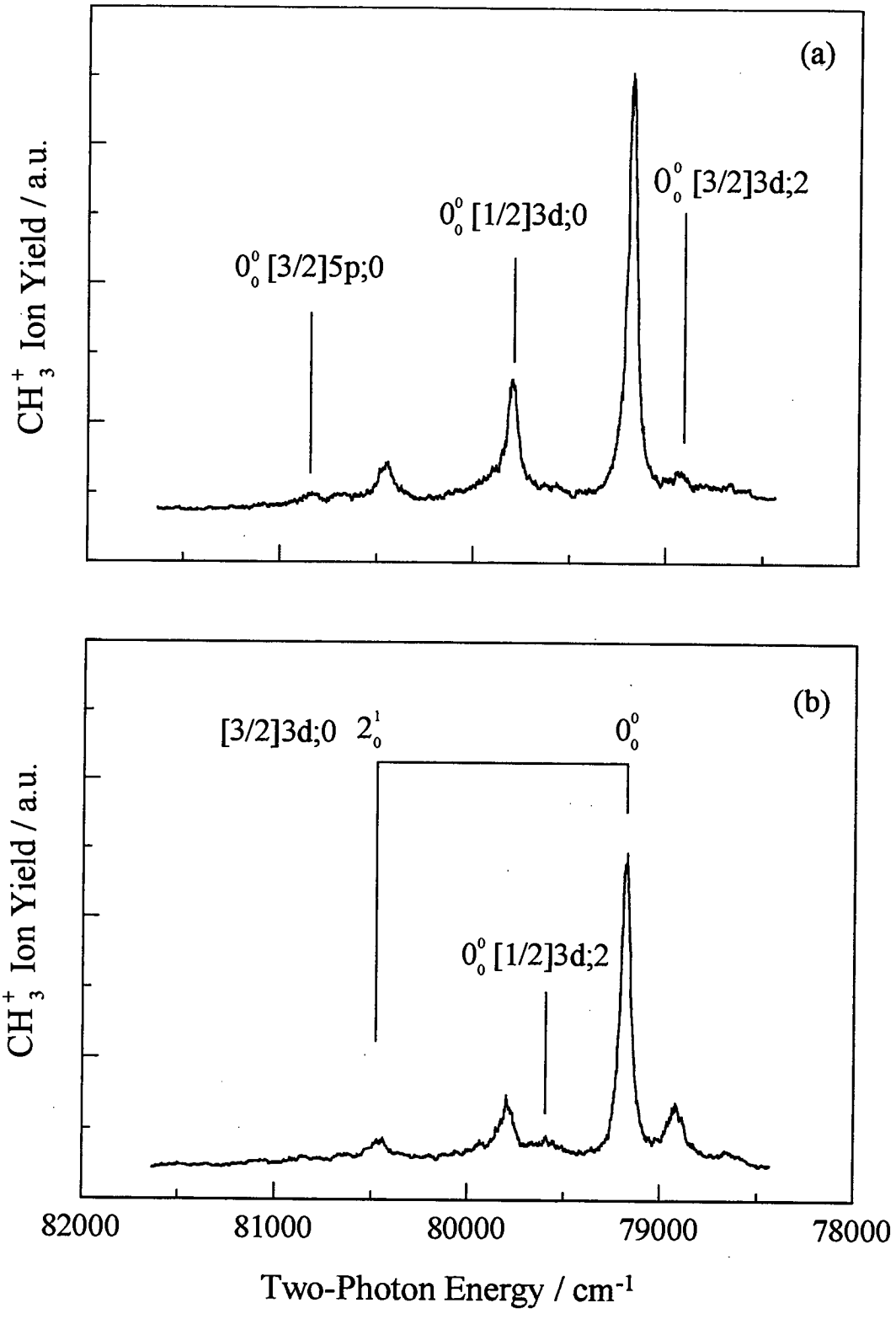

Figure 4-12: Two-photon polarisation behaviour of the 3d cluster of CH_3Cl. The spectrum recorded using linearly polarised light is shown in panel (a) while panel (b) depicts the spectrum recorded using circularly polarised light.

Band Positions cm^{-1}	Assignment	Vibrational Spacings cm^{-1}
78922	0_0^0 [3/2]3d;2	0
79181	0_0^0 [3/2]3d;0	0
79580	0_0^0 [1/2]3d;2	0
79795	0_0^0 [1/2]3d;0	0
79868	3_0^1 [3/2]3d;0	708
80443	2_0^1 [3/2]3d;0	1262
81112	2_0^1 [1/2]3d;0	1317
81311	5_0^1 [1/2]3d;0	1516
81879	1_0^1 [3/2]3d;0	2698
82757	1_0^1 [1/2]3d;0	2962

Table 4-10: Vibronic assignments of the 3d cluster in methyl chloride.

Band Positions cm^{-1}	Assignment	Vibrational Spacings cm^{-1}
82734	0_0^0 [3/2]4d;0′	0
83416	3_0^1 [3/2]4d;0′	682
83912	2_0^1 [3/2]4d;0′	1178
84333	0_0^0 [3/2]4d;2	0
84570	0_0^0 [3/2]4d;0	0
84973	0_0^0 [1/2]4d;2	0
85228	0_0^0 [1/2]4d;0	0
85290	3_0^1 [3/2]4d;0	720
85441	6_0^1 [3/2]4d;0	871
85669	2_0^1 [3/2]4d;2	1336
85889	2_0^1 [3/2]4d;2	1319

Table 4-11: Vibronic assignments of the 4d cluster in methyl chloride. In additional to the symmetric modes, ν_6, the CH_3 rock, also seems to be active.

molecules. Thus, some curtailment of the observed [3/2]*nd*;0 series can be attributed to predissociation.

Features arising from transitions to members of the *nd*;2 series are much weaker than those due to *nd*;0 states and are not observed above n=6. A greater

degree of predissociation could result in features arising from transitions to different states becoming blended. The ensuing congestion means that only features due to members of the dominant [3/2]*nd*;0 series can be assigned. This might also explain the apparent absence of features due to [1/2]*nd*;0 states with $n > 6$.

4.5.4 Additional Features in the 84000-91000 cm^{-1} Region of the Two-Photon Spectrum

The two-photon spectrum of CH_3Cl in the 84000-91000 cm^{-1} region, depicted in Figure 4-8, is somewhat richer than the spectrum of the equivalent region in CH_3Br. The spectrum in the 88000-91000 cm^{-1} region is of such complexity that, for the most part, only [3/2]*nd*;0 origin band assignments are made. In the 84000-88000 cm^{-1} region, there are other features, in addition to those assigned to the origin bands of *nd*;0 and *nd*;2 states and vibrational bands built upon them, to which assignments should be attributed. The presence of these resonances in both CH_3^+ and Cl^+ ionic channels confirm that they are due to the parent molecule and not any fragment species. Even electronic assignments to other Rydberg states, based upon the $^2E_{3/2}$ and $^2E_{1/2}$ ionic cores, do not explain all of the extra features. The appearance of features due to transitions to *np* states can be discounted given that the features comprising the 5p band system are so weak. The lack of an additional feature with similar intensity immediately to higher energy of the [3/2]4d;0 origin precludes any *nf* assignments. Also, in the light of the multiphoton spectroscopy of methyl bromide, discussed in the previous chapter, *nf* states are expected to lie below *nd*;0 states. This makes an *nf* assignment an even more unlikely possibility.

Another possibility is that the extra features in the 86500-88500 cm^{-1} region could appear as a result of coupling between members of the assigned [3/2]*nd*;0 series and nearby Ω=0 ion-pair states. However, this possibility can be dismissed on energetic grounds which are summarised in the potential energy diagram in Figure 4-13. The depicted potential curves were generated in the same manner, and using the same assumptions, as those depicted in Figure 3-9 in Chapter 3. To generate

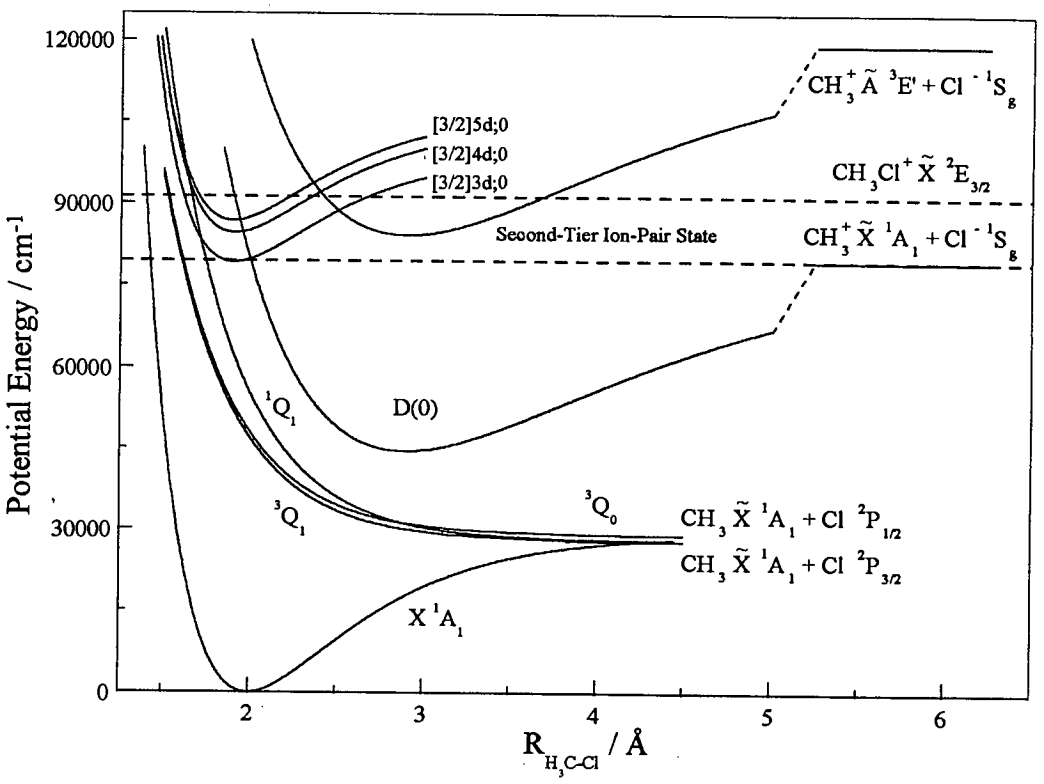

Figure 4-13: Schematic potential energy diagram depicting selected electronic states of CH_3Cl and showing that there is little scope for Rydberg~ion-pair coupling in the 86900-89600 cm^{-1} region. The depicted potential energy curves were generated in the same manner as those depicted in Figure 3-9 in Chapter 3.

Ion-Pair	I.E. cm^{-1}	E.A. cm^{-1}	$D_0(H_3C\text{-}I)$ cm^{-1}	Threshold Energy cm^{-1}
CH_3^+ ($\tilde{X}$ $^1A_1'$) + Cl^- ($^1S_0$)	79349 [25]	29141 [31]	29197 [29]	79405
CH_3^+ ($\tilde{A}$ $^3E'$) + Cl^- ($^1S_0$)	119047 [26]	29141 [31]	29197 [29]	119103
Cl^+ ($^3P_2$) + CH_3^- ($\tilde{X}$ $^1A_1'$)	84295 [21]	645 [28]	29197 [29]	133143

Table 4-12: Table of transition energies corresponding to the first three thermodynamic thresholds for ion-pair formation in methyl chloride and the values used to calculate them. The references from which values are taken are indicated in square brackets.

the potential energy curves for ion-pair states, values typical for ion-pair states in molecular chlorine[30] were used. The equilibrium bond length, $R_e(H_3C\text{-}Cl)$, adopted is 2.9 Å and 35000 cm^{-1} is used for the equilibrium dissociation energy, D_e. The equilibrium term values, T_e, for the depicted ion-pair states are obtained by subtracting the dissociation energy from the thresholds for ion-pair formation. The transition energies corresponding to the first three thresholds for ion-pair formation in methyl chloride, and the values used to calculate them, are given in Table 4-12. It can be seen from Figure 4-13 that the possibility of extra features arising as a result of coupling between Rydberg states and the first-tier ion-pair state, denoted D(0) in Figure 4-13, can be ruled out because it is unbound above 79405 cm^{-1}. Also, although curve-crossings between Rydberg states and a second-tier ion-pair state occur within the bound region of the latter, the crossings are expected to lie above 88500 cm^{-1} and high up the potential curves of the [3/2]5d;0 and [3/2]6d;0 Rydberg states. There is one further tier of ion-pair states which dissociate to give Cl^+ ($^3P_2$) and CH_3^- ($\tilde{X}\ ^1A_1$) but this tier of ion-pair states lies above the first ionisation energy. In light of all this, the additional features cannot be attributed to ion-pair states.

Some of the extra features are of comparable intensity to those assigned to the origin bands of nearby [3/2]*nd*;0 states. This is particularly true of the features at 86961 cm^{-1} and 88292 cm^{-1}. Given that these features cannot be assigned to Rydberg states based upon the $^2E_{3/2}$ ionic core or to ion-pair states, the possibility of features from transitions to Rydberg states based on other ionic cores must be considered. One such possibility is that the spin-orbit splittings between Rydberg states based on the $^2E_{3/2}$ and $^2E_{1/2}$ ionic cores is much reduced in the case of the 5d;0 and 6d;0 states. In fact, the spin-orbit splitting in the $\tilde{X}$ state of CH_3Cl^+ may be much smaller than the value of 650 cm^{-1} adopted here. If it were of the order of 200 cm^{-1}, which is in agreement with the separations between the bands at 86961 cm^{-1} and 88292 cm^{-1} and the features due to [3/2]5d; and [3/2]6d;0 states respectively, it might not be resolved in a He I photoelectron spectrum. Then, the greater spin-orbit splittings, of the order of 650 cm^{-1}, seen in lower energy clusters could be attributed to Rydberg~valence interactions. Also, the relative strengths of (Ω_c, ω_{Ryd}) coupling and spin-orbit coupling

could differ in methyl chloride from those in methyl bromide and methyl iodide. This may also alter the values of the ionic core splitting observed within a cluster of Rydberg states. This possibility is further discussed later regarding the re-assignment of the VUV spectrum of methyl chloride. In any case, the lowest energy band system in the photoelectron spectrum requires detailed examination at higher resolution using ZEKE-PFI PES before this can be established.

Band Positions cm^{-1}	**Assignment**	**Vibrational Spacing** cm^{-1}
86961	0_0^0	0
87650	3_0^1	689
87886	6_0^1	925
88292	2_0^1	1331
89564	2_0^2	2603

Table 4-13: Vibronic structure attributable to the $[^2A_1]4s;0$ state.

Yet another possibility is that the additional bands are due to a 4s Rydberg state based upon the $\tilde{A}\ ^2A_1$ ionic core. From photoelectron spectroscopy[24] it is seen that the ionisation energy corresponding to the $\tilde{A}\ ^2A_1$ ionic state is about 116547 cm^{-1}. With this as the ionisation limit, the $(n\text{-}\delta)$ value calculated for the 86961 cm^{-1} feature is 1.93, not untypical of a 4s state. The labelling of such a state would then be abbreviated to $[^2A_1]4s$. The spin-orbit components of the parent ionic state were unresolved, therefore they cannot be included in the labelling scheme used here. The presence of sharp features due to a transition to such a state is surprising in light of an examination of the photoelectron spectrum which indicates that this ionic state, upon which a $[^2A_1]4s$ Rydberg state is based, is repulsive in nature. This is because the $\tilde{A}\ ^2A_1$ ionic state results from the removal of an electron from a C-Cl bonding orbital. Moreover, another reason for surprise is that the greatest penetration of the ionic core is expected for a Rydberg electron in a 4s orbital. The possibility of vibronic transitions built upon the 86961 cm^{-1} band would explain most of the additional features in the 86900-89600 cm^{-1} region. Suggested assignments for these are given in Table 4-13 and indicated in Figure 4-8.

Several possible assignments for extra features in the 86500-88500 cm^{-1} region, which cannot be assigned to members of the dominant [3/2]*nd*;0 series, have been put forward. Of these possibilities, two can be dismissed more easily and these would involve assignments to members of *np*;0 and *nf*;0 series or assignment to transitions terminating in the vibrational levels of ion-pair states. The assignment of a single band system to a $[^2A_1]4s;0$ state seems odd in light of the appearance of the band due to the $\tilde{A}\ ^2A_1$ state in the photoelectron spectrum. However, it does explain most of the extra features in the 86500-88500 cm^{-1} region of the two-photon spectrum. A more radical suggestion is that the spin-orbit splitting in the $\tilde{X}\ ^2E$ state of CH_3Cl^+ is only about 200 cm^{-1} rather than 650 cm^{-1} as supposed heretofore. However, while this needs to be confirmed by a ZEKE-PFI photoelectron study of CH_3Cl, it does seem a more plausible explanation than the others proposed alongside it.

4.5.5 Features Exclusive to the Three-Photon Spectrum

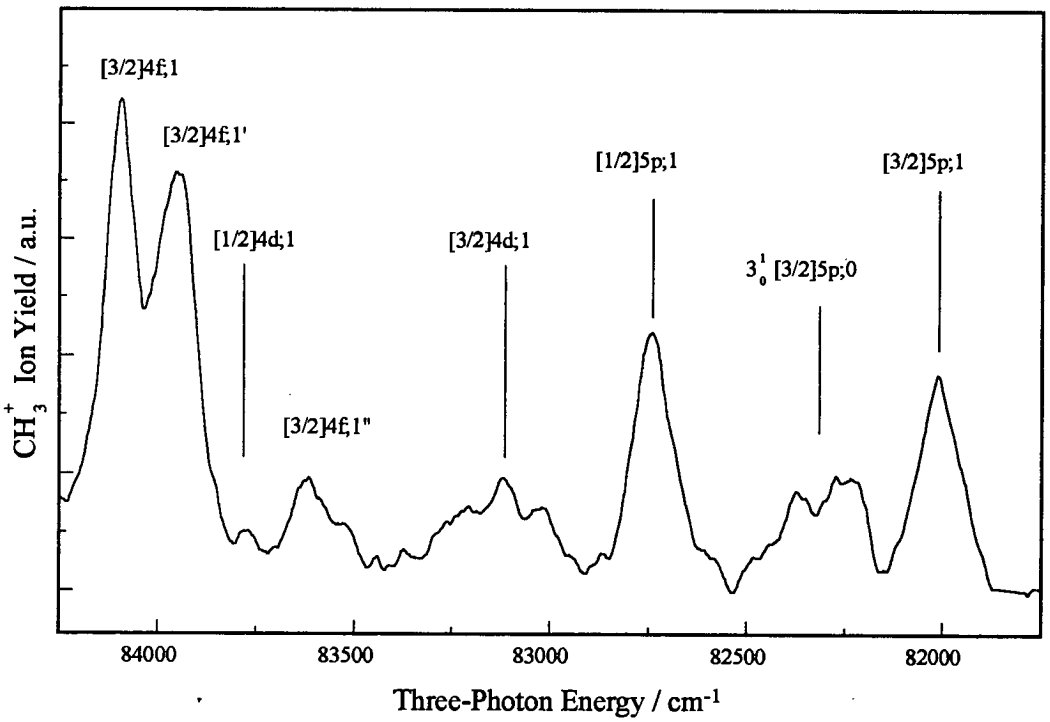

Figure 4-14: Three-photon spectrum of methyl chloride in the 81750-84250 cm^{-1} region.

The newly investigated 81750-84250 cm^{-1} region of the three-photon spectrum of CH_3Cl is depicted in Figure 4-14. The polarisation data presented for the 70000-84250 cm^{-1} region for the three-photon spectrum mean that a revision of some of the assignments suggested by Szarka et al.[3] is required. The three-photon polarisation behaviour of features occurring in both the two- and three-photon spectra confirm the assignments reported earlier for the 4p and 3d clusters. However, like methyl bromide and methyl iodide, some features appear in the three-photon spectrum of methyl chloride which are absent from the two-photon spectrum. In light of their polarisation behaviour and in common with the other methyl halides, these are assigned to states with Ω=1. Apart from the triplet [3/2]4p;1′ state already discussed, the other additional features are assigned to 3d;1, 5s;1 and 4f;1 states. A broad feature at 77000cm^{-1} can be attributed to 3d;1 states and this is more intense than those due to [3/2]3d;2 and [3/2]3d;0 states, suggesting that Ω=1 states dominate the three-photon spectrum of methyl chloride as they do in the spectra of methyl bromide and methyl iodide. Two features, one at 79655 cm^{-1} and the other at 80487 cm^{-1}, are assigned to 5s;1 states in line with their polarisation behaviour. Like methyl bromide and methyl iodide, features assignable to *nf*;1 states occur in the 83500-84000 cm^{-1} region. For reasons discussed earlier, only the [3/2]4f cluster was seen. Other features in the 81750-84250 cm^{-1} region are assigned to 5p;1, 5p;0 and 4d;1 states.

4.6 Discussion

4.6.1 Rydberg Transitions in CH_3Br, CD_3Br, CH_3I and CH_3Cl.

Given that, for the most part, Rydberg transitions in both methyl iodide and methyl chloride follow the same propensity rules as those in methyl bromide, it can be said that *l* and Ω remain good for all of these methyl halides. This means that the spin-orbit coupling in both the ionic core and the Rydberg orbital is sufficiently strong to justify the use of an (Ω_c, ω_{Ryd}) or (Ω_c, λ_{Ryd}, m_s) description for the Rydberg states in all molecules concerned. This replaces the descriptions used previously for the Rydberg states of methyl iodide and methyl chloride. In methyl iodide, Λ has been

used to describe the observed states[4] but the use of Ω is more correct because of the strong spin-orbit coupling observed. These comments even apply to methyl chloride where spin-orbit interactions are the weakest but remain sufficiently strong to justify the description introduced here. Heretofore, the Rydberg states of methyl chloride were described in terms of their molecular symmetry[3]. Also, Szarka et al.[3] concluded that *ns*, *np* and *nd* states displayed different amounts of atomic and molecular character which is not immediately apparent in this study. In fact, the atomic-like appearance of Rydberg transitions in the VUV spectra of the three methyl halides of interest meant that propensity rules and energetics from atomic spectroscopy were used to aid the assignments. Both can be discounted in light of the polarisation studies presented here. Also, the use of atomic energetics can be misleading when used to aid the assignment of molecular Rydberg spectra and this is especially shown in this work. Thus, in light of the new data presented here, the previous assignments of the VUV spectra of methyl iodide and methyl chloride need reconsideration.

4.6.2 Reconsideration of the VUV Spectrum of Methyl Iodide

In the preceding chapter, it was seen that the majority of the observed features in the VUV spectrum of methyl bromide could be reassigned to members of *np*;0, *nd*;0 and *nd*;1 series, with the latter dominating the spectrum. Like methyl bromide, several features apparent in the two- and three-photon spectra of CH_3I presented here also coincide with those observed in the VUV spectrum. Coincidences in band measurements, within their experimental errors, in the one-, two- and three-photon spectra suggest that *np*;0, *np*;1 and *nd*;0 series are likely assignments for features in the VUV spectrum. Thus, the features assigned to *ns* states with $n>6$ are more likely to be due to *nd*;0 states. Also, those features previously assigned[6] to 5d states can now be assigned to 6p;1 states. In later work[11], it was seen that *nd* states, re-assignable to *nd*;1 states, dominated the VUV spectrum, especially at higher energies. Thus, the VUV spectrum of methyl iodide can be understood in the same manner as that of methyl bromide. The additional richness of this spectrum vis-à-vis that of methyl bromide can be put down to more extensive *nd*;0 and *np*;0 series.

However, the assignments suggested above are at odds with the results of theoretical work[10,12] carried out in support of the previous assignments. As discussed earlier, an SQDT study[10] has been used and the results of this study supported assignments to *ns*, *np* and *nd* states. However, SQDT does not take interactions between Rydberg states and other electronically excited states into account. In the MQDT study[12] reported following the acquisition of higher resolution VUV data[11], only interactions between different Rydberg series were taken into account. This MQDT study[12] supported the assignment of features in the VUV spectrum to *ns*, *np*, *nd* and *nd'* states. Both studies were carried out assuming the Rydberg states of methyl iodide were atomic-like in nature. Also, the contribution of Rydberg~valence and Rydberg~ion-pair interactions were never considered. Moreover, there does appear to be some indication of Rydberg~valence and Rydberg~ion-pair interactions in the two- and three-photon spectra of methyl iodide. Therefore, these must be taken into account in any future MQDT study and may account for differences between the assignments suggested here and those supported by previous theoretical work[10,12].

4.6.3 Reconsideration of the VUV Spectrum of Methyl Chloride

The VUV absorption spectrum of methyl chloride should be understood in a manner similar to that already proposed for methyl bromide and methyl iodide. However, the spectrum of methyl chloride has only ever been examined at medium resolution[9,18]. Thus, any comments concerning the reassignment of this spectrum will be somewhat restricted. As in methyl bromide and methyl iodide, coincidences occur between features in the one-, two- and three-photon spectra. An example of this is seen for the features assigned to 4p;0 states in this study and 4p;E in that of Truch et al.[18] This means that *np*;0 states occur in the VUV spectrum of methyl chloride as they do in the spectra of the other methyl halides discussed. There is another relatively sharp feature in the VUV to higher energy of the 4p cluster, at 74250 cm^{-1}, whose assignment has attracted some discussion. This was because of the absence of any obvious spin-orbit partner. Rather than the [3/2]4p;A_1 assignment attributed to it by Truch et al.[18], a 4p;1 assignment seems more appropriate in light of the data available for the other methyl halides. The main point of contention regarding

the feature at 74250 cm^{-1} is absence of an obvious spin-orbit partner. However, it has been suggested already, regarding the additional features in the 86500-88500 cm^{-1} region of the two-photon spectrum, that the spin-orbit splitting in the $\tilde{X}\ ^2E$ state may be smaller than previously thought[24]. If this were so, the feature at 74250 cm^{-1} might result from the blending of features due to the [3/2]4p;1 and [1/2]4p;1 states. Also, the 4p;1 assignment implies a large splitting, of the order of 2500-3200 cm^{-1}, between the Ω=0 and Ω=1 components of the [3/2]4p and [1/2]4p clusters. This suggests that the relative strengths of spin-orbit coupling within the ionic core and (Ω_c, ω_{Ryd}) coupling may be different in methyl chloride to those on methyl bromide and methyl iodide. A reduced spin-orbit splitting in the ion and stronger (Ω_c, ω_{Ryd}) coupling could have consequences for the assignment of the rest of the VUV spectrum of methyl chloride also.

For the assignment of features in the VUV spectrum of methyl chloride to *nd*;1 series, features in the 78000-80000 cm^{-1} must have appreciable intensity. From an examination of the VUV spectrum of Truch et al.[18], this is apparently not the case. In fact, a feature at 84095 cm^{-1} is more intense than those at 79170 cm^{-1} and 79800 cm^{-1}. Thus, the assignment of features with near-unity quantum defects to *nf* states seems more probable. Then, the VUV spectrum of methyl chloride would be assigned to *np* and *nf* states, with the latter dominating. This situation is very unlike that for the other methyl halides, where *nd*;1 series apparently dominate their VUV spectra, but it is very like that of the homonuclear diatomic halogens. An assignment of the VUV spectrum of methyl chloride to *np* and *nf* states could mean that the VUV spectra of methyl bromide and methyl iodide need reconsideration in this light. It may be that *nf* states occur in the VUV spectra of methyl bromide and methyl iodide alongside the *nd*;1 states already discussed.

4.6.4 Summary of the New Assignments

The two-photon spectra of methyl bromide, methyl iodide and methyl chloride are dominated by *nd* series. Their three-photon spectra are dominated by states with

Ω=1. *nf*;1 states dominate the three-photon spectrum of methyl bromide and should be seen in the spectra of the others as well if the respective three-photon energy regions were accessible. The VUV spectra of methyl bromide and methyl iodide can be said to be dominated by *nd*;1 series. The VUV spectrum of methyl chloride, in contrast, appears to be dominated by *nf* states which would suggest that they occur in the VUV spectra of the other methyl halides as well. Transitions to *np* states are also apparent in one-, two- and three-photon spectra with *ns*;1 transitions with $n>6$ appearing in the three-photon spectrum.

4.7 Conclusion

This study of the multiphoton spectra of methyl iodide and methyl chloride has shown that the description of the Rydberg states discussed earlier in this thesis for methyl bromide is equally applicable here. It is also shown that, for the most part, the multiphoton spectra of methyl chloride and methyl iodide can be assigned using the propensity rules developed for understanding the spectra of methyl bromide. The system of assignments which applies here is almost identical to that previously employed to explain the VUV and two-photon spectra of the halogens[1,2]. The differences that do occur between the spectra of the different molecules have no effect on their overall understanding. Thus, a new and more consistent unified understanding of Rydberg transitions in methyl bromide, methyl chloride and methyl iodide has been achieved.

4.8 References

1. R. J. Donovan, A. C. Flexen, K. P. Lawley and T. Ridley, *Chem. Phys.*, **1998** 226 217.
2. R. J. Donovan, A. C. Flexen, K. P. Lawley, R. R. J. Maier, A. Mank and T. Ridley, *to be submitted.*
3. M. R. Dobber, W. J. Buma and C. A. de Lange, *J. Chem. Phys.*, **1993** 99 836.
4. M. G. Szarka, D. S. Green, D. T. Cramb and S. C. Wallace, *J. Phys. Chem. A*, 1997 101 1818.

5. A. Strobel, I. Fischer, A. Loschmidt, K. Müller-Dethlefs and V. E. Bondybey, *J. Phys. Chem.*, **1994** 98 2024.
6. W. C. Price, *J. Chem. Phys.*, **1936** 4 539.
7. A. Gedanken and M. D. Rowe, *Chem. Phys. Lett.*, **1975** 34 39.
8. A. T. J. B. Eppink and D. H. Parker, *J. Chem. Phys.*, **1998** 109 4758.
9. P. Hochmann, P. H. Templet, H.-T. Wang and S. P. McGlynn, *J. Chem. Phys.*, **1975** 62 2588.
10. H.-T. Wang, W. S. Felps, G. L. Findley, A. R. P. Rau and S. P. McGlynn, *J. Chem. Phys.*, **1977** 67 3940.
11. M. A. Baig, J. P. Connerade, J. Dagata and S. P. McGlynn, *J. Phys. B: At. Mol. Phys.*, **1981** 14 L25.
12. J. A. Dagata, G. L. Findley, S. P. McGlynn, J.-P. Connerade and M. A. Baig, *Phys. Rev. A*, **1981** 24 2485.
13. S. Felps, P. Hochmann, P. Brint and S. P. McGlynn, *J. Mol. Spectrosc.*, **1976** 59 355.
14. D. H. Parker, R. Pandolfi, P. R. Stannard and M. A. El-Sayed, *Chem. Phys.*, **1980** 45 27.
15. S. Couris, P. Agapaki and P. Brint, *Laser Chem.*, **1993** 13 151.
16. Z. Min, T. Ridley, K. P. Lawley and R. J. Donovan, *J. Photochem. Photobiol. A: Chem.*, **1996** 100 9.
17. A. Gedanken, M. B. Robin and Y. Yafet, *J. Chem. Phys.*, **1982** 76 4798.
18. D. T. Truch, D. R. Salomon and D. A. Armstrong, *J. Mol. Spectrosc.*, **1979** 78 31.
19. M. A. Baig, J. Hormes and J. P. Connerade, *J. Phys. B: At. Mol. Phys.*, **1982** 15 L5.
20. C. E. Moore, *Circ. Nat. Bur. Stand.*, **1958** 467 Vol. III 105.
21. L. J. Radzieminski and V. Kaufman, *J. Opt. Soc. Am.*, **1959** 59 424.
22. J. F. Black and I. Powis, *J. Chem. Phys.*, **1988** 89 3986.
23. T. N. Olney, G. Cooper and C. E. Brion, *Chem. Phys.*, **1998** 232 211.
24. J. L. Ragle, I. A. Stenhouse, D. C. Frost and C. A. McDowell, *J. Chem. Phys.*, **1970** 53 178.

25. J.A. Blush, P. Chen, R.T. Wiedmann and M. G. White, *J. Chem. Phys.*, **1993** 98 3557.

26. J. Dyke, N. Jonathan, E. Lee and A. Morris , *J. Chem. Soc. Faraday Trans. 2*, **1976** 72 1385.

27. D. Hanstorp and M. Gustafson, *J. Phys. B. At. Mol. Phys.*, **1992** 25 1773.

28. P. S. Przaic, J. Marks and J. I. Brauman, in *Gas Phase Chemistry Vol. 3* (Edited by M. T. Bowers), Academic Press, Orlando, **1984**.

29. E. Ofako and E. Whittle, *Int. J. Chem. Kin.*, **1975** 7 287

30. M. S. N. Al-Kahali, Ph. D. Thesis, University of Edinburgh, **1996**.

31. R. Trainham, G. D. Fletcher and D. J. Larson, *J. Phys. B. At. Mol. Phys.*, **1987** 20 L777.

Chapter 5

Multiphoton Rydberg Transitions in CF_3I

5.1 Introduction

In preceding chapters, a systematic study of the multiphoton spectra of methyl bromide, methyl iodide and methyl chloride has been discussed. Here, the multiphoton Rydberg transitions of CF_3I are discussed. Since similarities are expected between methyl iodide and trifluoromethyl iodide, the same description will be employed also for Rydberg states of the latter. The multiphoton polarisation selection rules employed in previous chapters also prove useful here. Together with the foregoing, the propensity rules seen in the spectra of the other methyl halides are used here to aid the assignment of the spectra of CF_3I. However, it will be seen that several differences are apparent in the spectra of CH_3I and CF_3I. The fluorine substitution has some role in these differences and this is also discussed.

5.1.1 UV and VUV Spectroscopy

Like methyl iodide, the UV spectrum of CF_3I is composed of a single continuum absorption band extending from 312 nm to 220 nm[1]. The repulsive valence states not only lie in a similar energy region in CF_3I to those in methyl iodide but also display very similar properties. Like methyl iodide, CF_3I is also a model system for the study of the photodissociation dynamics of a polyatomic molecule.

However, the VUV spectroscopy of trifluoromethyl iodide has not attracted the same level of attention. This begins at 174nm with a sharp well resolved system with more diffuse systems seen to higher energy. The band system at about 174 nm have been studied in the greatest detail, attracting two studies[2,3]. Sutcliffe and Walsh[2] reported the earlier study containing a detailed vibrational analysis of the 6s cluster. One difference between the appearance of [3/2]6s systems in methyl iodide[4] and

trifluoromethyl iodide, apart from their energies, is the greater amount of sequence band structure in the spectrum of the latter. Herzberg[3] followed this up with a more detailed study of the [3/2]6s state, assigning it as an E (Ω=1 in an (Ω_c, ω_{Ryd}) coupling scheme) state on the basis of a detailed analysis of the Jahn-Teller splitting in the lowest energy sequence bands. As regards the higher energy bands, these have only been studied in any detail by Sutcliffe and Walsh[2]. The [1/2]6s system was seen about 160 nm while higher energy features were assigned to higher members of *ns* series, up to n=9, based upon energetic considerations. Some of these were seen to be more diffuse than the [3/2]6s system. Upon nearing the first ionisation energy, it is likely that the spectrum became too congested for it to be analysed. Some vibrational analysis of the [1/2]6s and [3/2]7s states was reported also. Surprisingly, no evidence of transitions to *np* states was presented. Equally surprising is the fact that further examinations of the VUV spectrum extending its understanding have not been reported given that methyl iodide has been subject of so much interest[5-7].

5.1.2 Previous Multiphoton Studies

Some REMPI studies have been reported[8-10] for CF_3I. Recently, Stolte and co-workers[8,9] have re-examined the 6s cluster in some detail. In addition to the 6s states discussed above, which have Ω=1, features were also assigned to [3/2]6s;2 and [1/2]6s;0 states. Two-photon polarisation studies were used to aid the vibronic analysis of the [1/2]6s cluster. The bands comprising the [1/2]6s cluster were seen to be much broader than those comprising the [3/2]6s cluster, in agreement with previous VUV studies[2]. This was attributed to an interaction of the [1/2]6s states with a nearby $^1A_1$ (or Ω=0) valence state. The unusual intensity distribution exhibited by bands comprising the [1/2]6s;0 system was also attributed to this state. Also, some new two-photon resonances in CF_3I were observed by Waits et al.[10] in their photofragmentation study of CF_3I^+. These features occurred in the 65300-66700 cm^{-1} region but no features were seen to higher energy of these. The new features were tentatively ascribed to a [3/2]6p state but no vibronic analysis was presented, possibly because the unexpected appearance of the observed band system prevented its easy

assignment. It is interesting to note that these features were absent from the one-photon spectrum in the same energy region.

5.1.3 Photoelectron Spectroscopy

Since this study is only concerned with Rydberg states based upon the two lowest energy ionic states, discussion of the photoelectron spectroscopy of CF_3I will centre upon these ionic states. One of the better resolved He I photoelectron spectra of trifluoromethyl iodide was reported by Cvitaš et al.[11]. Like methyl iodide[12], there is again a spin-orbit splitting of the $\tilde{X}\ ^2E$ ionic state in CF_3I and a splitting of 5888 cm^{-1} was observed. However, some differences in the photoelectron spectra of both molecules are evident. Firstly, the entire photoelectron spectrum of the $\tilde{X}\ ^2E$ cluster is shifted to much higher energy and this can be attributed to the fluorine substitution. Another difference possibly due to the fluorine substitution is apparent when the vibronic structure of the $\tilde{X}\ ^2E_{3/2}$ and $\tilde{X}\ ^2E_{1/2}$ states of methyl iodide[12] and trifluoromethyl iodide[11] are compared. A greater degree of vibrational excitation was seen in the spectrum[11] of CF_3I, although again only symmetric modes were seen.

The differences between the $\tilde{X}\ ^2E_{3/2}$ ionic states in $CH(D)_3I$ and CF_3I are also borne out in ZEKE-PFI photoelectron spectroscopy. In a recent one-colour coherent two-photon (C2P) study[13] of CF_3I, an adiabatic ionisation energy of 83652±2 cm^{-1} was obtained for the $\tilde{X}\ ^2E_{3/2}$ ionic state. This is much higher than the first ionisation energy of methyl iodide. However, any attempt to obtain a spectrum of the higher spin-orbit state proved unsuccessful. Like the He I spectrum[11], there is also a great degree of vibrational activity seen in the C2P ZEKE-PFI spectrum[13] of CF_3I and, apart from the origin, the observed features are assigned to the fundamentals, overtones and combinations of the symmetric modes ν_1 (C-F stretch), ν_2 (CF_3 bend) and ν_3 (C-I stretch). However, unlike the one-colour two-photon ZEKE-PFI spectrum of methyl iodide[14], where evidence of bond-stretching at the first photon level is seen, the extensive vibrational structure in the C2P ZEKE-PFI spectrum of CF_3I is more likely to be due exclusively to transitions within the Frank-Condon window of the

neutral electronic ground state. Bond-stretching at the intermediate level can be further discounted in the two-photon ionisation of CF_3I because the first photon energy lies within the high energy tail of the A-band. This means that C2P ionisation via virtual intermediate states gives rise to the observed ZEKE signal in the case of CF_3I. Therefore, a more meaningful comparison would be with the VUV ZEKE-PFI spectrum of methyl iodide reported by Zhu and Grant[15]. It is in this comparison that one immediately can see that there is a greater degree of vibrational activity in the spectrum of trifluoromethyl iodide.

Given that one-colour C2P ZEKE-PFI is more likely to result from the simultaneous absorption of two photons, one further factor must be considered before the ZEKE spectrum is used to predict the appearance of the Rydberg band systems. In ZEKE spectroscopy, the relative intensities of features comprising the observed spectrum are not due entirely to Franck-Condon and Hönl-London factors because of the indirect ionisation scheme involved. However, upon comparison with the conventional photoelectron spectrum, it is seen that the intensities of the observed features are more likely due solely to the Franck-Condon factors for the underlying vibronic transitions. This means that the vibronic band system is indicative of the orbital from which the electron is being removed. While the HOMO (Highest Occupied Molecular Orbitals) in methyl iodide are mainly non-bonding in character meaning that they are localised upon the iodine atom, this does not appear to be the case in CF_3I. A possible explanation for this would be if the HOMO in CF_3I were to contain more bonding character than they do in methyl iodide. This could arise through mixing of the I($5p\pi$) orbitals with unoccupied orbitals of *e* symmetry resulting from antibonding combinations of the three F($2p\sigma$) orbitals with the C($2p\sigma$) and C($2p\pi$) ones. This, coupled with the strong spin-orbit quenching of any Jahn-Teller interaction, a similar vibronic envelope would be expected for the $\tilde{X}\ ^2E_{1/2}$ ionic state which was not seen in the ZEKE-PFI spectrum, possibly as a result of enhanced spin-orbit autoionisation of the very high *n* Rydberg doorway states based upon it.

The altered properties of the HOMO in trifluoromethyl iodide would have repercussions for Rydberg transitions resulting from promotion of an electron from them. Thus, unless Rydberg~valence or Rydberg~ion-pair interactions were to distort the appearance of the observed band systems, the VUV and multiphoton spectra are expected to display Rydberg transitions with a great deal of vibrational structure. Not only would this be a departure from the type of spectra seen for methyl iodide but it would also mean more spectral congestion which could make the spectral analysis less tractable.

5.2 Additional Experimental Details

The one-colour (2+1) and (3+1) REMPI spectroscopy of trifluoromethyl iodide was studied using UV and visible light in the 280-470 nm region. Two-colour experiments were carried out using both bound-free-bound and non-resonant two-photon excitation schemes. In non-resonant two-colour two-photon excitation, the energy of the first photon was fixed at various wavelengths between 211.5 nm and 215 nm, immediately outside the continuum UV absorption band, while the second photon energy was scanned in the 385-555 nm wavelength range. For the bound-free-bound experiments, the wavelength of the first photon was scanned in the 220-275 nm region with the energy of the second photon being fixed at various values (for example, at 362.5 nm or 380 nm for the [3/2]6p system) according to the system being studied. The molecular beam was produced by pulsing the sample seeded in helium through a nozzle. The total backing pressures used were typically 700 torr with the proportion of total pressure due to the sample typically being 20%. Spectra are normalised to the square or the cube of the laser power only where relative intensities of different features are sought and it is easy to do so reliably. Where polarisation behaviour is discussed, comparisons often are made between two spectra that are not power normalised. However, these comparisons still remain valid because both spectra concerned were recorded sequentially thus ensuring that little or no change in dye laser power occurs between both scans. The majority of the tabulated band positions have been calibrated using transitions in atomic iodine[16].

5.3 Spectroscopic Survey

Since a thorough examination of the one-colour two-photon spectrum of trifluoromethyl iodide in the 57000-84000 cm^{-1} region has remained unreported, this was one of the aims of this study. The 6s cluster was re-examined with two-photon excitation and the two-photon spectrum extended to higher energy. However, it did not prove possible to extend the two-photon spectrum to higher energy of the [3/2]6p cluster. Like methyl iodide, two-photon Rydberg transitions in trifluoromethyl iodide proved to be of insufficient strength to compete effectively with the one-photon dissociation process. This was in spite of the greater transition strengths expected for CF_3I Rydberg states than for those occurring in the same energy region in methyl iodide because the former are of lower *n*. However, the more extensive vibronic envelopes suggested by photoelectron spectroscopy of trifluoromethyl iodide would dilute Rydberg state transition strengths. This would prevent two-photon Rydberg transitions from competing effectively with one-photon dissociation and preclude their observation.

Given that the A-band continuum was avoided by the wavelengths involved, it was hoped that three-photon spectroscopy might prove more fruitful in extending the Rydberg spectrum up to and including the first ionisation energy. However, the higher energy features were seen to be more diffuse which suggests that predissociation greatly curtails Rydberg series in CF_3I.

Also, with a view to extending the two-photon spectrum, a two-colour coherent two-photon excitation scheme was employed such that the resonances giving rise to the continuum UV band could be avoided. However, only diffuse structure was observed.

Two-colour bound-free-bound experiments were tried for states comprising the [1/2]6s and [3/2]6p clusters. Based upon the observations of Min et al. for the [1/2]6s;0 state in methyl iodide[17], extended progressions in ν_3, the C-I stretch, were

expected for the states in CF_3I. While little change is seen in the spectrum of the [3/2]6p cluster with respect to the one-colour REMPI spectrum, no bound-free-bound spectrum was attainable for the [1/2]6s;0 state. This is at least partly due to the low transition strength of the [1/2]6s;0 transitions. For instance, the origin band of the [1/2]6s;0 state is between two and three orders of magnitude less intense than the most intense band in the [3/2]6p system.

Most of the attention regarding the multiphoton spectra of methyl bromide, methyl iodide and methyl chloride centred upon electronic assignments and not vibrational ones. However, it was possible only to examine a smaller number of Rydberg states in the case of trifluoromethyl iodide. Also, since a greater degree of vibronic activity is observed for these Rydberg transitions, greater attention is paid to vibronic analysis in this study. The observed Rydberg systems of CF_3I will be discussed in turn with most attention being centred on the [3/2]6p system. Although it has been studied in detail before[8,9], the 6s cluster will be discussed here in light of the recent ZEKE-PFI spectrum[13] and for sake of comparison with the former system. The assignment of the [3/2]6p cluster, aided by ZEKE-PFI PES[13] and multiphoton polarisation studies, are then discussed in greater depth. Finally, some higher energy resonances seen in the one-colour three-photon spectrum are briefly mentioned and possible assignments suggested for some of them.

5.4 Two-Photon Spectroscopy of the 6s Cluster

Although studied in detail before[8,9], the 6s cluster in CF_3I was re-investigated in preparation for the study of its higher energy states. Here, some comments are made regarding the appearance of the vibronic band systems due to the 6s states. Two-photon polarisation studies were carried out for the [1/2]6s states for their use as models for the polarisation behaviour of higher energy two-photon transitions. These confirm that Ω remains good even with some differences in geometry of CF_3I in its excited states relative to methyl iodide. The assignments of Taatjes et al.[9] are accepted for the most part with only a few changes being made.

If, as in the methyl halides, the vibronic envelopes of any observed Rydberg states follow closely that of the state of the ion upon which they are based, then there is little suggestion from the C2P ZEKE spectrum that the vibronic envelopes of the CF_3I Rydberg states will be in any way similar to those of the methyl halides. In this light, the appearance of the band systems exhibited by the states comprising the 6s cluster is somewhat surprising. This is especially the case for the [3/2]6s;1 and [1/2]6s;1 band systems, the appearances of which are alike. This similarity might not be so apparent from Figure 5-1 or Figure 5-2. The intensity of the [3/2]6s;1 origin band is quite likely exaggerated by the nature of the dye laser power spectrum in the wavelength regions depicted. However, the similarity between the two Ω=1 states becomes more apparent when the more reliable intensity data available for the [3/2]6s;1 band system from the study of van den Hoek et al.[8] is used. This shows a band system for the [3/2]6s;1 state which is very like that for the [1/2]6s;1 state, the latter depicted in Figure 5-1. The departures in the appearances of the 6s;1 band systems might be explained if the greater amount of penetration of the ionic core by the Rydberg electron occupying a 6s orbital were to mean that the underlying states were to possess a greater degree of valence character. This could also occur through a linear combination of 6s and σ^* orbitals, the latter arising from combinations of the three F(2pσ) orbitals with the C(2pσ) and C(2pπ) ones. If the 6s Rydberg orbital were to gain an increased amount of valence character in this manner, this might explain the similarities in geometry between the electronic ground and 6s Rydberg states and why vibronic envelopes unlike those of the two lowest-lying ionic states are observed.

However, an increased amount of valence contamination of the 6s Rydberg orbital would not explain the intensity distribution of the features comprising the [1/2]6s;0 band system, also depicted in Figure 5-3. The intensity distribution of this band system more closely follows that seen for the $\tilde{X}\ ^2E_{3/2}$ ionic state in the ZEKE spectrum than the 6s;1 states already discussed. It is surprising that different

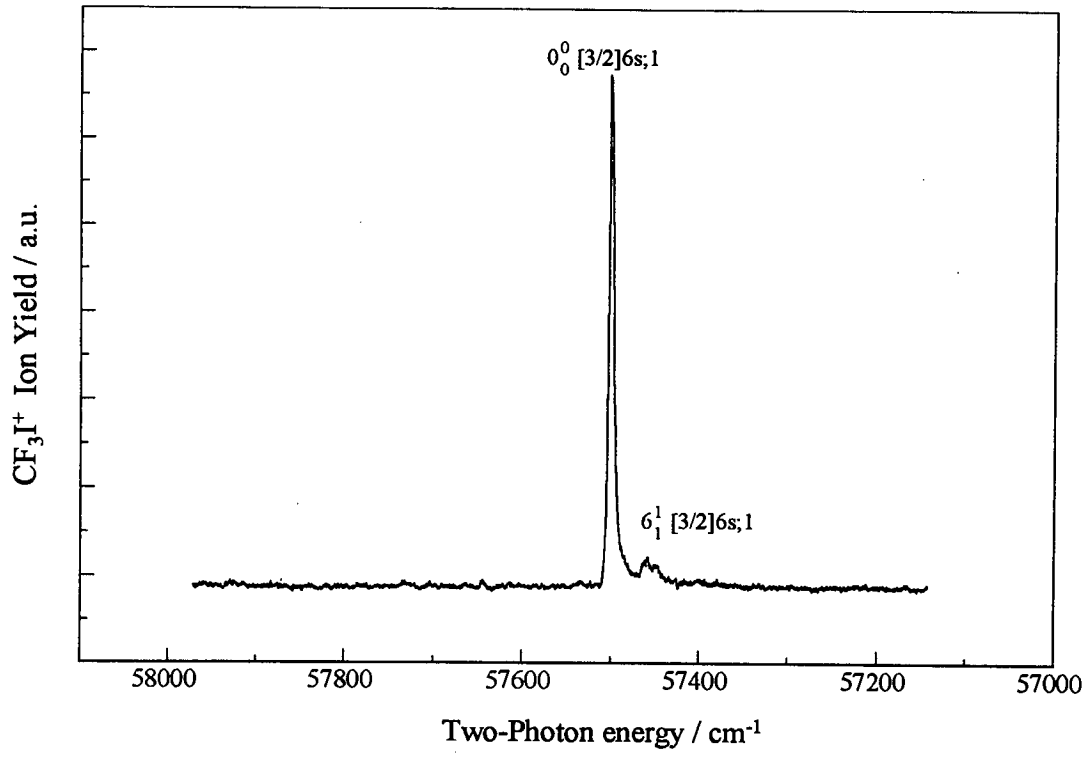

Figure 5-1: The two-photon spectrum of the [3/2]6s;1 state of CF_3I detailing the intensity of the origin band relative to any vibrational structure that may be built upon it. Care is required when interpreting relative intensities because the spectrum has not been normalised to the square of the laser power. See text for more details.

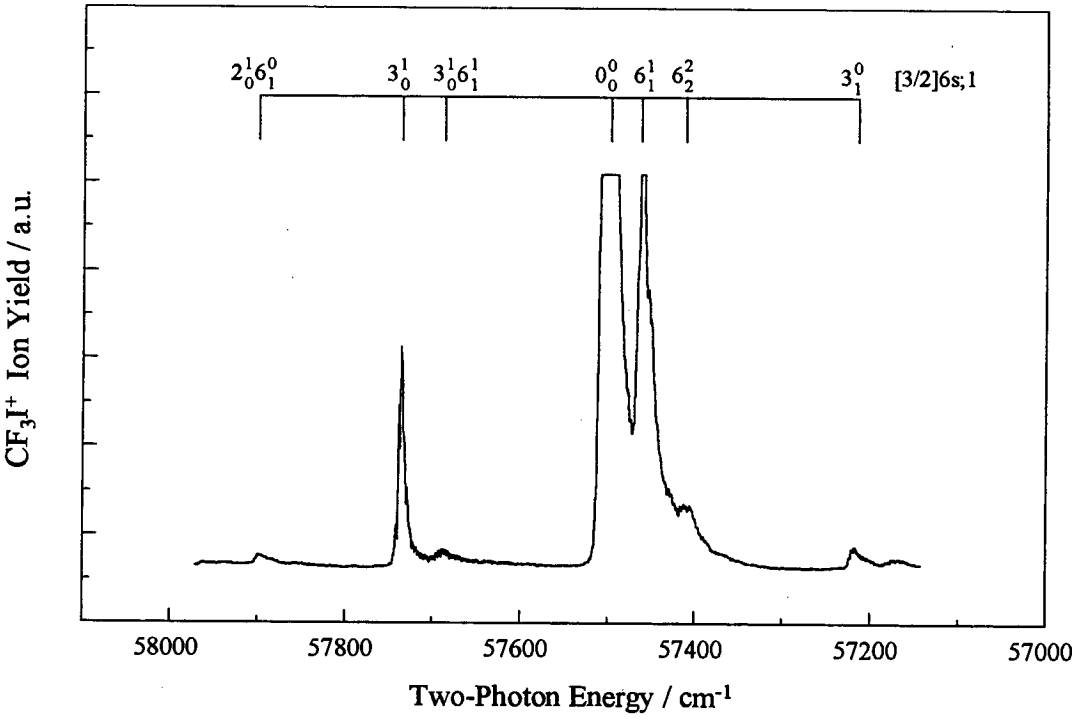

Figure 5-2: Intensity expansion of the two-photon spectrum of the [3/2]6s;1 state of CF_3I depicting its vibrational structure. The assignments adapted are from the work of Taatjes et al.[9] Again, the spectrum has not been power normalised.

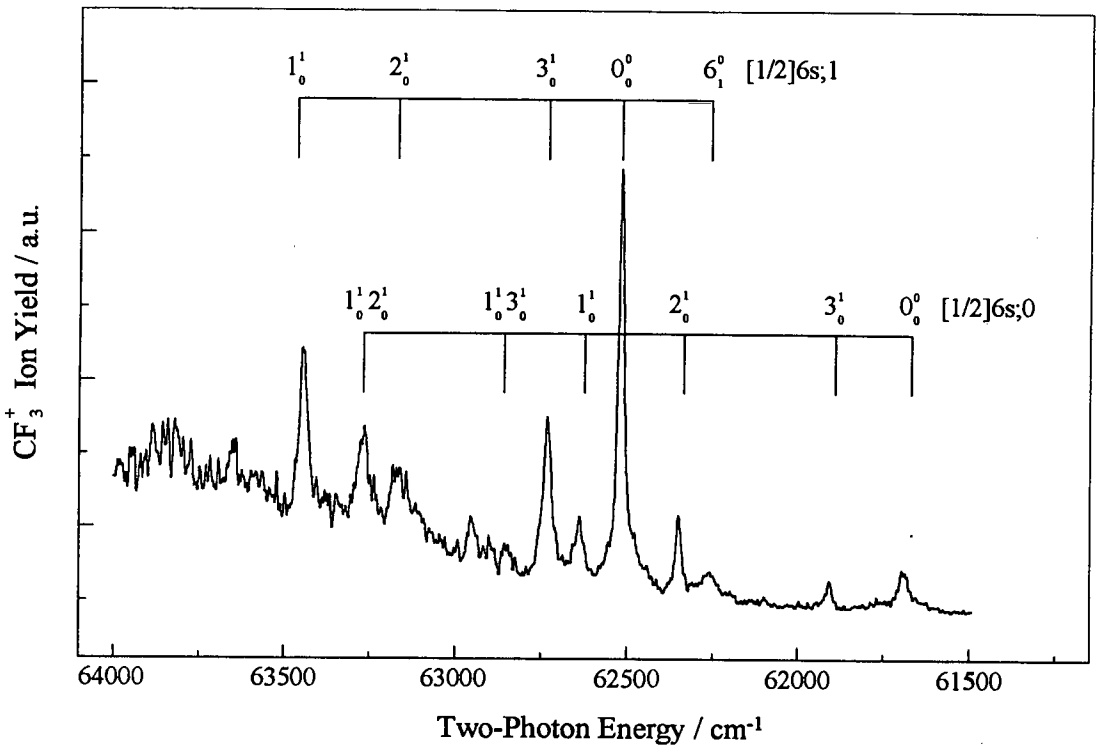

Figure 5-3: The power-normalised two-photon spectrum of [1/2]6s states of CF_3I. The rising background in this region is more likely due to a nearby Ω=0 continuum valence state and not any spectral aberration. The vibronic assignments have been adapted from the work of Taatjes et al.[9] with minor revisions.

components of the same Rydberg cluster would display varying degrees of Rydberg or valence character unless these Rydberg states were to interact to different extents with a nearby ion-pair state. Taatjes et al.[9] used density functional SCF calculations to predict where valence or ion-pair states might lie within the energy region occupied by components of the 6s cluster but these only indicate the presence of a singlet state with Ω=0 within the energy region of interest. The appearance of a perceptible rise in background signal in the vicinity of the [1/2]6s cluster, depicted in Figure 5-3, would seem to justify the occurrence of such a state. In fact, the broad background feature centred about 63200 cm^{-1} has been assigned to a singlet Ω=0 valence state by Taatjes et al.[9]. Homogeneous interaction of the [1/2]6s;0 state with a nearby valence or ion-pair state might explain the different appearance of its band system to those of the 6s;1 states but seems surprising in that an intensity distribution more like that of the two low-lying ionic states is produced.

Although most of the assignments of the 6s cluster proposed by Taatjes et al.[9] are accepted here, some amendments are made. One of the more notable of these regards a feature at 62362 cm^{-1} which was attributed a $5^1_0 6^1_0$ [1/2]6s;0 assignment. The reason given in support of the $5^1_0 6^1_0$ assignment was that a large distortion in molecular geometry, mixing the normal co-ordinates through Duschinsky rotation, had occurred. Some dynamic Jahn-Teller splittings were seen in the spectra of the 6s cluster but are not extensive enough to suggest that this kind of distortion occurs. Thus, this band is attributed the more likely 2^1_0 [1/2]6s;0 assignment. Another point regarding the vibronic structure of the 6s cluster in CF_3I is that there is a perceptible amount of sequence band excitation, in ν_6, seen even though the spectra have been obtained using jet-cooled sample. This is not the case in methyl iodide. The greater population in ν_6=1 in the electronic ground state is most likely due to the lower vibrational frequencies in CF_3I. The vibrational assignments of the [1/2]6s cluster are given in Table 5-1.

Band Measurements cm^{-1}	**Assignments**	**Vibrational Spacings** cm^{-1}
61695	0^0_0 [1/2]6s;0	0
61906	3^1_0 [1/2]6s;0	211
62264	6^0_1 [1/2]6s;1	-258
62351	2^1_0 [1/2]6s;0	656
62520	0^0_0 [1/2]6s;1	0
62640	1^1_0 [1/2]6s;0	945
62734	3^1_0 [1/2]6s;1	214
62858	$1^1_0 3^1_0$ [1/2]6s;0	1163
63182	2^1_0 [1/2]6s;1	662
63269	$1^1_0 2^1_0$ [1/2]6s;0	1574
63447	1^1_0 [1/2]6s;1	927

Table 5-1: Vibrational assignments of the [1/2]6s cluster.

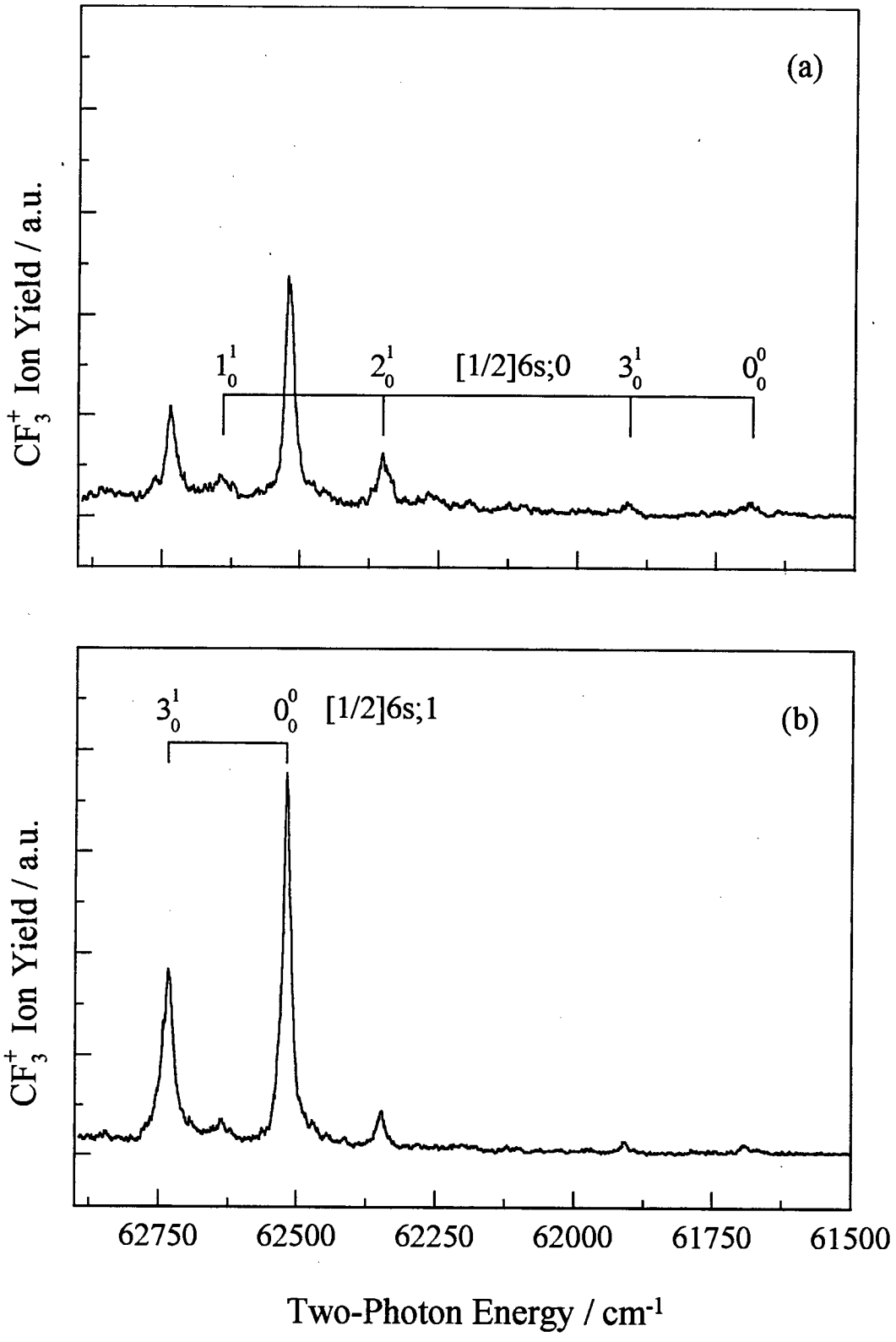

Figure 5-4: Polarisation dependence of some features comprising the [1/2]6s cluster in CF_3I. The spectrum recorded with linearly polarised light is depicted in panel (a) while panel (b) shows the one recorded using circularly polarised light.

Although the polarisation behaviour of the [1/2]6s cluster has been studied by Taatjes et al.[9], it is was reinvestigated as a benchmark for interpreting the polarisation behaviour that might be observed for the [3/2]6p cluster. The results of this study are shown in Figure 5-4. However, the two-photon polarisation ratio, ρ_2, of the features making up the [1/2]6s;0 band system is nearly unity for some of the features comprising it. In contrast, ρ_2 for features due to the [1/2]6s;1 state is near 1.5 as expected. This is similar to the situation seen in the (2+1) REMPI spectrum of Br_2 previously[20]. The two-photon polarisation ratio of features due to the [1/2]5s;0 state of molecular bromine were nearly 1.5 and this was attributed to differences between the excitation pathway terminating in the [1/2]5s;0 state and those terminating in *nd*;0 states. These differences were attributed to the pure triplet character of the [1/2]5s;0 state and the possible contribution of the B $^3\Pi_{0^+}$ to the virtual intermediate state involved. Similarly in CF_3I, the near unity two-photon polarisation ratios seen for some features comprising the [1/2]6s;0 band system could result from its pure triplet character and contribution of the $^3Q_0$ state to the virtual intermediate state involved. Therefore, the observed polarisation behaviour of the [1/2]6s cluster implies that Ω remains good in CF_3I and that the polarisation selection rules already described for the methyl halides should also apply here. This will prove especially useful when assigning the features making up the [3/2]6p band system.

Several departures from the expected behaviour for molecular Rydberg states are seen in the 6s cluster of CF_3I. In light of the perturbations seen in the [3/2]6s cluster, the vibrational frequencies do seem amazingly regular. In the [3/2]6p cluster, described below, where the latter does not hold, several departures occur which may not be so surprising in light of the 6s cluster.

5.5 Two- and Three-Photon Spectroscopy of the [3/2]6p System

A complete vibronic analysis is carried out newly for the [3/2]6p cluster because the unexpected appearance of its band systems has previously precluded such analysis[10]. Electronic assignment of the different components is established in

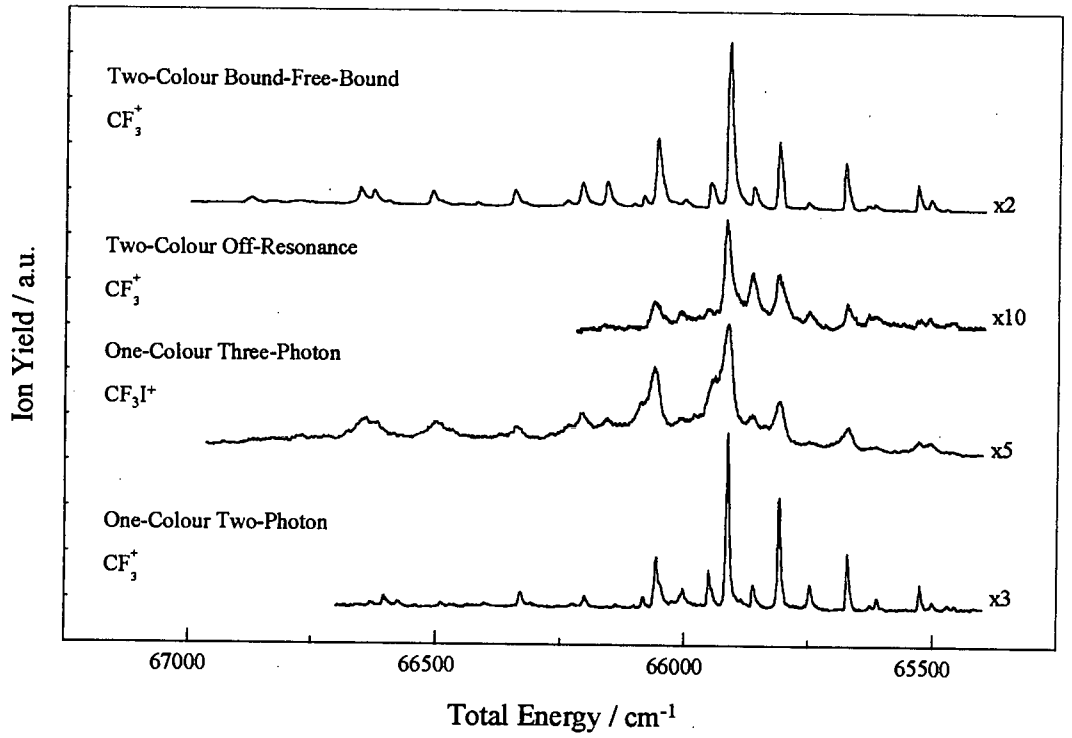

Figure 5-5: The [3/2]6p system in CF_3I accessed using different excitation schemes. The depicted spectra have been displaced for sake of clarity.

the light of two- and three-photon polarisation data. Given the complexity of the band systems, even this additional information is insufficient for their full vibrational analysis. The use of different excitation schemes confirms that the appearance of the vibronic band systems is intrinsic to the excited states involved and does not arise as a result of the excitation scheme used. The spectra obtained using these different excitation schemes are depicted in Figure 5-5. Individual vibrational assignments can only be made using the additional information provided by (2+1') ZEKE-PFI PES[13]. Following this analysis, it is seen that the [3/2]6p cluster is perturbed and is made up of band systems unlike those of the ionic ground state or the 6s states. Possible explanations for this are given. Perturbations of the [3/2]6p cluster in CF_3I become more apparent in a comparison with the equivalent states in methyl iodide in terms of propensity rules and the appearances of their respective band systems.

5.5.1 Electronic Assignments

Because the spectral appearance of the [3/2]6p system, depicted in Figure 5-5, contrasts so sharply with that of the 6s cluster, discussed earlier, each of the observed features would have to form part of overlapping band systems arising from different substates if the states themselves were well-behaved. In view of this, two- and three-photon polarisation studies were carried out in order to identify the underlying components of the [3/2]6p cluster giving rise to the individual features. As discussed earlier, two-photon polarisation studies of the [1/2]6s cluster appear to confirm that Rydberg states in CF_3I can be described using Ω and exhibit a similar kind of polarisation dependence to those in methyl iodide. Most of the features comprising the [3/2]6p system which lie above 66800 cm^{-1}, do in fact behave in a similar manner to the singlet-singlet $\Delta\Omega=0$ transitions in the methyl halides. Thus, these are attributed to the singlet [3/2]6p;0 state, as depicted in Figure 5-7. Features forming part of the [3/2]6p cluster but occurring in the 65400-66800 cm^{-1} region were found to have $\rho_2>1$. This leaves several possibilities open. These features could arise from $\Omega=1$ or $\Omega=2$ states or both possibilities together. The usefulness of three-photon polarisation studies has already been shown in preceding chapters for the analysis of Rydberg transitions in the methyl halides and is evident again here. It is seen that most of the features in the 65400-66800 cm^{-1} region have $\rho_3\cong2.5$ which implies that they arise from transitions with $\Delta\Omega=2$. Examples of this type of polarisation behaviour are shown in Figure 5-6. However, it also can be seen in Figure 5-6 that there is one exception to this general trend, the feature at about 65489 cm^{-1}. This feature arising has $\rho_3 \cong 1$ and $\rho_2 \leq 1.5$ which is consistent with an assignment to a [3/2]6p;1 state. Thus, the polarisation studies suggest that there is a single strong $\Omega=2$ state, a weaker $\Omega=0$ state and an $\Omega=1$ state which gives rise to one of the less intense features. The band positions of the [3/2]6p;2 and [3/2]6p;0 states as well as that for the only band attributable to a [3/2]6p;1 state are in given in Table 5-2.

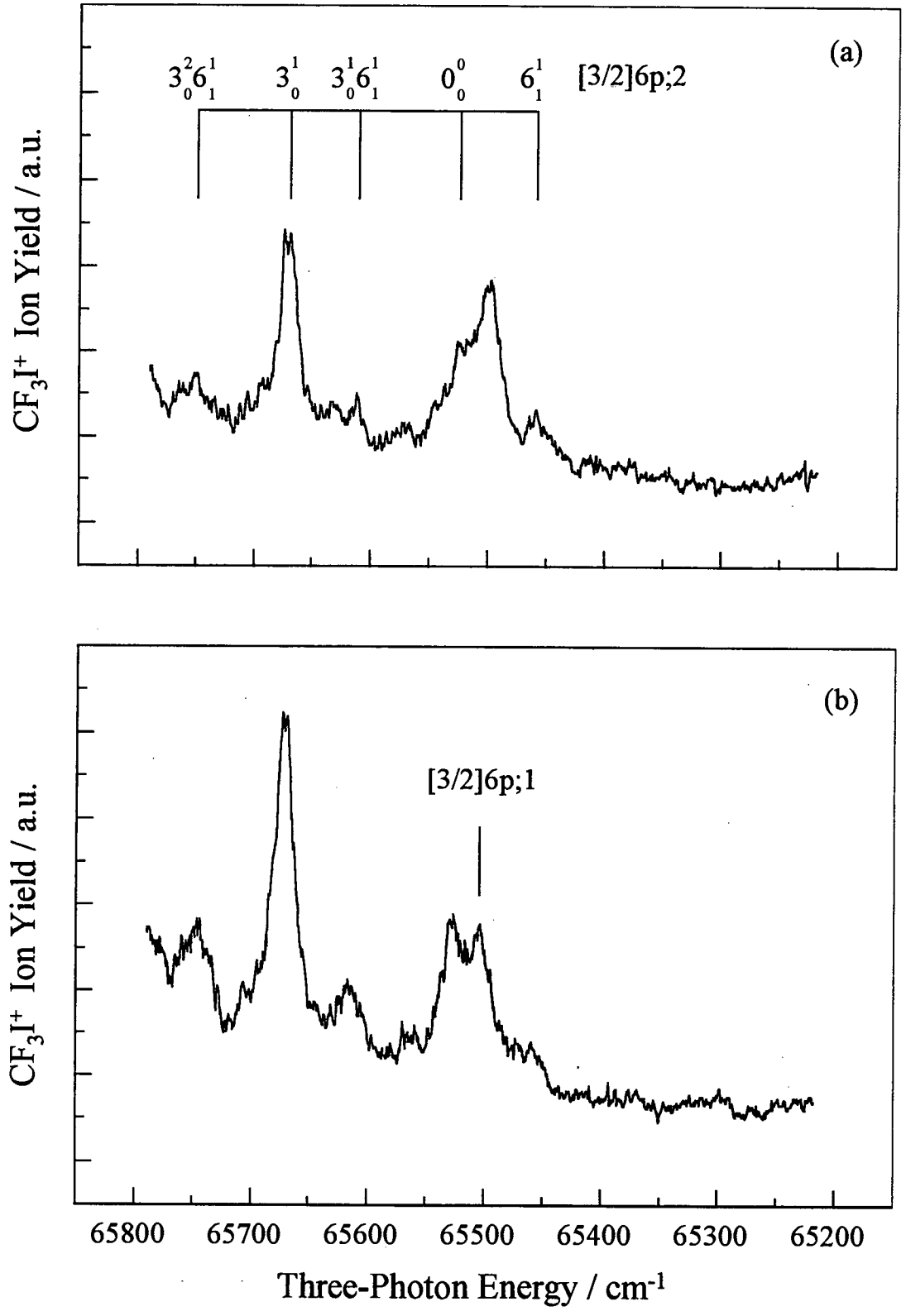

Figure 5-6: Expansion of the (3+1) REMPI spectrum detailing the polarisation behaviour of a [3/2]6p;1 state. Panel (a) depicts the spectrum recorded using linearly polarised light and panel (b) depicts the one recorded with circularly polarised light.

Assignment	One-Colour		Two-Colour	
	Two-Photon Energy / cm^{-1}	Three-Photon Energy / cm^{-1}	Off-Resonance Energy / cm^{-1}	Bound-Free-Bound Energy / cm^{-1}
6p;1	65489	65501	65494	65494
6p;2	65514	65519	65514	65517
6p;0	~	~	~	66889

Table 5-2: Electronic assignment of the [3/2]6p cluster in CF_3I. See Ref. 13 for a discussion of the one-colour two-photon spectroscopy of the [3/2]6p;0 state. Apart from the feature assigned to a [3/2]6p;1 state, for which a vibrational assignment is unknown, all band measurements are for electronic origins.

5.5.2 Vibrational Assignments

The agreement between the two- and three-photon polarisation studies suggests that the observed structure does not result from a bound-free-bound excitation involving the continuum valence states underlying the A-band in CF_3I. To add to this, two-colour bound-free-bound and off-resonance experiments were carried out with little or no change in the observed spectra, depicted in Figure 5-5. While the similarity of the two-colour bound-free-bound spectrum to the one-colour two-photon spectrum would suggest the involvement of a real intermediate state, the similarity of two-colour off-resonance spectrum, where any real intermediate resonance has been avoided, confirms the coherent nature of the two- and three-photon excitation pathways. This, together with the polarisation data, confirms that any features seen arise from transitions taking place within the Franck-Condon window of the ground state.

To aid the vibrational assignment of the [3/2]6p;2 band system, a ZEKE-PFI photoelectron study[13] was carried out for CF_3I, pumping at its stronger resonances in a (2+1') REMPI scheme. Vibrational assignments are generally made, assuming diagonal transitions, based on the most intense transition observed in the obtained ZEKE spectra[13]. This results in the assignment of progressions in ν_3 and $\nu_5 + \nu_3$, ν_5 being the asymmetric CF_3 bend. A short progression in ν_6 and combination bands built upon the 1_0^1 and 2_0^1 bands can account for the majority of the remaining structure. In

line with the [3/2]6s;1 state, some sequence band structure is also seen, again in ν_6. There still remain some bands for which no assignment can be found but these are very weak. Also, they are most likely to be due hot band excitations as they are not apparent in a two-photon spectrum of the same region recorded with a skimmed molecular beam[13]. Vibrational assignments of the ZEKE spectra themselves were made with reference to the vibrational spacings of the ground state of the neutral molecule[18,19].

Mode	CF_3I			CF_3I^+
	$\tilde{X}\ ^1A_1$	[3/2]6s;1	[3/2]6p;2	$\tilde{X}\ ^2E_{3/2}$
	$\bar{\nu}$/cm^{-1}	$\bar{\nu}$/cm^{-1}	$\bar{\nu}$/cm^{-1}	$\bar{\nu}$/cm^{-1}
ν_1	1073	970	984	978
ν_2	741	681	715	733
ν_3	286	232	150	205
ν_4	1185	1282	-	-
ν_5	540	525	394	540
ν_6	265	223	225	221

Table 5-3: The vibrational frequencies of the ground[18,19], [3/2]6s;1[9] and [3/2]6p;2 states of CF_3I, and the ground state[13] of CF_3I^+.

However, there is some disagreement between the ZEKE spectra and the polarisation studies. The most intense band in the [3/2]6p system, positioned at about 65902 cm^{-1}, would be assigned as an origin band based on the ZEKE spectrum obtained from it. If this were so, it would imply that there are two Ω=2 states are being seen. However, from the expected electronic structure of CF_3I, one of these would be a pure triplet state. Also, it has been seen in the methyl halides and diatomic halogens[20,21] that singlet-singlet transitions are favoured. Thus, as seen in the [1/2]6s cluster, any triplet state should be seen far more weakly than a singlet state. However, it is clear from the intensity of the features depicted in Figure 5-7 that this is unlikely to be the case here. Also, since the vibrational frequencies differ greatly from those of the neutral[18,19] and ionic ground states[13], which are shown in Table 5-3, it is more

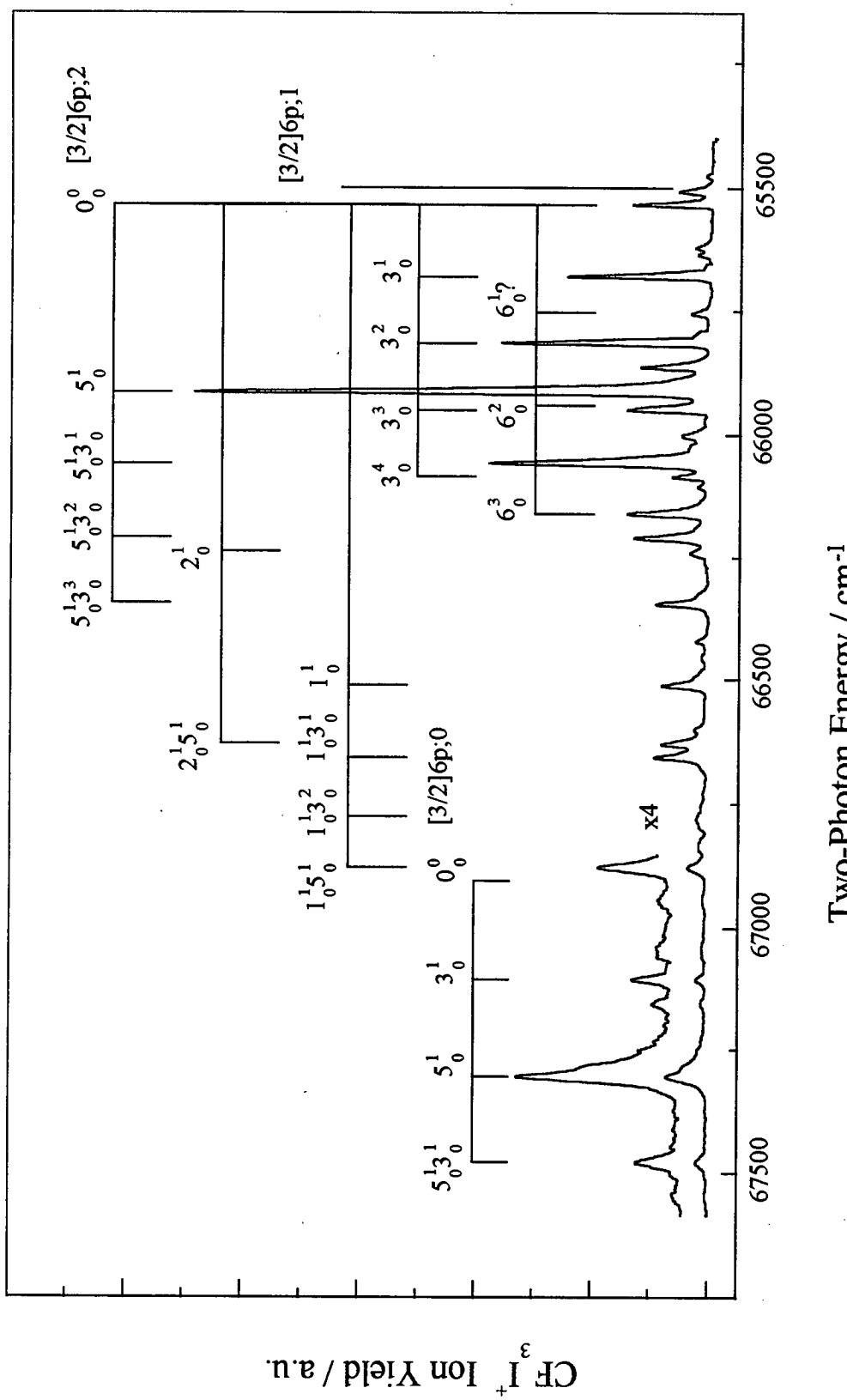

Figure 5-7: Two-colour bound-free-bound-spectrum of CF_3I detailing the vibronic assignments of the [3/2]6p cluster made in light of polarisation and ZEKE-PFI photoelectron studies.

Assignment	One-Colour		Two-Colour	
	Two-Photon Energy / cm^{-1}	Three-Photon Energy / cm^{-1}	Off-Resonance Energy / cm^{-1}	Bound-Free-Bound Energy / cm^{-1}
6_1^1	65459	-	-	65463
0_0^0	65514	65519	65514	65517
$3_0^1 6_1^1$	65605	-	-	65603
$5_0^1 3_1^0$	65620	-	65617	65619
3_0^1	65664	65669	65661	65662
$3_0^2 6_1^1$	65739	-	65738	65738
3_0^2	65802	65806	65798	65801
$5_0^1 6_1^1$	65848	65862	65852	65851
5_0^1	65902	65913	65904	65905
6_0^2	65933	-	-	-
3_0^3	65940	-	65937	65942
$5_0^1 3_0^1 6_1^1$	65996	65997	66996	66996
$5_0^1 3_0^1$	66045	66060	66050	66051
3_0^4	66072	-	-	66079
6_1^4	66100	-	-	-
6_0^3	66152	66160	-	66149
$5_0^1 3_0^2$	66197	66207	-	66197
2_0^1	66227	66238	-	66232
$5_0^1 3_0^3$	66326	66332	-	66332
$1_0^1 6_1^1$	66452	-	-	-
$5_0^1 3_0^4$	66460	66476	-	-
1_0^1	66501	66503	-	66501
$1_0^1 3_0^1$	66614	-	-	66612
$1_0^1 3_0^2$	-	-	-	66765
$1_0^1 5_0^1$	-	-	-	66862

Table 5-4: Vibrational assignments of the [3/2]6p;2 state of CF_3I. All band positions were independently calibrated using atomic iodine lines[16] apart from those in the three-photon spectrum, the uncertainties in which were sufficient that the uncalibrated positions proved to be in good agreement with the calibrated values measured from other spectra.

likely that the state causing the observed features is extremely perturbed. This would mean that any ZEKE transitions starting from vibrational levels of the [3/2]6p;2 state as intermediates are not necessarily diagonal, so some caution must be exercised when using the ZEKE spectra alone to aid the spectral assignment. Thus, on using the ZEKE data in combination with the polarisation data, the band at 65902 cm^{-1} is assigned to the 5_0^1 band built upon the origin of a [3/2]6p;2 state. Thus, the assignment of a strong vibronic system to one Ω=2 state, rather than two, seems more likely. The vibrational assignments for a single [3/2]6p;2 state are given in Table 5-4.

Although no ZEKE spectra were recorded using resonances due to the [3/2]6p;0 state, vibrational assignments can be made based upon those for the [3/2]6p;2 system. As in the case of Ω=2 system, ν_3, ν_5, ν_1 and ν_2 are the active vibrational modes[13]. The vibrational assignments for the [3/2]6p;0 state are given in Table 5-5. One interesting point is that it is apparent from Table 3-7 in Chapter 3 that only one *np*;0 state can exist with the $^2E_{3/2}$ ionic core in the methyl halides and this also applies to CF_3I. Thus, the nature of the vibronic envelope of the [3/2]6p;0 state in CF_3I further confirms the assignment of only one [3/2]6p;2 state, which has been discussed already. While vibrational analysis of the [3/2]6p;2 and [3/2]6p;0 band systems has been possible, the feature assigned to a [3/2]6p;1 state is left with no

Assignment	**Band Position** cm^{-1}	**Vibrational Spacing** cm^{-1}
6p;0 0_0^0	66889	0
6p;0 3_0^1	67089	200
6p;0 5_0^1	67286	397
6p;0 $5_0^1 3_0^1$	67459	570

Table 5-5: Vibronic assignments for the [3/2]6p;0 state seen in the two-colour bound-free-bound spectrum of CF_3I. See Ref. 13 for a discussion of the same state in the one-colour two-photon spectrum.

vibrational assignment. Because of its low intensity, no ZEKE spectrum could be recorded using this feature but a 5_0^1 assignment is the most likely in light of the vibronic structure of the other states in this region. However, a more definite vibrational assignment cannot be made for this band.

5.5.3 Discussion of the [3/2]6p Cluster

The apparent absence of the [3/2]6p band system from the VUV spectrum[2] of trifluoromethyl iodide suggests the operation of propensity rules which differ somewhat from those in methyl iodide. In methyl iodide, the [3/2]6p cluster is as prominent in its VUV spectrum[13] as it is in its multiphoton spectra, discussed in the previous chapter. These trends are consistent with the dominant [3/2]6p component in CF_3I having Ω=2 while the [3/2]6p;0 state is strongest in methyl iodide. The one-photon allowed Ω=0 and Ω=1 substates are much weaker than the one-photon forbidden Ω=2 component in CF_3I and this would preclude their observation in a VUV spectrum recorded with a weaker radiation source. Some disruption in the energy ordering of the [3/2]6p states in CF_3I is evident when compared with the same system in methyl iodide. The [3/2]6p;1 state is much lower lying in trifluoromethyl iodide than it is in CH_3I (CD_3I) but this may well be due to an interaction with a nearby ion-pair state.

Of much more interest are the vibronic envelopes of the observed [3/2]6p states in CF_3I. In methyl iodide, the vibronic envelopes follow closely those of the ionic state upon which the Rydberg state is based but the [3/2]6p states in CF_3I depart significantly from this. There are two possible causes of this. Firstly, some mixing of the 6p Rydberg orbital with unoccupied σ^* orbitals may occur. If this were the case, one might expect band systems more like those exhibited by the 6s;1 states as the molecular geometry would become more like that of the neutral electronic ground state. Consequently, other explanations are sought. For instance, some evidence of interactions between Rydberg states and other states such as valence and ion-pair states seems apparent in the REMPI spectra of methyl iodide. Also, it is known that the lowest *np* states in the diatomic halogens and interhalogens[20,21] as well as those in

the hydrogen halides[22] are most likely to interact with nearby ion-pair states. However, in CF_3I the first thermodynamic threshold for ion-pair formation is calculated to be 66705 cm^{-1}. The values used for this calculation included: 72993 cm^{-1} for the first ionisation energy[23] of CF_3, 18393 cm^{-1} for $D(F_3C\text{-}I)$[24] and 24681 cm^{-1} for the electron affinity of atomic iodine[25]. The first ionisation energy of CF_3 is still subject of much debate and the only available values come from photoionisation studies. The differences in the geometries of the electronic ground states of the neutral and ionic species make any determination difficult. This adds some uncertainty to the determination of the first ion-pair threshold but the value obtained here is sufficiently indicative for the purposes of this discussion. Therefore, given the observed vibrational spacings, interactions with states of the 6p cluster with the first tier $\Omega = 0$ ion-pair state can be ruled out. Nevertheless, an interaction with an ion-pair state belonging from the second tier cannot be ruled out and is in fact quite likely. Also, the vibrational frequency for ν_3 in the [3/2]6p cluster is typically 150 cm^{-1} which is consistent with an ion-pair state given the trends in the diatomic halogens[26]. Thus, the unusual vibrational spacings can be attributed to extensive Rydberg~ion-pair interactions.

5.6 Higher Energy Structure in the Three-Photon Spectrum

Some additional structure is seen in the three-photon spectrum to higher energy of the [3/2]6p cluster that is absent from the two-photon spectrum. An example of this is shown in Figure 5-8. It is clear from the figure that the observed features are far broader than those comprising the [3/2]6p cluster. Upon examination of the spacings between the observed bands, it might be said that any state causing is more ion-like than the lower energy [3/2]6p system although the appearance of the band systems may not always bear this out.

The best resolved features in the three-photon spectrum apart from those due to [3/2]6p states lie within the 68500-72500 cm^{-1} region, depicted in Figure 5-8. Upon examination of the dye laser power spectrum in this region, it is possible to

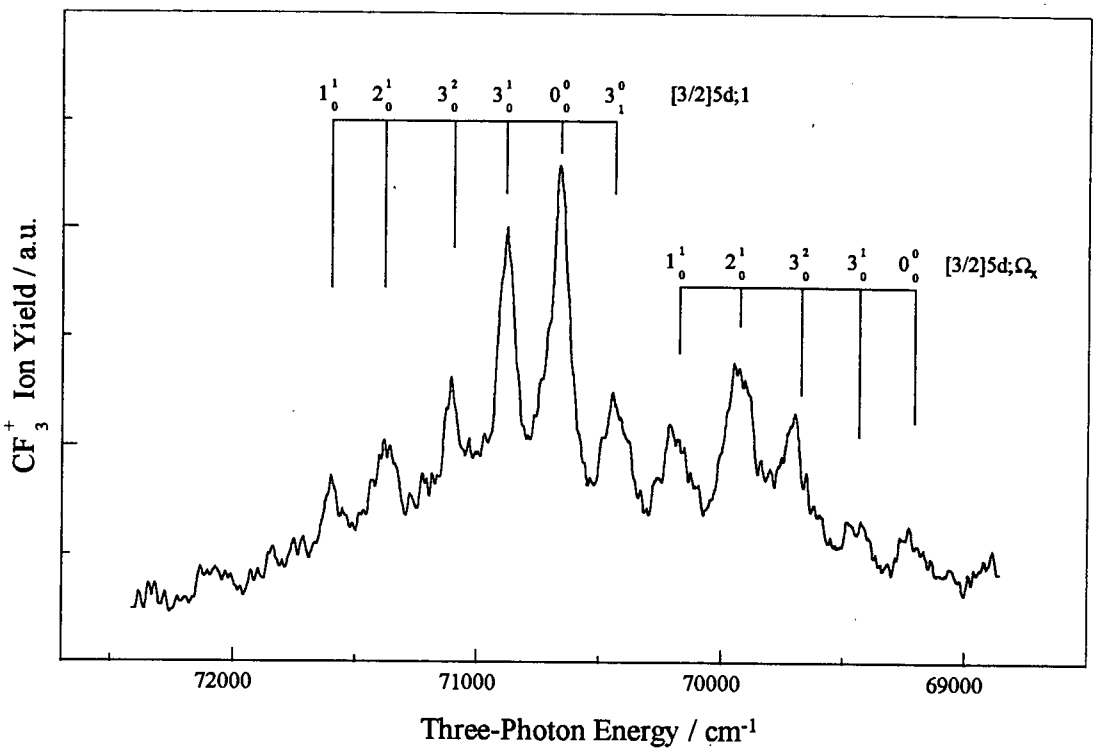

Figure 5-8: Three-photon spectrum of CF_3I in the 68500-72500 cm^{-1} region. The depicted spectrum has not been normalised to cube of the dye laser power so caution must be exercised when comparing the intensities of the observed features.

distinguish two band systems which share similar vibrational structure. On energetic grounds, both [3/2]7s and [3/2]5d assignments for these band systems seem plausible while a [1/2]6p assignment is not impossible either. However, the observed structure bears little resemblance to any state comprising the [3/2]6p cluster. Also, in methyl bromide, the intensity of the [1/2]5p;0 origin band is seen to be about an order of magnitude weaker than the [3/2]5p;0 origin band. Therefore, in light of these considerations, the [1/2]6p assignment can be ruled out. With regard to the [3/2]7s possibility, some bands in the three-photon spectrum do coincide with those seen in the VUV spectrum[2] within the combined uncertainties of their measurements. These resonances have been attributed previously to a [3/2]7s state[2] but in light of the work on methyl iodide presented in the preceding chapter, re-assignment of members of Walsh's *ns* series[2] with $n>6$ to *(n-2)d*;1 series seems more reasonable. Thus, the band

[3/2]5d;Ω_x			[3/2]5d;1		
Band Position cm^{-1}	Vibronic Assignment	Vibrational Spacing cm^{-1}	Band Position cm^{-1}	Vibronic Assignment	Vibrational Spacing cm^{-1}
68897	3_1^0	-311	70441	3_1^0	-267
69208	0_0^0	0	70662	0_0^0	0
69423	3_0^1	215	70883	3_0^1	221
69667	3_0^2	459	71100	3_0^2	438
69928	2_0^1	720	71386	2_0^1	724
70174	1_0^1	966	71602	1_0^1	940

Table 5-6: Vibronic assignments of the [3/2]5d band systems. Because of the uncertainties in the band measurements, which are of the order of 30-40cm^{-1}, wavelength calibration was not attempted.

system lying to higher energy is tentatively assigned to a [3/2]5d;1 state. As regards the lower energy band system, this most likely due to another [3/2]5d state. As regards the Ω-value for this state, this remains unknown because no polarisation studies were undertaken in this region. For a vibronic analysis of these two band systems, one similar to that of Sutcliffe and Walsh[2] is adopted as detailed in Table 5-6.

To even higher energy in the three-photon spectrum, about 77000 cm^{-1}, additional structure is seen but this is again much broader and hence, even more difficult to analyse. Among the electronic states possibly responsible for this band system are [3/2]6d or [3/2]4f;1 states or even a 6s state based upon the $\tilde{A}\ ^2A_1$ ionic core. No structure is seen to higher energy of this band system until an onset is seen in the molecular ion channel near the first ionisation energy at the two-photon level. In light of this observation, the $[^2A_1]$6s assignment does not appear that unlikely. Also, from the ionisation onset in the molecular ion channel, a value for the $\tilde{X}\ ^2E_{3/2}$ ionisation energy can be obtained and, after field-correction, this agrees with the one

obtained using ZEKE-PFI PES within the combined uncertainties in both measurements.

5.7 Conclusion

The REMPI spectroscopy of CF_3I has been discussed in light of the recently reported ZEKE-PFI PES study[13] which shows that significant differences arise between trifluoromethyl iodide and methyl iodide. However, it is seen that the observed Rydberg vibronic envelopes depart from that observed in the ionic ground electronic state in terms of intensity distributions and vibrational spacings. This is attributed to valence contamination of the Rydberg orbitals through mixing with unoccupied σ^* orbitals as well as Rydberg~ion-pair interactions. While the vibronic envelopes of the states comprising the 6s cluster are commented upon, the main focus of attention in this study is the [3/2]6p cluster. In the light of multiphoton polarisation studies, assignments are made to Ω=1, Ω=2 and Ω=0 states, each having at least some singlet character. (2+1') ZEKE-PFI PES has been used to simplify the vibrational analysis. No features assignable to Rydberg states were observed to higher energy of the [3/2]6p level in the one-colour two-photon spectrum. This is at least partially due to the inability of two-photon transitions to compete with one-photon dissociation, like in methyl iodide. Other experiments were carried out with the aim of extending the multiphoton spectrum of trifluoromethyl iodide. Of these, one-colour three-photon spectroscopy proved most successful but any structure observed in the spectrum proved to become progressively more diffuse, and hence more difficult to assign conclusively, with increasing energy. In this respect, it is similar to the VUV spectrum for which an assignment to 6s;1 states and *nd*;1 series would now seem more reasonable in light of the work on the methyl halides presented in earlier chapters.

5.8 References

1. A. Gedanken, *Chem. Phys. Lett.*, **1987** 137 462.
2. L. H. Sutcliffe and A. D. Walsh, *Trans. Faraday Soc.*, **1961** 57 873.

3. G. Herzberg, *Faraday Diss.*, **1961** 35 7
4. S. Felps, P. Hochmann, P. Brint and S. P. McGlynn, *J. Mol. Spectrosc.*, **1976** 59 355.
5. P. Hochmann, P. H. Templet, H-T. Wang and S. P. McGlynn, *J. Chem. Phys.*, **1975** 62 2588.
6. H. T. Wang, W. S. Felps, G. L. Findley, A. R. P. Rau and S. P. McGlynn, *J. Chem. Phys.*, **1977** 67 3940.
7. M. A. Baig, J. P. Connerade, J. Dagata and S. P. McGlynn, *J. Phys. B: At. Mol. Phys.*, **1981** 14 L25.
8. G. van den Hoek, J. W. Thoman, D. W. Chandler and S. Stolte, *Chem. Phys. Lett.*, **1992** 188 413.
9. C. A. Taatjes, J. W. G. Mastenbroek, G. van den Hoek, J. G. Snijders and S. Stolte, *J. Chem. Phys.*, **1993** 98 4355.
10. L. D. Waits, R. J. Horwitz, R. G. Daniel, J. A. Guest and J. R. Appling, *J. Chem. Phys.*, **1992** 97 7263.
11. T. Cvitaš, H. Gusten, L. Klasinc, I. Novadj & H. Vancik, *Z. Naturforsch.*, **1978**, 33a, 1528.
12. A. W. Potts, H. J. Lempka, D. G. Streets and W. C. Price, *Phil. Trans. Roy. Soc. Lond. A.*, **1970** 268 59.
13. N. A. Macleod, S. Wang, J. Hennessy, T. Ridley, K. P. Lawley and R. J. Donovan, *J. Chem. Soc. Faraday Trans.*, **1998** 94 2689.
14. A. Strobel, I. Fischer, A. Loschmidt, K. Müller-Dethlefs and V. E. Bondybey, *J. Phys. Chem.*, **1994** 98 2024.
15. Y-F. Zhu and E. R. Grant, J. Phys. Chem., **1993** 97 9582.
16. C. E. Moore, *Circ. Nat. Bur. Stand.*, **1958** 467 Vol. III 105.
17. Z. Min, T. Ridley, K. P. Lawley and R. J. Donovan, *J. Photochem. Photobiol. A: Chem.*, **1996** 100 9.
18. G. Herzberg, *Molecular Spectra and Molecular Structure III: Electronic Spectra and Electronic Structure of Polyatomic Molecules*, Van Nostrand Reinhold, 1966.
19. W. Fuss, *Spectrochemica Acta A*, **1982** 38 829

20. R. J. Donovan, A. C. Flexen, K. P. Lawley and T. Ridley, *Chem. Phys.*, **1998** 226 217.

21. R. J. Donovan, A. C. Flexen, K. P. Lawley, R. R. J. Maier, A. Mank and T. Ridley, *to be submitted.*

22. Á. Kvaran, A. Logadóttir and H. Wang, *J. Chem. Phys.*, **1998** 109 5856.

23. R. L. Asher and B. Ruscic, *J. Chem. Phys.*, **1997** 106 210.

24. E. Ofako and E. Whittle, *Int. J. Chem. Kinetics*, **1975** 7 287.

25. D. Hanstrop and M. Gustafson, *J. Phys. B: At. Mol. Opt. Phys.*, **1992** 96 7191.

26. K. P. Lawley and R. J. Donovan, *J. Chem. Soc. Faraday Trans.*,**1993** 89 1885.

Chapter 6

(2+1) REMPI of Jet-Cooled CH_2Cl_2

6.1 Introduction

Following on from the success of the systematic assignment of multiphoton Rydberg transitions in the methyl halides, it was hoped that this could be repeated for the equivalent transitions in dihalomethanes. However, it was seen that, of the molecules studied, only dichloromethane displayed features which could not be attributed to any species but the parent molecule. As a result, most of this chapter will be concerned with two-photon Rydberg transitions in CH_2Cl_2. For the other molecules which were studied, extensive photofragmentation, as evidenced by the radical resonances observed, is probably to blame for the non-appearance of their two-photon Rydberg transitions.

As will be seen later, the overall appearance of the two-photon spectrum of dichloromethane is very different to that of methyl chloride. However, this is hardly surprising given the appearance of its photoelectron spectrum[1,2]. For instance, the greater number of lower-lying bound ionic states present in the dihalomethanes vis-à-vis the methyl halides[1] increases the number of Rydberg states lying within the region of interest in CH_2Cl_2 with respect to the equivalent region in CH_3Cl. Also, the appearance of a great deal of vibrational activity in the photoelectron spectrum[1,2] of CH_2Cl_2 indicates that its Rydberg transitions should display a similar amount of vibrational activity. In fact, the vibrational envelopes exhibited by the ionic states which form the ionic core of those Rydberg states for which transitions are observed can be used to aid the vibrational analysis of the Rydberg band systems. However, while some Rydberg states, such as those in methyl bromide, discussed in Chapter 3, are well-behaved in this respect, others may not. An example of Rydberg states displaying the latter kind of behaviour is seen in the multiphoton spectra of CF_3I, discussed in the Chapter 5. Therefore, caution is required when using photoelectron

data to aid the assignment of Rydberg transitions. While this is the case, there remains the possibility that Rydberg states in dichloromethane may be well-behaved and the assignment of its VUV[3,6] and two-photon spectra assisted by the consideration of photoelectron data. Therefore, even though no ZEKE-PFI photoelectron data is available for any of the dihalomethanes, a discussion of their photoelectron spectroscopy remains useful and, so, is included here.

6.1.1 Photoelectron Spectroscopy

Not all the dihalomethanes display a He I photoelectron spectrum which is as complex as that of dichloromethane[1,2]. Even so, four low-lying ionic states appear in the case of all dihalomethanes. These $\tilde{X}$, $\tilde{A}$, $\tilde{B}$ and $\tilde{C}$ states result from the reduction in point group symmetry from C_{3v} to C_{2v} (CH_2X_2) or C_s (CH_2XY) in the dihalomethanes. Of all the states observed in the photoelectron spectra of the dihalomethanes, the ones listed are of most interest because only Rydberg states based upon them lie within the spectral region of interest. The symmetry assignment of the listed states has been subject of some discussion even for dibromomethane and diiodomethane where a lesser degree of vibrational excitation is seen than in dichloromethane[3,6]. Even less vibrational activity is seen in the heterogeneously bihalogenated methanes, of which chloroiodomethane is an example[7]. Here, ionisation from the 7a', 3a", 2a" and 6a' orbitals give rise to the $\tilde{X}$ ^{2}A', $\tilde{A}$ ^{2}A", $\tilde{B}$ ^{2}A" and $\tilde{C}$ ^{2}A' ionic states. Given the appearance of the photoelectron spectrum, it appears that these orbitals are essentially non-bonding in character with the 7a' and 3a" orbitals based upon the iodine atom and the 2a" and 6a' orbitals based upon the chlorine atom. This interpretation is consistent with sharpness of the features comprising the first two sets of bands with those comprising the next pair of band systems being broader and more overlapped. The observed vibrational structure in the photoelectron spectrum of chloroiodomethane amounted to short progressions in ν_3, the C-Cl stretch, observed and assigned for the $\tilde{X}$ ^{2}A', $\tilde{A}$ ^{2}A" and $\tilde{C}$ ^{2}A' states, while the $\tilde{C}$ ^{2}A' state also exhibited a short progression in ν_2, the CH_2 scissoring mode. These bear out the increased non-bonding character of the outer valence orbitals in this class

of molecules. The photoelectron spectrum of dichloromethane is much more complex than any of the other molecules mentioned above. This would seem to suggest that Rydberg transitions in dibromomethane, diiodomethane or chloroiodomethane may well be easier to analyse. The greater degree of vibrational activity in the photoelectron spectrum of dichloromethane also suggests a greater degree of bonding or antibonding character is possessed by its four outermost valence orbitals than those in any of the other dihalomethanes discussed.

The greater complexity of the photoelectron spectrum of CH_2Cl_2 vis-à-vis those of other dihalomethanes discussed above means that additional data are necessary for its interpretation. In this respect, theoretical calculations[8,9] can be useful and they have been used to aid the elucidation of the symmetry assignments for the four low-lying ionic states in dichloromethane. Li et al.[8] predicted the ordering of the first four ionic states to be $^2B_1$, $^2B_2$, $^2A_1$ and $^2A_2$ but Takeshita[9] subsequently predicted the ordering to be $^2B_2$, $^2B_1$, $^2A_1$ and $^2A_2$. Takeshita[9] also predicted the geometries of the four low-lying ionic states and these would be very different to that of the ground state with any transition to the $^2B_2$ state exhibiting the largest change in geometry. Thus, the differences between the two studies can be rationalised if the order predicted by Li et al.[8] corresponds to that of the vertical ionisation energies and that of Takeshita[9] follows the order in terms of adiabatic energies.

Figure 6-1 shows an overview of the most recently reported He (I) photoelectron spectrum[2] of CH_2Cl_2 while Figure 6-2 is an expansion of this depicting the band systems arising from the $\tilde{X}$, $\tilde{A}$, $\tilde{B}$ and $\tilde{C}$ ionic states. The symmetry assignments for these states have been adopted from the theoretical work of Takeshita[9]. Takeshita's calculations[9] of the geometries of the ionic states were used as a guide in assigning long vibrational progressions in each of the low-lying ionic states. Pradeep and Shirley[2] find three long vibrational progressions where the $\tilde{X}$ $^2B_2$ and $\tilde{A}$ $^2B_1$ ionic states are expected, two in ν_3 and one in ν_4. The modes ν_3 and ν_4 have been defined for the states of interest by Takeshita[9]. The former of these, ν_3, is

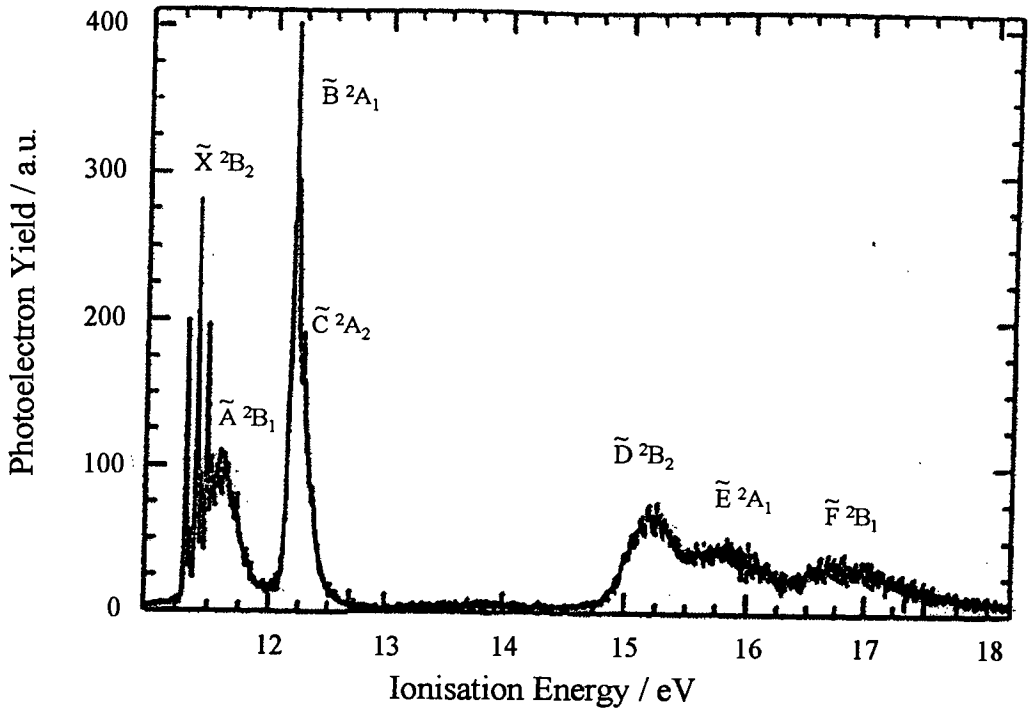

Figure 6-1: Overview of the He I photoelectron spectrum of dichloromethane recorded at a resolution of 13meV. Adapted from Pradeep and Shirley (Ref. 2).

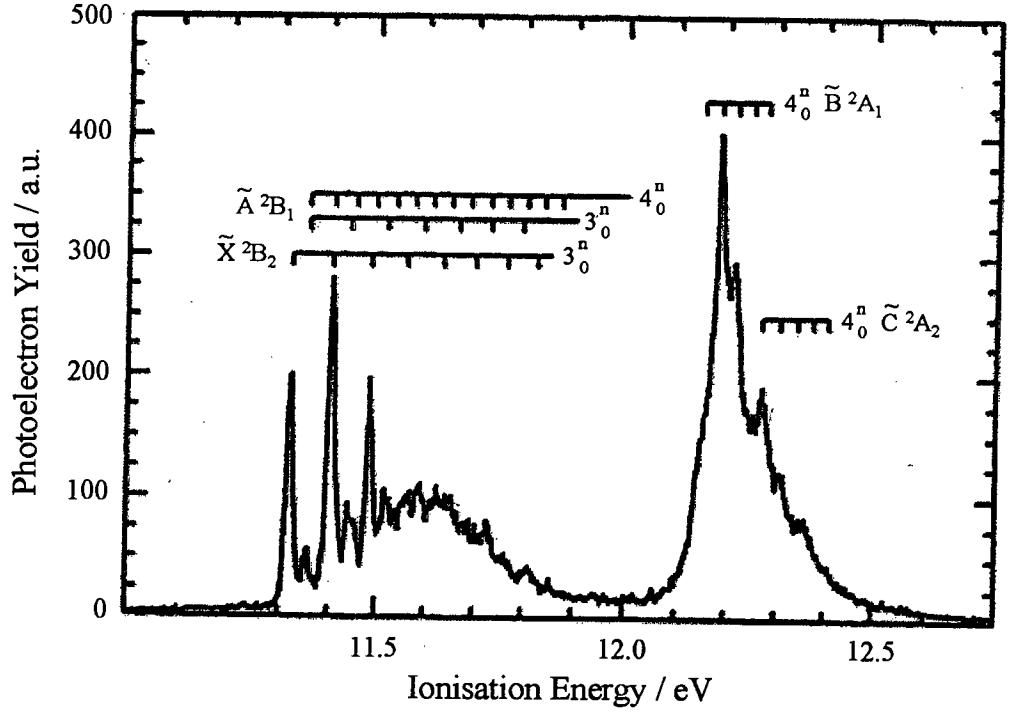

Figure 6-2: Expansion of the above He I Photoelectron spectrum of CH_2Cl_2 detailing the low-lying ionic states, their vibronic band systems and assignments. Adapted also from Pradeep and Shirley (Ref. 2).

said to involve a combination of C-Cl stretching and Cl-C-Cl bending for all of the states concerned here except the $\tilde{A}\ ^2B_1$ state. In the $\tilde{A}\ ^2B_1$ state, it is said to be a combination of C-Cl stretching, Cl-C-Cl and H-C-H bending. The latter mode, ν_4, is defined as Cl-C-Cl bending for all states of interest. From the results of Takeshita[9], a long progression in ν_4 would be expected for the $\tilde{X}\ ^2B_2$ state while progressions in $\nu_1$and ν_3 would be expected for the $\tilde{A}\ ^2B_1$ state. Since this is clearly at odds with what is observed, Pradeep and Shirley[2] assigned the first band system to the $\tilde{X}\ ^2B_2$ state with a long progression in ν_3 built upon its electronic origin. The origin of the $\tilde{A}\ ^2B_1$ state was assigned on the basis that long progressions in ν_3 and ν_4 could be built upon it which is somewhat in line with its predicted geometry. Progressions in ν_4 could be fitted to the origins of the $\tilde{B}\ ^2A_1$ and $\tilde{C}\ ^2A_2$ states.

6.1.2 Near and Far Ultraviolet Absorption Spectra

The very different photoelectron spectra of methyl chloride and dichloromethane suggest that they should have very different UV and VUV spectra and indeed they do. However, in the dihalomethanes, the one thing held in common with the methyl halides is that the lowest energy band in the electronic spectrum is extremely broad, arising from transitions to continuum valence states in each case. To higher energy of this band lie the sharper features which are due to Rydberg transitions, which are expected to show some differences.

The complexity of the photoelectron spectrum of dichloromethane suggests that its VUV spectrum should be similarly difficult to analyse. In fact, the appreciable amount of Rydberg state predissociation apparent from the observed bandwidths of the features in the spectrum further complicates matters. Therefore, given their simpler photoelectron spectra, an analysis of the VUV spectra of other dihalomethanes such as dibromomethane or diiodomethane should be more tractable. So, examination of the VUV absorption spectra of these molecules should simplify the analysis of that for CH_2Cl_2. In this light, a review of the VUV spectroscopy of some other dihalomethanes such as dibromomethane[10], diiodomethane[11,12] and

bromoiodomethane is included here. Of these the spectrum of CH_2Br_2 has received the most detailed analysis[10]. To summarise this electronic assignment, three *ns* series were fitted to ionisation limits whose values are in good agreement with those available from previous photoelectron spectra[1]. Assignments to *5p* and *4d* states were also made any attempt to find higher members of these series proved unsuccessful. In marked contrast, the VUV spectrum of CH_2I_2 has been reported[11,12] without any detailed analysis. Okabe et al.[11] included a VUV spectrum in a report of their study of the VUV photolysis of CH_2I_2. This covered the 110-150 nm region and, although the spectrum was of poor quality, a series converging on the first ionisation limit was indicated. More recently, Frey et al.[12] have reported an improved spectrum over a wider region (200-120 nm) obtained using synchrotron radiation but no analysis was presented. Only a portion of the VUV spectrum of CH_2IBr has been reported[13] and although the spectrum was recorded using a supersonic molecular beam, the observed features for CH_2IBr were still much broader than those arising in methyl iodide and methyl bromide within the same region (160-210 nm). These were attributed to the first members of *ns* states converging upon the $\tilde{X}\ ^2A'$, $\tilde{A}\ ^2A''$, $\tilde{B}\ ^2A''$ and $\tilde{C}\ ^2A'$ ionisation limits but no vibrational analysis was presented.

Unlike the molecules discussed above, several studies of the VUV spectrum of dichloromethane have been reported[3-6]. Not surprisingly in light of its photoelectron spectrum, an analysis of the observed features as complete as that reported by Causley and Russell for dibromomethane[10] has yet to be reported. The greater degree of vibrational activity in conjunction with the decrease in transition strength of successive members in a Rydberg series, with n^3, mean that Rydberg series like those exhibited in the spectra of the methyl halides cannot be expected. This has hampered the spectral analysis of the Rydberg transitions in previous studies. Despite this, features were assigned to *np* series in an early study of the VUV spectrum[3] with bands incompatible with an assignment as members of Rydberg series, denoted as X bands, being attributed to valence transitions. Robin[14] has commented that the X bands of Zobel and Duncan[3] could well be assigned to members of *np* series converging on higher ionisation limits. In a later study, lower energy features were tentatively

assigned to 4s and 4p states and not surprisingly, an analysis of the sharper features above 77280 cm^{-1} using the Rydberg formula was unsuccessful. In a more recent study[6] using synchrotron radiation, Lee and Suto re-examined the VUV spectrum at somewhat higher resolution but were unable to advance the electronic analysis of the VUV spectrum greatly. Even so, six possible vibrational progressions were highlighted but few suggestions were made regarding their electronic assignment.

6.1.3 Other Details Regarding Rydberg Transitions in Dihalomethanes

Because Ω can no longer be defined with respect with any chemical bond in a dihalomethane, its Rydberg states cannot be described in a like manner to those of the methyl halides. Thus, a labelling scheme involving C_{2v} or C_s symmetry has to be used instead. Therefore, the Rydberg states of dichloromethane are labelled $\tilde{S}\,[\Gamma_c]nl;\Gamma_{Ryd}$ where $\tilde{S}$ is the state label of the ionic state upon which the Rydberg state is based, Γ_c is the symmetry species of this ionic state, n is the principal quantum number, l is the Rydberg orbital angular momentum and Γ_{Ryd} is the symmetry species of the Rydberg state.

Given that polarisation studies have greatly simplified the assignment of Rydberg transitions in the methyl halides and trifluoromethyl iodide, discussed in previous chapters, they are also used here where appropriate. However, as indicated above, Ω is no longer a good quantum number. Therefore, the polarisation selection rules have to be redefined here. The two-photon polarisation behaviour of molecules with the C_{2v} point group is summarised by Williams and Cool[15], in their study of the two-photon spectroscopy of a number of dichloroethylenes, from the work of M^{c}Clain and Harris[16]. The polarisation selection rules described here were used to aid the assignment of two-photon transitions for 1,1-dichloroethylene and cis-1,2-dichloroethylene, both of which have C_{2v} symmetry, in that study[15]. In these molecules, several features were seen to have $\rho_2 < 1.5$ and thus were assigned to A_1 transitions while features with $\rho_2 \cong 1.5$ were assigned to transitions of other symmetry.

6.2 Experimental Details Regarding the Spectroscopic Survey

The (2+2) and (2+1) REMPI spectroscopy of several dihalomethanes was surveyed using UV radiation in the 217-320 nm region. The molecular beam was produced by pulsing the sample gas seeded in helium through a nozzle. The total backing pressures used were typically 500 torr with the proportion of total pressure due to the sample typically being 4-20% depending upon the room temperature vapour pressure of the sample being used. The molecules which were included in this survey included dichloromethane, dibromomethane, diiodomethane and chloroiodomethane. The latter was chosen because analysis of its two-photon spectrum was expected to be more tractable on the basis of its photoelectron spectrum. Of all the dihalomethanes listed, dichloromethane showed the most promise with the others only giving rise to spectra identifiable as being due to fragment species if any signal was observed at all. The dye laser power spectrum was monitored in each case to ensure that any features observed were real. Reasons for the lack of success in the case of dibromomethane, diiodomethane and chloroiodomethane include a greater degree of predissociation than seen in dichloromethane and, especially in the case of the iodinated compounds, the inability of two-photon Rydberg transitions to compete with one-photon photodissociation.

As in previous studies, spectra are normalised to the square of the laser power only where relative intensities of different features are sought and it is easy to do so reliably. Where polarisation behaviour is discussed, comparisons often are made between two spectra that are not power normalised. However, these comparisons still remain valid because both spectra concerned were recorded sequentially thus ensuring that little or no change in dye laser power occurs between both scans. Any band systems that are reported have not been calibrated. This is because any correction due to calibration is more likely less than the uncertainty in the band measurements themselves as result of the observed bandwidths.

6.3 Observed Radical Resonances

As indicated earlier, some of the dihalomethanes underwent photolysis rather than excitation into Rydberg transitions. In this light, it is felt that a discussion of observed radical resonances is appropriate, especially since radical spectroscopy and reaction dynamics is of such interest. In particular, photodissociation of chloroiodomethane and dichloromethane was seen to yield CH, CH_2 and CCl radicals which were detected via their electronic transitions. Photodissociation of the parent molecules and subsequent photoexcitation of any radicals produced all occurred at the same laser wavelength.

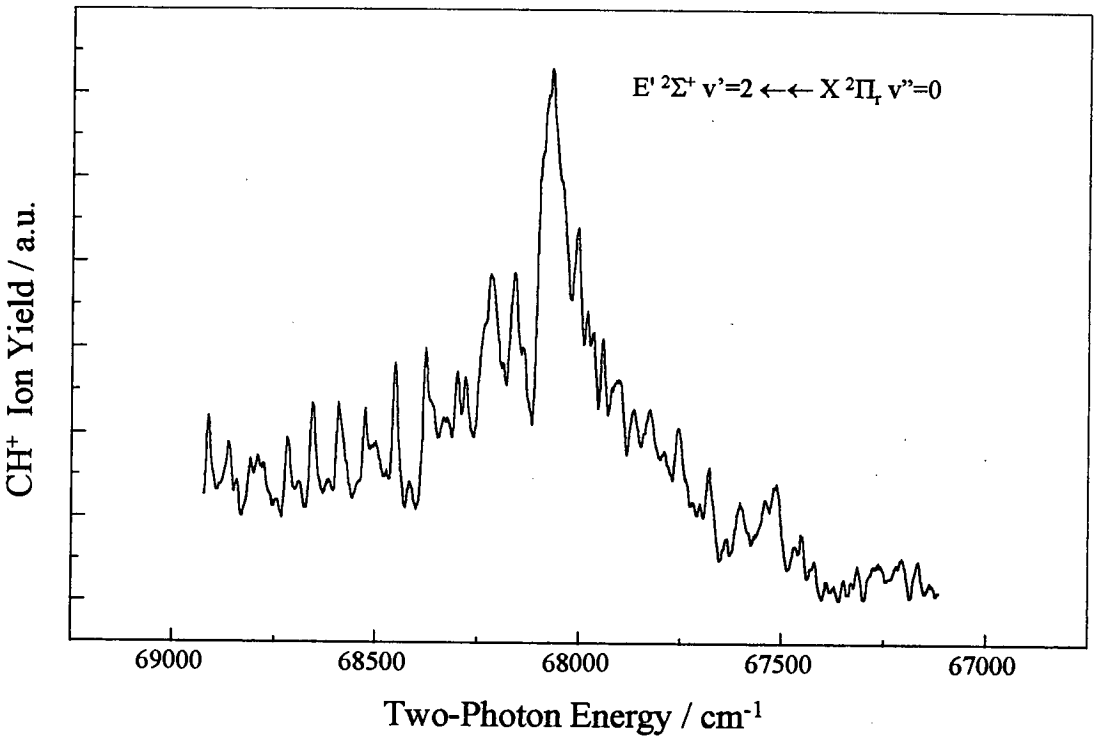

Figure 6-3: Two-photon resonances in CH arising from the previously reported[17] E'←←X transition. Partial rotational resolution, at least, is achieved for this system.

Photodissociation of dichloromethane in the energy region where features arising from $\tilde{X}\,[^2B_2]4s$ and $\tilde{A}\,[^2B_1]4s$ states are expected, yielded ground state CH which was then excited into its E' state[17]. The observed features are due to rotational

lines arising from the E' $^2\Sigma^+$ v'=2 ←← X $^2\Pi_r$ v"=0 vibronic transition. Because dichloromethane does not absorb into any real electronic state at the one-photon level, the dissociation must occur at the two-photon level. Hence, it could be said that the $\tilde{X}[^2B_2]4s$ and $\tilde{A}[^2B_1]4s$ states are extremely predissociated by some continuum valence state and only transitions in photofragments are observed, not those of the parent molecule.

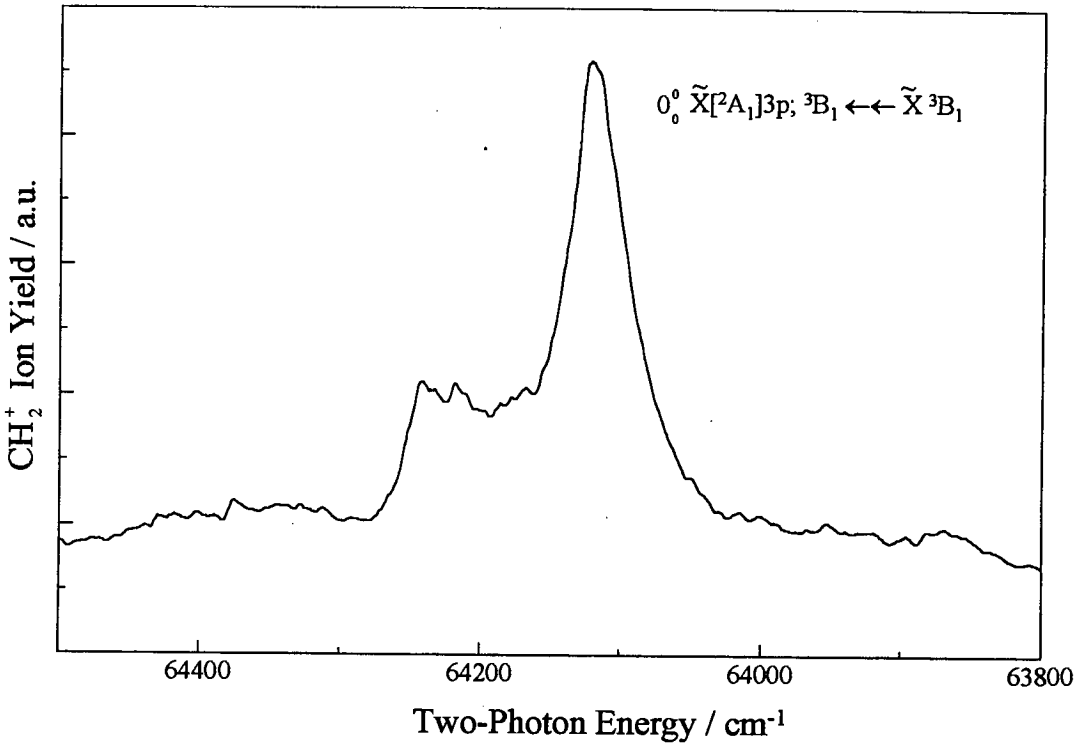

Figure 6-4: Two-photon resonance in triplet methylene.

Photolysis of CH_2ICl, in the region where resonances arising from the $\tilde{X}[^2A']6p$ state are expected, resulted in the production of CH_2. This radical can be produced in both singlet ($\tilde{a}$ $^1A_1$) and triplet ($\tilde{X}$ $^3B_1$) forms, depending on the precursor and the reaction conditions. It is well known that the molecules in the $\tilde{a}$ $^1A_1$ states are collisionally quenched to produce the $\tilde{X}$ $^3B_1$ state. Irikura et al.[19] have previously reported the feature depicted in Figure 6-4 and assigned it to a two-photon transition to a 3p Rydberg state in triplet methylene. Unlike Irikura et al.[18], the polarisation behaviour of this band is noted here. When circularly

polarised light was used, the intensity of the observed feature is found to decrease. Thus, we can assign its symmetry as B_1 because only transitions that are totally symmetric would be expected to display the observed polarisation behaviour.

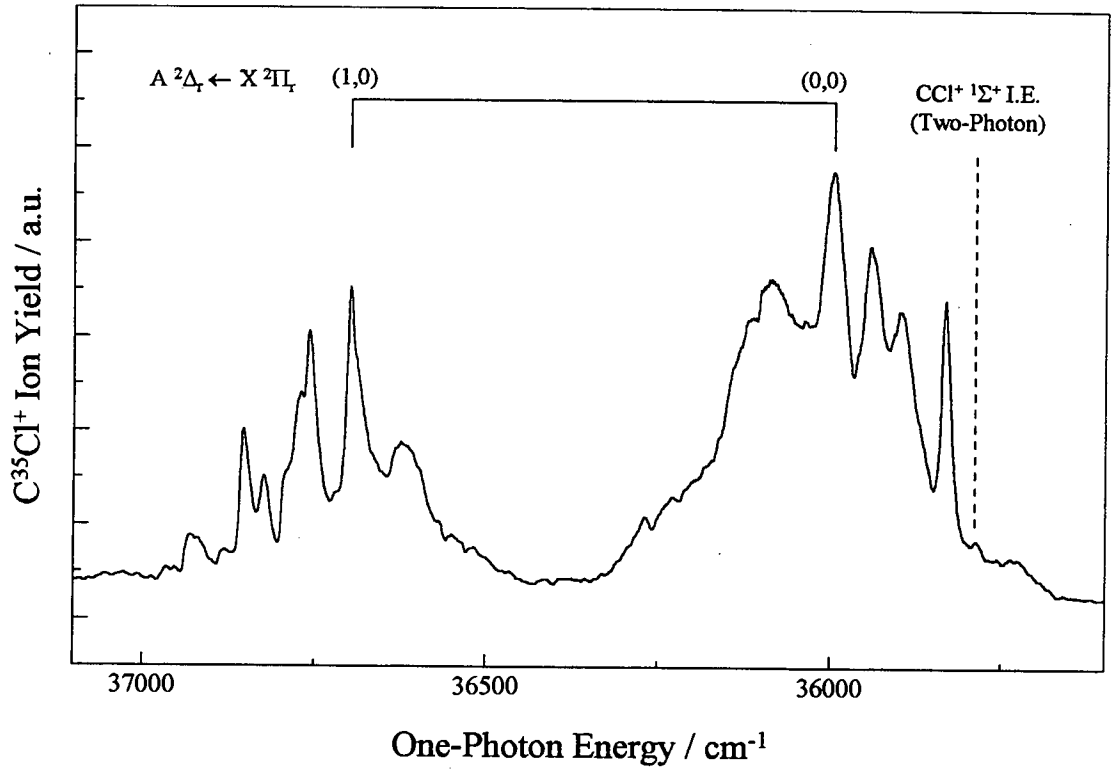

Figure 6-5: One- and two-photon resonances in CCl radical. The partially-resolved rotational band contours of the depicted vibronic bands are discussed in the text. The first ionisation potential at the two-photon level is also shown.

Similarly, ground state CCl was produced from both CH_2Cl_2 and CH_2ICl but the best quality spectrum, shown in Figure 6-4, was obtained from the latter. One-photon A-X resonances were observed in this study at partial rotational resolution but have been studied at higher resolution previously[19]. The A $^2\Delta_{3/2} \leftarrow$ X $^2\Pi_{1/2}$ and A $^2\Delta_{5/2} \leftarrow$ X $^2\Pi_{3/2}$ transitions overlap each other giving rise to the observed rotational band contours for the (0,0) and (0,1) bands. The position of the first ionisation energy, at the two-photon level, of CCl is also indicated in Figure 6-5. This is reported to be 71783 cm^{-1} by Hepburn et al.[20] and so can contributed to the appearance of the (0,0) band This means that the observed

resonances result from (1+1) REMPI. These resonances were found instead of the expected $\tilde{X}[^2A']4f$ resonances in CH_2ICl and $\tilde{X}[^2B_2]4p$ and $\tilde{A}[^2B_1]4p$ resonances expected for dichloromethane.

6.4 Identification of Features as Being Due to Transitions in CH_2Cl_2

As indicated in the previous section, a spectral search for features arising from two-photon transitions to 4s, $\tilde{X}[^2B_2]4p$ and $\tilde{A}[^2B_1]4p$ states proved unsuccessful. It is seen in the VUV spectrum of dichloromethane that features assigned to $\tilde{X}[^2B_2]4s$ and $\tilde{A}[^2B_1]4s$ transitions are extremely broad while those associated with $\tilde{X}[^2B_2]4p$ and $\tilde{A}[^2B_1]4p$ states are somewhat sharper but are superimposed upon a continuum absorption. Thus, it may not be unreasonable to observe radical production from photodissociation or predissociation in these energy regions. However, it is not immediately clear how the parent molecule might photolyse to produce the observed radical species.

In contrast to the forgoing, some features were observed in both CH_2^+ and CCl^+ channels in the 76000-82000 cm^{-1} region where $\tilde{X}[^2B_2]3d$ and $\tilde{A}[^2B_1]3d$ resonances should be seen. This leaves only CH_2Cl and CH_2Cl_2 as the carriers of this structure. As we are above the first ionisation energy[21] of CH_2Cl at 70573 cm^{-1}, any observed features could only be one-photon in nature. However, the intensity of these observed features were seen to decrease in the presence of circularly polarised light, indicating that they are due to multiphoton transitions and therefore should be due to the parent molecule and not any of its photolysis products.

Above 84000 cm^{-1}, additional features are observed and they too decrease in intensity in the presence of circularly polarised light. Although these resonances only appear in the spectrum recorded on the CH_2^+ mass channel and not the one recorded on the CCl^+ channel, they are not likely to be due to CH_2^+ for several reasons. Firstly, there is no continuum absorption at the first-photon level in this energy region for the

parent molecule. However, the production of free radicals could still result from predissociation of some electronically excited state in the parent molecule. Also, at the two-photon level, these bands lie above the first ionisation limit of CH_2 which has been obtained by Herzberg to be 83851 cm^{-1} by extrapolation from a short $\tilde{X}\,[^2A_1]nd;\,^3A_2$ Rydberg series[22]. Although this still leaves open the possibility of the features arising from autoionising Rydberg states, the appearance of one-photon resonances would be a more likely explanation. Not only have there been no one-photon resonances been reported for methylene in this wavelength region[23,24] but the polarisation behaviour of the features here is at odds with the observed bands being one-photon in nature. All this still does not discount the appearance of autoionising Rydberg resonances. However, the features show separations of the order of 200-300 cm^{-1} with little decrease as higher energies are reached. Hence, it would be difficult to analyse the observed bands in terms of Rydberg series. Also, the Rydberg spectra of methylene have been studied in some detail[22-24] and these show little evidence for vibronic activity. Thus, the observed bands are unlikely to result from autoionising Rydberg series in CH_2 but are almost certainly due to Rydberg transitions in the parent molecule which are expected to show a reasonable amount of vibronic activity based on the appearance of the photoelectron spectrum[2].

The above band system continues to 86500 cm^{-1} but additional structure follows on from this and is continued up to 90800 cm^{-1}. These bands appear in both CH_2^+ and CCl^+ channels, hinting that they too may be due to the parent molecule. Again, no dissociative resonance is encountered at the first-photon level, further supporting the conclusion that resonances in dichloromethane are being seen. The other possibility is that they may be due to CH_2Cl. However, since these features occur about 17000 cm^{-1} above its first ionisation energy at the two-photon level, this is unlikely. In addition to this, molecular ion signal is seen in the region about the first ionisation limit and some discrete structure is seen below the observed ionisation threshold. This is the only portion in the two-photon spectrum where molecular ion signal is actually observed. There is reasonable agreement between the spectra recorded in the CH_2^+, CCl^+ and $CH_2Cl_2^+$ channels. So, the features in the

87000-91000 cm^{-1} are more likely to be due to CH_2Cl_2. Also, when field corrected, the ionisation energy obtained is in agreement with that from the most recent photoelectron study[2]. Thus, it seems that a two-photon spectrum of dichloromethane has been obtained and its analysis will be discussed later.

Most of the spectra produced by dichloromethane can be attributed to the parent molecule and not radical species. However, the only instance of strong signal in the parent molecular ion channel occurs near the first ionisation threshold. Thus, extensive fragmentation of the parent ion must occur subsequent to ionisation because any excess energy above the ionisation limit in a 2+1 process will be removed by the ejected electron in the form of kinetic energy. Hence, this process will require at least one further photon. In the case of CH_2Cl_2, it is possible to access continuum electronically excited ionic states with photon energies greater than 31000 cm^{-1}, that is, at wavelengths less than 316 nm. Thus, fragmentation will be a one-photon process and given the selection rules, some information pertaining to the higher ionic states may be obtained. Spectra of the $\tilde{X}[^2B_2]3d;A_1$ and $\tilde{A}[^2B_1]3d;A_1$ states were observed on both CH_2^+ and CCl^+ ion channels. The one-photon energy in this region is sufficient to pump the $\tilde{E}\ ^2A_1 \leftarrow \tilde{X}\ ^2B_2$ transition in the ion. As this transition is allowed, it is not unreasonable to say that the $\tilde{E}\ ^2A_1$ state fragments to give CH_2^+ and CCl^+, even if two pathways might be involved. For the $\tilde{X}[^2B_2]4d/\tilde{A}[^2B_1]4d/\tilde{B}[^2A_1]3d$ system, fragmentation of a different ionic state must be involved as the observed features only occur in the CH_2^+ ion channel. However, the final state in this case would be the $\tilde{F}\ ^2B_1$ state and a transition terminating in this state from the $\tilde{X}\ ^2B_2$ state would be forbidden. Similarly, it is less clear how fragmentation of the ion might occur in the case of higher energy resonances to give spectra in the CH_2^+ and CCl^+ ion channels. Ultimately, a study into the dynamics of the ionic states using a technique such as Photoelectron Photoion Coincidence (PEPICO) would be helpful here. However, to date, such a study apparently has yet to be reported for dichloromethane. Until then, it will remain an open question as to

why features comprising the $\tilde{X}\,[^2B_2]4d/\tilde{A}\,[^2B_1]4d/\tilde{B}\,[^2A_1]3d$ system are absent from the CCl^+ channel.

6.5 Electronic Assignment of the (2+1) REMPI Spectrum of CH_2Cl_2

As discussed above, there is a substantial amount of structure attributable to CH_2Cl_2. An overview of the observed features is given in Figure 6-6. On first sight, the two-photon spectrum of CH_2Cl_2 bears little resemblance to its VUV absorption spectrum[3-6]. Many bands present in the former are noticeably absent from the latter, and vice versa. The electronic assignments of bands attributable to dichloromethane will be discussed in light of this.

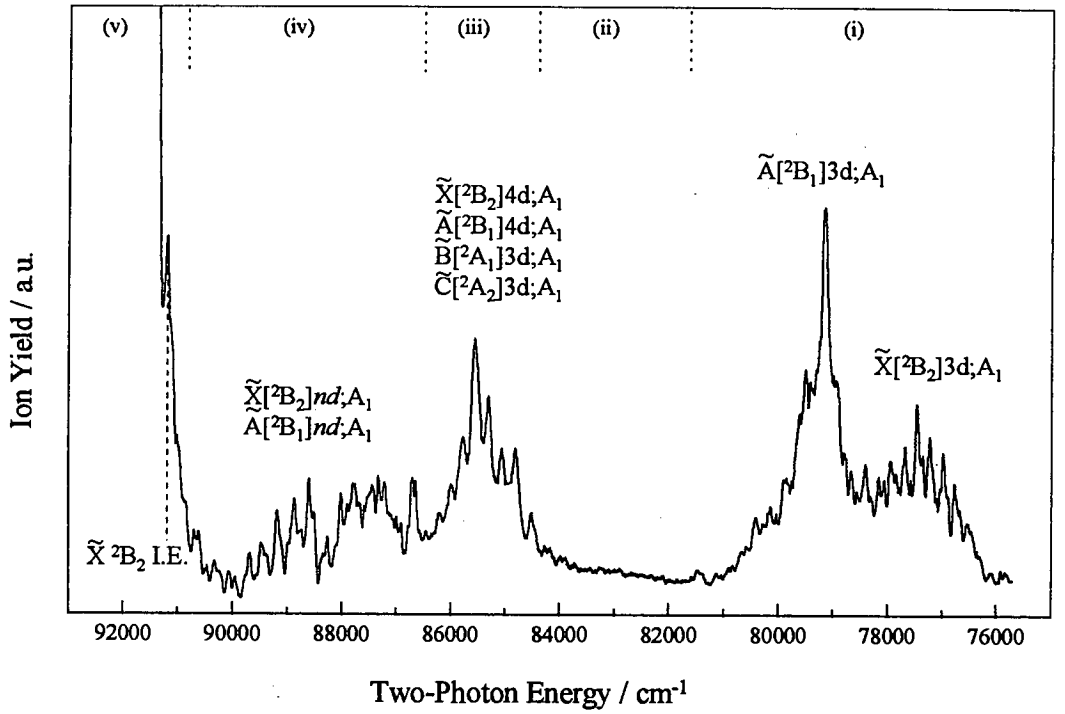

Figure 6-6: Composite plot detailing the two-photon spectroscopy of dichloromethane. The component spectra have not been power normalised so caution is required when comparing the relative intensities of the observed features. The relevant laser dye regions have been demarcated at the top of the plot: (i) Coumarin 307, (ii) Coumarin 102, (iii) Coumarin 47, (iv) and (v) Coumarin 2. Regions (i)-(iv) have been recorded in the CH_2^+ mass channel while region (v) was recorded in the $CH_2Cl_2^+$ channel. The expected Rydberg transitions are highlighted next to the relevant traces as is the first ionisation energy[2].

The absence of features present in the two-photon spectrum from the VUV spectrum can be rationalised in terms of C_{2v} point group symmetry. Bands arising from transitions to states with A_2 symmetry are one-photon forbidden but two-photon allowed. However, this assertion is inconsistent with the polarisation behaviour of features in the 76500-87000 cm^{-1} region of the two-photon spectrum of CH_2Cl_2. All of these bands had $\rho_2 < 1$ which is consistent with totally symmetric transitions, that is, transitions involving no change in symmetry between the ground and excited states. Also, the ground state of dichloromethane is closed shell and hence has A_1 symmetry, that is, it is totally symmetric. Therefore, the features comprising the two-photon spectrum of dichloromethane arise from transitions to states with A_1 symmetry. Therefore, other propensity rules must be dictating whether transitions are allowed or forbidden in the spectra of CH_2Cl_2.

Also indicative of the operation of propensity rules other than those expected is the absence of band systems seen with appreciable intensity in the VUV spectrum[6] of dichloromethane from its two-photon spectrum. Since some of the features concerned can be assigned to *np* states, it would appear that transitions to *np* states are absent from the two-photon spectrum of CH_2Cl_2. This situation is like that known for homonuclear diatomic molecules where *np* transitions are one-photon allowed but two-photon forbidden. Thus, it appears that dichloromethane displays propensity rules for electronic transitions which are analogous to the parity selection rules well known for homonuclear diatomics. So, in this light, the absence of *np* resonances from the two-photon spectrum of CH_2Cl_2, would imply that no two-photon *nf* transitions should be seen either. Therefore, the two-photon spectrum of dichloromethane should be composed of *ns* and *nd* resonances. However, no features arising from transitions to 4s states were seen which suggests that the resonances that are observed are most likely to be due to *nd* states. This conclusion is entirely consistent with the propensity rules seen in the two-photon spectra of both the methyl halides, discussed in earlier chapters, and the diatomic halogens[24].

Figure 6-6 depicts an overview of the two-photon spectrum of dichloromethane. From polarisation studies, all observed features in the 76000-81000 cm^{-1} region have a polarisation ratio $\rho<1.5$ which would indicate that they all belong to the same totally symmetric electronic state. Because of the absence of 4s, $\tilde{X}[^2B_2]4p$ and $\tilde{A}[^2B_1]4p$ states, assignments to $\tilde{B}[^2A_1]4p$, $\tilde{C}[^2A_2]4p$, $[^2B_2]5s$ and $[^2B_1]5s$ states can be discounted. There still remains the possibility of $\tilde{X}[^2B_2]3d$ and $\tilde{A}[^2B_1]3d$ assignments which are feasible in light of the calculated quantum defects for features in the 76000-81000 cm^{-1} energy region. However, from the photoelectron spectrum, at least two states are expected, one member of each series converging on the $\tilde{X}\ ^2B_2$ and $\tilde{A}\ ^2B_1$ ionisation limits. With respect to that number of substates that are expected with each symmetry for each ionic core, it is useful to refer to the halogens[24], and the methyl halides, which have been discussed in preceding chapters. In those molecules, at least two totally symmetric *nd* substates are expected to be seen on each ionic core. However, one of these is a pure triplet state and consequently was not observed. By analogy with this, only one symmetric substate based on each ionic core. This analogy, not unreasonable given that the electronic configuration of a Rydberg state in any of the three classes of molecule should be equivalent, helps to simplify the assignment of this band system, and the rest of the spectrum, substantially.

While there can be little doubt about the electronic assignment of the lower energy system discussed above, the electronic analysis becomes more complex because the density of states becomes higher with increasing energy. As above, assignments of features in the 84000-86500 cm^{-1} region to *ns* and *np* states are eliminated easily. The apparent propensity rules also rule out two-photon transitions to *nf* states. This means that our two-photon spectrum is dominated by transitions to *nd* states. However, at least three *nd* states, $\tilde{B}[^2A_1]3d$, $\tilde{X}[^2B_2]4d$ and $\tilde{A}[^2B_1]4d$, are predicted to lie in this region using the Rydberg equation with the most recent photoelectron data[2]. Again, the observed features display $\rho_2 < 1.5$ which indicates that

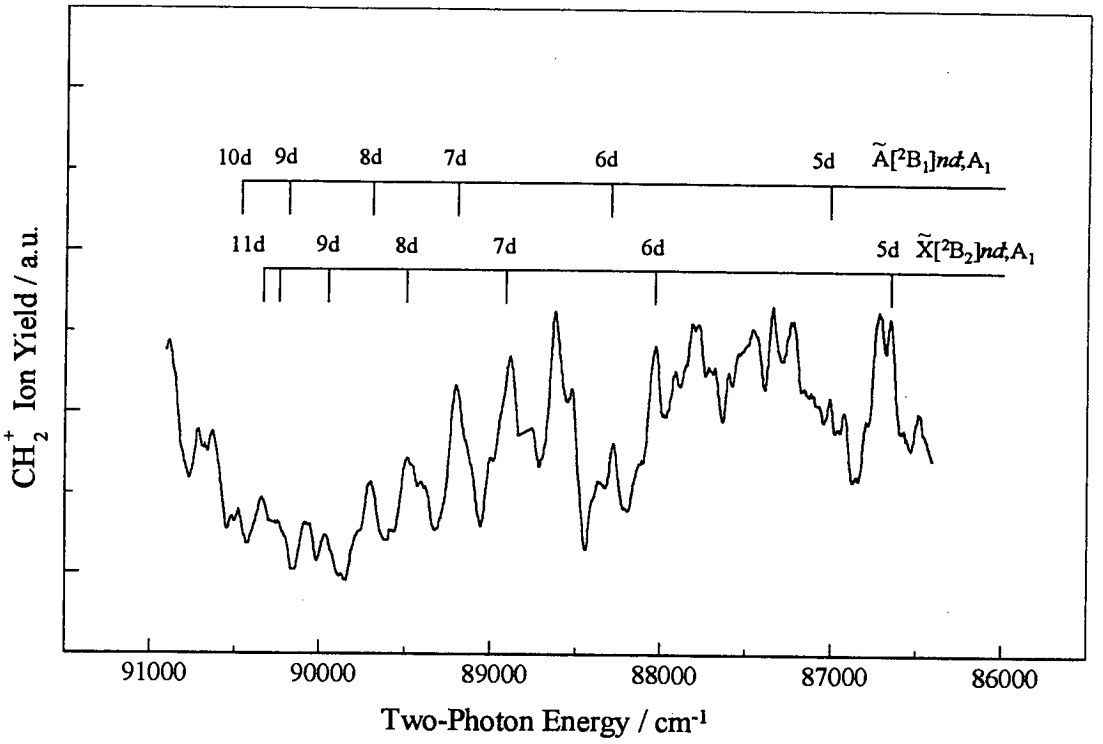

Figure 6-7: Indication of the band positions possibly coinciding with the electronic origins of *nd* series for dichloromethane.

Band Position cm^{-1}	**Electronic Assignment** cm^{-1}	**(*n*-δ)**
76513	$\tilde{X}[^2B_2]3d;A_1$	2.72
79167	$\tilde{A}[^2B_1]3d;A_1$	2.97
84528	$\tilde{X}[^2B_2]4d;A_1$	4.02
84825	$\tilde{A}[^2B_1]4d;A_1$	4.02
85561	$\tilde{B}[^2A_1]3d;A_1$	2.97
86660	$\tilde{X}[^2B_2]5d;A_1$	4.90
86725	$\tilde{C}[^2A_2]3d;A_1$	2.99
86922	$\tilde{A}[^2B_1]5d;A_1$	4.84
88032	$\tilde{X}[^2B_2]6d;A_1$	5.79
88281	$\tilde{A}[^2B_1]6d;A_1$	6.75

Table 6-1: Band Positions of members of the *nd* series observed in dichloromethane. Any (*n*-δ) values have been calculated using the Rydberg equation. The values for the ionisation limits used to calculate the (n-δ) values are those of Pradeep and Shirley[2] which are as follows: 91302 cm^{-1}, 91600 cm^{-1}, 98012 cm^{-1} and 98972 cm^{-1} for $\tilde{X}\ ^2B_2$, $\tilde{A}\ ^2B_1$, $\tilde{B}\ ^2A_1$ and $\tilde{C}\ ^2A_2$ states, respectively. The 5d and 6d states have been tentatively assigned A_1 symmetry for consistency.

the transitions are totally symmetric. Thus, as for the $\tilde{X}\,[^2B_2]3d$ and $\tilde{A}\,[^2B_1]3d$ states, only one component of each state is expected. This simplifies the vibronic analysis which will be discussed in detail later.

As can be seen in Figure 6-6 and Figure 6-7, some additional structure is seen to higher energy of the $\tilde{X}\,[^2B_2]4d/\tilde{A}\,[^2B_1]4d/\tilde{B}\,[^2A_1]3d$ system. Although *nd* series converging upon the first two ionisation limits can be continued in the 86500-91000 cm^{-1} region, the effect of increased vibronic activity, apparent from both the photoelectron spectrum[2] and the lower energy regions of the two-photon spectrum, must be considered. This increased level of vibronic activity, coupled with well known trend in Rydberg series that transition strength decreases with n^3, negates the possibility of seeing long Rydberg series like those discussed in earlier chapters for methyl chloride and methyl bromide. Figure 6-7 shows the result of an attempt to fit *nd* series to the observed features in this energy region. It is noticeable that this analysis also leaves an appreciably intense feature at 88623 cm^{-1} unassigned. However, the band system in the 87000-88000 cm^{-1} region can be said to be vibrational structure built upon the origins of $\tilde{X}\,[^2B_2]5d$ and $\tilde{A}\,[^2B_1]5d$ states. Hence, higher members of the series should behave in a similar manner. In fact, as will be seen in a later subsection, vibronic band systems arising from $\tilde{X}\,[^2B_2]6d$ and $\tilde{A}\,[^2B_1]6d$ states can account for most of the features above 88000cm^{-1}. Thus, the observed features are assigned to band systems arising from $\tilde{C}\,[^2A_2]3d;A_1$, $\tilde{X}\,[^2B_2]5d$, $\tilde{A}\,[^2B_1]5d$, $\tilde{X}\,[^2B_2]6d$ and $\tilde{A}\,[^2B_1]6d$ states.

Table 6-1 summarises the electronic assignments of the (2+1) REMPI spectra and their quantum defects. The 3d and 4d states are known to have A_1 symmetry form polarisation studies and there is good reason that the 5d and 6d states also possess the same symmetry because members of a Rydberg series should all follow the same trend. However, there is some scatter is scatter in the calculated quantum defects which not only arises from the uncertainties of the ionisation limits used but also reflects the different vibronic envelopes seen as higher energy is reached. As will be emphasised in the discussion of the vibronic analysis, exact agreement with the

photoelectron spectrum is not attained. Thus, interactions between electronic states also may be responsible for any perturbations present in the observed spectra.

6.6 Vibronic Analyses of the Observed Band Systems

As a molecule in a Rydberg state is expected to display a similar geometry to the ionic state upon which the Rydberg state is based, the appearance of the photoelectron spectrum can be used as a guide in the vibronic analysis of the observed band systems. Also, as the first-photon energy is always less than that corresponding to the A-band continuum, any vibronic transition observed is most likely to lie within the Franck-Condon window of the ground state. Thus, the most probable source of any departure from the vibronic envelope of the relevant ionic state would be through interaction with valence or ion-pair states. Another factor to be taken into account when comparing vibrational envelopes is the resolution of the spectrometer upon which the most recent photoelectron spectrum[2] is recorded. The spectrum was recorded using a He I light source but using a molecular beam. Hence, the fact that the resolution of the spectrometer is 13 meV (about 104cm^{-1}) means that some low frequency vibrations may not be resolved. However, the overall shapes of the ionic band systems can still be used as a guide for assigning the REMPI spectra, which have been recorded at much higher resolution.

6.6.1 The $\tilde{X}[^2B_2]3d/\tilde{A}[^2B_1]3d$ System

Figure 6-8 depicts the features observed in the 76000-82000 cm^{-1} region with the suggested vibronic assignments. Because of the observed intensity distribution, some caution must be exercised when analysing the spectrum on the basis of the photoelectron spectrum[2]. It can be seen that the observed features are separated by 200-300 cm^{-1}. This allows long progressions in ν_3, the C-Cl stretch, built upon two electronic origins, to be fitted easily to the observed spectrum. However, this assignment does not follow the intensity pattern of the observed band system. Thus, another assignment, that depicted in Figure 6-8, is suggested instead. This again favours two electronic states but with each having a different vibronic envelope. This

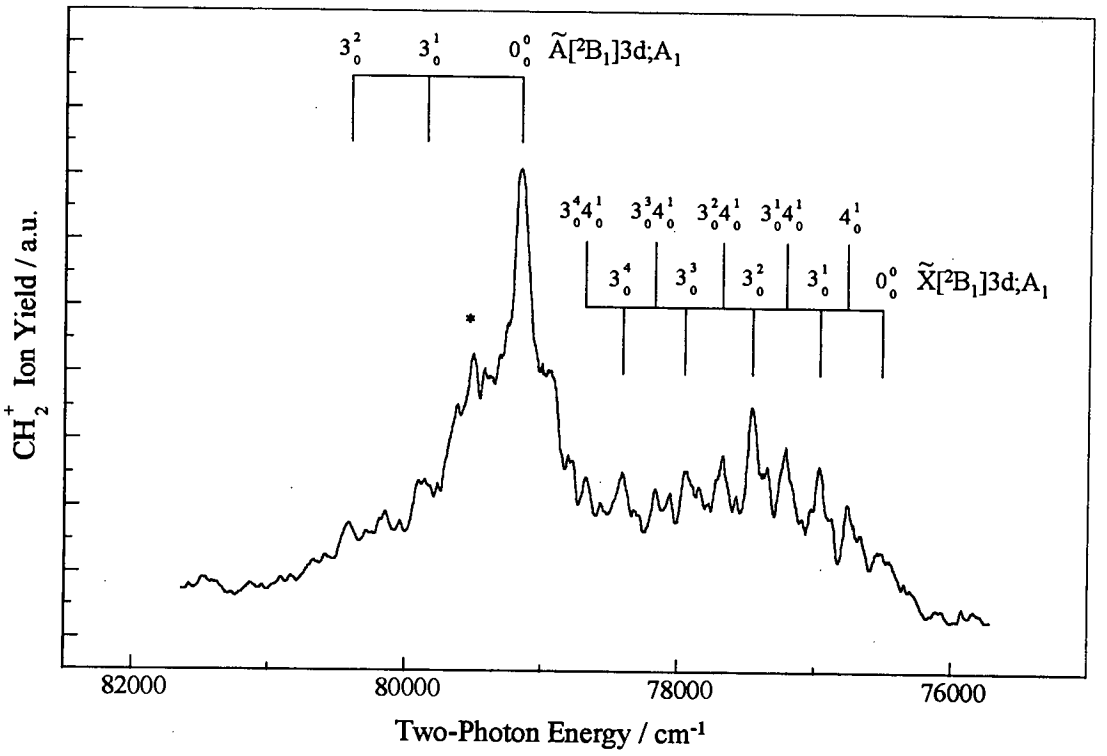

Figure 6-8: The (2+1) REMPI spectrum in the 75000-82000 cm^{-1} region where 3d states based upon the lower ionic cores are expected to exist. Because of an aberration, the depicted spectrum is only normalised to the dye laser power and not its square as is usually done for a two-photon spectrum. The asterisk (*) highlights the area of the spectrum where this aberration is apparent.

behaviour is not unreasonable when the symmetries of the Rydberg states are considered group theoretically. Because the two states observed share the same symmetry but are based upon different ionic cores, it is possible that the Rydberg electrons occupy *nd* orbitals with different orientations in space and hence display very different vibronic envelopes. Thus, an assignment can be arrived at where progressions in ν_3 and $\nu_3 + \nu_4$ are built upon the first origin and a progression in ν_3 is built upon the second origin. Alternatively, based solely upon the appearance of the vibronic band systems in the photoelectron spectrum[2], the band systems assigned above to $\tilde{X}[^2B_2]3d;A_1$ and $\tilde{A}[^2B_1]3d;A_1$ states could well be re-assigned to $\tilde{A}[^2B_1]3d;A_1$ and $\tilde{C}[^2A_2]4p;A_1$ states, respectively. In the case of the first band system, the $\tilde{A}[^2B_1]3d$ assignment would appear more likely than the alternative $\tilde{X}[^2B_2]3d$ one. However, states based upon the $\tilde{C}\ ^2A_2$ ionic core will differ hugely

from those built upon the $\tilde{A}\ ^2B_1$ ionic core. However, a large dip occurs in the dye laser power curve immediately to the blue of the origin band of the second band system in this region. This makes it difficult to distinguish between a perturbed state based upon the $\tilde{A}\ ^2B_1$ ionic core and a one that is largely unperturbed and based upon the $\tilde{C}\ ^2A_2$ core. Even so, a progression in ν_4 alone is expected on the basis of the photoelectron spectrum, cannot account for consideration of the absence of $\tilde{X}[^2B_2]4p;A_1$ and $\tilde{A}[^2B_1]4p;A_1$ states, the assignment to a heavily perturbed $\tilde{A}[^2B_1]3d$ state, depicted in Figure 6-8, is more likely correct. As will be seen from

Band Position cm^{-1}	**Electronic Assignment** cm^{-1}	**Vibrational Assignment** cm^{-1}	**Vibrational Spacing** cm^{-1}
76517	$\tilde{X}[^2B_2]3d;\ A_1$	0_0^0	0
76765	$\tilde{X}[^2B_2]3d;\ A_1$	4_0^1	248
76980	$\tilde{X}[^2B_2]3d;\ A_1$	3_0^1	463
77223	$\tilde{X}[^2B_2]3d;\ A_1$	$3_0^1 4_0^1$	706
77469	$\tilde{X}[^2B_2]3d;\ A_1$	3_0^2	952
77681	$\tilde{X}[^2B_2]3d;\ A_1$	$4_0^1 3_0^2$	1164
77933	$\tilde{X}[^2B_2]3d;\ A_1$	3_0^3	1416
78171	$\tilde{X}[^2B_2]3d;\ A_1$	$4_0^1 3_0^3$	1654
78400	$\tilde{X}[^2B_2]3d;\ A_1$	3_0^4	1883
78678	$\tilde{X}[^2B_2]3d;\ A_1$	$4_0^1 3_0^4$	2161
79167	$\tilde{A}[^2B_1]3d;\ A_1$	0_0^0	0
79630	$\tilde{A}[^2B_1]3d;\ A_1$	3_0^1	463
80051	$\tilde{A}[^2B_1]3d;\ A_1$	3_0^2	884
80410	$\tilde{A}[^2B_1]3d;\ A_1$	3_0^3	1243

Table 6-2: Band measurements and suggested assignments for the $\tilde{X}[^2B_2]3d/\tilde{A}[^2B_1]3d$ system of dichloromethane.

the following discussion of the higher energy features seen in the two-photon spectrum, the assignment of vibronic band systems to two perturbed 3d states is the more consistent.

6.6.2 The $\tilde{X}[^2B_2]4d/\tilde{A}[^2B_1]4d/\tilde{B}[^2A_1]3d$ System

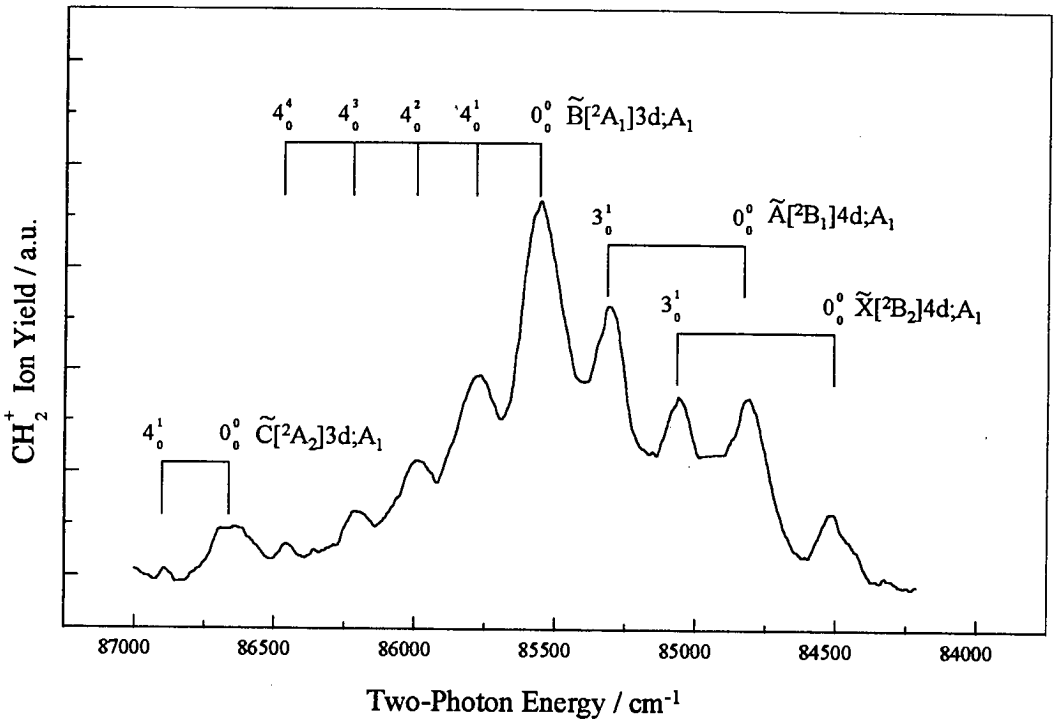

Figure 6-9: Assignments of the (2+1) REMPI spectrum of CH_2Cl_2 in the 84000-87000 cm^{-1} region. The spectrum has not been power normalised so some care must be exercised when comparing intensities of the observed bands. The $\tilde{C}[^2A_2]3d$ state will be discussed in the following subsection.

At first sight, the band system observed in the 84000-86500 cm^{-1} region has an appearance very like that of the previously discussed $\tilde{X}[^2B_2]3d;A_1$ system. Likewise, this band system displays similar polarisation behaviour. Thus, it could be assigned to a $\tilde{X}[^2B_2]4d;A_1$ or $\tilde{A}[^2B_1]4d;A_1$ state, in consideration of the possibilities suggested previously for the lower energy band systems. Although this would seem to account for all of the observed bands, some variation is seen in the vibrational frequency of ν_4 in the $4_0^1 3_0^n$ progression. In addition to this, $\tilde{B}[^2A_1]3d$, $\tilde{X}[^2B_2]4d$ and $\tilde{A}[^2B_1]4d$ states are expected in this region and are predicted to lie in close proximity to each

other. Far from complicating the spectral analysis, the presence of a number of electronically excited states in this region aid the vibronic assignment because the observed vibrational coarse structure can be analysed simply using the photoelectron data[2]. Thus, in this region, 4d states expected to display progressions in ν_3 and 3d states progressions in ν_4. Although this seems to better fit the observed band system observed in this region, as depicted in Figure 6-9 below, one would not expect only one member of a progression in ν_3 to be seen, while the photoelectron spectrum indicates that there should be extended progressions in this vibration. However, it is well known that transition strength decreases with n^3 in a Rydberg series. Thus, if higher core 3d bands were to overlap those arising from lower core 4d states, it would not be unreasonable to observe the 3d resonances in place of the 4d ones. Another point to note is that there is an apparent continuum underneath the observed features. This may well be due to the density of vibronic Rydberg transitions rather than some dissociative electronic state. In light of this, the initial assignment as illustrated in Figure 6-9 remains the more plausible.

Band Position cm^{-1}	**Electronic Assignment** cm^{-1}	**Vibrational Assignment** cm^{-1}	**Vibrational Spacing** cm^{-1}
84528	$\tilde{X}\,[^2B_2]4d;\ A_1$	0_0^0	0
84831	$\tilde{A}\,[^2B_1]4d;\ A_1$	0_0^0	0
85067	$\tilde{X}\,[^2B_2]4d;\ A_1$	3_0^1	539
85322	$\tilde{A}\,[^2B_1]4d;\ A_1$	3_0^1	491
85561	$\tilde{B}\,[^2A_1]3d;\ A_1$	0_0^0	0
85761	$\tilde{B}\,[^2A_1]3d;\ A_1$	4_0^1	200
86002	$\tilde{B}\,[^2A_1]3d;\ A_1$	4_0^2	441
86201	$\tilde{B}\,[^2A_1]3d;\ A_1$	4_0^3	640
86463	$\tilde{B}\,[^2A_1]3d;\ A_1$	4_0^4	902

Table 6-3: Band measurements and suggested assignments for the second strong band system in dichloromethane.

6.6.3 Features Observed in the 86500-91000 cm^{-1} Region

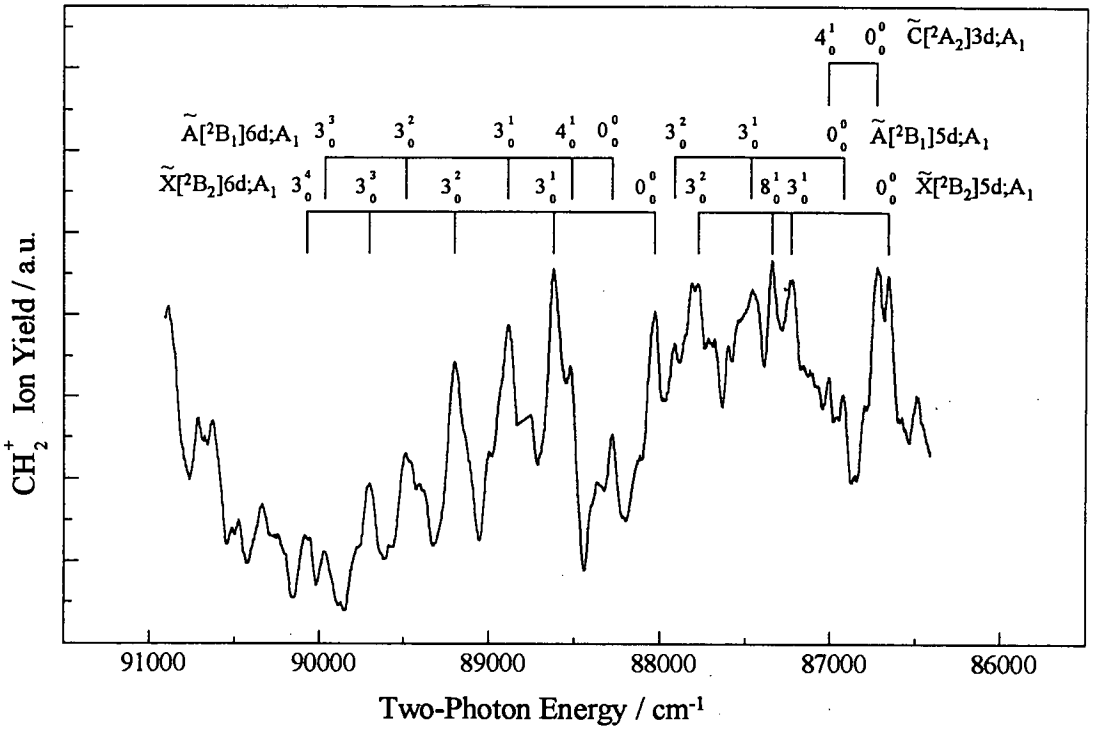

Figure 6-10: Spectrum depicting bands attributed to vibrational structure arising from higher members of *nd* series observed in CH_2Cl_2. The spectrum has been normalised to the square of the dye laser power.

The assignment of features in this region is more complex than that of the lower energy band systems. The additional spectral congestion in this region is caused by the greater density of electronic states and each state exhibiting an appreciable amount of vibrational activity. From Figure 6-9, it can be seen that the 4d/3d band system diminishes in intensity above 85500 cm^{-1}. This would suggest that any bands observed above 86500 cm^{-1} are not due to these Rydberg states. Although the spectrum depicted in Figure 6-9 is not power normalised, the drop-off in dye laser power is insufficient to explain the observed intensity distribution. On this basis, the states comprising the $\tilde{X}[^2B_2]4d/\tilde{A}[^2B_1]4d/\tilde{B}[^2A_1]3d$ system can be eliminated from our analysis in the 86500-91000 cm^{-1} region. Also, assignments to $\tilde{B}[^2A_1]4d$ and $\tilde{C}[^2A_2]4d$ transitions can be discounted on energetic grounds. These are expected to

Band Position cm^{-1}	**Electronic Assignment** cm^{-1}	**Vibrational Assignment** cm^{-1}	**Vibrational Spacing** cm^{-1}
86660	$\tilde{X}\,[^2B_2]5d;\ A_1$	0_0^0	0
86725	$\tilde{C}\,[^2A_2]3d;\ A_1$	0_0^0	0
86922	$\tilde{A}\,[^2B_1]5d;\ A_1$	0_0^0	0
87012	$\tilde{C}\,[^2A_2]3d;\ A_1$	4_0^1	287
87232	$\tilde{X}\,[^2B_2]5d;\ A_1$	3_0^1	572
87344	$\tilde{X}\,[^2B_2]5d;\ A_1$	8_0^1	684
87468	$\tilde{A}\,[^2B_1]5d;\ A_1$	3_0^1	546
87778	$\tilde{X}\,[^2B_2]5d;\ A_1$	3_0^2	1118
87918	$\tilde{A}\,[^2B_1]5d;\ A_1$	3_0^2	996
88032	$\tilde{X}\,[^2B_2]6d;\ A_1$	0_0^0	0
88282	$\tilde{A}\,[^2B_1]6d;\ A_1$	0_0^0	0
88520	$\tilde{A}\,[^2B_1]6d;\ A_1$	4_0^1	238
88623	$\tilde{X}\,[^2B_2]6d;\ A_1$	3_0^1	591
88891	$\tilde{A}\,[^2B_1]6d;\ A_1$	3_0^1	609
89202	$\tilde{X}\,[^2B_2]6d;\ A_1$	3_0^2	1170
89490	$\tilde{A}\,[^2B_1]6d;\ A_1$	3_0^2	1208
89700	$\tilde{X}\,[^2B_2]6d;\ A_1$	3_0^3	1668
89969	$\tilde{A}\,[^2B_1]6d;\ A_1$	3_0^3	1687
90070	$\tilde{X}\,[^2B_2]6d;\ A_1$	3_0^4	2038

Table 6-4: Vibronic Assignments of the 86600-90100 cm^{-1} region of the two-photon spectrum of dichloromethane.

lie above the energy region of interest. As discussed previously, an analysis involving Rydberg series can also be ruled out. This leaves open the possibility of band systems arising from $\tilde{X}\,[^2B_2]5d$ and $\tilde{A}\,[^2B_1]5d$ states. Then, most of the observed bands above 88000 cm^{-1} can be assigned to progressions in ν_3 arising from $\tilde{X}\,[^2B_2]6d$ and

$\tilde{A}\,[^2B_1]6d$ states, as depicted in Figure 6-10. Another possible assignment which would account for the majority of these features is that to a progression in ν_4 arising from a $\tilde{C}\,[^2A_2]5p$ state. However, this assignment is less cohesive because accounting for features in the 86500-88000 cm^{-1} region is now more difficult. Thus, as depicted in Figure 6-10 and shown in Table 6-4, assignments to vibronic systems arising from $\tilde{C}\,[^2A_2]3d;A_1$, $\tilde{X}\,[^2B_2]5d;A_1$, $\tilde{A}\,[^2B_1]5d;A_1$, $\tilde{X}\,[^2B_2]6d;A_1$ and $\tilde{A}\,[^2B_1]6d;A_1$ states can account for the majority of bands in the 86500-91000 cm^{-1} region. It is only bands beyond 90000 cm^{-1} that remain unassigned but these are more likely due to higher members of *nd* series.

6.7 Conclusion

As can be seen from the VUV absorption spectra of several dihalomethanes, the observed features are much broader. This most probable reason for this is a greater degree of predissociation. This is shown by the generation of CH radicals from dichloromethane. Also, not only are their spectra complicated by the presence of Rydberg series converging on the four low-lying ionisation limits, but there is a greater degree of vibrational excitation. All of these factors make any analysis of the observed spectra more difficult than it is in the case of the methyl halides. Even so, it possible to achieve at least a partial understanding of their spectra on the basis of their photoelectron spectra and a comparison with the spectra of the halogens[24] and the methyl halides.

Any attempt to see two-photon resonances in chloroiodomethane yielded little except the observation of resonances in radical species resulting from photodissociation of the parent at the first-photon stage. However, in the case of dichloromethane, many two-photon resonances are seen and these can only be attributed to the parent molecule. These are assigned to *nd* states but show somewhat different vibronic envelopes. The lowest energy band systems are assigned to $\tilde{X}\,[^2B_2]3d;A_1$ and $[^2B_1]3d;A_1$ states which show vibronic envelopes and vibrational frequencies which depart significantly from those seen in the photoelectron spectrum[2].

The $\tilde{X}[^2B_2]4d;A_1$, $\tilde{A}[^2B_1]4d;A_1$, $\tilde{X}[^2B_2]5d;A_1$, $\tilde{A}[^2B_1]5d;A_1$, $\tilde{X}[^2B_2]6d;A_1$ and $\tilde{A}[^2B_1]6d;A_1$ states display envelopes and spacings which increasingly approach those of the ionic states upon which they are based. Other possibilities are suggested also but then are discounted in favour of consistency.

6.8 References

1. D. W. Turner, C. Baker, A. D. Baker and C. R. Brundle, *Molecular Photoelectron Spectroscopy: A Handbook of He 584 P. E. Spectra*, Wiley-Interscience, London, **1970**.
2. T. Pradeep and D. A. Shirley, *J. Electron Spectrosc. Relat. Phenom.*, **1993** 66 125.
3. C. R. Zobel and A. B. F. Duncan, *J. Am. Chem. Soc.*, **1955** 77 2611.
4. B. R. Russell, L. O. Edwards and J. W. Raymonda, *J. Am. Chem. Soc.*, **1973** 95 2129.
5. L. E. Edwards and J. W. Raymonda, *J. Am. Chem. Soc.*, **1969** 91 5937.
6. L. C. Lee and M. Suto, *Chem. Phys.*, **1987** 114 423.
7. I. Novak, J. M. Benson and A. W. Potts, *Chem. Phys.*, **1986** 107 129.
8. D. Li, J.-K. Zhu, J.-G. Li and Y.-K. Pani, *Chem. Phys. Lett.*, **1982** 87 463.
9. K. Takeshita, *Chem. Phys.*, **1990** 143 239.
10. G. C. Causley and B. R. Russell, *J. Chem. Phys.*, **1975** 62 848.
11. H. Okabe, M. Kawasaki and Y. Tanaka, *J. Chem. Phys.*, **1980** 73 6162.
12. J. G. Frey, A. J. Bell, N. Shaw, M. J. Crawford, C. G. Hickman and A. Hopkirk, *VUV Molecular Photochemistry*, 152.
13. A. Penner and A. Amirav, *J. Chem. Phys.*, **1990** 93 8576.
14. M. B. Robin, *Higher Excited States of Polyatomic Molecules* Vol. 1, Academic Press, New York, **1974**.
15. B. A. Williams and T. A. Cool, *J. Phys. Chem.*, **1993** 97 1270.
16. W. M. McClain and R. A. Harris, in *Excited States Vol. 3* (Edited by E. C. Lim), Academic Press, New York, **1977**.

17. P. Chen, J. B. Pallix, W. A. Chupka and S. D. Colson, *J. Chem. Phys.*, **1987** 86 516.

18. K. K. Irikura, R. D. Johnson and J. D. Hudgens, *J. Phys. Chem.*, **1992** 96 6131.

19. F. Mélen, Y. Houbrechts, I. Dubois and H. Bredohl, *J. Phys. B: At. Mol. Phys.*, **1983** 16 2523.

20. J. W. Hepburn, D. J. Trevor, J. E. Pollard, D. E. Shirley and Y. T. Lee, *J. Chem. Phys.*, **1982** 76 4287.

21. L. Andrews, J. M. Dyke, N. Jonathan, N. Keddar and A. Morris, *J. Am. Chem. Soc.*, **1984** 106 299.

22. G. Herzberg, *Can. J. Phys.*, **1961** 39 1511.

23. G. Herzberg, *Proc. Royal Soc. Lond. A*, **1961** 262 291.

24. G. Herzberg and J. W. C. Johns, *Proc. Roy. Soc. Lond. A*, **1966** 295 107.

25. R. J. Donovan, A. C. Flexen, K. P. Lawley and T. Ridley, *Chem. Phys.*, **1998** 226 217.

Chapter 7

The Vacuum Ultraviolet Laser Spectroscopy of Molecular Chlorine in the Vicinity of the $1\,^1\Sigma_u^+$ (0_u^+) Double Minimum State.

7.1 Introduction

In previous chapters, the multiphoton spectroscopy of some small halogenated molecules was discussed. Here, in contrast, a discussion of the one-photon spectroscopy of Cl_2 in the 72200-77000 cm^{-1} is presented. While the assignments of the VUV spectra of some other diatomic halogens have been reviewed recently[1], molecular chlorine was not included in this. This might be at least partly due to differences between the VUV spectroscopy of chlorine and other halogens such as bromine or iodine. In fact, the understanding of the VUV spectrum of chlorine has been hindered by strong interactions between Rydberg and ion-pair states. These interactions are manifest in the perturbed irregularly spaced vibrational progressions which are apparent in VUV spectrum and this has made its analysis difficult. This is especially the case in the region studied here.

From the early work of Ickowski et al.[2] and Lee and Walsh[3] through to Douglas[4], little headway was made in reaching an understanding the VUV spectrum of Cl_2. In Douglas's study[4], the absorption spectrum of isotopically pure $^{35}Cl_2$ was recorded at rotational resolution in the 69000-82000 cm^{-1} region. Bands resulting from transitions to ion-pair and Rydberg states were categorised on the basis on their

rotational band contours. Red-degraded bands were taken to be due to ion-pair bands whilst blue-shaded bands were identified as Rydberg bands. The simulation of rotational band contours was used to distinguish Σ and Π excited states. This was more successful for the better resolved bands below 76000 cm^{-1}. For the blue-shaded bands in the 72000-77000 cm^{-1} region, three vibrational progressions were suggested as being due to Rydberg states. No state assignments were present for these and the observed progressions were labelled arbitrarily as I, II and III. Identification of the electronic states responsible for the observed features proved impossible until after the theoretical work of Peyerimhoff and Buenker[5].

Peyerimhoff and Buenker[5] undertook an extensive theoretical study of the electronic states of Cl_2, Cl_2^+ and Cl_2^-. Their predictions of the avoided crossings of the potential curves of Rydberg and ion-pair states in Cl_2 have contributed much towards reaching an understanding of its VUV spectrum. Following this, the VUV absorption spectrum was re-examined in the 73000-82000 cm^{-1} region using a synchrotron radiation source and the UV and VUV fluorescence spectra were newly reported[6,7]. In light of the preceding theoretical work[5], Moeller et al.[6] attributed Progressions III, II and I seen by Douglas to 2 $^3\Pi_u$ (1_u), 2 $^3\Pi$ (0_u^+) and 2 $^1\Pi_u$ states, respectively. Incidentally, the unexpectedly appreciable amount of intensity displayed by the features due to the 2 $^3\Pi$ (0_u^+) attracted the attention of Grein et al.[9] who attributed this to spin-orbit mixing with the nearby 2 $^1\Pi_u$ state in their theoretical study. The majority of the features in the 71000-76000 cm^{-1} were assigned to a 1 $^1\Sigma_u^+$ state and these were examined in some detail, using both absorption and bound-free fluorescence experiments. Analytical expressions describing the 1 $^1\Sigma_u^+$ double minimum potential curve were derived from the experimental data[6,7]. Moeller et al.[6] also studied higher energy features lying above 77000 cm^{-1}, the most of which were found to be assignable to a 2 $^1\Sigma_u^+$ state. These features are not of interest here because they lie outside the region of the VUV spectrum studied. All states and state interactions were considered adiabatically.

The greater resolution afforded by the use of coherent VUV excitation has been demonstrated by both Tsuchiya and his co-workers[10,11] and Wang et al.[12] for Cl_2 in their studies of the one-photon spectrum in the 72000-77000 cm^{-1} region. The coherent VUV radiation was generated using four-wave difference frequency (FWDM) mixing in krypton. Tsuchiya and his co-workers[10,11] used laser induced fluorescence (LIF) to study the 1 $^1\Sigma_u^+$ state while the 2 $^3\Pi_u$ (0_u^+) state was examined using (1+1') REMPI[7]. The vibrational numbering of the 1 $^1\Sigma_u^+$ ion-pair state was altered slightly for each of the $^{35}Cl_2$ and $^{35}Cl^{37}Cl$ isotopes[7]. Assignments for the same system in $^{37}Cl_2$ isotope were newly reported. Rotational analysis of the mass-resolved VUV laser spectra of the (39,0) 1 $^1\Sigma_u^+$ band in $^{35}Cl_2$ and $^{35}Cl^{37}Cl$, and the (40,0) 1 $^1\Sigma_u^+$ band in $^{37}Cl_2$ confirm that they are largely localised in the v'= 0 in the Rydberg well of the double minimum potential[12]. Assignments to progressions in the 1 $^1\Sigma_u^+$ and 2 $^3\Pi_u$ (0_u^+) states accounted for most of the observed bands. Extra bands were observed and these were said to be due to an interaction with the α $^3\Sigma_u^-$ state on the basis of rotational simulation of the relevant bands. Surprisingly, features arising from transitions to the 2 $^1\Pi_u$ and 2 $^3\Pi_u$ (1_u), so strong in the absorption spectrum, are apparently absent here.

Possible candidates for curve crossings with the ion-pair well of the 1 $^1\Sigma_u^+$ state have been examined by Al-Kahali et al.[13] using multiphoton excitation. Using a one-colour (1+2) excitation scheme, they[13] explored the spectroscopy of several ion-pair states of pure triplet character. However, because ion-pair states tend to have a much longer equilibrium internuclear distance than the neutral electronic ground state, they generally reside outside its Franck-Condon window, meaning that a vertical excitation pathway cannot be used to access them. To circumvent this, Al-Kahali et al.[13] used the continuum of the B $^3\Pi_{0_u^+}$ state as a real intermediate state at the first photon level. Exciting into the continuum of this state results in bond-stretching which expands the Franck-Condon window of the electronic ground state, allowing transitions to the ion-pair states of interest to be studied. This

excitation pathway resulted in the observation of vibrational progressions in the $\alpha\,^3\Sigma_u^-$ and $\gamma\,^3\Pi_u$ ion-pair states. These were seen to be perturbed by the $^1\Sigma_u^+$ state to be discussed here. It was found that the γ state interacted with the $^1\Sigma_u^+$ state more strongly than the α state. As will be discussed later, this has some consequences for the VUV spectroscopy of Cl_2 in the 72000-77000 cm^{-1} region.

7.2 Additional Experimental Details

In this work, tunable coherent vacuum ultraviolet radiation was generated in the 129-139 nm region using FWDM in krypton. The experimental arrangement used here differs to some extent from that discussed in earlier chapters for multiphoton experiments. An overview of the setup used for FWDM in this study is given in Figure 7-1. The frequency-doubled output of the Lambda Physik FL2002 dye laser (the UV laser) was used to pump a two-photon 5p←←4p transition in atomic krypton. For the majority of this work, the $[1/2,0]^{14}$, 94094 cm^{-1}, resonance was used while the $[5/2,2]^{14}$, 92308 cm^{-1}, resonance was used also. The emission of coherent VUV radiation was stimulated using the fundamental output of the Lambda Physik FL3002E dye laser (the visible laser). To generate VUV radiation, visible radiation in the 468-590 nm was used. The scheme used for generating coherent VUV is depicted in Figure 7-2. The bandwidth of the VUV radiation produced is of the order of 0.3 cm^{-1}. For the four wave mixing to occur, the beams from both dye lasers were passed collinearly through a beam combiner and focused into a static gas cell containing 10-20 torr of krypton (Krypton 4.0, Messer Griesheim) using a quartz lens of focal length 20cm. The VUV radiation was focused onto a molecular beam of 700 torr Cl_2 seeded in 300 torr He using a translatable LiF lens of focal length 5cm. However, not only can VUV radiation cross the molecular beam but the UV and visible radiation can do so also. This may lead to a variety of two-colour excitation schemes but the three beams have different focal points as a result of their very different wavelengths. Therefore, judicious positioning of both the quartz and LiF lenses allows selection of the 1+1' (excitation by one VUV photon followed with ionisation by one visible photon) scheme used for the most of this study.

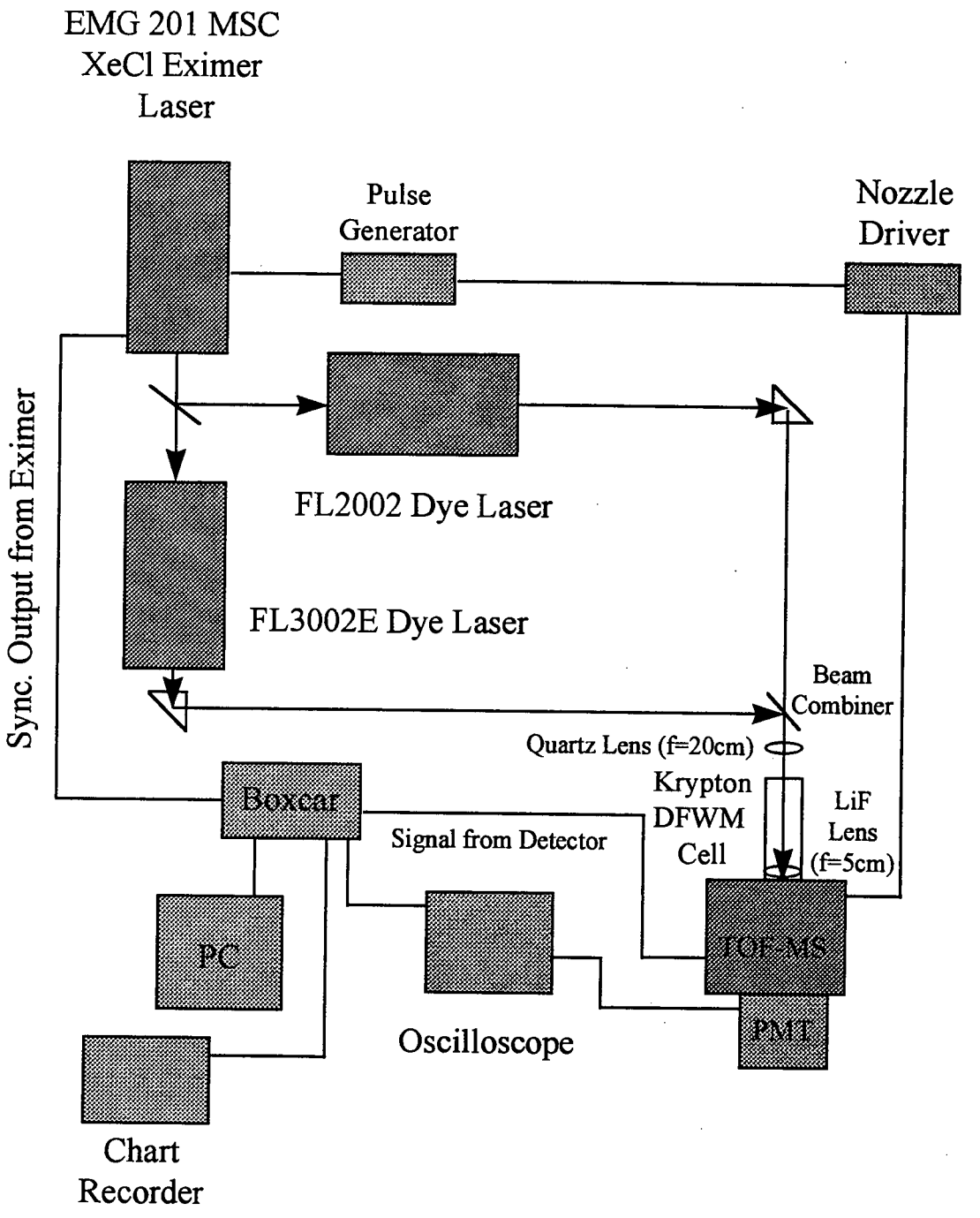

Figure 7-1: The experimental setup employed mass-resolved VUV laser spectroscopy.

The VUV radiation was monitored through directing the beam exiting the ionisation chamber via an Acton Research Corporation vacuum monochromator onto

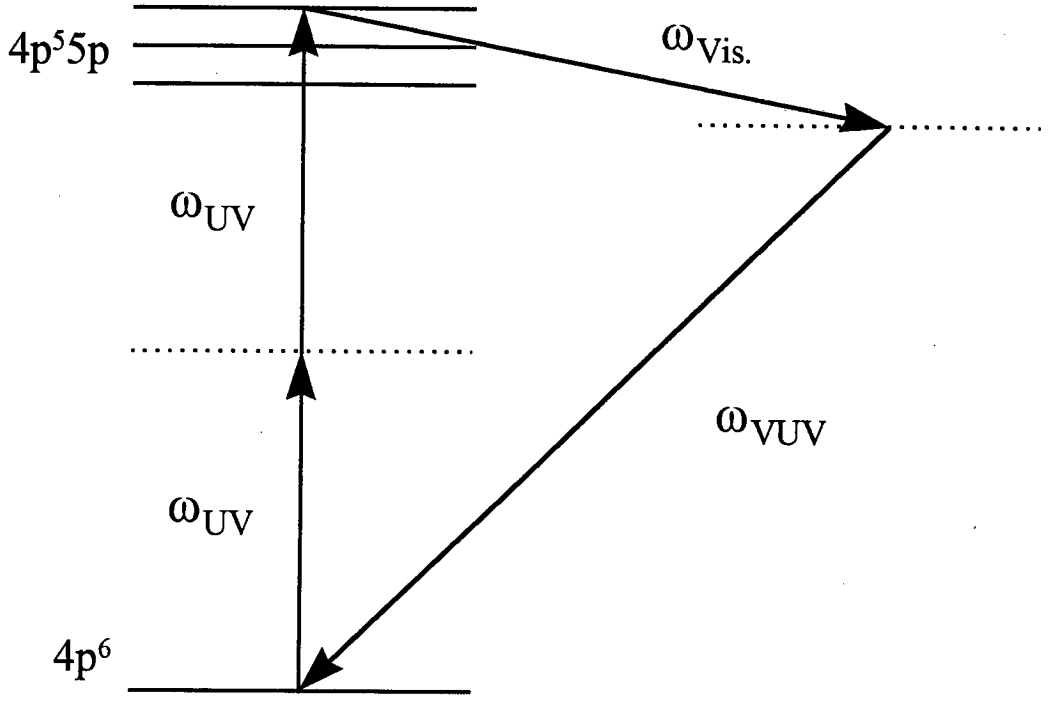

Figure 7-2: The FWDM scheme for coherent VUV generation in atomic krypton.

a Hamamatsu R1459 solar blind photomultiplier tube (PMT). However, this does not allow for direct monitoring of VUV power and an attempt to replace the PMT with a photodiode proved unsuccessful. Consequently, and since variation in VUV power was not monitored in any other way, the power normalisation of any VUV spectra obtained was not possible. Power normalisation is desirable because one source of variation in the VUV power results from the power spectrum of the visible laser. Therefore, a degree of caution must be exercised when comparing peak intensities on any of the obtained spectra. Some comparison of the relative intensities of nearby features is allowed because the major variation in VUV intensity should be due to the power spectrum of the visible laser and this is not expected to be dramatic, except at its extremities. Hence, where composite plots made up of a number of laser scans are presented, the regions corresponding to different laser scans are indicated. The band measured quoted in this discussion have not been calibrated but sufficiently agree, typically within 3 cm^{-1}, with those reported by Douglas[5] and Tsuchia et al.[11] to be reported without any calibration.

7.3 Results and Discussion

In this study of the VUV spectrum of Cl_2 in the 72000-77000 cm^{-1} region, all of the states reported by Moeller et al.[6] are seen although they will be labelled differently here. This is in order to ensure consistency with the labelling used for other diatomic halogens. Previously. the Rydberg and ion-pair states of Cl_2 have been labelled in a manner consistent with a Hund's case (a) coupling scheme. However, given the appreciable spin-orbit splitting seen in the X and A ion states, Λ is more likely to be decoupled from the molecular axis, leaving Ω as the more appropriate quantum number. Therefore, for Rydberg states, a description involving (Ω_c, ω_{Ryd}) or (Ω_c, λ_{Ryd}, m_s) coupling will be adopted here and the states labelled accordingly. Thus, a similar labelling scheme will adopted for the Rydberg states of Cl_2 as for the methyl halides, described in Chapter 3, with Ω_c being indicative of the component of the X ionic state forming the basis for the Rydberg state concerned. Also, ion-pair states are labelled in accordance with a Hund's case (c) description. Therefore, the ion-pair states of most interest in this study, the $^1\Sigma_u^+$ (0_u^+), $\gamma\ ^3\Pi_u$ and $\alpha\ ^3\Sigma_u^-$ (0_u^+) states, are relabelled F′ (0_u^+), F (0_u^+) and D (0_u^+), respectively, in line with those of other halogens such as Br_2 or I_2.

In most of the previous work dealing with the VUV spectroscopy of molecular chlorine in the 72000-77000 cm^{-1} region, the interactions between Rydberg and ion-pair states are described adiabatically and the relevant states labelled accordingly. Here, in contrast, the excited state interactions are discussed using a diabatic representation and the observed states are labelled in keeping with this. The diabatic description is used here because it is in keeping with the labelling used for the heavier diatomic halogens. Not only this but it also demonstrates any perturbation of vibrational spacings which can occur as a result of interactions between electronic states. Therefore, it is equally useful in showing which states remain unperturbed by excited state interactions as well as maintaining a consistent labelling scheme.

In the free-ion VUV laser spectra of I_2 and ICl, the positions of the 20 cm quartz and 5 cm LiF lenses were optimised such that only VUV radiation intersected the molecular beams. Any ion signal observed was a result of Rydberg state predissociation by the continuum of a first-tier ion-pair state. That this does not occur here would seem to be indicated by the dominance of molecular ion signal when the 94094 cm^{-1} krypton resonance is used for coherent VUV generation. It is also consistent with the first thermodynamic threshold for ion-pair formation being 95727 cm^{-1}, calculated using values of 104591 cm^{-1} for the energy of the Cl^+ $^3P_2$ state[15], 20277 cm^{-1} for D_e(Cl-Cl)[6] and 29141 cm^{-1} for the electron affinity of atomic chlorine[16]. However, atomic ion signal is the more apparent when 92308 cm^{-1} krypton resonance is used for FWDM. This behaviour can be explained when it is considered that the first ionisation energy[17] of Cl_2 lies at 92616 cm^{-1}. Since this lies below the higher energy krypton resonance, it means that the combined energy of one VUV and

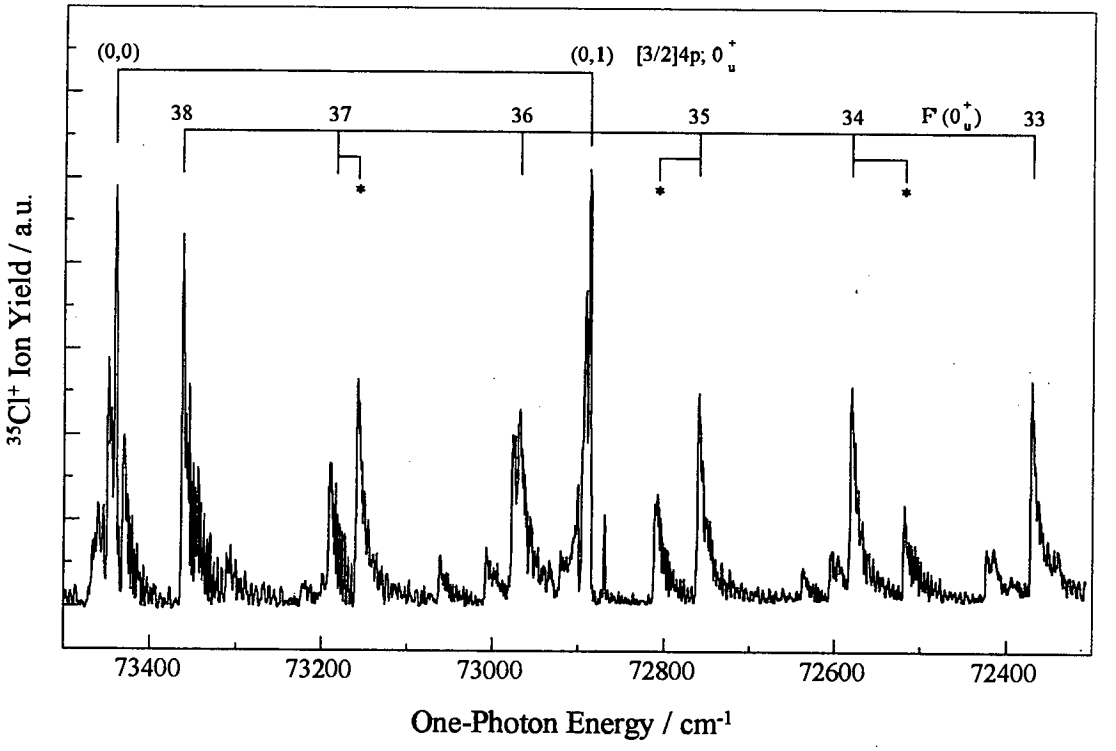

Figure 7-3: The VUV Excitation Spectrum Recorded in the $^{35}Cl^+$ Channel. The peaks denoted by an asterisk (*) are due to the interaction with the F (0_u^+) state. These are not assigned as it proved impossible to extend the progression reported by Al-Kahali et al.[13] into our energy region. Any additional unassigned peaks present correspond to the $^{35}Cl^{37}Cl$ isotopomer.

one visible photon is sufficient to ionise the molecule when this krypton resonance is used. This is not the case for the 92308 cm^{-1} resonance so the dominance of atomic signal may not be entirely surprising. Therefore, a different ionisation mechanism must be involved. One possibility consistent with the appearance of dominant atomic ion signals is that dissociation occurs prior to ionisation and the appearance of a greater amount of rotational structure would be in keeping with this. However, this would suggest neutral species which must then be ionised by at least three UV photons or seven visible ones which seems rather unlikely. Another alternative would involve a VUV + UV ionisation pathway followed by UV fragmentation of the ion. This seems more likely because less photons, and hence a lower laser power, are required.

Given that most of the spectra are recorded in the molecular ion channels, separation of signals due $^{35}Cl_2$ and $^{35}Cl^{37}Cl$ is possible. As can be seen in Figure 7-3, this is not possible for the atomic fragment. Therefore, the benefit of using mass-resolved spectra only comes about when molecular ion channels are used unless a separate $^{37}Cl^+$ channel can be monitored.

7.3.1 The $1\,^1\Sigma_u^+$ State

The most perturbed of the 4p states in molecular chlorine is the $[3/2]4p;0_u^+$ state. This strongly interacts, through an avoided crossing near its v' = 0 level, with the third-tier F' (0_u^+) ion-pair state. This curve crossing is indicated diabatically in a schematic potential energy diagram displaying potential energy curves for some electronic states in $^{35}Cl_2$, shown in Figure 7-4. The curve crossing is avoided because of the two electron shift between the electron configurations of the original states: the Rydberg state has a 2431 (or $\sigma_g^2\pi_u^4\pi_g^3 4p^1$) configuration while the electronic configuration of the ion-pair state is 1441 (or $\sigma_g^1\pi_u^4\pi_g^4\sigma_g^1$). The position on the potential curve of the Rydberg state means that all the observed bands due to it will be perturbed by the ion-pair interaction. However, the Rydberg vibrational levels will

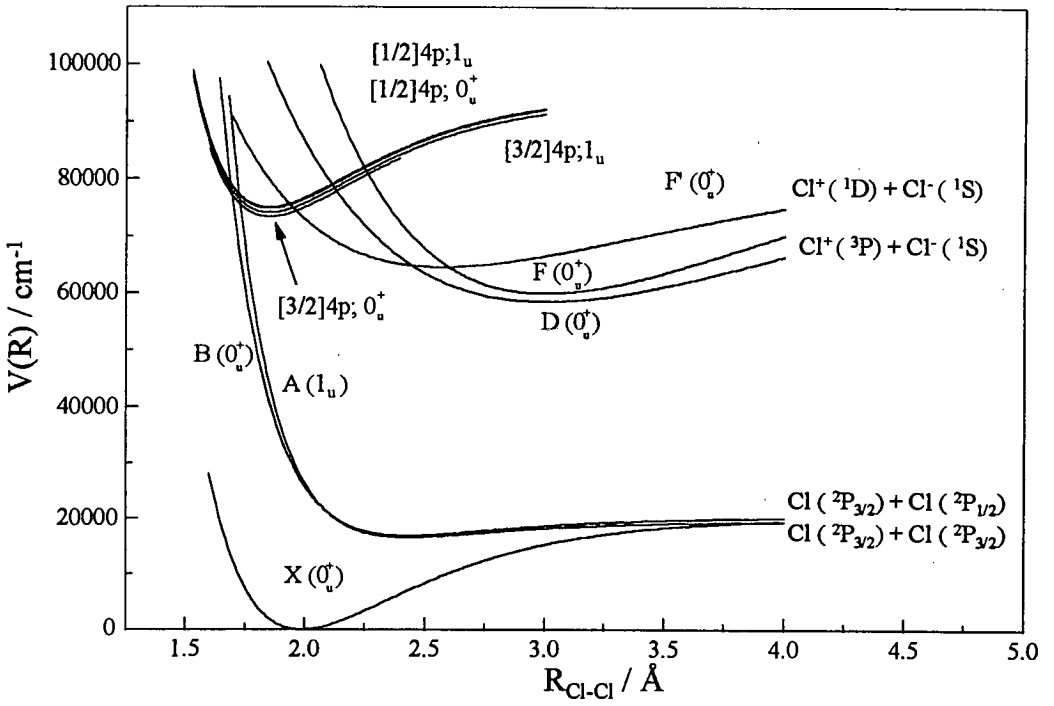

Figure 7-4: Schematic diabatic potential energy diagram of selected electronic states of $^{35}Cl_2$. The ion-pair states interacting with the [3/2]4p;1_u, [1/2]4p;0_u^+ and [1/2]4p;1_u states are not shown for sake of clarity and because they are not apparent in the spectra presented here.

be seen to be only partially delocalised into the ion-pair potential well. Moreover, some delocalisation of the ion-pair vibrational levels into the Rydberg well allows intensity borrowing and transition which otherwise might not take place due to Franck-Condon restrictions are seen.

In this discussion, the vibronic assignments of the Rydberg and ion-pair states are treated separately to show any perturbations more clearly. The assignments for the ion-pair system are given in Table 7-1 which those for the Rydberg state are detailed in Table 7-2. Some localisation of vibrational levels in Rydberg and ion-pair potential wells remains apparent. The first indication of this come from intensity data. While the spectra recorded in this study have not been power normalised, some useful intensity information remains available as long as extra caution is taken. It can be seen that transitions to vibrational levels originating within the Rydberg potential well are much stronger than those to vibrational levels occurring within the ion-pair well. The more favourable Franck-Condon factors for Rydberg transitions together with a greater

one-photon ionisation cross-section due to similarities in electronic configuration between the Rydberg state and the ionic ground state ensure that Rydberg bands are the more intense. That some localisation of vibrational levels occurs is also consistent with the observed rotational band contours. Rotational band systems are blue-degraded for Rydberg transitions but red-degraded for those to ion-pair states. This is a consequence of the magnitudes of the rotational constants for the relevant display longer bondlengths while, in the diatomic halogens, Rydberg states display slightly shorter ones relative to the neutral electronic ground state. Since $B_e \propto 1/R_e$, differences in B_e values also occur between the neutral ground state and the different excited states, resulting in different rotational contours. However, perturbation of the rotational contours as a result of Rydberg~ion-pair interaction can occur. This means that care is required in their analysis but the perturbations are not sufficiently severe to disqualify the qualitative interpretation employed here. That rotational contours can still be useful here is shown in Figure 7-3. Therefore, in spite of the strong Rydberg~ion-pair interaction, the vibrational levels in the double minimum potential seem to display a significant degree of localisation in their original potential wells: Rydberg or ion-pair. Hence, a diabatic description as employed in the schematic potential energy diagram in Figure 7-4 is not unreasonable.

The vibrational progression in the ion-pair state, detailed in Table 7-1, has been extended in this work. These and the vibrational assignments of the other Rydberg states observed, are illustrated in Figures 7-5 and 7-6 for $^{35}Cl_2$ and Figures 7-7 and 7-8 for $^{35}Cl^{37}Cl$. Because these figures do not depict the origin of the $[3/2]4p;0_u^+$ state to its full extent, this is detailed in Figure 7-9 with the (0,1) band include for the sake of comparison. As in the VUV LIF spectrum[10,11], additional bands due to one or more nearby ion-pair states are also seen in the spectrum reported here. Tsuchizawa et al.[11] analysed interactions the rotational contour of the additional bands and found them to be in agreement with the values of Ishiwata et al.[18] Because of this Tsuchizawa et al.[11] argued that the D (0_u^+) state was interacting with the F′ (0_u^+) state. But Al-Kahali et al.[13] reported new data from a study involving the use of the B state as an intermediate in a one-colour (1+2) excitation of some candidates for interaction

with the F′ (0_u^+) state. This strongly suggests that a strong interaction, enhanced by spin-orbit coupling, should occur between the triplet F (0_u^+) and singlet F′ (0_u^+) states. This implies that the additional bands seen on our spectra are due to the F state and not the D state as stated by Tsuchiya et al.[11] Since, these bands also possess irregular vibrational spacings, a vibrational numbering based upon the

Vibrational Assignment	$^{35}Cl_2^+$	$^{35}Cl^{37}Cl^+$
(v',v")	**Band Measurement cm^{-1}**	**Band Measurement cm^{-1}**
(33,0)	72370	~
(34,0)	72582	~
(35,0)	72759	~
(36,0)	72977	72872
(37,0)	73159	73074
(38,0)	73362	73268
(39,0)	73562	73482
(40,0)	73755	73657
(41,0)	73915	73815
(42,0)	74142	74056
(43,0)	74305	74218
(44,0)	74464	74381
(45,0)	~	~
(46,0)	~	~
(47,0)	~	~
(48,0)	75385	75266
(49,0)	75545	75443
(50,0)	~	75443
(51,0)	75846	~
(52,0)	76006	~

Table 7-1: Vibronic assignments for the F′ (0_u^+) ion-pair state.

Vibrational Level	$^{35}Cl_2^+$	$^{35}Cl^{37}Cl^+$
(v',v")	**Band Measurement** cm^{-1}	**Band Measurement** cm^{-1}
(0,2)	72340	~
(0,1)	72887	72914
(0,0)	73440	73435
(1,0)	74017	73963
(2,0)	74616	74520
(3,0)	75226	75119
(4,0)	~	75613
(5,0)	76166	~

Table 7-2: Vibronic assignments for the [3/2]4p;0_u^+ Rydberg state.

extension of the progression seen by Al-Kahali et al.[13] has not proved possible.

While some vibrational levels, especially the higher lying ones, of the F' (0_u^+) ion-pair state may be accessible from the ground state in a one-photon excitation, their intensity enhancement is most likely a result of the interaction with the [3/2]4p;0_u^+ Rydberg state. This also would increase the number of observed transitions to vibrational levels in the potential well of the F' (0_u^+) ion-pair state. Lower-lying vibrational levels are placed outside the Franck-Condon window of the ground state by the elongated equilibrium bondlength of an ion-pair state and intensity borrowing from a nearby Rydberg state may well be the only means for observing transitions to at least some of these levels when vertical excitation is used. This is pertinent when it is considered that the ion-pair bands were found to be of lower intensity for $^{35}Cl^{37}Cl$ than for $^{35}Cl_2$ in comparison to the intensities of the Rydberg bands observed for both isotopomers. This would be consistent with a weaker interaction between the Rydberg and ion-pair states in the former. One possible explanation for this is that isotope shifts of the vibrational levels in both the Rydberg and ion-pair potential wells must reduce the strength of the interaction

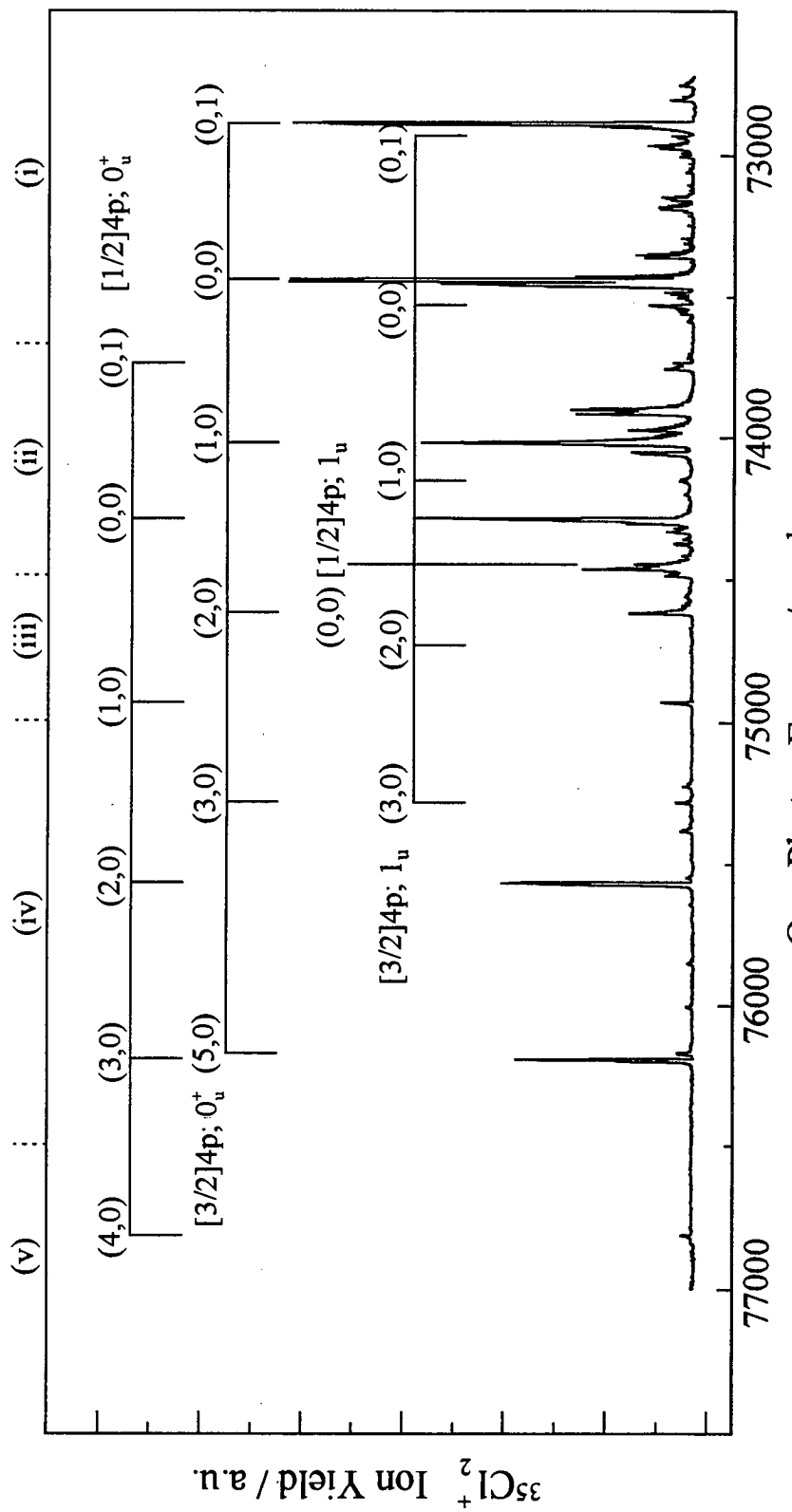

Figure 7-5: Composite plot detailing the appearance of the ungerade 4p Rydberg band systems in the VUV laser spectrum of $^{35}Cl_2$. The component spectra have not been power normalised so caution is required when comparing the relative intensities of the observed features. Also, the origin of the [1/2]4p;0_u^+ band system is not shown to its full extent. The different laser scans comprising the composite plot are denoted at the top of the figure. The dyes used were Coumarin 47, (i); Coumarin 307, (ii) and (iii); and Coumarin 153, (iv) and (v).

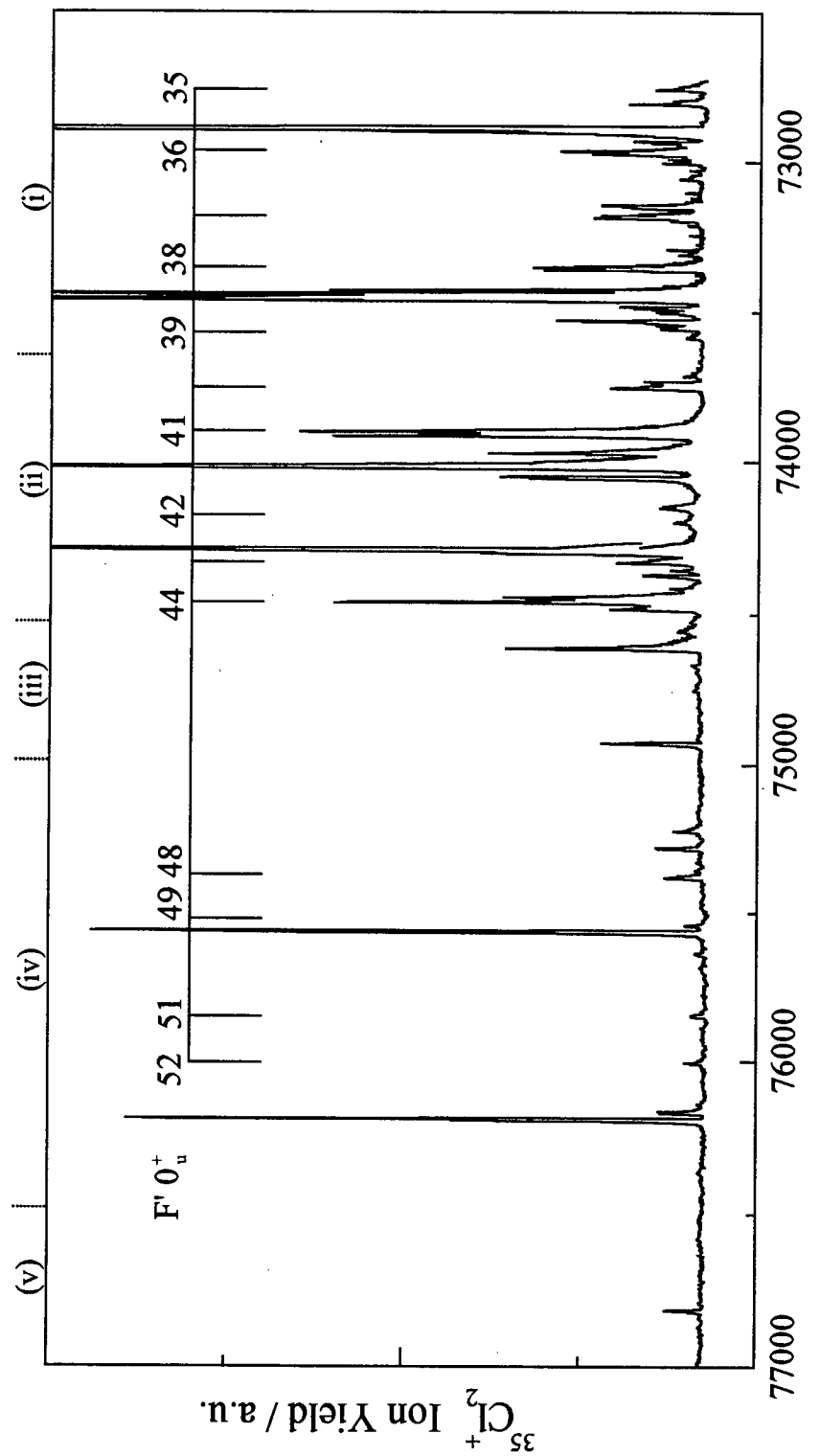

Figure 7-6: Composite plot with an expanded intensity scale detailing the appearance of the band system due to the F'0_u^+ ion-pair state in the VUV laser spectrum of $^{35}Cl_2$. As in the previous figure, the component spectra have not been power normalised so caution is required when comparing the relative intensities of the observed features. The different laser scans comprising the composite plot are denoted at the top of the figure. The dyes used were Coumarin 47, (i); Coumarin 307, (ii) and (iii); and Coumarin 153, (iv) and (v).

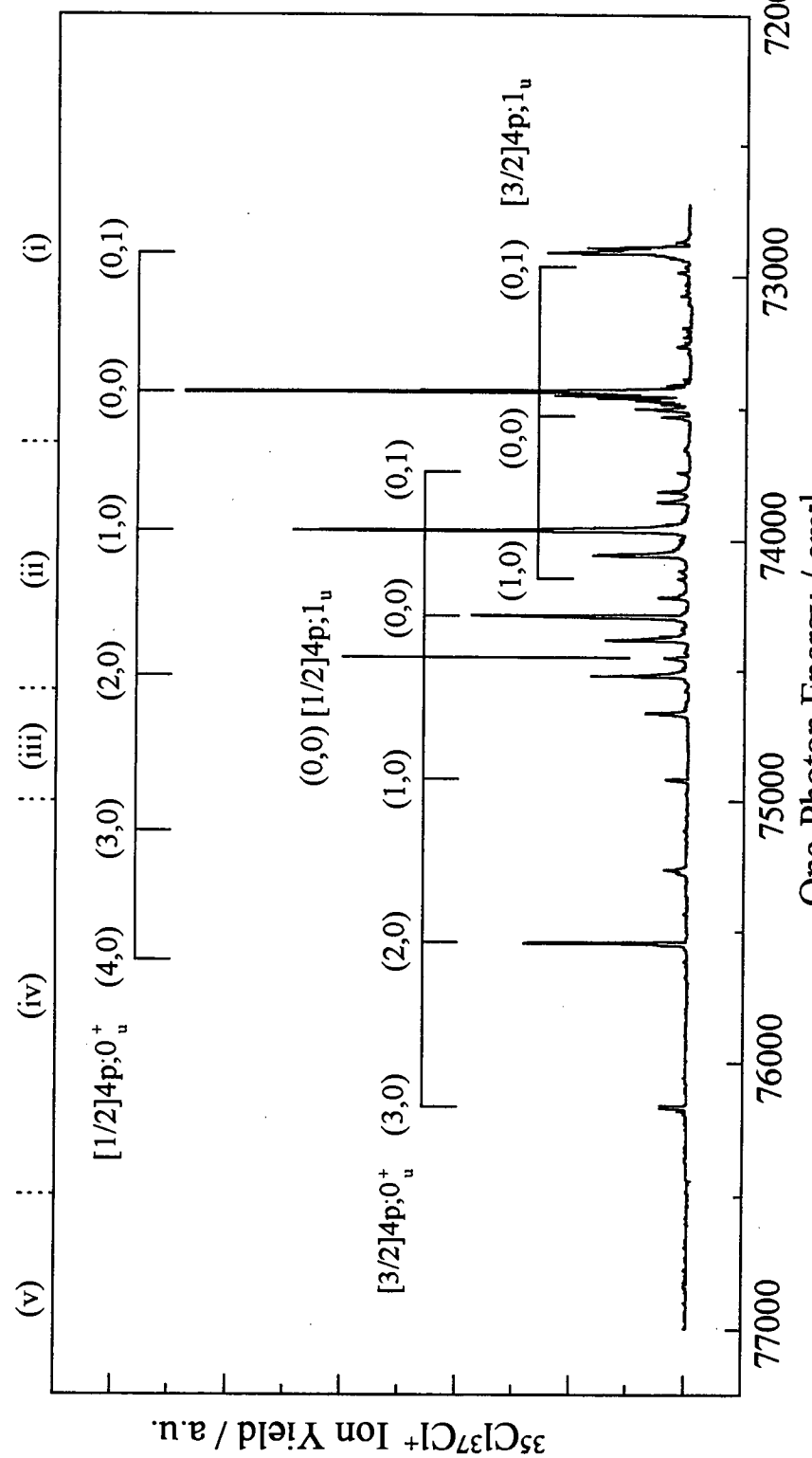

Figure 7-7: Composite plot detailing the appearance of the ungerade 4p Rydberg band systems present in the VUV laser spectrum of $^{35}Cl^{37}Cl$. As in the previous figures, the component spectra have not been power normalised so caution is required when comparing the relative intensities of the observed features. Again, the full intensity of the origin of the $[3/2]4p;0^+_u$ band system is not shown. The different laser scans comprising the composite plot are denoted at the top of the figure. The dyes used were Coumarin 47, (i); Coumarin 307, (ii) and (iii); and Coumarin 153, (iv) and (v).

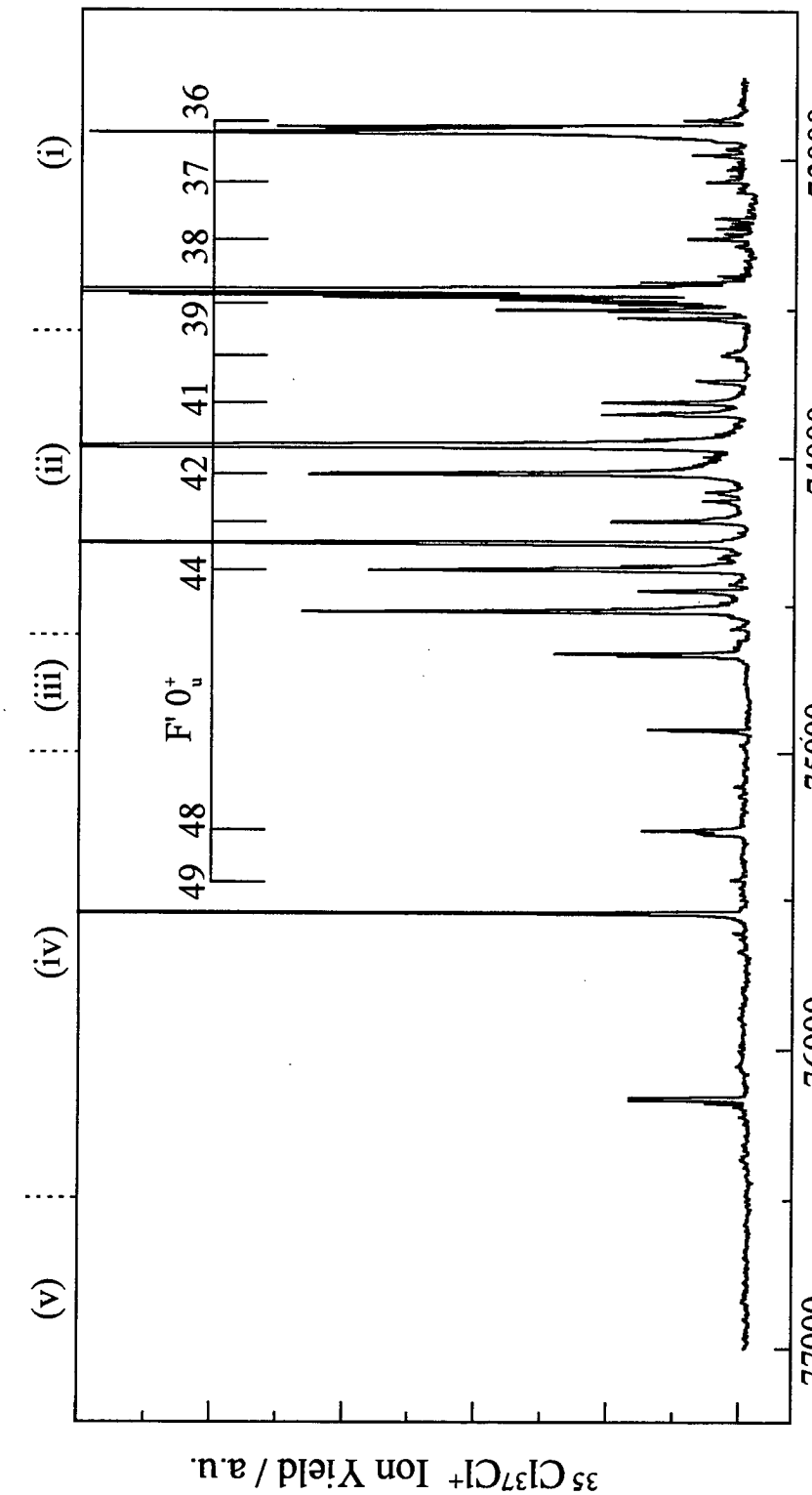

Figure 7-8: Composite plot with an expanded intensity scale detailing the appearance of the band system due to the F'0_u^+ ion-pair state in the VUV laser spectrum of $^{35}Cl^{37}Cl$. As in the previous figures, the component spectra have not been power normalised so caution is required when comparing the relative intensities of the observed features. The different laser scans comprising the composite plot are denoted at the top of the figure. The dyes used were Coumarin 47, (i); Coumarin 307, (ii) and (iii); and Coumarin 153, (iv) and (v).

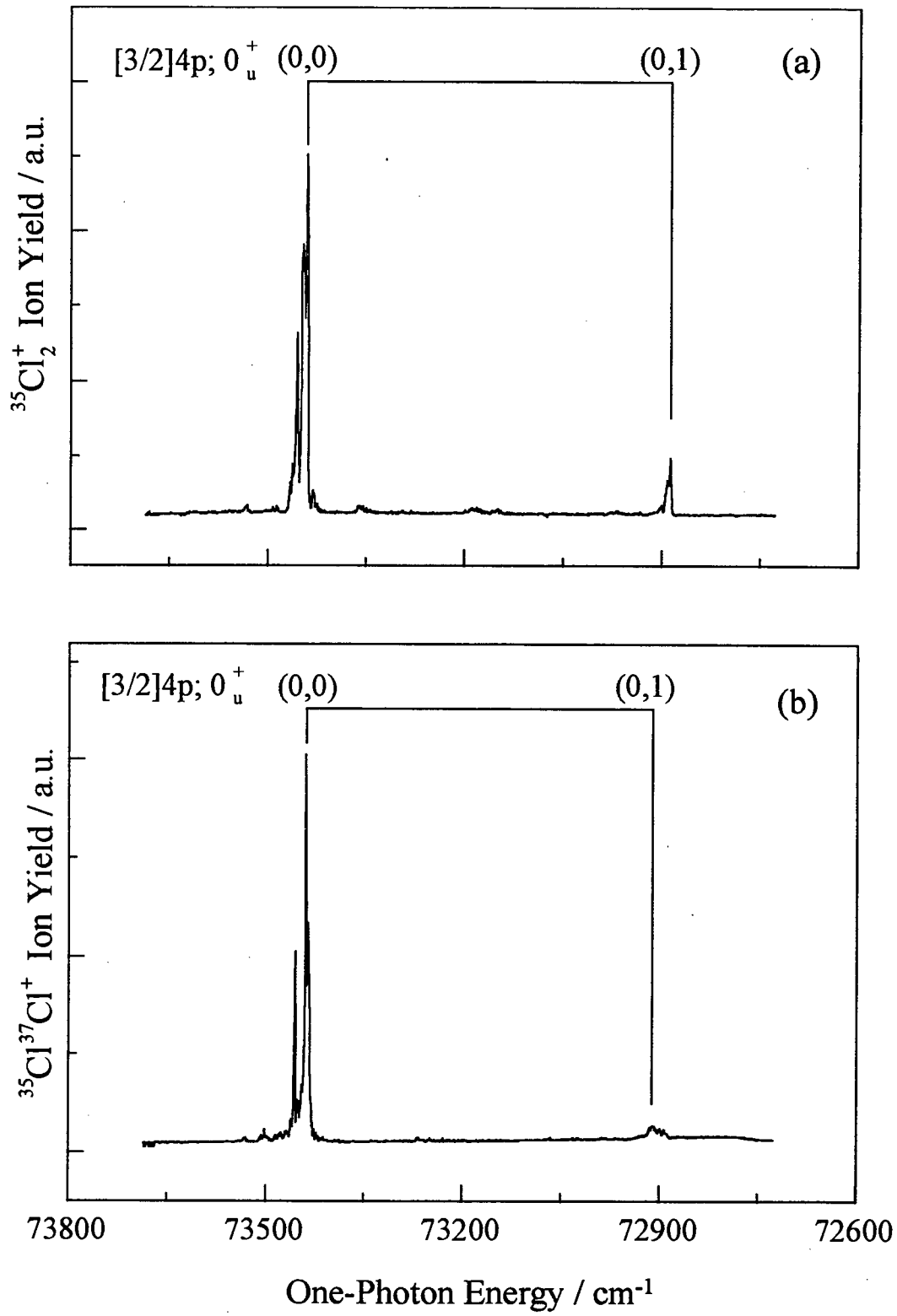

Figure 7-9: Attenuated VUV spectra detailing the full extent of the (0,0) [3/2]4p;0_u^+ band for (a) $^{35}Cl_2$ and (b) $^{35}Cl^{37}Cl$.

between the two states. This would occur if the interacting Rydberg and ion-pair vibrational levels were closer together for the lighter isotopomer, hence inducing a stronger interaction and more intensity borrowing, than in the heavier.

Even in a diabatic description, the perturbation of the [3/2]4p;0_u^+ remains quite apparent. The first indication of this is the divergence of the vibrational spacings in the 4p state. Normally, convergence is expected as the dissociation limit of the electronic state is being reached. This is most likely a direct result of the interaction with the F′ state. In the absence of any interaction, some of the vibrational levels in both potential wells would be incident on one another but are displaced by the interaction between them. The interaction also results in perturbation of the rotational band contours of the interacting states. As discussed earlier, features arising from transitions to Rydberg states tend to display blue-degraded rotational structure while bands due to ion-pair states have red-degraded band contours. When an ion-pair state interacts with a Rydberg state, the rotational contour can deviate from this, in some cases being a mixture of both types. These comments also apply to the F′ 0_u^+ ion-pair state which displays even more irregular vibrational spacings. Even with the perturbed vibrational spacings, the vibrational levels do seem to be localised for the most part within their original potential wells. This may well be a consequence of the avoided curve crossing and also means that a diabatic description used here is not unsuitable in this case. However, differences are apparent between the 4p Rydberg states observed and they are discussed below.

7.3.2 The Other States Examined

While most of the bands in the 72000-77000 cm^{-1} region can be attributed to the 1 $^1\Sigma_u^+$ double minimum state, features due to other double minimum states are present also. These are the 2 $^3\Pi$ (0_u^+), 2 $^3\Pi$ (1_u) and 2 $^1\Pi$ states[6]. However, these band systems show less perturbation than the 1 $^1\Sigma_u^+$ system discussed already. Also, the observed band systems are remarkably Rydberg-like in character. This is

confirmed by the appearance of blue-degraded rotational contour for these bands in Douglas's VUV spectrum[5]. This implies that any crossing involving the relevant Rydberg and ion-pair states must occur much higher up the Rydberg potential curves here than in the case of the [3/2]4p;0_u^+ state. The band measurements and quantum defects of the electronic origins of all the 4p states observed are given in Table 7-3. Note the perceptible isotope shift of the origin of the [3/2]4p;0_u^+ state as a result of strong interaction with the F′ (0_u^+) state while the band measurements for all of the others agree within 1 cm^{-1}. Some differences are noticeable between the 4p cluster in molecular chlorine and the lowest *np* clusters in other diatomic halogens[1]. The first of these arises as a result of the smaller degree of spin-orbit interaction present. This results not only in smaller spin-orbit splittings in the ion but lessens the amount of spin-orbit splitting in the Rydberg orbital as evidenced by the smaller splittings between different Ω components based upon the same ionic core. However, the extent of Rydberg~ion-pair interaction taking place can only exacerbate this. This may account for the departures in the spin-orbit splittings observed in the 4p cluster from that seen in the ion states. Rydberg~ion-pair interactions could account also for the reversed ordering of Ω=0 and Ω=1 in Cl_2 relative to Br_2 or I_2.

Assignment	$^{35}Cl_2^+$		$^{35}Cl^{37}Cl^+$	
$[\Omega_c]nl;\Omega$	$\bar{\nu}$/cm^{-1}	$(n-\delta)$	$\bar{\nu}$/cm^{-1}	$(n-\delta)$
[3/2]4p;0_u^+	73440	2.39	73435	2.39
[3/2]4p;1_u	73531	2.40	73530	2.40
[1/2]4p;0_u^+	74286	2.40	74287	2.40
[1/2]4p;1_u	74446	2.41	74446	2.41

Table 7-3: The electronic origins of the 4p Rydberg states observed in this work. The ionisation limits used to claculate the quantum defects for these states were 92616 cm^{-1} and 93366 cm^{-1}, for the X $^2\Pi_{g,3/2}$ and X $^2\Pi_{g,1/2}$ ion states, respectively. These values were obtained from a recent threshold photoelectron study[17].

Apart from the [3/2]4p;0_u^+ state, the other 4p states observed are the [1/2]4p;0_u^+ ($2\ ^3\Pi\ (0_u^+)$), [3/2]4p;1_u ($2\ ^3\Pi\ (1_u)$) and [1/2]4p;1_u ($2\ ^1\Pi_u$) states. Although two components of the 4p cluster based upon each ionic core are seen as expected on the basis of the propensity rules described in Chapter 3, the identities of some of the double minimum states, given above in brackets beside the relevant Rydberg state label, are somewhat surprising. The assignment of transitions to a $2\ ^3\Pi\ (0_u^+)$ state is the most surprising while the $2\ ^3\Pi\ (1_u)$ state can acquire some singlet character through spin-orbit coupling. To return to the $2\ ^3\Pi\ (0_u^+)$ double minimum state, the Hund's case (a) label for the observed [1/2]4p;0_u^+ state should be $^{1,3}\Sigma_u^+$ given the intensity of the features due to it and not $^3\Pi\ (0_u^+)$, even though Ω would be the same in both cases. It is difficult to see how a triplet state might be observed in place of a singlet state given the expected propensity rules. Thus, the [1/2]4p;0_u^+ state should interact with the F′ 0_u^+ state, $^1\Sigma_u^+$ in Hund's case (a), as its counterpart based upon the lower ionic core does. That it clearly does not is apparent from the regularity of the vibrational spacings. The band positions for features arising from transitions to this state are given in Table 7-4. Why it should interact with a

Vibrational Level	$^{35}Cl_2^+$	$^{35}Cl^{37}Cl$
(v',v")	**Band Measurement cm^{-1}**	**Band Measurement cm^{-1}**
(0,1)	73733	73738
(0,0)	74286	74287
(1,0)	74927	74918
(2,0)	75562	75544
(3,0)	76190	76164
(4,0)	76812	~

Table 7-4: Vibronic assignments for the [1/2]4p;0_u^+ Rydberg state.

nearby $^3\Pi$ (0_u^+) ion-pair state and not the F' 0_u^+ one is not immediately clear, especially as an interaction involving the former would have to be facilitated by appreciable spin-orbit interaction because such a Rydberg~ion-pair interaction would be both spin- and λ-forbidden in a Hund's case (a) description. The effect of spin-orbit coupling in the low-lying ionic states, which increases the number of Rydberg states upon the electronic structure of Cl_2 does not seem to have been considered by Peyerimhoff and Buenker[5]. In fact, a new theoretical study carried out in this light may further elucidate the properties of the [1/2]4p;0_u^+ state discussed here.

Vibrational Level	$^{35}Cl_2^+$	$^{35}Cl^{37}Cl^+$
(v',v")	**Band Measurement** cm^{-1}	**Band Measurement** cm^{-1}
(0,1)	72977	72966
(0,0)	73531	73530
(1,0)	74152	74144
(2,0)	74753	~
(3,0)	75281	~

Table 7-5: Vibronic assignments for the [3/2]4p;1_u Rydberg state.

4p;1_u states give rise to the strongest features in the VUV absorption spectrum. However, this intensity distribution is not repeated here and no features due to these states were reported by Tsuchia and co-workers[10,11]. However, the latter observation may well be due to curtailment of fluorescence by predissociation of the Rydberg states concerned. This is an important consideration when it is remembered that Tsuchia and co-workers[10,11] only examined the energy region in which the 4p;1_u states lie using LIF and not REMPI. Also, the features due to the [1/2]4p;0_u^+ state are seen using (1+1') REMPI but not LIF which is consistent with this increased rate of predissociation. Still, the weakness of the features seen in the REMPI spectrum due to these states is surprising. especially as only the origin band of the [1/2]4p;1_u state is

seen the REMPI spectra reported here when features arising from transitions to this state are the strongest in the VUV absorption spectrum[4,6,7]. Because one-photon excitation is used in each case, this leads one to suspect that an inefficient ionisation step is the cause of this. The vibrational assignment of the [3/2]4p;1_u state is detailed in Table 7-5.

7.4 Conclusion

Using VUV laser spectroscopy, the ion-pair and Rydberg states of Cl_2 were examined in the 72200-77000cm^{-1} energy region with high resolution. Like in Br_2 and I_2, the relevant excited states have been labelled in a manner consistent with a diabatic description of the excited state interactions. Adiabatic descriptions have been used heretofore. The validity of a diabatic description is supported by the rotational band contours displayed by the observed features here and in other studies[4,6,7,10,11]. These rotational contours suggest significant localisation of vibrational levels within the potential wells from which they originate. If this were not the case, a diabatic description could not be used.

Upon qualitative examination of rotational contours, vibrational progressions are assigned to all expected 4p states and the F' 0_u^+ ion-pair state. The vibrational progression arising from the F' 0_u^+ ion-pair state is extended up to v'=52 for $^{35}Cl_2$ and v'=50 for $^{35}Cl^{37}Cl$. However, regarding the Rydberg states, a number of matters arise. Firstly, the 4p;0_u^+ states dominate the spectrum reported here while the VUV absorption spectrum[4,6,7] in the same region is dominated by 4p;1_u states. For example, in the VUV spectrum reported by Moeller et al.[6], the origin of the [1/2]4p;1_u state appeared to be a factor of ca. 2.5 more intense than that of the [1/2]4p;0_u^+ state. In line with what is seen in this study, Tsuchiya and his co-workers[10,11] did not report any 1_u states at all but this might be explained by the use of fluorescence detection in their study. The identical excitation schemes used both here and by Moeller et al.[6] would seem to suggest that a one-photon ionisation from the 1_u states, as used here,

might not be as favourable as that from the 0_u^+ states. Also, there would seem to be an anomaly regarding the [1/2]4p;0_u^+ state. One might expect it to interact with the F' 0_u^+ ion-pair state which it clearly does not. Further theoretical work, including the contribution of spin-orbit coupling, needs to be carried out before this inconsistency can be explained.

Overall, good agreement is seen between the results of this study and those of earlier studies[4,6,7,10,11]. All the electronically excited states reported by Moeller et al.[6] can be seen. The diabatic description used here remains valid and can be used to identify states which are perturbed. This is possible when irregular vibrational spacings are displayed. However, an adiabatic description can still be employed because the excited state interactions are intermediate between the adiabatic and diabatic limiting cases.

7.4 References

1. R. J. Donovan, A. C. Flexen, K. P. Lawley, R. R. J. Maier, A. Mank and T. Ridley, *to be submitted.*
2. R. P. Ickowski, J. L. Margrave and J. W. Green, *J. Chem. Phys.*, **1960** 33 1261.
3. J. Lee and A. D. Walsh, *Trans. Faraday Soc.*, **1959** 55 1281.
4. A. E. Douglas, *Can. J. Phys.*, **1981** 59 835.
5. S. D. Peyerimhoff and R. J. Buenker, *Chem. Phys.*, **1981** 57 279.
6. T. Moeller, B. Jordan, P. Gürtler, G. Zimmerer, D. Haaks, J. Le Calve and M-C Castex, *Chem. Phys.*, **1983** 76 295.
7. J. Wörmer, T. Moeller, J. Staplefeldt, G. Zimmerer, D. Haaks, S. Kampf, J. Le Calve and M. C. Castex, *Z. Phys. D.*, **1988** 7 383.
9. F. Grein, S. D. Peyerimhoff and R. J. Buenker, *Can. J. Phys.*, **1984** 62 1928.
10. K. Yamanouchi, T. Tsuchizawa and S. Tsuchia, *Chem. Phys. Lett.*, **1989** 156 301.
11. T. Tsuchizawa, K. Yamanouchi and S. Tsuchia, *J. Chem. Phys.*, **1990** 93 111.

12. P. Wang, I. V. Okuda, S. S. Dimov and R. H. Lipson, *Chem. Phys.*, **1994** 229 370.

13. M. S. N. Al-Kahali, R. J. Donovan, K. P. Lawley and A. J. Yarwood, *J. Phys. Chem.*, **1995** 99 3978.

14. J. Sugar and A. Musgrove, *J. Phys. Chem. Ref. Data*, **1991** 20 859.

15. L. J. Radzieminski and V. Kaufman, *J. Opt. Soc. America.*, **1969** 59 424.

16. R. Trainham, G. D. Fletcher and D. J. Larson, *J. Phys. B. At. Mol. Phys.*, **1987** 20 L777.

17. A. J. Yencha, A. Hopkirk, A. Hiraya, R. J. Donovan, J. G. Goode, R. R. J. Maier, G. C. King and A. Kvaran, *J. Phys. Chem.*, **1995** 99 7231.

18. T. Ishiwata, I. Fujiwara, T. Shinzawa and I. Tanaka, *J. Chem. Phys.*, **1983** 79 4779.

Chapter 8

Conclusions

8.1 Introduction

In this thesis, systematic assignments of the spectra of several different classes of molecule are presented. The greater part of the thesis is taken up with the detailed analysis of Rydberg transitions in the heavier methyl halides CH_3X (X= Cl, Br and I). This detailed systematic analysis was made possible by the relative simplicity of the observed spectra. That this is not always so is exemplified by the studies of the spectroscopy of Rydberg transitions in such diverse molecules as CF_3I and CH_2Cl_2 and Cl_2.

8.2 Spectroscopy of Rydberg States in the Methyl Halides

The spectroscopy of the methyl halides is similar in many respects to the that of the diatomic halogens[1,2]. In fact, the same propensity rules prove useful in both cases. Like the diatomic halogens, the two-photon spectra of the methyl halides are found to be dominated by *nd*;0 series with weaker *nd*;2 series also apparent. Because the parity restrictions of homonuclear diatomic molecules no longer apply, *np*;0 transitions are apparent in methyl halides as in the heteronuclear diatomic halogens. Another likeness to the diatomic halogens is that transitions to states with Ω=1 are almost completely absent. Also, the spectra can be understood in terms of Rydberg state microconfigurations which apply equally well to the diatomic halogens. Despite the strong spin-orbit coupling, transitions to states with at least some singlet character are dominant. This similarity between the two-photon spectra of the diatomic halogens and those of the methyl halides seems somewhat surprising given the apparent differences between the two classes of molecules. However, this can be explained by the similarity of Rydberg state microconfigurations and the presence of strong spin-orbit coupling in the methyl halides.

The propensity rules which prove so successful in obtaining an understanding of the two-photon spectroscopy of the methyl halides can also be applied equally well to their three-photon spectra. While the transitions present in the two-photon spectra are still apparent in the three-photon ones, they are much weaker than those with $\Delta\Omega = 1$. In fact, the strongest features in the three-photon spectrum of the methyl bromide are those due to *nf*;1 series. There would appear to be evidence that *nf*;1 states dominate the three-photon spectra of methyl chloride and methyl iodide as well. Other features can be assigned to *ns*;1 and *nd*;1 series. Extending the system of assignments used in the two- and three-photon spectra of the methyl halides to their VUV absorption spectra results in an understanding where *nd*;1 series are dominant with *np*;0 and *nd*;0 series also present. The absence of *nf*;1 series from the VUV absorption spectra can be explained if *l* remains good in the methyl halides with Ω and spin multiplicity in turn introducing further restrictions.

While the same propensity rules can be used to explain the spectra of methyl chloride, methyl bromide and methyl iodide, some differences are evident. For example, the spectra of methyl iodide appear to show signs of strong vibronic coupling between Rydberg and ion-pair states. Also, an additional set of strong features is seen in the two-photon spectrum of methyl chloride. These are ascribed to a 4s Rydberg state based upon the $\tilde{A}\ ^2A_1$ ionic core. However, on the whole, these are only minor departures and the same systematic assignment can be applied to all three molecules.

8.3 Rydberg Transitions in Other Molecules which are not Well-behaved

One of the reasons why the analysis of the Rydberg spectra of the methyl halides has proved tractable is the relative simplicity of their vibrational structure. This reflects the simplicity of the photoelectron spectroscopy of these molecules. However, photoelectron spectra are not always as simple of those of methyl chloride, methyl bromide or methyl iodide, and this can have a dramatic effect upon the spectral

complexity. Further adding to the difficulty in analysing spectra is the presence of Rydberg~ion-pair interactions and valence contamination of the Rydberg orbitals.

Many similarities would be expected in the spectroscopy of Rydberg transitions in both CF_3I and methyl iodide. However, it turns out that there are more differences than similarities between the two. The first difference is that there is strong vibrational activity in the photoelectron spectrum of trifluoromethyl iodide[3] compared with methyl iodide[4]. This suggests that there is a greater degree of anti-bonding character in the HOMO of trifluoromethyl iodide. There are also some clear departures from the vibronic envelope seen in the photoelectron spectrum. This is most clearly apparent in the [3/2]6p cluster but the 6s and [3/2]5d clusters also display departures. These departures can be explained by extensive Rydberg~ion-pair interaction and some valence contamination of the Rydberg orbitals.

Even greater spectral complexity is seen in the photoelectron spectrum of dichloromethane[5] with respect to its methyl halide counterpart, methyl chloride[6]. Not only does a greater number of lower-lying ion states increase the number of Rydberg states present but a much greater degree of vibrational activity is predicted as well. These two factors, taken together, make the analysis of Rydberg transitions in CH_2Cl_2 much more difficult. Long Rydberg series like those seen in the two-photon spectrum of methyl bromide cannot be expected because of the much greater degree of vibrational activity seen in the photoelectron spectrum. However, the propensity rules for electronic transitions in dichloromethane would appear to be much stricter than in methyl chloride. This is because all of the observed features in the two-photon spectrum of CH_2Cl_2 are best assigned to $nd;A_1$ transitions. Nevertheless, there is some uncertainty in these electronic assignments, especially for those features which lie to higher energy. This uncertainty results from departures from the vibronic envelopes exhibited by the four low-lying electronic states of the ion. Rydberg~ion-pair or Rydberg~valence interactions and valence contamination of Rydberg orbitals cannot be ruled out here also.

The VUV absorption spectrum of molecular chlorine was not understood until after the theoretical work reported by Peyerimhoff and Buenker[7] in 1981. Following this, the Rydberg~ion-pair interactions predicted by Peyerimhoff and Buenker[7] were verified and proved of great use in analysing the spectrum[8]. The complexity of the spectrum is increased by interactions of the 4p cluster, especially the [3/2]4p;0_u^+ state, with nearby ion-pair states. The [3/2]4p;0_u^+ state interacts strongly with the nearby F′ 0_u^+ ion-pair state. The other three 4p Rydberg states apparent in the same energy region, 72000-77000 cm^{-1}, are not as perturbed and display more Rydberg character. While this can be explained by the positions of the curve crossings on the Rydberg state potential curves, it is still surprising that the [1/2]4p;0_u^+ state is apparently unperturbed. One point to note is that the calculations of Peyerimhoff and Buenker[7] did not take account of the effect of spin-orbit splittings in Cl_2^+ upon the electronic structure of Cl_2. A theoretical re-examination but taking spin-orbit splittings into account might explain this apparent inconsistency.

8.4 Conclusions and Extensions

The understanding of Rydberg transitions in the methyl halides has been significantly advanced by this work. It has been seen that propensity rules recently applied to the spectra of the diatomic halogens can also be applied to the spectra of the methyl halides. Attempts to extend this systematic approach has not proved entirely successful in molecules such as CF_3I, CH_2Cl_2 and Cl_2. This was mainly because of the increased amount of spectral complexity produced by perturbations in these molecules.

Recently, work[9] has been carried out on the two-photon spectroscopy of several substituted benzenes along with a re-examination of the two-photon spectra of benzene and benzene-d_6. It was found that similar propensity rules also applied to this completely different class of molecule. This seems to suggest that the propensity rules

described in this thesis might well apply to other classes of molecules completely unrelated to those considered here.

8.5 References

1. R. J. Donovan, A. C. Flexen, K. P. Lawley and T. Ridley, *Chem. Phys.*, **1998** 226 217.
2. R. J. Donovan, A. C. Flexen, K. P. Lawley, R. R. J. Maier, A. Mank and T. Ridley, *to be submitted.*
3. T. Cvitaš, H. Gusten, L. Klasinc, I. Novadj & H. Vancik, *Z. Naturforsch.*, **1978**, 33a, 1528.
4. Y-F. Zhu and E. R. Grant, *J. Phys. Chem.*, **1993** 97 9582.
5. T. Pradeep and D. A. Shirley, *J. Electron Spectrosc. Relat. Phenom.*, **1993** 66 125.
6. J. L. Ragle, I. A. Stenhouse, D. C. Frost and C. A. McDowell, *J. Chem. Phys.*, **1970** 50 178.
7. S. D. Peyerimhoff and R. J. Buenker, *Chem. Phys.*, **1981** 57 279.
8. T. Moeller, B. Jordan, P. Gurtler, G. Zimmerer, D. Haaks, J. Le Calve and M-C Castex, *Chem. Phys.*, **1983** 76 295.
9. S. Wang, R. J. Donovan, T. Ridley and K. P. Lawley. *Resonance Ionisation Spectroscopy*, **1998** CP454 325.

Appendix

A.1 Lectures Attended

In accordance with the regulations of the Department of Chemistry, University of Edinburgh, the following courses were attended:

1. Excited States and Ions

2. Advanced Spectroscopic and Dynamic Techniques

3. Lasers I and II

4. Reaction Dynamics

5. Atmospheric Chemistry

6. Molecular Quantum Mechanics

In addition to these, Physical Chemistry colloquia and laser group meetings were attended at the University of Edinburgh as well as some invited lectures at Heriot-Watt University.

A.2 Conferences Attended

1. Annual Northern Universities Meeting on Chemical Physics, July 1996.

2. The Autumn Meeting of the Royal Society of Chemistry, September 1997.

A.3 Publications

Ionic and Rydberg states of CF_3I studied by high resolution photoelectron (ZEKE-PFI) and resonance-enhanced multiphoton ionisation spectroscopy, N. A. Macleod, S. Wang, J. Hennessy, T. Ridley, K. P. Lawley and R. J. Donovan, *J. Chem. Soc. Faraday Trans.*, **1998**, 94, 2689-2694.